United States
Environmental Protection
Agency

Environmental Sciences Research
Laboratory
Research Triangle Park NC 27711

EPA-600/2-80-024
January 1980

Research and Development

EPA

Kinetic Studies of Simulated Polluted Atmospheres

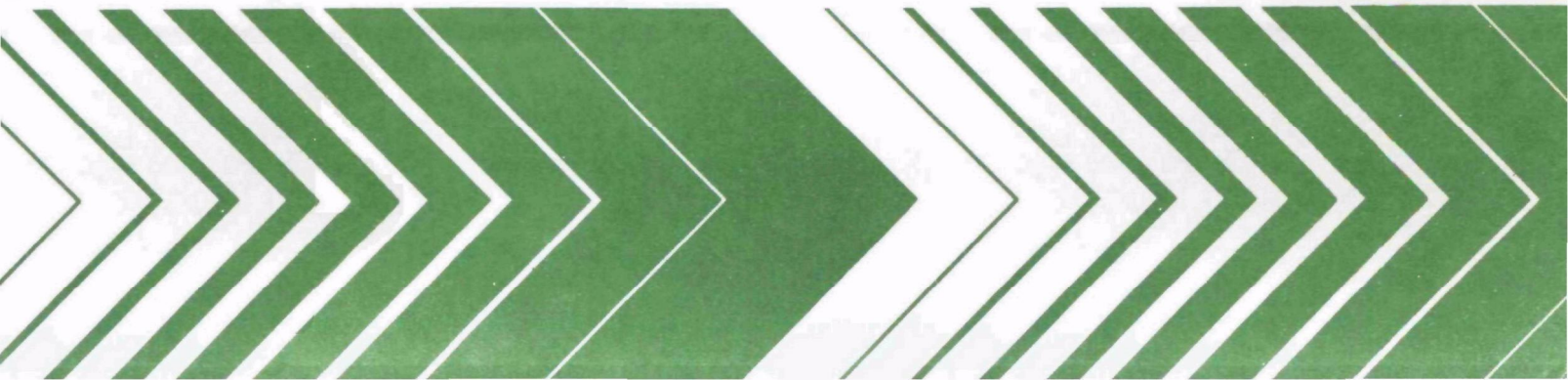

RESEARCH REPORTING SERIES

Research reports of the Office of Research and Development, U.S. Environmental Protection Agency, have been grouped into nine series. These nine broad categories were established to facilitate further development and application of environmental technology. Elimination of traditional grouping was consciously planned to foster technology transfer and a maximum interface in related fields. The nine series are:

1. Environmental Health Effects Research
2. Environmental Protection Technology
3. Ecological Research
4. Environmental Monitoring
5. Socioeconomic Environmental Studies
6. Scientific and Technical Assessment Reports (STAR)
7. Interagency Energy-Environment Research and Development
8. "Special" Reports
9. Miscellaneous Reports

This report has been assigned to the ENVIRONMENTAL PROTECTION TECHNOLOGY series. This series describes research performed to develop and demonstrate instrumentation, equipment, and methodology to repair or prevent environmental degradation from point and non-point sources of pollution. This work provides the new or improved technology required for the control and treatment of pollution sources to meet environmental quality standards.

This document is available to the public through the National Technical Information Service, Springfield, Virginia 22161.

EPA-600/2-80-024
January 1980

KINETIC STUDIES OF SIMULATED POLLUTED ATMOSPHERES

BY

Jack G. Calvert
Department of Chemistry
The Ohio State University
Columbus, Ohio 43212

Grant Number R804348-01

Project Officer

Joseph J. Bufalini
Atmospheric Chemistry and Physics Division
Environmental Sciences Research Laboratory
U.S. Environmental Protection Agency
Research Triangle Park, North Carolina 27711

ENVIRONMENTAL SCIENCES RESEARCH LABORATORY
OFFICE OF RESEARCH AND DEVELOPMENT
U. S. ENVIRONMENTAL PROTECTION AGENCY
RESEARCH TRIANGLE PARK, NORTH CAROLINA 27711

DISCLAIMER

This report has been reviewed by the Gas Kinetics and Photochemistry Branch, U.S. Environmental Protection Agency, and approved for publication. Approval does not signify that the contents necessarily reflect the views and policies of the U.S. Environmental protection Agency, nor does mention of trade names or commercial products constitute endorsement or recommendation for use.

ABSTRACT

This research was initiated to help quantify several key aspects of the chemistry of the polluted atmosphere which remain ill-defined. Kinetic and mechanistic studies were made related to several important atmospheric contaminants: sulfur dioxide, formaldehyde, nitrous acid, and the nitrosamines.

Through the use of laser excitation, sulfur dioxide has been excited at selected wavelengths to characterize the reactions and lifetimes of the several common excited states of this species with various atmospheric components. The reactions of sulfur dioxide with the methylperoxy radical were also studied by flash spectroscopy. All of these data and other published rate data were reviewed and evaluated. It was concluded that the homogeneous oxidation of sulfur dioxide in the atmosphere is initiated largely by way of three free radical intermediates; the hydroxyl radical (HO) is the most important of these. The hydroperoxy (HO_2) and methylperoxy (CH_3O_2) may contribute significantly for certain highly polluted atmospheres.

The present studies have shown that the ubiquitous formaldehyde molecule can be a major source of the important hydroperoxyl radical through the photolysis process, CH_2O + sunlight $\rightarrow$ HCO + H, followed by, HCO + O_2 $\rightarrow$ HO_2 + CO and H + O_2 + M $\rightarrow$ HO_2 + M. Our data allow a quantitative evaluation of the apparent first order rate constants for the rates of HO_2 generation by this process within the troposphere at various solar zenith angles.

The absolute extinction coefficients for nitrous acid were determined, and estimates were made of the rates of hydroxyl radical generation in the troposphere through the reaction, HONO + sunlight $\rightarrow$ HO + NO.

Long-path Fourier transform infrared spectroscopy was employed in one phase of the work to help evaluate the potential for nitrosamine formation in the polluted atmosphere. It was found that the dimethylamino radical, $(CH_3)_2N$, is 1.5×10^{-6} -times and 3.9×10^{-7} times less reactive toward oxygen than nitric oxide and nitrogen dioxide, respectively. Thus alkyl amino radicals formed by H-atom abstraction from amines by HO-radical attack in the atmosphere have a reasonable chance of forming nitrosamines (R_2N-N=O) and nitramines (R_2N-NO_2) even though nitric oxide and nitrogen dioxide impurities are at concentrations in the pphm range.

This report was submitted in fulfillment of grant number R804348-01 by Ohio State University under the sponsorship of the U.S. Environmental Protection Agency. This report covers a period from January, 1976, to April, 1979, and work was completed as of March 1979.

CONTENTS

Abstract		iii
Figures		vi
Tables		xi
1.	Introduction and Conclusions	1
2.	Studies Related to Sulfur Dioxide Removal Mechanisms in the Atmosphere	5
	Kinetics of fluorescence decay of SO_2 excited in the 2662-3273Å region	5
	References	35
	The mechanism of photochemical reactions of SO_2 with isobutane excited at 3130Å	37
	References	60
	A kinetic flash spectroscopic study of the CH_3O_2-CH_3O_2 and CH_3O_2-SO_2 reactions	63
	References	77
	Mechanism of the homogeneous oxidation of sulfur dioxide in the troposphere	79
	References	129
3.	Studies Related to Formaldehyde Removal Mechanism in the Atmosphere	141
	Quantum efficiency of the primary processes in CH_2O photolysis at 3130Å and 25°C	141
	References	159
	The wavelength dependence of the quantum efficiencies of the primary processes in CH_2O photolysis at 25°C	162
	References	178
	An unusual H_2-forming reaction in the 3130Å photolysis of CH_2O-O_2 mixtures at 25°C	180
	References	198
4.	Studies Related to the Removal Mechanisms of Nitrogenous Compounds in the Atmosphere	201
	The near uv absorption spectrum of gaseous HONO and N_2O_3	201
	References	214
	The kinetics of dimethylamino radical reactions in simulated atmospheres: the formation of dimethyl-nitrosamine and dimethylnitramine	216
	References	263

FIGURES

Number		Page
1.	Comparison of the wavelength dependence of the transmission of filters used.	7
2.	Time resolved fluorescence decay curves of SO_2 excited at 3020 Å.	9
3.	Stern-Volmer plot of the long-lived component of SO_2 fluorescence excited at 3107 Å.	11
4.	Stern-Volmer plot of the short-lived component of SO_2 fluorescence excited at 3107 Å.	11
5.	Plot of the radiative lifetime of the long-lived fluorescing species versus excitation energy of SO_2.	13
6.	Plot of the radiative lifetime of the short-lived fluorescing species versus excitation energy of SO_2.	13
7.	Plot of the rate constant for the quenching of the L state by SO_2 versus the excitation energy.	13
8.	Plot of the rate constant for the quenching of the S state by SO_2 versus the excitation energy.	13
9.	Semilog plot of the intensity of the total fluorescence of the SO_2 molecule versus time with excitation at 2998 Å.	18
10.	Plot of the calculated initial rate of decay of the L species of SO_2 versus the excitation energy.	18
11.	Plot of the apparent first-order rate constant for the diffusional loss of the L state versus $1/P_{SO_2}$.	20
12.	Plot of the ratio I_S°/I_L° versus pressure: excitation wavelength 3107 Å; assuming $^1S \rightarrow L$ conversion.	20
13.	Plot of the ratio I_S°/I_L° versus pressure: excitation wavelength 3107 Å; assuming $^1S \rightleftarrows L$ interconversion.	24
14.	Plot of the ratio I_S°/I_L° versus pressure for excitation at 3211, 3225, 3275 Å.	24
15.	Plot of the Brus and McDonald data for the ratio I_S°/I_L° as a function of pressure of SO_2.	29

16. Semilog plot of the fluorescence intensity versus time for SO_2 under collision free conditions. 30

17. Example of the pressure variation in the 3130 Å photolysis of SO_2 with isobutane; P_{SO_2} = 15.0 Torr. 39

18. Light scattering observed in the photolysis of SO_2-isobutane mixtures. 40

19. Example of the pressure variation in the 3130 Å photolysis of SO_2 with isobutane; P_{SO_2} = 0.195 Torr. 40

20. Plot of quantum yields as a function of light intensity. 41

21. Plot of quantum yields as a function of $[RH]/[SO_2]$ ratio. 44

22. Plot of the function of the quantum yield, relation C, versus the benzene pressure. 44

23. Plot of the function of the left-hand term in relation D as a function of the $[SO_2]/[RH]$ ratio. 47

24. Plot of $P_j(I_a/I_o)$ as a function of P_{SO_2}. 51

25. Plot of quantum yields as a function of $P_{C_4H_{10}}$; P_{SO_2} = 5 Torr. 52

26. Plot of quantum yields as a function of $P_{C_4H_{10}}$; P_{SO_2} = 2.5, 5.0, 10.0, and 15.0 Torr. 55

27. Plot of the function of quantum yield, relation C, versus benzene pressure. 56

28. Plot of quantum yields as a function of the CO_2 pressure. 58

29. Plot of the rate of increase of initial light scattering as a function of the rate of pressure drop. 59

30. The measured initial absorbance of CH_3O_2 at 265 nm versus azomethane pressure in the flash photolysis of Me_2N_2-O_2. 66

31. The gas phase extinction coefficients of CH_3O_2 as a function of wavelength. 67

32. Plot of the rate constant function $k'_{16}[SO_2] + k'_5[Me_2N_2]$ versus P_{SO_2}. 74

33. Comparison of the extinction coefficients of SO_2 within the first allowed band, the "forbidden" band, and a typical wavelength distribution of the flux of solar quanta at ground level. 81

34. Relation between the rate constants for the triplet quenching reactions with oxygen and $E_{T_1} - E_{S_o}$. 89

35. Relation between the rate constant for the triplet quenching reactions with nitric oxide and $E_{T_1} - E_{S_o}$. 90

36. The theoretical percentage of HO_2 in the Gas phase which is complexed with H_2O vapor as a function of the temperature and relative humidity. 101

37. Variation of the apparent second order rate constant for the reaction 57 with pressure of the added gases. 108

38. Plot of the reciprocal of the apparent second order rate constant for the reaction 39 versus the reciprocal of the pressure of the added gas. 109

39. Plot of the ratio of rate of O_3 loss to rate of SO_3 formation versus $[SO_2]^{-1}$. 119

40. Plot of the ratio of slope/intercept for the plots of Figure 7 versus $[H_2O]$. 119

41. The theoretical monthly average of the rate (% hr^{-1}) of SO_2 oxidation within the northern atmosphere as a function of the month of the year. 123

42. The theoretical rate (% hr^{-1}) of SO_2 oxidation by HO (reaction 39) and HO_2 (reaction 31) at various elevations within the troposphere and at various N latitudes. 123

43. The theoretical rate of attack of various free radical species on SO_2 (% hr^{-1}) for a simulated sunlight-irradiated polluted atmosphere. 125

44. First-order plot of a function of the pressure in CH_2O photodecomposition at 3130 Å. 145

45. Effect of incident light intensity on the rate of CH_2O photodecomposition at 3130 Å. 145

46. Plot of $(\Phi_{H_2} - \Phi_2) - 1$ versus $[C_4H_8]/[CH_2O]$. 153

47. The previously published estimates of the primary quantum yield of the free radical-forming process 1 in CH_2O photolysis. 163

48. The wavelength dependence of the primary quantum yield of the free radical-forming process 1 in CH_2O photolysis. 171

49. Variation with solar zenith angle of the apparent first order rate constants for sunlight absorption by CH_2O and the decomposition of CH_2O by primary process 1. 176

50. Pressure-time profiles in the photooxidation of CH_2O. 183

51. Beer's law plots for $N_2O_3(g)$ at some representative wavelengths. 204

52. The absorption cross section for $N_2O_3(g)$ as a function of wavelength. 208

53. The absorption cross section for HONO(g) as a function of wavelength. 209

54. Estimated first order rate constants for HONO(g) photolysis in sunlight. 213

55. Comparison of irradiance inside photolysis cell with solar irradiance. 220

56. Gas handling system for introducing known amounts of chemicals into the photolysis cell. 222

57. Optical paths in a standard White cell(4n pass). 223

58. Placement of images on M_f in a standard White cell. 224

59. Mirror system for the modified White cell. 225

60. Optical transfer system from interferometer to photochemical cell. 227

61. Optical diagram of interferometer. 228

62. Concentration/time profile for the reaction of dimethylamine with nitrous acid. 230

63. Plot of the disappearance of dimethylnitrosamine as a function of photolysis time. 232

64. Plot of the logarithm of dimethylnitrosamine concentration as a function of time. 233

65. Plot of the reciprocal concentration of dimethylnitrosamine as a function of time for the photolysis of DMN with 5.0 ppm NO in N_2. 235

66. Initial data from the photolysis of DMN in N_2. 236

67. Plot of ln(Absorbance) for three low pressure photolyses of NO_2. 239

68. Concentration-time profile for the photolysis of dimethylnitrosamine in a mixture of 49 Torr O_2 and 651 Torr of N_2. 245

69. Concentration-time profile for the photolysis of dimethylnitrosamine in a mixture of 140 Torr of O_2 and 560 Torr of N_2. 246

70. Concentration-time profile from the photolysis of dimethylnitrosamine in a mixture of 730 Torr O_2. 247

71. Concentration-time profile from photolysis of dimethylnitrosamine with 5.4 ppm NO in a mixture with 23 Torr O_2 and 677 N_2. 248

72. Concentration-time profile from the photolysis of dimethylnitrosamine with 5.5 ppm NO in a mixture of 69 Torr O_2 and 621 N_2. 249

73. Concentration-time profile from the photolysis of dimethylnitrosamine with 5.5 ppm NO in a mixture with 138 Torr O_2 and 562 Torr N_2. 250

74. Concentration-time profile for the photolysis of dimethylnitrosamine with 5.0 ppm NO in 700 Torr O_2. 251

75. Concentration-time profile from the photolysis of dimethylnitrosamine with 25 ppm NO in a mixture of 145 Torr oxygen and 555 Torr N_2. 252

76. Plot of functions B and B' as a function of $[O_2]/[NO]$ used to extimate k_4/k_3. 256

77. Plot of functions C and C' as a function of $[O_2]/[NO_2]$ for the estimation of the rate constant ratio k_{5a}/k_3 and k_{5b}/k_3. 259

TABLES

Number		Page
1.	Lifetime and quenching rate constants for long-lived and short-lived species excited in SO_2.	14
2.	Stern-Volmer parameters of the L and S components as a function of the fluorescence wavelengths monitored.	15
3.	Reciprocal lifetimes of the S and L components and I^o/I_L^o as a function of the fluorescence wavelengths monitored.	16
4.	The effect of pressure on the I_S^o/I_L^o values and reciprocal lifetimes of the L and S components of SO_2 fluorescence excited at 3107Å.	25
5.	The estimated fraction of the total fluorescence intensity from the L species in SO_2 steady state irradiations.	32
6.	Rate constants for the quenching by various atmospheric gases of the L and S components of the SO_2 fluorescence excited at 3130 and 2662Å.	34
7.	Quantum yields for the photolyses of SO_2 and isobutane mixtures under low pressure conditions.	42
8.	Quantum yields for the photoreaction of SO_2 with isobutane in the presence of benzene under low pressure conditions.	43
9.	Quantum yields for the photolysis of SO_2-isobutane mixtures under medium pressure conditions.	49
10.	Quantum yields for the photolyses of SO_2-isobutane-C_6H_6 mixtures under medium pressure conditions.	54
11.	Quantum yields for the photolyses of SO_2-isobutane-CO_2 mixtures under medium pressure conditions.	57
12.	Estimates of the apparent rate constant for the reaction 4.	68
13.	Rate data for the reaction, $CH_3O_2 + SO_2$.	73
14.	Extimated rates of $SO_2(^3B_1)$ generation by solar radiation in the lower troposphere.	85

15. Percentage of $SO_2(^3B_1)$-quenching by various atmospheric gases in air at 25°C and 1 atm. 86

16. $SO_2(^3B_1)$ "chemical" quenching rate constants for various atmospheric components and impurity species in the overall reaction shown. 91

17. The theoretical rate of reaction of $SO_2(^3B_1)$ reactions with various impurity species and O_2 in a hypothetical sunlight-irradiated lower troposphere. 94

18. Enthalpy changes and recommended rate constants for potentially important reactions of ground state SO_2 and SO_3 molecules in the lower troposphere. 95

19. Experimental data from the photolysis of formaldehyde at 3130Å and 25°C. 144

20. Experimental data from the photolysis of formaldehyde in the presence of trimethylsilane. 149

21. Experimental data from the photolysis of formaldehyde in the presence of isobutene. 152

22. The rates of H_2 formation in formaldehyde photolysis with small amounts of added isobutene. 153

23. Experimental data from the photolysis of formaldehyde in the presence of nitric oxide. 156

24. The effect of isobutene on hydrogen formation in the photolysis of formaldehyde at 25°C and with excitation at 2890 to 3380Å. 166

25. The effect of CO_2 on hydrogen formation in the photolysis of formaldehyde at 25°C. 167

26. The wavelength dependence of the primary quantum efficiency of the photodecomposition of formaldehyde into H and HCO. 169

27. Estimated apparent first order rate constants for sunlight absorption by CH_2O and for photodecomposition by reaction 1 in sunlight in the lower atmosphere. 175

28. Experimental data from the photolysis of CH_2O-O_2 mixture at 3130Å and 25°C. 185

29. The effect of absorbed light intensity on the product quantum yields in the photolysis of CH_2O-O_2 mixtures. 186

30. Experimental data from the photolysis of CH_2O-O_2-CO_2 mixtures at 3130Å and 25°C. 187

31. Summary of the reaction mechanism and rate constants employed in the simulation of the CH_2O, O_2, and CO_2 mixture photolyses. 194

32. Dinitrogen trioxide absorption cross sections. 205

33. Nitrous acid absorption cross sections. 207

34. Values of the rate constant for the photolysis of dimethylnitrosamine obtained from the initial slope of the logarithm of the dimethylnitrosamine concentration as a function of time. 238

35. Extinction coefficients, quantum yields and values of the light intensity within the cell used in the determination of the photolysis rate of dimethylnitrosamine. 241

36. Calculated values of B and B' used in the estimation of k_4/k_3. 254

37. Calculated values of C and C' used in the estimation of k_{5a}/k_3 and k_{5b}/k_3. 257

SECTION 1

INTRODUCTION AND CONCLUSIONS

OBJECTIVES

There are several aspects of the chemistry of the polluted atmosphere which remain ill-defined. The research effort supported by this grant was designed to elucidate some of the remaining key problem areas. (1) The atmospheric removal and transformation mechanisms for sulfur dioxide remain a major area of concern and interest. In spite of the rather general concensus that sulfuric acid, ammonium sulfate, and ammonium bisulfate are ultimate major sinks for atmospheric sulfur dioxide, the mechanism by which the SO_2 is transformed to these and other products is not clear. The research on this grant has provided some new insights into these processes and some important information related to the SO_2 tropospheric reactions.

(2) In recent years it has become increasingly clear that the aldehydes are significant participants in the chemical transformations which occur within the troposphere. Thus the photodissociation of formaldehyde and the higher aldehydes generates H-atoms and HCO and alkyl free radicals:

$$CH_2O + h\nu \rightarrow H + HCO$$

$$RCHO + h\nu \rightarrow HCO + R$$

Each of these radicals can generate HO_2 radicals by reactions with oxygen:

$$H + O_2 \ (+M) \rightarrow HO_2 \ (+M)$$

$$HCO + O_2 \rightarrow HO_2 + CO$$

$$R + O_2 \rightarrow RO_2$$

$$RO_2 + NO \rightarrow RO + NO_2$$

$$RO + O_2 \rightarrow HO_2 + R'CHO$$

The HO_2 and RO_2 radicals can initiate the chain photooxidation reactions of NO to NO_2:

$$HO_2 + NO \rightarrow NO_2 + HO$$

$$HO + RH \rightarrow H_2O + R$$

$$R + O_2 \rightarrow RO_2$$

$$RO_2 + NO \rightarrow RO + NO_2$$

$$RO + O_2 \rightarrow R'CHO + HO_2$$

Since the $[NO_2]/[NO]$ ratio is increased by the occurrence of these reactions, O_3 builds up in the sunlight-irradiated atmosphere as the NO_2-NO-O_3 reaction sequence occurs:

$$NO_2 + h\nu \rightarrow O + NO$$

$$O + O_2 (+M) \rightarrow O_3 (+M)$$

$$O_3 + NO \rightarrow O_2 + NO_2$$

Although it has been recognized for years that the aldehydes may play an important role in the initiation of chain reactions responsible for photochemical smog, the quantitative aspects of this thesis, so necessary for accurate, realistic modelling efforts and control strategy development, remain unevaluated. In particular, the quantum efficiency of the radical formation from CH_2O and RCHO, irradiated at the wavelengths of sunlight within the troposphere, have not been characterized well. In this work several studies have been completed which help define these important parameters.

(3) The nature of the chemical transformations among the nitrogen-containing molecules such as NO, NO_2, HONO, $HONO_2$, HO_2NO_2, NH_3, RNH_2, R_2NH, etc., are directly related to the NO_x balance and ultimately to the O_3 generation potential within the troposphere. The amines are of special concern in our considerations of tropospheric chemistry by virtue of their potential transformation to the highly carcinogenic compounds such as the nitrosamines and the nitramines. Our work of the past year has provided some new quantitative kinetic information which should allow a realistic evaluation of the significance of nitrosamine and nitramine generation by free radical reactions in the troposphere.

The following section A-2 provides a brief summary of our several findings. In the section B, Parts I, II, III, the detailed reports on each of the several aspects of our studies are given.

SUMMARY OF FINDINGS DURING THE PROJECT PERIOD

a) Several key points related to the tropospheric removal mechanism of sulfur dioxide have been established in this work:

i) Through the use of laser excitation of SO_2 at selected wavelengths within the region, 2662-3273 A, we have defined the lifetimes and quenching rate constants for the $SO_2(^1B_1)$ and $SO_2(^1A_2)$ excited states of SO_2 with various atmospheric gases. The $SO_2(^1A_2)$ state is quenched extremely effectively by all of the molecules studied. For example N_2 and O_2 quench

this molecule with rate constants: 1.9×10^{12} l/mole-sec, respectively. The $SO_2(^1B_1)$ species is quenched less efficiently; for example, $k = 3.5 \times 10^{10}$ and 3.4×10^{10} l/mole-sec by N_2 and O_2, respectively. These data suggest that SO_2 excited by sunlight within the troposphere will be quenched to other longer lived states of SO_2 very quickly. The $SO_2(^3B_1)$ state is a dominant one which is clearly involved in SO_2 photochemistry.

ii) In a further quantitative study we have established the mechanism of the reactions of the singlet $[SO_2(^1B_1)]$ and triplet $[SO_2(^3B_1)]$ states of SO_2 with isobutane. The reaction in the absence of a large excess of quencher molecules involves both the $SO_2(^1B_1)$ and the $SO_2(^3B_1)$ species with rate constants: 8.4×10^9 and 8.7×10^8 l/mole-sec, respectively.

iii) The reaction of CH_3O_2 with SO_2 was studied using kinetic flash spectroscopy to monitor the CH_3O_2 radical directly. The results give the rate constant for the reaction $CH_3O_2 + SO_2 \rightarrow$ Products, $k = (3.2 \pm 0.7) \times 10^6$ l/mole-sec. In the same study we derived the rate constant for the reaction, $CH_3O_2 + CH_3O_2 \rightarrow$ Products, $k = (2.4 \pm 0.1) \times 10^8$ l/mole-sec.

iv) All of our existing data related to SO_2 atmospheric transformation paths and that of the literature were reviewed carefully in another phase of our work, and a quantitative evaluation has been made of the significance of various pathways for SO_2 reaction in the troposphere. The results suggest that the oxidation occurs largely by way of the reactions: $HO + SO_2 (+M) \rightarrow HOSO_2 (+M)$ (a); $HO_2 + SO_2 \rightarrow HO + SO_3$ (b); $CH_3O_2 + SO_2$ $CH_3O + SO_3$ (or CH_3OOSO_2) (c). Through computer simulations of the chemistry within both "clean" and polluted atmospheres, the theoretical rates of SO_2 conversion were estimated. Our present evaluation for the case of the highly polluted atmosphere, suggests the three reactions (a), (b), and (c) may all occur and with near equal rates. In these cases, the total of the rate corresponds to an SO_2 removal as high as 4%/hr. The many remaining uncertainties and alternatives in the mechanisms for SO_2 atmospheric removal have been discussed in detail in an attempt to provide a reasonable basis for the planning of the further studies.

b) In three detailed kinetic studies which were carried out on this grant, we determined the quantum efficiency of the two photochemical decomposition paths in formaldehyde in experiments at a variety of wavelengths:

$$CH_2O + h\nu \rightarrow H + HCO \qquad (I)$$

$$CH_2O + h\nu \rightarrow H_2 + CO \qquad (II)$$

The kinetics and the quantum yields of the products of the photolysis of CH_2O-NO, CH_2O-Me_3SiH, CH_2O-iso-butene, and CH_2O-O_2, CH_2O-O_2-CO_2 mixtures have been studied. The wavelength dependence of the absolute quantum yields of the primary processes (I) and (II) have been established. From these results and solar irradiance estimates, the apparent first order rate constants for CH_2O dissociation by process (I) at various solar zenith angles (in parentheses parentheses) are: $2.31 \times 10^{-3}(0^o)$; $2.17 \times 10^{-3}(20^o)$; $1.71 \times 10^{-3}(40^o)$;

$0.92 \times 10^{-3}(60^{\circ})$; and 0.17×10^{-3} $min^{-1}(78^{\circ})$. In further studies of CH_2O-O_2 mixtures we discovered an unexpected reaction leading to the formation of H_2, CO, and HCO_2H in a chain reaction. From the unusual kinetics observed we concluded that the reaction involves HO_2 and/or HO-radical addition to CH_2O. These considerations bear directly upon the mechanism of transformation of formaldehyde to formic acid with the polluted troposphere.

c) Two detailed studies have been made in this grant period of the atmospheric reactions of some important nitrogen-containing species.

i) The absolute extinction coefficients of nitrous acid vapor have redetermined. The large disagreement between the previous literature values has been resolved, and apparent first order rate constants for the reaction (III),

$$HONO + h\nu \rightarrow HO + NO \qquad \text{(III)}$$

in the sunlight-irradiated lower atmosphere have been derived for various solar zenith angles (in parentheses): 0.089 (0°); 0.086 (20°); 0.077 (40°); 0.054 (60°); 0.017 $min^{-1}(78^{\circ})$.

ii) In the second phase of our work on nitrogen compounds of atmospheric interest, we have used the long-path FT-IRS photolysis system to study the reaction modes of atmospheric generation of the $(CH_3)_2N$ radical and the kinetics of its subsequent reaction with O_2, NO, and NO_2: $(CH_3)_2N + O_2 \rightarrow CH_2{=}NCH_3 + HO_2$ (d); $(CH_3)_2N + NO \rightarrow (CH_3)_2NNO$ (e); $(CH_3)_2N + NO_2$ $(CH_3)_2NNO_2$ (f). The rate data give the following preliminary estimates of the rate constant ratios near 25°C: $k_d/k_e = (1.48 \pm 0.072) \times 10^{-6}$; $k_d/k_f = (3.90 \pm 0.28) \times 10^{-7}$. The very large reactivity of the $(CH_3)_2N$ radical with NO and NO_2 compared with that with O_2 suggests that the alkyl amino radicals formed by HO abstraction from amines present in the atmosphere have a reasonable chance of forming nitrosamines and nitramines even though the NO and NO_2 impurities are at concentrations in the pphm range.

SECTION 2

STUDIES RELATED TO SULFUR DIOXIDE REMOVAL MECHANISMS IN THE ATMOSPHERE

KINETICS OF FLUORESCENCE DECAY OF SO_2 EXCITED IN THE 2662-3273Å REGION

Introduction

A thorough understanding of the photochemistry of SO_2 excited within the first allowed electronic absorption region, 2500-3400 Å, has been impossible, since the nature of the excited species and their mechanisms of population and decay are poorly characterized today. The spectroscopic assignment of this band of SO_2 has puzzled spectroscopists for many years. Both the $^1B_1$ and the $^1A_2$ states of SO_2 are predicted to lie in this energy region,[3-5] and although only the $^1B_1 \leftarrow \tilde{X}\ ^1A_1$ transition is formally allowed, the vibronically induced transition to the $^1A_2$ state may also occur. The Renner-Teller coupling between the $^1B_1$ and $\tilde{X}\ ^1A_1$ states of SO_2, the Jahn-Teller interaction between the $^1B_1$ and $^1A_2$ states, and the spin-orbital coupling between the triplet states ($^3A_2$, $^3B_1$, and $^3B_2$) and singlet states ($^1B_1$, $^1A_2$), make the singlet electronic transitions in the 2500-3400 Å region extremely difficult to analyze. It was generally believed that this absorption system belonged to the allowed $^1B_1 \leftarrow \tilde{X}\ ^1A_1$ electronic transition.[6-9] However Dixon and Halle[10] did a partial rotational analysis of the 3340 Å band, and they suggested that it corresponded to a vibronically induced $^1A_2 \leftarrow \tilde{X}\ ^1A_1$ electronic transition. Hamada and Merer [11,12] carried out a much more detailed rotational analysis of twelve bands of $S^{16}O_2$ and two bands of $S^{18}O_2$ in the 3000-3400 Å region; they concluded that all of the obvious banded structure in this wave length region could indeed be assigned to the $^1A_2 \leftarrow \tilde{X}\ ^1A_1$ transition and that its origin was near 3580 Å. Analyzable vibrational or rotational structure which might be attributed to the $^1B_1 \leftarrow \tilde{X}\ ^1A_1$ transition has not been observed, but on the basis of the other less direct evidence at hand, Hamada and Merer[12] tentatively suggested that the band origin of the $^1B_1 \leftarrow \tilde{X}\ ^1A_1$ transition lay between 3100 and 3160 Å. Brand, et al.[13] have rationallized the observed Zeeman effect within the $^1A_2 \leftarrow \tilde{X}\ ^1A_1$ band system in terms of coupling of the $^1A_2$ state with a background of interacting vibrational levels of the ground state and the low lying states of the triplet manifold.

Recently Shaw, et al., have carried out an analysis of the fluorescence of SO_2 from single vibronic level excitation in the 3150-3080 Å[14] and the 3070-2930 Å[15] regions. The qualitative conclusions from the data support the view that the SO_2 ($^1B_1$) excited state, with an origin near 3160 Å, provides

the major component of the emitting levels. In time-resolved fluorescence studies of SO_2 excited in the 2617-3350 Å region, Brus and McDonald[16] and Butler and McDonald[17] found double exponential decay of the excited SO_2. The long-lived (L) state and the short-lived (S) state which contribute to this emission were attributed tentatively to the $^1B_1$ and $^1A_2$ states of SO_2, respectively. McDonald and co-workers concluded that the $^1B_1$ state of SO_2 could be populated even at wavelengths as short as 3350 Å, in seeming contradiction of the tentative band origin assignment from the data of Hamada and Merer[12] and Shaw, et al.[14,15] It was not possible to choose between alternative mechanisms of independent generation and decay of the L and S species and that involving generation of one from the other by way of first order or second order, collisionally perturbed processes.

Heicklen and his co-workers[18-21] have presented a great deal of indirect evidence for the existence of some other ill-defined, non-emitting singlet state of SO_2 which they designate as SO_2*. This hypothesis was formulated in view of the observed kinetics of product formation resulting from excited SO_2 interactions with various reactants as well as in SO_2 and biacetyl emission studies in various mixtures using steady illumination. These workers have concluded that excitation of SO_2 within the first allowed singlet band leads directly to the SO_2* state; they speculated that its radiative lifetime was about 6×10^{-7} sec, corresponding to that expected from simple theory relating lifetime and integrated absorption data for the first excited singlet band of SO_2.[1,22] They further suggested that the emitting singlet, presumably the long-lived state usually seen by previous workers, was formed by internal conversion from the SO_2* species. However there is no correspondence between the observed kinetic properties of the SO_2* state suggested by Heicklen, et al., and the Stern-Volmer quenching parameters derived for the emitting states of SO_2. Obviously firm conclusions concerning the true nature of the excited singlet states involved in the photochemistry of SO_2 are not now possible from the information at hand.

This study was initiated in an attempt to define better the kinetic properties of the first excited singlet states of SO_2. We have excited SO_2 at discrete wavelengths in the range 2662-3273 Å employing a quadrupled neodymium laser and a powerful, frequency doubled, tunable dye laser. We have studied the fluorescence decay kinetics of SO_2 at finite pressures and under essentially collision free conditions, and in SO_2-added gas mixtures. Some significant new evidence has been obtained which provides a clearer understanding of the kinetic mechanisms which control the generation and decay of the singlet emitting species in SO_2 excited at wavelengths in the 2662-3273 Å range.

Experimental Section

The experimental apparatus used in most of these studies was similar to that employed by Brus and McDonald.[16] A flashlamp pumped dye laser, Candela model ED-66, was used to excite SO_2 molecules at low pressures (0.05-12 mTorr) with a light pulse covering a narrow band of wavelengths (~1 Å). With a Rhodamine-B (Eastman No. 4453) solution (10^{-4}M) in ethanol, this laser produced approximately 400 kW of light at 6260 Å, or approximately 150 kW of light at 6522 Å with an optimum mixed solution of Rhodamine-6G

(Eastman No. 10724 and Cresylviolet (Eastman No. 11884) in ethanol. Kiton Red (Exciton No. 620) in methanol was used in some experiments to obtain a better output around 6400 Å. The pulse length of this laser was about 200 nsec. These laser pulses were frequency-doubled with a KDP crystal to give the corresponding uv-output with a power of 3 to 20 kW. The dye laser system was employed to secure pulses of near monochromatic ultraviolet radiation over the wavelength range, 2975-3273 Å. Wavelength determinations were performed with a Jarrell-Ash 3.4 m Ebert spectrograph.

In all of the lifetime studies at low pressures we used a cell of 22 ℓ. volume, similar to that employed by Sackett, et al.[23] Two cylindrical sidearms with Brewster angle windows of Suprasil were fused directly to the spherical cell body through quartz-Pyrex graded seals; these served as the entrance and exit routes for the exciting laser light pulse. The uv laser pulse passed an appropriate filter (Corning 7-54) to exclude the fundamental. At 90° to the excitation path a third sidearm, 3.5 in. long, was fused to the cell; it had a 2 in. diameter Suprasil window to which an RCA 7265 photomultiplier was positioned as closely as possible. Various cut-off filters were inserted between the window and the photomultiplier; the transmission of these is shown in Figure 1. The fluorescence signal from the photomultiplier was monitored via a Tektronix model 7704 oscilloscope, and stored on a Biomation model 610 transient digitizer. With the help of the interactive light pen display of a PDP-7 computer interfaced with a Datacraft 6024 computer for computations, the data tape could be transformed into semi-logarithmic form, displayed on the screen, judged to be a double or single exponential decay, and resolved by least squares computer fit accordingly.

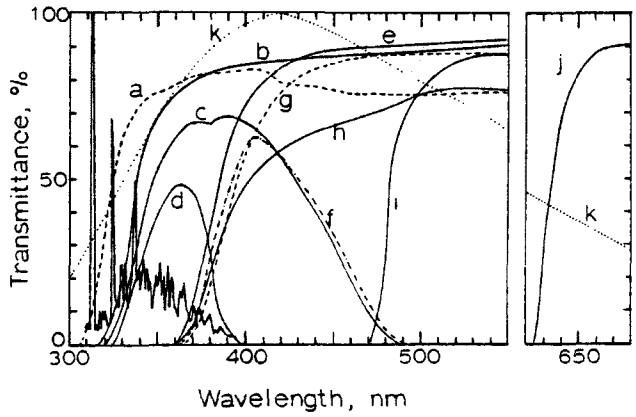

Figure 1. Comparison of the wavelength dependence of the transmission of filters used in front of the fluorescence intensity detector in this study, the photomultiplier response, and a typical SO_2 fluorescence envelope for SO_2 excited at 3133 Å [12]. Curve k represents the relative photomultiplier response.

In the quenching experiments of the long-lived singlet with various reactant gases at 2662 Å, a separate laser system and cell were employed, and a 20 nsec pulse of 2662 Å light was generated using a neodymium laser source. The oscillator was a 9 in. neodymium-doped glass rod, excited by three linear xenon flash lamps placed symmetrically about the rod; these provided an input of about 4000 J. Q-switching was accomplished with a rotating prism (24,000 rpm), and the laser beam was polarized by an angled Pyrex plate. A dielectric coated mirror completed the oscillator cavity. The peak intensity of the beam from the oscillator was of the order of 10 MW at a wavelength of 1.064 μ. A ten-fold increase in peak intensity was obtained by use of an amplification system. This consisted of a 12 in. neodymium-doped glass rod which was excited by a 700 J linear xenon flash lamp. The Q-switch was used to time the flash of both the oscillator and amplifier flash lamps; the amplifier flash was delayed with respect to that of the oscillator lamps by an electronic network. Both oscillator and amplifier were forced air cooled. The 100 MW 1.064 μ laser beam was twice frequency doubled to produce the desired uv pulse. The first frequency doubling was effected by a precisely oriented potassium dihydrogen phosphate (KDP) crystal. Any scattered flash lamp ultraviolet light was filtered from the beam by a Corning 7-57 filter, and the resultant beam contained about 1 MW of peak power at 5324 Å, together with unchanged fundamental neodymium frequency. The latter was removed by a Corning 4-96 filter which also served as a beam splitter. The light from the beam splitter activated the oscilloscope trace by means of a phototube (RCA 922) and allowed the recording of the fluorescence from the reaction cell. For doubling the green light, an ammonium dihydrogen phosphate (ADP) crystal was chosen to minimize absorption of the ultraviolet frequency. The arrangement employed generated about 10 kW peak power at 2662 Å with a half-intensity peak duration of 20 nsec. A Corning 7-54 filter placed before the sample cell, removed the green radiation from the beam. The fourth harmonic of the fundamental Nd centered at 2662 Å was found to have a band width of 1.2 Å for our system. In these studies at relatively high pressures where only the long-lived singlet emission was followed, the reaction cell was constructed from a Pyrex tube, 25 mm in diameter and 88 cm long, with Brewster angle windows of Suprasil sealed to the ends. The emission beam was filtered with a Corning 7-60 filter and the intensity of the fluorescence was monitored at right angles to the excitation beam.

The grease-free, mercury-free, high vacuum system employed was equipped with Teflon and metal valves (Granville Phillips). Pressure was measured with a MKS Baratron capacitance manometer (MKS-1H). The SO_2 reactant used in this study was purchased from the Baker Chemical Co. The condensed gas was distilled from trap to trap at -196°C, retaining only the middle third; this was degassed many times. In the quenching experiments we used high purity gases from Phillips Petroleum Company (isobutane, trans-2-butene, cis-2-butene, methane), Fisher Scientific Company (Benzene), Matheson Company (argon, oxygen, nitric oxide), and Airco (carbon monoxide, carbon dioxide). All gases except nitrogen were distilled on the vacuum line and only the middle fraction was retained.

Results and Discussion

The Double Exponential Decay of SO_2 Fluorescence--

The time resolved emission from SO_2 excited within the first allowed band shows a most interesting behavior first observed by Brus and McDonald.[16] Tupical fluorescence decay curves for SO_2 excited at 3020Å, 0.97 mTorr pressure, and 27°C, are shown in Figure 2. Only the time scale of the observations has been changed in the different experiments shown in order to accent the nature of the short- and long-time decay regions and the degree of the fit of the data to the kinetic equations employed. Clearly the

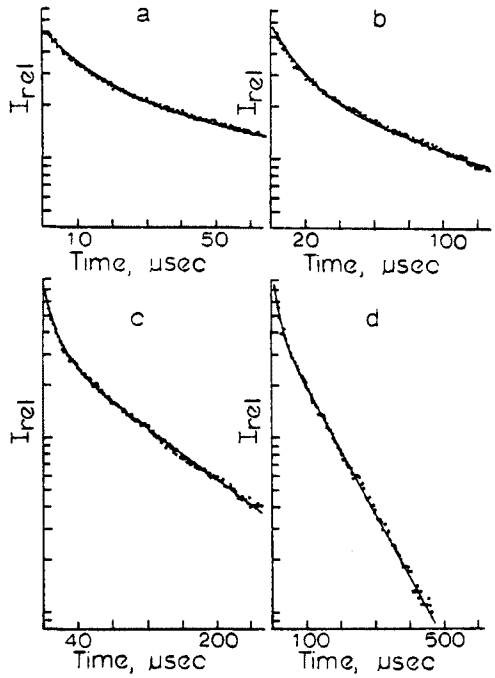

Figure 2. Time resolved fluorescence decay curves of SO_2 excited at 3020 Å and 0.97 mTorr. The solid lines are calculated assuming a double exponential decay as outlined in the text.

fluorescence intensity does not follow a simple, single exponential decay. However the results are described well using a double exponential decay formula:

$$I = I_S^o e^{-t/\tau_S} + I_L^o e^{-t/\tau_L} \qquad (1)$$

$$\text{or } I_{rel} = (I_S^o/I_L^o)e^{-t/\tau_S} + e^{-t/\tau_L} \qquad (2)$$

where I and I_{rel}, respectively, are the total intensity of the fluorescence

and the relative fluorescence intensity at time t, and I_S^o and I_L^o are the initial intensities of the short-lived and long-lived components, respectively. The solid curves shown in Figure 2 have been calculated from equation (2) using a single set of parameters for the components of emission: $1/\tau_S = 6.93 \times 10^4$; $1/\tau_L = 8.46 \times 10^3$; $(I_S^o/I_L^o) = 1.36$. Obviously the locus of the data points are reproduced well assuming the double exponential decay of the fluorescence, in confirmation of the observations of Brus and McDonald.[16] Failure to observe this phenomenon in our previous study at wavelength 2662 Å[24] was the result of the wavelength choice and the relatively high pressure range employed (2-80 mTorr) in this study. Even at low pressures of SO_2 the short-lived component of the fluorescence is not readily detected using 2662 Å excitation. This is confirmed by the fact that Brus and McDonald did not attempt to derive Stern-Volmer quenching data related to the short-lived species only in their experiments at 2617.4 and 2715.1 Å.

All of the fluorescence intensity-time data observed in this work could be fitted well in terms of relation (2) to derive τ_S, τ_L, and I_S^o/I_L^o values. It should be noted that a third exponential component to the fluorescence decay is observed at very long times; this emission which originates from the $SO_2(^3B_1)$ state is the subject of a further study in a subsequent report.

The Lifetimes and Stern-Volmer Quenching Parameters for the Short-Lived (S) and the Long-Lived (L) Components of the SO_2 Fluorescence-- The values of $1/\tau_S$ and $1/\tau_L$ determined at each excitation wavelength (2975-3273 Å) were plotted versus the SO_2 pressure over the range 0.5 to 12 mTorr. Typical data obtained in experiments with the excitation at 3107 Å are shown for the L and S components in Figures 3 and 4, respectively. It is seen that the emission from the S component shows Stern-Volmer behavior down to the lowest pressure at which data could be obtained. The data from the L component also shows Stern-Volmer behavior down to a pressure of about 1 mTorr; below this pressure the $1/\tau_L$ versus P_{SO_2} plot shows upward curvature. We will consider this deviation later and merely note here that this appears to arise from diffusional loss of the L species from the observation zone during their lifetimes.

Stern-Volmer quenching constants for each of the emitting species were derived from the linear portion of the $1/\tau$ versus pressure plots. These data are summarized in Table 1, and they may be compared with those published by Brus and McDonald[16] in Figures 5-8. The error bars shown for both sets of data correspond to ± twice the standard deviation. It is seen that the two studies are in general agreement within the error limits for most of the parameters determined. The one apparent difference between the two studies is the lifetime of the L species excited near 31833 cm^{-1}; see Figure 5. Thus Brus and McDonald found a lifetime of 617 ± 103 μsec for excitation at 3140.5 Å, while we observed a value of τ_L = 220 ± 30 μsec in the same general wavelength region at 3143 Å. The effect may result from the selective excitation of a peculiar, narrow region of SO_2 states for which perturbations of near lying states are less important; the band width of the laser light employed by Brus and McDonald is somewhat narrower (~3 cm^{-1}) than that which

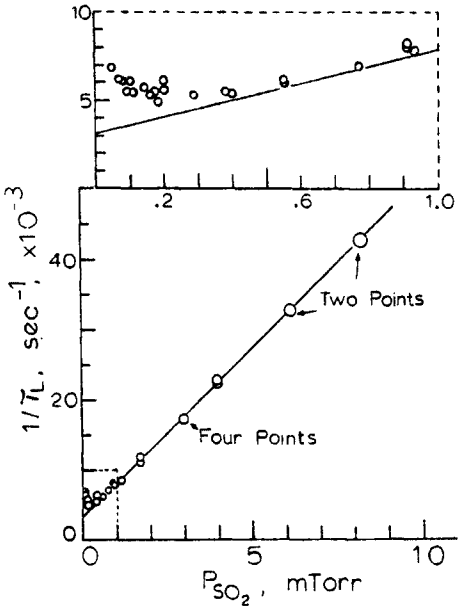

Figure 3. Stern-Volmer plot of the long-lived (L) component of SO_2 fluorescence excited at 3107 Å.

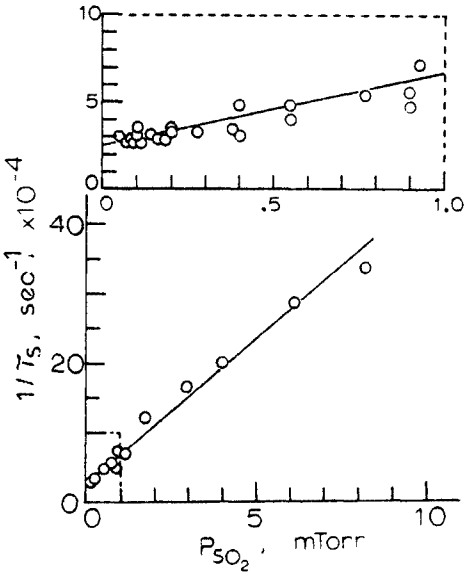

Figure 4. Stern-Volmer plot of the short-lived (S) component of SO_2 fluorescence excited at 3107 Å.

we employed (~10 cm^{-1}). However this difference may in part result from the choice of cut-off filter which was placed before the detector in the Brus and McDonald experiments; they switched from a 3100 Å to a 3550 Å cut-off filter in experiments at 3140.5 Å excitation and the longer wavelengths. The influence of the apparent lifetime on the choice of fluorescence wavelengths monitored for excitation at a given wavelength can be seen in the data of Tables 2 and 3. We found that the observed τ_L^o values varied from extremes of 224 to 646 μsec with a 3300 Å or a 6000 Å cut-off filter in place.

In both the study of Brus and McDonald and the present work the observation was made that the apparent lifetime of the L component increased as the observed fluorescence was restricted to the longer wavelength region. Since the emission intensity-time profile of the S species is obtained by subtracting the intensity of the L state extrapolated from the data at long times, the τ_S, and I_S^o/I_L^o values are somewhat dependent on the choice of filters employed; see Table 3. In general the τ_S^o and the quenching rate constants for the S and L species all decrease as the fluorescence is observed at increasing wavelengths. As Brus and McDonald have pointed out previously, the filter effect on the Stern-Volmer parameters indicates that the L and S species created at a given excitation wavelength, must be a group of rovibronic states with a range of τ_S^o and τ_L^o values. Therefore the lifetimes and quenching rate constants obtained from the Stern-Volmer plots must be only an average value of this group of states. To overcome the potential problem of enhancement of the fraction of the L or S fluorescence envelope observed, we have employed a cut-off filter and photomultiplier response which maximized the width of the band of wavelengths monitored in each experiment. See Figure 1.

The dependence of the apparent values of I_S^o/I_L^o on the choice of cut-off filter suggests that the emission spectrum of the S component is somewhat shifted to longer wavelengths than the L component. If one accepts the premise that the S and L components arise from the $^1A_2$ and $^1B_1$ states of SO_2, respectively, then the minor differences in emission profiles can be rationalized in terms of the differences in the geometry of the $^1A_2$, $^1B_1$, and $\tilde{X}$, $^1A_1$ states of SO_2 predicted in theoretical studies.[3-5] Thus Lindley[5] has estimated that the S-O bond distances in the $^1A_2$ and $^1B_1$ states are 1.50 and 1.49 Å, respectively, compared to 1.40 Å in the ground state; the O-S-O angles in the $^1A_2$, $^1B_1$, and ground states, respectively, are 92.6°, 117.3°, and 119°. The relatively large difference between the equilibrium O-S-O angles in the $\tilde{X}$ $^1A_1$ and the $^1A_2$ states is expected to enhance the transition probability for radiative decay of the $^1A_2$ to the higher vibrational levels of the ground state, and hence shift the fluorescence envelope to somewhat longer wavelengths than the $^1B_1$ emission.

Vibrational relaxation of the long-lived excited SO_2 molecules, first observed by Sidebottom, et al.,[24] and confirmed by Brus and McDonald,[16] was also observed in this work. The effect arises largely from the variation in quenching rate constant and radiative lifetime with excitation energy; see Table 1 and Figure 10. As an excited molecule is vibrationally relaxed to

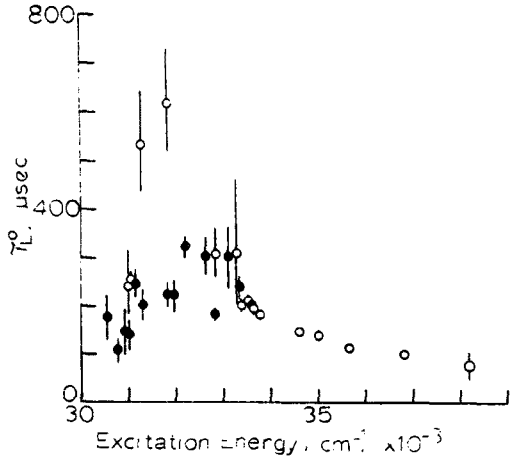

Figure 5. Plot of the radiative lifetime of the long-lived (L) fluorescing species versus excitation energy of SO_2. Closed circles - this work; open circles - [14].

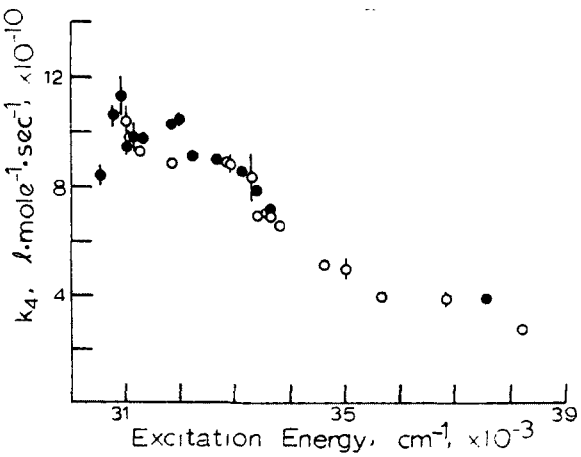

Figure 7. Plot of the rate constant k_4 for the quenching of the L state by SO_2 versus the excitation energy. Closed circles - this work; open circles - [14].

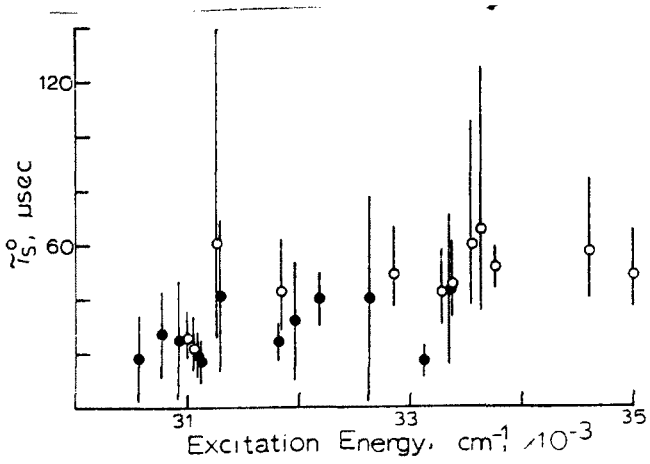

Figure 6. Plot of the radiative lifetime of the short-lived (S) fluorescing species versus excitation energy of SO_2. Closed circles - this work; open circles - [14].

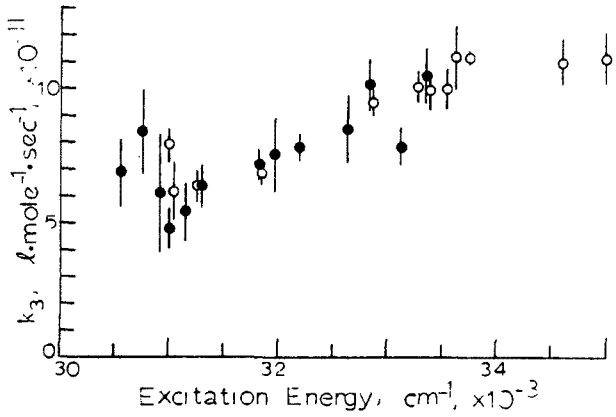

Figure 8. Plot of the rate constant k_3 for the quenching of the S state by SO_2 versus the excitation energy. Closed circles - this work; open circles - [14].

TABLE 1. LIFETIMES AND QUENCHING RATE CONSTANTS FOR THE LONG-LIVED(L) AND SHORT-LIVED(S) SPECIES EXCITED IN SO_2 AT VARIOUS WAVELENGTHS[a]

λ_{exc}, Å	$\tau_L°$, sec, x 10^4	$\tau_S°$, sec, x 10^5	k_4, $\ell.mole^{-1}sec^{-1}$ x 10^{-10}	k_3, $\ell.mole^{-1}sec^{-1}$ x 10^{-11}	Filter[b]
2662			3.8 ± 0.1		d
2975	2.0 ± 0.1		7.2 ± 0.1		c
2998	2.4 ± 0.2	4.3 ± 2.8	7.9 ± 0.1	10.5 ± 1.1	c
3020	3.0 ± 0.6	1.7 ± 0.6	8.5 ± 0.2	7.9 ± 0.7	c
3046	1.8 ± 0.1	8.3 ± 10.6	8.9 ± 0.1	10.2 ± 1.0	d
3065	3.0 ± 0.4	4.0 ± 3.8	9.0 ± 0.1	8.5 ± 1.3	c
3107	3.2 ± 0.2	4.0 ± 1.0	9.1 ± 0.1	7.8 ± 0.5	c
3129	2.2 ± 0.3	3.2 ± 2.2	10.4 ± 0.2	7.6 ± 1.4	d
3143	2.2 ± 0.3	2.4 ± 0.7	10.2 ± 0.1	7.2 ± 0.6	d
3196	2.0 ± 0.3	4.1 ± 2.8	9.7 ± 0.2	6.4 ± 0.8	d
3211	2.5 ± 0.4	1.7 ± 0.8	9.8 ± 0.5	5.4 ± 1.1	c
3225	1.4 ± 0.3	1.9 ± 0.8	9.4 ± 0.2	4.8 ± 0.7	b
3235	1.5 ± 0.5	2.5 ± 2.2	11.3 ± 0.7	6.1 ± 2.2	d
3251	1.1 ± 0.3	2.7 ± 1.6	10.5 ± 0.4	8.4 ± 1.6	d
3273	1.8 ± 0.5	1.8 ± 1.6	8.4 ± 0.4	6.9 ± 1.3	f

[a]Temperature, 25 ± 2°C; error limits shown here and elsewhere throughout this work are ± twice the standard deviation. [b]Transmission curves for the filters referenced here are shown in Figure 1; these were placed before the fluorescence detector.

TABLE 2. STERN-VOLMER PARAMETERS FOR THE L AND S COMPONENTS AS A FUNCTION OF THE FLUORESCENCE WAVELENGTHS MONITORED[a]

τ_L°, sec, x 10^4	τ_S°, sec, x 10^5	k_4, $\ell.mole^{-1}sec^{-1}$ x 10^{-10}	k_3, $\ell.mole^{-1}sec^{-1}$ x 10^{-11}	Detector Filter[b]
2.1 ± 2.5	2.4 ± 8.4	10.1 ± 0.5	9.5 ± 4.3	(a) $\lambda \geq 3200$ Å
2.8 ± 2.5	4.2 ± 4.6	10.0 ± 0.6	9.2 ± 0.4	(b) $\lambda \geq 3300$ Å
2.2 ± 0.3	3.2 ± 2.2	10.4 ± 0.2	7.6 ± 1.4	(d) $3400 \leq \lambda \leq 3800$ Å
2.9 ± 0.8	3.3 ± 0.7	7.9 ± 0.3	8.4 ± 0.2	(e) $\lambda \geq 3700$ Å
2.5 ± 1.2	2.3 ± 0.9	7.7 ± 0.6	7.5 ± 0.5	(h) $\lambda \geq 3800$ Å
3.1 ± 1.0	2.2 ± 2.2	7.8 ± 0.3	7.9 ± 0.4	(g) $\lambda \geq 3850$ Å
6.5 ± 4.2	2.4 ± 0.6	6.6 ± 0.3	5.9 ± 0.5	(j) $\lambda \geq 6000$ Å

[a] Excitation wavelength, 3130 Å; temperature, 25 ± 2°C; [b] See Figure 1 for complete transmission curves of the filters employed which are designated by the letters.

TABLE 3. RECIPROCAL LIFETIMES OF THE S AND L COMPONENTS AND I_S^o/I_L^o AS A FUNCTION OF THE FLUORESCENCE WAVELENGTHS MONITORED[a]

$1/\tau_L$, sec^{-1}, $\times 10^{-3}$	$1/\tau_S$, sec^{-1}, $\times 10^{-4}$	I_S^o/I_L^o	T[b], μsec/div.	Detector Filter[c]
16.9 ± 0.3	10.9 ± 0.6	1.08 ± 0.08	10	(b) $\lambda > 3300$ Å
16.5 ± 0.2	10.6 ± 0.4	1.14 ± 0.06	20	
15.7 ± 0.3	12.4 ± 0.5	1.16 ± 0.07	10	(e) $\lambda > 3700$ Å
15.4 ± 0.3	13.9 ± 0.9	1.58 ± 0.13	10	
14.3 ± 0.3	8.9 ± 0.5	0.97 ± 0.07	20	
14.5 ± 0.5	9.4 ± 0.7	0.95 ± 0.11	20	
13.0 ± 0.3	12.1 ± 0.8	1.42 ± 0.13	10	(i) $\lambda > 4800$ Å
12.6 ± 0.2	11.4 ± 1.2	1.40 ± 0.17	20	
10.7 ± 0.1	13.3 ± 0.1	2.22 ± 0.04	10	(j) $\lambda > 6000$ Å
11.4 ± 0.1	12.4 ± 0.2	----------	20	

[a]Excitation wavelength, 3130 Å; P_{SO_2} = 2.96 mTorr in all runs except those with filter (j) where 2.85 mTorr was used; [b]sweep time of the oscilloscopic trace employed; [c]see Figure 1 for complete transmission curves of the filters.

the lower vibrational levels, its larger quenching rate constant and somewhat shorter radiative lifetime, increases its chance for decay; thus in theory the slope of the $\ell n\, I_L$ versus time plot should become increasingly more negative with increasing time. At sufficiently high pressures ($p > 8$ mTorr) where collisional deactivation is significant, this vibrational relaxation phenomenon can be seen in the emission of SO_2 excited in the 2662-3107 Å region; typical data from SO_2 excited at 2998 Å are shown in Figure 9. The phenomenon is almost undetectable at 8 mTorr for 3211 Å excitation, where the original vibrational excitation is near that of the completely relaxed molecule. From the data of Figure 9 and similar decay curves from excitations at other wavelengths, we can estimate the average internal energy removed per collision. From the change in slope of the $\ell n\, I$ versus time plot, and the initial rates of decay of the L component anticipated for the SO_2(8.08 mTorr) excited at various energies (See Figure 10), we estimate that the approximate loss in energy (kcal/mole) per collision is: 1.2 (2998 Å); 0.8 (3020 Å); 0.9 (3065 Å); 1.3 (3107 Å). Thus among those excited SO_2 molecules which do not suffer electronic quenching on collision, about 1 kcal/mole per collision appears to be lost by SO_2(L) species excited in the 2998 to 3107 Å region.

The Diffusional Loss of Excited L Molecules--

In their earlier study of the time dependence of the fluorescence of the L and S states of SO_2, Brus and McDonald[16] considered the kinetics of the emission in terms of two contrasting mechanisms: (1) essentially independent population and decay of the L and S states; (2) collisional conversion of one state into the other (S L). They used the variation in the I_S^o/I_L^o ratio as a function of pressure in an attempt to choose between these mechanism. They felt that their data obtained at 3225.9Å provided the most sensitive test of the mechanism. From these data they concluded that an upper limit of 15% of the S state deactivating collisions gave L state molecules for excitation at this wavelength; that is, the L and S states decayed essentially independently of one another. Data from the shorter excitation wavelengths were not accurate enough over a wide pressure range to provide a choice between the mechanism alternatives. The main difficulty in the experimental test of the mechanism lies in the necessary limit in the low pressure range in which the experiments can be performed. Diffusional loss of the excited molecules and the very low initial population of the states at low SO_2 pressures, limit the useful range of pressures. As we noted previously in Figure 4, the S state with its very short lifetime, follows Stern-Volmer behavior down to the lowest limit of pressures which we could employ (0.05 mTorr). This is expected since essentially none of the S species is lost from the observation zone by diffusion during their very short lifetimes. However the L state shows a departure from Stern-Volmer behavior below about 1 mTorr: see Figure 3. Since the data below 1 mTorr are very important in allowing a mechanism choice, we have attempted to understand the origin of the upturn in the $1/\tau_L$ versus P_{SO_2} plot in this region. The increasing importance of L loss at the walls at low pressures may be the origin of this effect. Low pressure deviations from the Stern-Volmer relation for excited $SO_2(^3B_1)$ molecules were observed by Otsuka and Calvert,[25] Strickler, et al.,[26] and Briggs, et al.[27] In view of the much shorter lifetime of the L component of the excited SO_2 compared to that of the $^3B_1$ state, one expects the dif-

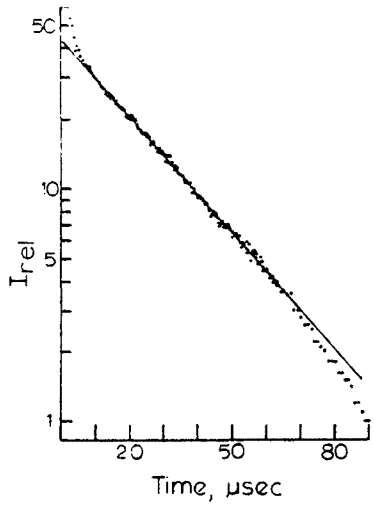

Figure 9. Semilog plot of the intensity of the total fluorescence of the SO_2 molecule versus time with excitation at 2998 Å and P_{SO_2} = 8.06 mTorr; note the downward curvature at long times which is thought to result from vibrational relaxation of the L state.

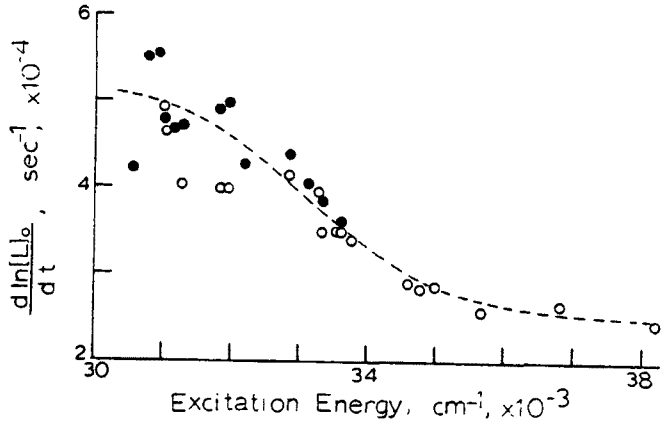

Figure 10. Plot of the calculated initial rate of decay of the L species of SO_2 versus the excitation energy; P_{SO_2} = 8.08 mTorr. Closed circles - kinetic data from this work; open circles - data from [14].

fusional loss of the L species to become important in a ten-fold lower pressure range than in the case of $SO_2(^3B_1)$. Indeed this is the pressure range for the L state deviations seen here. Theory requires that at sufficiently low pressures the rate of diffusional loss of excited molecules from the observation zone will be determined solely by their molecular velocities and the geometry of the cell and the observation zone, provided that excited molecules which reach the wall are deactivated effectively. At an SO_2 pressure of 0.9 mTorr and excitation at 3107 Å, an L molecule will undergo about 1 collision during its lifetime, and its mean free path is about 4.8 cm. Obviously below this pressure region we expect the molecular velocities of the excited molecules to be a major factor in controlling the diffusional loss rate. At somewhat higher pressures diffusion out of the observation zone will be controlled largely by molecular diffusion and collisionally controlled processes. In this latter case the kinetic theory the Brownian motion can be applied.[28] The time t required for a molecule to diffuse a distance x is given approximately by: $t = x^2/D$, where D is the pressure dependent diffusion constant: $D = a/p$. Thus we would expect for these conditions that the apparent first order constant for diffusion of excited molecules out of the observation zone of average radius $\bar{r}$ will be given by: $k_{diff} \simeq D\sqrt{r^2} \simeq a/p\bar{r}^2$. Experimentally we can estimate k_{diff} from the measured lifetimes of the excited species at low pressures (τ_{exp}) and that anticipated in the absence of diffusional loss from an extrapolation of the Stern-Volmer lifetime plot from the higher pressure region (τ_{calc}): $k_{diff} = (1/\tau_{exp}) - (1/\tau_{calc})$. Thus if the molecular diffusion mechanism is operative then we expect that $(1/\tau_{exp}) - (1/\tau_{calc})$ to be a linear function of $1/p$. Such a plot is shown in Figure 11 for the data from the L state excited at 3107 Å. It can be seen that the functional form of the highest pressure regime ($1/p \rightarrow 0$) is near linear as anticipated from simple theory, but the values become less dependent on the pressure as the pressure is reduced ($1/p \rightarrow \infty$) and collisionally controlled diffusion becomes less important.

The data of Figure 11 fit well the empirical equation: $k_{diff}(sec^{-1}) = 5.0 \times 10^3[1 - e^{-0.060/p(mTorr)}]$. If we interpret this equation in terms of the simple diffusion model outlined, then the experimental limiting slope of the k_{diff} versus $1/p$ plot as $1/p \rightarrow 0$, is 300 sec^{-1} $mTorr^{-1}$. For gaseous SO_2 at 25°C we can estimate that $D \simeq 7.9 \times 10^4/p$ (mTorr). Thus simple theory suggests: 300 sec^{-1} $mTorr^{-1} \simeq 7.9 \times 10^4\sqrt{r^2}$, from which $\bar{r} \simeq 16$ cm, a physically realistic result. At the low pressure limit ($1/p \rightarrow \infty$), the empirical experimental law gives $k_{diff} = 5.0 \times 10^3$ sec^{-1}. Then according to the simple theory, $\bar{v}/\bar{r} \simeq 5.0 \times 10^3$ sec^{-1}; taking $\bar{v} = 3.2 \times 10^4$ cm/sec, $\bar{r} \simeq 6$ cm. This is in qualitative accord with the alternate estimate made from the higher pressure limit and as good an agreement as one might expect from the very approximate model assumed here. In $SO_2(^3B_1)$ lifetime studies carried out in this same system, the k_{diff} versus $1/p$ plot was linear as expected for this longer lived species, and $\bar{r} \simeq 10$ cm was estimated. Certainly the deviation of the L state lifetime data from Stern-Volmer

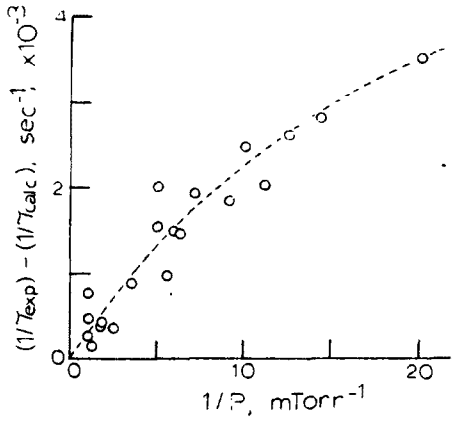

Figure 11. Plot of the apparent first-order rate constant for the diffusional loss of the L state [$k_{diff} = (1/\tau_{exp}) - (1/\tau_{calc})$] versus the reciprocal of the pressure of SO_2. The dashed line is the calculated fit of the data by the empirical equation given in the text.

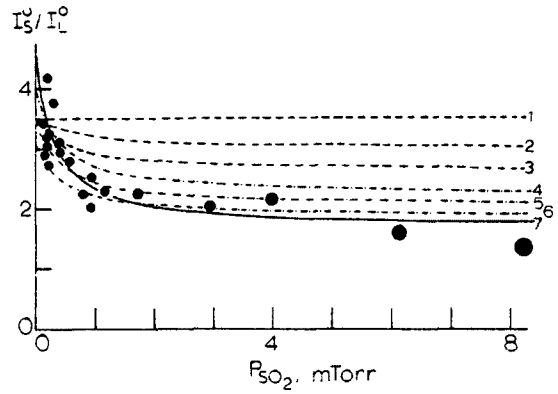

Figure 12. Plot of the ratio I_S^o/I_L^o versus pressure: excitation wavelength 3107 Å. The curves shown are the theoretical fits to the data assuming the S → L conversion calculated from the nonequilibrium model [eq. (24)]. The parameters chosen to obtain the various curves are outlined in the text.

behavior at low pressures is consistent with the diffusional loss of the L species from the observation zone, and it is reasonable to use the experimentally determined k_{diff} equation to estimate the diffusional loss term for L at low pressures.

The Kinetics of the Formation and Decay of the L and S Components of SO_2 Fluorescence --

It seems highly probable that the two components of the SO_2 fluorescence seen here involve two excited species as suggested by Brus and McDonald.[16] It will be convenient to consider the results in terms of the following general reaction scheme:

$$SO_2 + h\nu \rightarrow SO_2(S) \qquad (I_\alpha)$$

$$SO_2 + h\nu \rightarrow SO_2(L) \qquad (I_\beta)$$

$$SO_2(S) + SO_2 \rightarrow SO_2(L) + SO_2 \qquad (3a)$$

$$SO_2(S) + SO_2 \rightarrow (2SO_2) \qquad (3b)$$

$$SO_2(L) + SO_2 \rightarrow SO_2(S) + SO_2 \qquad (4a)$$

$$SO_2(L) + SO_2 \rightarrow (2SO_2) \qquad (4b)$$

$$SO_2(S) \rightarrow SO_2 + h\nu_S \qquad (5a)$$

$$SO_2(S) \rightarrow SO_2(L) \qquad (5b)$$

$$SO_2(S) \rightarrow (SO_2) \qquad (5c)$$

$$SO_2(L) \rightarrow SO_2 + h\nu_L \qquad (6a)$$

$$SO_2(L) \rightarrow SO_2(S) \qquad (6b)$$

$$SO_2(L) \rightarrow (SO_2) \qquad (6c)$$

In reactions (3b), (4b), (5c), and 6c above, $(2SO_2)$ and (SO_2) symbolize $SO_2(\tilde{X}\,{}^1A_1)$, $({}^3B_1)$, $({}^3A_2)$ or other long-lived or non-emitting product molecules. In terms of the above mechanism the following decay laws may be written:

$$d[S]/dt = -k_S[S] + k_{t'}[L] \qquad (7)$$

$$d[L]/dt = -k_L[L] + k_t[S] \qquad (8)$$

where $k_S = (k_{3a} + k_{3b})\,[SO_2] + k_{5a} + k_{5b} + k_{5c}$ (9)

$$k_L = (k_{4a} + k_{4b})\,[SO_2] + k_{6a} + k_{6b} + k_{6c} \qquad (10)$$

$$k_t = k_{3a}\,[SO_2] + k_{5b} \qquad (11)$$

$$k_{t'} = k_{4a}[SO_2] + k_{6b} \tag{12}$$

Solving the coupled differential equations (7) and (8) gives expressions for the time dependence of [S] and [L]:

$$[S] = Ae^{-\zeta t} + Be^{-\xi t} \tag{13}$$

$$[L] = Ce^{-\zeta t} + De^{-\xi t} \tag{14}$$

where $\zeta = (1/2)\,[(k_S + k_L) + \omega]$ (15)

$$\xi = (1/2)\,[(k_S + k_L) - \omega] \tag{16}$$

and $\omega = [(k_S - k_L)^2 + 4k_t k_{t'}]^{1/2}$

$$A = \omega^{-1}\,\{(1/2)\,(\omega + k_S - k_L)[S]_o - k_{t'}[L]_o\} \tag{17}$$

$$B = \omega^{-1}\,\{(1/2)\,(\omega - k_S + k_L)[S]_o + k_{t'}[L]_o\} \tag{18}$$

$$C = \omega^{-1}\,\{-k_t[S]_o + (1/2)\,(\omega - k_S + k_L)\,[L]_o\} \tag{19}$$

$$D = \omega^{-1}\,\{k_t[S]_o + (1/2)\,(\omega + k_S - k_L)\,[L]_o\} \tag{20}$$

Clues concerning the relative significance of the various reactions in the general mechanism outlined can be had from a consideration of the variation of the I_S^o/I_L^o ratio with pressure. Values of this ratio estimated for experiments at 3107 Å are summarized in Table 4 . The plot of these data shown in Figures 12 and 13 may be considered in view of the trends expected for various mechanism choices.

Mechanism I--

The simplest possible mechanism choice, that favored by Brus and McDonald for their experiments at 3225.9Å, involves the independent decay of the S and L species; that is the rate constants k_{3a}, k_{4a}, k_{5b}, and k_{6b} all are equal to zero. For this condition the fluorescence intensity and the I_S^o/I_L^o values are described by the simple expressions (21) and (22):

$$I = \alpha\,[S]_o e^{-k_S t} + \beta\,[L]_o e^{-k_L t} \tag{21}$$

$$I_S^o/I_L^o = (\alpha/\beta)\,([S]_o/[L]_o) \tag{22}$$

Thus for this condition we expect I_S^o/I_L^o to be independent of the pressure. It is seen in Figures 12, 13, and 14 that the data for 3107, 3211, and 3225 Å

excitation do not follow this expectation. There is a strong increase in the I_S^o/I_L^o ratio at the low pressures. Only one set of data derived from our experiments with 3273 Å excitation appear to follow relation (22); note the points marked by triangles in Figure 14. However in this case the results are least accurate since the extinction coefficient of SO_2 is very low, and the necessarily limited pressure range employed (1.8-12 mTorr) could not be extended to the region in which I_S^o/I_L^o is most sensitive to the pressure. Clearly we can conclude from the present results that the L and S states of SO_2 excited at 3107, 3211, and 3225 Å do not decay independent of one another; it is possible that this mechanism is operative at excitation wavelength 3273 Å. Thus it is necessary to consider these results in terms of alternative mechanisms which involve S to L conversions. We will consider two such mechanisms.

Mechanism II--

The least complex of the alternative L and S interconversion mechanisms is one chich allows only the S L transformation; that is, $k_{t'} = 0$, $k_t \neq 0$. This non-equilibrium mechanism leads to the following relations for the fluorescence intensity and the I_S^o/I_L^o values:

$$I = \{\alpha [S]_o - \frac{k_t}{k_S - k_L}[S]_o\}e^{-k_S t} + \{\frac{k_t}{k_S - k_L}[S]_o + [L]_o\}e^{-k_L t} \qquad (23)$$

$$I_S^o/I_L = \{(\alpha/\beta) - k_t/(k_S - k_L)\}/\{[L]_o/[S]_o + k_t/(k_S - k_L)\} \qquad (24)$$

We may test the compatibility of this mechanism using the data set for 3107 Å excitation (Table 4); in this case the strong absorption by SO_2 allowed study of the fluorescence to very low pressures (0.05 mTorr) corresponding to nearly collision-free conditions. The 3107 Å data can be fitted well employing the following experimentally determined rate constant expressions:

$$k_S(\text{sec}^{-1}) = 2.51 \times 10^4 + 4.19 \times 10^4 p \qquad (25)$$

$$k_L(\text{sec}^{-1}) = 3.11 \times 10^3 + 4.86 \times 10^3 p + 5.0 \times 10^3[1 - e^{-0.060/p}] \qquad (26)$$

where the pressure p is expressed in mTorr units. Equation (24) contains three unknown rate parameters: α/β, $[L]_o/[S]_o$, and k_t. Since the decay of both the S and L states was determined in the same experiment using a fixed geometry of the cell and the detector, α/β should be a constant which depends only on the lifetimes of the emitting species, the detector wavelength response, and the relative emission envelopes of the S and L states. From the effect of filters on the apparent I_S^o/I_L^o values, Brus and McDonald have concluded that the emission envelopes for the two species are not greatly different, and in this case, $\alpha/\beta = \tau_L^o/\tau_S^o = 8.08$ (3107 Å) is a good approximation. However it is seen in Table 3 that the calculated I_S^o/I_L^o

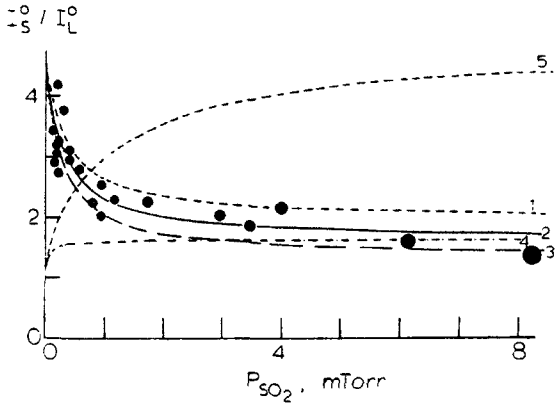

Figure 13. Plot of the ratio I_S^o/I_L^o versus pressure: excitation wavelength 3107 Å. The curves shown are the theoretical fits to the data assuming the $S \rightleftarrows L$ interconversion calculated from the equilibrium model [eq. (31)]. The parameters chosen to obtain the various curves are outlined in the text.

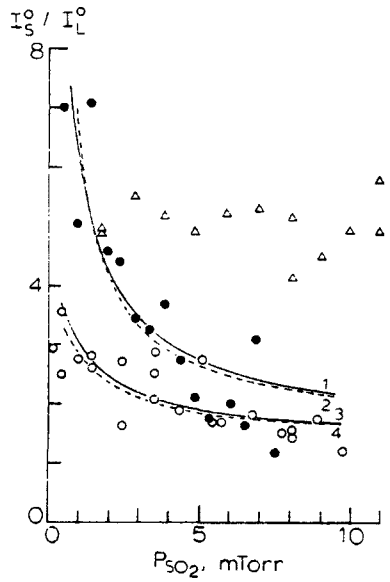

Figure 14. Plot of the ratio I_S^o/I_L^o versus pressure. Excitation wavelengths, open circles - 3211 Å; closed circles - 3225 Å; triangles - 3275 Å; the solid curves are the theoretical fits to the 3211 - and 3225 Å data calculated from eq. (24) for curves 2 and 4, and eq. (31) for curves 1 and 3; values of the parameters used for curves 1, 2, 3, and 4, respectively, are α/β = 8.26, 8.26, 3.2, 4.3: $[L]_o/[S]_o$ 0.50, 1.67, 0.03, 1.0; $k_{3a} = k_{4a}$ = 8.64 x 10^3, 3.40 x 10^3, 2.91 x 10^4, 2.56 x 10^4, 2.56 x 10^4 sec^{-1}. $mTorr^{-1}$.

TABLE 4. THE EFFECT OF PRESSURE ON THE I_S^o/I_L^o VALUES AND RECIPROCAL LIFETIMES OF THE L AND S COMPONENTS OF SO_2 FLUORESCENCE EXCITED AT 3107Å

Pressure, mTorr	T, μsec/div.[a]	$1/\tau_L$, sec^{-1}, x 10^{-3}	$1/\tau_S$, sec^{-1}, x 10^{-4}	I_S^o/I_L^o
8.19	5	42.9	33.6	1.34
8.19	10	43.0	----	----
6.12	5	32.7	28.5	1.58
6.12	10	32.8	----	----
3.99	10	22.6	19.8	2.14
3.99	20	22.6	----	----
2.93	10	17.1	16.5	2.00
2.93	20	17.3	(10.3)[b]	(0.92)[b]
2.93	20	17.4	(10.9)	(0.88)
2.93	50	17.5	----	----
1.71	10	11.7	12.]	2.24
1.71	20	11.2	----	----
1.14	20	8.54	6.93	2.25
0.93	20	7.88	7.13	2.52
0.91	20	8.00	5.54	2.00
0.91	50	8.29	(4.73)	(1.72)
0.77	20	7.01	5.36	2.23
0.55	20	6.15	4.73	2.78
0.55	50	6.19	(3.94)	(2.08)
0.40	20	6.30	4.73	2.95
0.40	50	5.41	(3.00)	(2.84)
0.38	50	5.50	3.37	3.10
0.29	50	5.33	3.21	3.76
0.20	50	6.08	3.48	2.73
0.20	50	5.60	3.39	3.24
0.18	50	4.94	2.80	4.18
0.17	50	5.41	2.86	3.04
0.16	50	5.34	2.86	3.18
0.14	50	5.70	3.02	2.88
0.11	50	5.46	2.60	3.42

[a] Sweep time of the oscilloscope; [b] these data in parentheses were determined using longer sweep times for which the S component data were highly compressed on the time scale; they are not considered as accurate at the small T runs; the runs at large T served as a check on the L component analysis at small T values.

values may differ by a significant factor depending on the wavelength region monitored. The emission of the S state appears to be shifted somewhat toward the longer wavelengths. In consideration of these results it appears to us that a realistic choice of α/β for 3107 Å excitation is in the range: $\tau_L^o/\tau_S^o = 8.08 > \alpha/\beta > 4.7$. The choice of magnitude and kinetic form of k_t in this case is somewhat arbitrary. Theoretically[29] one expects that non-radiative unimolecular processes such as (5b), (5c), (6b), and (6c) will be unimportant in a small molecule such as SO_2. In studies of SO_2 fluorescence excited within the second allowed band, Hui and Rice[30] have found that the quantum yield of radiative decay of the $SO_2(^1B_2)$ state is near unity at excitation energies less than the dissociation limit. The magnitude of the fluorescence quantum yields at zero pressure of SO_2 excited within the first allowed band have been the subject of some disagreement.[1, 2] The failure in the earlier work to recognize two emitting species, the very great efficiency of the collisional quenching of the S species, and the very long lifetime of the L species, together with the use of cells too small to avoid diffusional loss of the L state with these unrecognized properties, all contributed to this problem. However most workers and we now agree that the limiting quantum yield of fluorescence at zero pressure is probably near unity, in accord with the original suggestions of Mettee.[31] Therefore it is reasonable to assume that only second order reactions such as (3a) should be important in converting S to L states, and we may take k_t equal to some fraction (F) of the observed bimolecular quenching rate constant for the S state; for the experiments at 3107 Å, $k_t(sec^{-1}) = k_{3a}p = F \times 4.19 \times 10^4 p$ (mTorr).

Using reasonable choices for the various parameters in equation (24) does provide a good fit of the experimental I_S^o/I_L^o variation with pressure. In Figure 12 the effect of various choices of F on the fit can be seen. Taking $[L]_o/[S]_o = 2.3$, and $\alpha/\beta = 8.08$, F was varied; 0, 0.25, 0.5, 1.0 in curves 1, 2, 3, and 5 respectively. Obviously the F = 1 curve best describes the experimental results. The sensitivity of the theoretical curve shape to the choice of the unknown variable $[L]_o/[S]_o$, taking f = 1, is also shown in Figure 12; for the choices of $\alpha/\beta = 8.08$, the value of $[L]_o/[S]_o$ was varied: 2.0, 2.3, and 2.6 in curves 4, 5, and 6, respectively. The best match of the data is had for $[L]_o/[S]_o = 2.3$. As we pointed out previously, α/β may be somewhat less than τ_S^o/τ_L^o, and we may investigate the effect of this choice on the results. Taking the apparent lower extreme for this ratio, $\alpha/\beta = 4.7$, F = 1, and $[L]_o/[S]_o = 1.0$, gives a somewhat better fit (curve 7 of Figure 12) at higher pressures. It is evident that this mechanism involving the efficient, second order S → L conversion is consistent with our data at 3107 Å. For other excitation wavelengths where fairly complete I_S^o/I_L^o versus pressure data were determined in this work (3215 and 3225 Å), the mechanism II also fits well; see Figure 14.

The mechanism II appears to be unattractive in one sense; the physical circumstances which would favor the conversion of S ➤ L, without the reverse reaction occurring significantly, are hard to imagine. It is not likely that the density of states available to the L species is much greater

than that for the S species in the region of the potential energy surfaces to which excitation occurs. In fact if we associate the L species with $SO_2(^1B_1)$ and the S species with $SO_2(^1A_2)$, one might expect the density of the states available to the S species to be somewhat greater since this molecule is formed in a highly vibrationally excited state where anharmonicity would create a close packing of the states. If there is no energy difference between the states, then microscopic reversibility requires that L → S conversion occur as well as S → L. In this light a test of the compatibility of the more complete, "equilibrium" mechanism with our data is in order.

Mechanism III--

In this equilibrium mechanism we may make the reasonable assumption that $k_t = k_t$. It is important to recognize that under these conditions the experimentally determined decay constants for the L and S states no longer are equal to the real decay constants; i.e., $\zeta \neq k_L$ and $\zeta \neq k_S$. From equations (13)-(16) we obtained the following relationships:

$$\zeta + \xi = k_S + k_L \tag{27}$$

$$\zeta - \xi = [(k_S - k_L)^2 + 4k_t^2]^{\frac{1}{2}} \tag{28}$$

$$\text{Let } \psi = \zeta - \xi \tag{29}$$

$$\text{Then } \phi = (\psi^2 - 4k_t^2)^{\frac{1}{2}} = k_S - k_L \tag{30}$$

Now equation (20) reduces to (31):

$$I_S^{\,o}/I_L^{\,o} = \frac{(\alpha/\beta)\{(\psi + \phi)([S]_o/2[L]_o) - k_t\} + \{-k_t([S]_o/[L]_o) + (\psi - \phi)/2\}}{(\alpha/\beta)\{(\psi - \phi)([S]_o/2[L]_o) + k_t\} + \{k_t([S]_o/[L]_o) + (\psi + \phi)/2\}} \tag{31}$$

Again three parameters must be specified to test the fit of this equation to the data: α/β, $[S]_o/[L]_o$, and k_t. For various "reasonable" choices of these parameters the fit to the 3107 Å data is shown in Figure 13. For curves 1, 2, and 3 we have assumed $[L]_o/[S]_o = 1.67$ and $\alpha/\beta = 8.08$, but we have varied the second order rate constant k_t ($mTorr^{-1}\ sec^{-1}$): 3×10^3, 4×10^3, 5×10^3, respectively. Note that the choice of $k_t = 5.0 \times 10^3\ mTorr^{-1}\ sec^{-1}$ gives an excellent fit of the data.

It is instructive to observe the expected influence on the $I_S^{\,o}/I_L^{\,o}$ -pressure relationship of a significant first order component to the intersystem crossing constant k_t; i.e., $k_{5b} = k_{6b} \neq 0$. Taking $k_{5b} = k_{6b} = 3.1 \times 10^3\ sec^{-1}$ and no second order component ($k_{3a} = k_{4a} = 0$) gives curve 5 in Figure 13. With the same value for k_{5b} and k_{6b} but taking $k_{3a} = k_{4a} = 5.0 \times 10^3\ mTorr^{-1}\ sec^{-1}$, curve 4 results. It is evident that both curves have the incorrect form of $I_S^{\,o}/I_L^{\,o}$ variation with pressure and that first order

interconversion of S and L at any significant rate appears to be an inappropriate choice.

Our only other extensive data sets for excitation at 3225 and 3211 Å are also described well by this equilibrium mechanism III. Obviously one cannot differentiate between mechanisms II and III on the basis of the fit to the I_S^o/I_L^o -pressure data alone. However out results do exclude the mechanism I in every case where reliable, low pressure results are available, and they are incompatible with the significant occurrence of first-order intersystem crossing between the L and S systems.

It is interesting to note that the $[S]_o/[L]_o$ values which we estimate using either of the two $S \rightleftarrows L$ interactive mechanisms are relatively higher for experiments with excitation at 3225 Å than at other wavelengths which we employed. Brus and McDonald observed a jump in I_S^o/I_L^o to 19 in this wavelength region (3226 Å), which seems consistent with our present result. However in their work the I_S^o/I_L^o values appeared to be independent of the pressure, so it is not clear that the two results apply to the same phenomenon; the somewhat smaller excitation bandwidth in the Brus and McDonald experiments may have led to a rather different set of states. In any case, our observations for 3225 Å excitation and Brus and McDonald's results at 3226 Å both are consistent with the work of Hamada and Merer[11] who reported that the absorption band of SO_2 at 3226 Å is less perturbed than its neighbors in the spectrum.

Brus and McDonald's data for 3140.5, 2981, 2961.6, and 2889.3 Å did not extend to pressures below 0.4 mTorr where the most sensitive test of the mechanism can be made, but their data also can be fitted well to both the mechanisms II and III outlined here, using reasonable choices for the parameters; see Figure 15.

Mechanism IV--

One might question whether the present data could support equally well the hypothesis that only one excited state of SO_2 is involved in the emission. Presumably a variation in the radiative and nonradiative decay constants may occur with change in vibrational excitation within the single state, in a somewhat more dramatic fashion than we believe occurs in the L species. Then a "step-ladder" collision dynamics scheme such as that outlined by Freed and Heller[34] may be used to rationalize the non-exponential behavior. This case is approximated in terms of the present mechanism taking $\beta = 0$ and $[L]_o = 0$ in equation (20):

$$I_S^o/I_L^o = (\omega + k_S - k_L)/(\omega - k_S + k_L) \qquad (32)$$

If k_t and k_t' involve only the bimolecular quenching terms then $I_S^o/I_L^o \rightarrow \infty$ as the pressure approaches zero. Thus at the very low pressures the collisionally induced internal conversion becomes negligible and single exponential decay should be observed. However even at the lowest pressure at which we could carry out the experiments successfully, 0.05 mTorr, the fluorescence of SO_2 follows double exponential decay; see Figure 16. Furthermore the decay constant of the L component does depend on the excitation

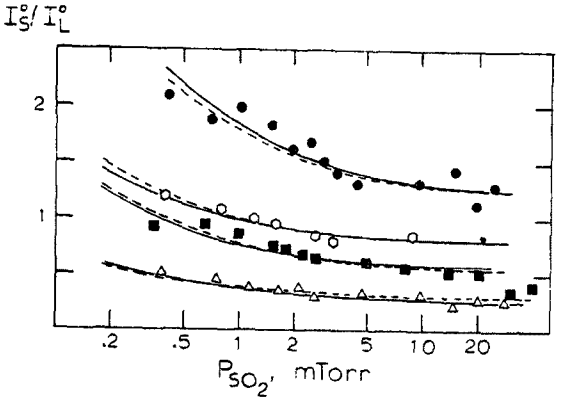

Figure 15. Plot of the Brus and McDonald [14] data for the ratio I_S°/I_L° as a function of pressure of SO_2; excitation wavelengths, hexagons -- 2961.6 Å; squares -- 2981 Å; triangles -- 2889.3 Å; circles -- 3140.5 Å; the solid curves are the theoretical fits to the data calculated from eq (24); the dashed curves are the theoretical fits calculated from eq. (31); values for the parameters used for the excitation wavelengths, 3140.5, 2981, 2961.8, and 2889.3 Å, respectively, are: α/β 4.0, 2.0, 2.7, 2.0 for mechanism II; 8.0, 15, 14, 15 for mechanism III; $[L]_o/[S]_o$ = 1.15, 0.60, 1.0, 2.0 for mechanism II; 2.11, 5.71, 5.88, 12.5 for mechanism III; k_{3a} = 3.67 x 10^4, 5.90 x 10^4, 6.00 x 10^4, 5.90 x 10^4 sec^{-1} $mTorr^{-1}$ for mechanism II, and $k_{3a} = k_{4a}$ = 4.27 x 10^3, 4.24 x 10^3, 3.48 x 10^3, 2.67 x 10^3 sec^{-1} $mTorr^{-1}$ for mechanism III.

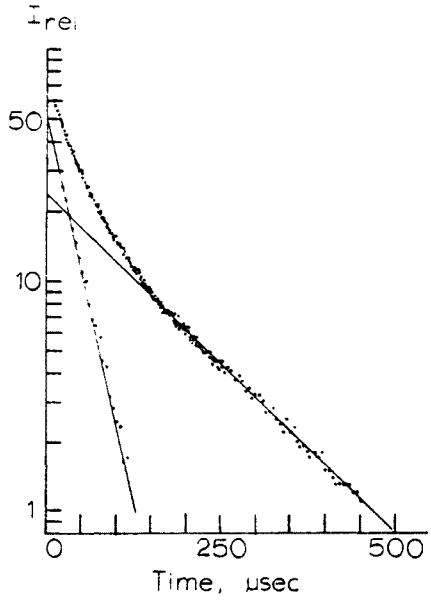

Figure 16. Semilog plot of the fluorescence intensity versus time for SO_2 under essentially collision free conditions; excitation wavelength 3107 Å; P_{SO_2} = 0.05 mTorr.

energy (see Table 1), in contrast to the expectations of the one state, vibrational relaxation model. Thus the single state model seems inappropriate to explain the present double exponential decay data. However it appears to us that the fluorescence behavior of the L state of SO_2 would be an excellent example to test quantitatively the Freed and Heller model, in that the properties of the L state appear to follow, at least qualitatively, all of the predictions from their theory.

The Nature of the S and L Species -- The tentative assignment of Brus and McDonald of the S species to the $SO_2(^1A_2)$ state and L species to the $SO_2(^1B_1)$ state seems to be in accord with most of the experimental data available today, including our own. Strong evidence for this is provided by the observed enhancement of the $[S]_o/[L]_o$ state population ratio on excitation within the relatively unperturbed spectral region near 3226 Å, attributed to the $^1A_2 \leftarrow \tilde{X}\ ^1A_1$ transition. We would like to point out that the tentative identification of the structure in the fluorescence emission excited within the 3150-2930 Å region [14,15] as originating from the $^1B_1 \leftarrow \tilde{X}\ ^1A_1$ transition, when coupled with the present results, also supports this assignment indirectly. It may appear incongruous that absorption by SO_2 in a structured region characteristic of a $SO_2(^1A_2) \leftarrow SO_2(\tilde{X}\ ^1A_1)$ transition should yield fluorescence which on analysis appears to support the $^1B_1$ state as the emitter. However from the kinetic parameters derived in this work, it can be seen that in the steady state experiments of Shaw, et al.[14,15] carried out a 2 and 1 mTorr pressure, the dominant intensity of the fluorescence could originate from the L species for most excitation wavelengths

they employed. From the kinetic mechanisms II and III presented, we would expect the equations (33) and (34) to describe the ratio of the intensities for the steady state condition $(I_S/I_L)_{ss}$:

$$\text{Mechanism II:} \quad (I_S/I_L)_{ss} = (\alpha/\beta)([S]_o/[L]_o)k_L/\{k_S + k_{3a}([S]_o/[L]_o)p\} \quad (33)$$

$$\text{Mechanism III:} \quad (I_S/I_L)_{ss} = \frac{(\alpha/\beta)\{([S]_o/[L]_o)(k_4 p + k_6) + k_{4a}p\}}{k_3 p + k_5 + k_{4a}([S]_o/[L]_o)p} \quad (34)$$

Using equations (33) and (34) and the appropriate kinetic data which we obtained from the fitting of the I_S^o/I_L^o-pressure data and the Stern-Volmer quenching constants, we simulated the conditions employed by Shaw, et al. We estimated the ratio $(I_S/I_L)_{ss}$ and the fraction of the total fluorescence from the long-lived state $[I_L/(I_S + I_L)]$ for the two seemingly realistic mechanism choices II and III; see Table 5. One evident feature of these data is the rather striking difference between the $I_L/(I_S + I_L)$ values expected for the two mechanism models. The choice of mechanism II, invoking only S → L conversion, leads to fractions in the range 0.94 to 0.72 for wavelengths in the 2889 to 3211 Å range, while there is a near equal fluorescence from the L and S components expected if the mechanism III, involving S ⇄ L interconversion, is operative. Thus the observations of Shaw, et al., who observed only $^1B_1 \rightarrow \tilde{X}\ ^1A_1$ structure, coupled with the present work, appear to favor indirectly the choice of mechanism II as well as add further support for the L and S state assignments as $^1B_1$ and $^1A_2$, respectively. These considerations indicate that additional fluorescence steady-state studies should be made with excitation near wavelength 3225 Å, where it appears that $^1A_2$ emission should be more intense than that of the $^1B_1$ component if the interpretation outlined here is correct.

One important experimental result remains to cloud the assignment of the L and S states. Both states can be readily populated with excitation wavelengths as long as 3273 Å, while the tentative spectroscopic assignment of the $SO_2(^1B_1) \leftarrow SO_2(\tilde{X}\ ^1A_1)$ transition is near 3150 Å.[12,14,15] If one is to accept the L and S states as $SO_2(^1B_1)$ and $SO_2(^1A_2)$, respectively, then the origin of the transition $^1B_1 \leftarrow \tilde{X}\ ^1A_1$ must be at some wavelength greater than 3273 Å, since the direct population of the L state at this wavelength is too large to reflect absorption from vibrationally rich ground state molecules.

The Quenching of the S and L States by Some Atmospheric Gases--

The quenching rate constants for the first excited singlet states of SO_2 with various common atmospheric gases and pollutant molecules are of interest to many atmospheric scientists and photochemists. These data for excitation at 3130Å are of special value since many photochemical experiments have been carried out at this wavelength. We have determined rate constants for both the L and S states of SO_2 excited at 3130Å for quenching by some important atmospheric gases through direct lifetime studies in gaseous SO_2

TABLE 5. THE ESTIMATED FRACTION OF THE TOTAL FLUORESCENCE INTENSITY DERIVED FROM THE L SPECIES IN SO_2 STEADY STATE IRRADIATIONS

Excitation wavelength, Å	$[I_L/(I_L + I_S)]_{ss}$[a] Mechanism II[b]		$[I_L/(I_L + I_S)]_{ss}$[a] Mechanism III[c]		Source of kinetic data employed
2889.3	0.94	(0.90)	0.59	(0.60)	Ref. 16
2961.6	0.88	(0.85)	0.52	(0.53)	Ref. 16
2981	0.88	(0.85)	0.44	(0.45)	Ref. 16
3020	0.92	(0.91)	0.51	(0.58)	This work
3065	0.85	(0.86)	0.46	(0.49)	This work
3107	0.74	(0.76)	0.46	(0.43)	This work
3140.5	0.80	(0.81)	0.51	(0.47)	Ref. 16
3211	0.72	(0.72)	0.51	(0.45)	This work
3225	0.44	(0.42)	0.26	(0.23)	This work

[a]The values shown were calculated for steady state irradiations of SO_2 at 2 mTorr and 1 mTorr pressure (in parentheses); [b]estimated using equation (24) of the text; [c]estimated using equation (31) of the text; the parameters chosen for α/β, $[S]_o/[L]_o$, and k_t were those providing the best fit of the data for I_S°/I_L° versus pressure data.

-quencher molecule mixtures. The quenching rate constants for the L state were also determined using 2662 Å excitation. In this case the emission from the S state was too weak to allow estimates of rate constants. All of these data are summarized in Table 6. Several features of these results should be noted. The quenching rate constants for the S state are significantly larger than the gas collision number for each of the quencher molecules. Only a very minor perturbation is effective in quenching the short-lived component, and this presumably leads to the L state. Thus it is highly unlikely that the S state is involved in any chemical reactions.

The data of the last column of Table 6 show the ratio of the quenching constant for the long-lived species to that of the short-lived species, k_4/k_3. Observe that this ratio is approximately constant for the great variety of reactant molecules studies. For the potentially chemically reactive gases such as O_2, isobutane, and trans-2-butene, the ratio may be somewhat larger than in the case of the chemically unreactive species; if this difference is real, some chemical contribution to the observed total quenching of the L species may occur in these cases. Another interesting feature of these data is the regular enhancement of the quenching rate constant for the L state with excitation at the longer wavelengths; $k_{4(2662)}/k_{4(3130)}$ is approximately constant, independent of the nature of the quenching gas. This effect has been inferred from less direct measurements of k_4/k_{6a} by Mettee[35] and Horowitz and Calvert[36] from steady state fluorescence studies. The effectiveness of the L state quenchers appears to be related to the polarizability of the molecules as suggested in other studies of excited SO_2 singlet and triplet quenching.[35-40] Presumably the excited SO_2 molecule acts as an electrophilic reactant on collision with polarizable molecule to form a highly polarized charge-transfer complex which may enhance intersystem crossing or internal conversion of the excited SO_2 species. The constancy of the $k_{4(2662)}/k_{4(3130)}$ ratio may merely reflect the relative density of states ($\tilde{X}\,^1A_1$; B_1, A_2, B_2) in the two regions of the L state potential energy surface which correspond to these excitations. The strength of the SO_2-quencher molecule encounter involving molecules of different polarizability may govern the extent of this enhancement of crossover at each region of the potential energy surface.

The present work gives no new insight into the mysterious, non-radiative, reactive singlets of SO_2 invoked by Heicklen, et al. If as seems likely the S state is indeed the $SO_2(^1A_2)$ and the L state is the $SO_2(^1B_1)$, then these states are excluded as condidates for the SO_2* species since the quenching properties do not correlate with those of SO_2*. It appears to us that the only other potentially important excited singlet reactant which remains a viable candidate for the Heicklen SO_2* species is a highly vibrationally excited ground state molecule, $SO_2(\tilde{X}\,^1A_1)$. It is probable that these species are formed in a large fraction of the quenching collisions, and they could be highly reactive toward some reactants employed by researchers. It is not clear that they could survive the usually rapid vibrational relaxation processes to be important reactants with CO, C_2H_2, C_2F_4, etc., in mixtures at the relatively high N_2 and CO_2 concentrations which were employed.

TABLE 6. RATE CONSTANTS FOR THE QUENCHING BY VARIOUS ATMOSPHERIC GASES OF THE L(k_q^L) AND S(k_q^S) COMPONENTS OF THE SO_2 FLUORESCENCE EXCITED AT 3130 AND 2662Å[a]

Quenching gas	Quenching rate constants, $\ell.mole^{-1}sec^{-1}, x\ 10^{-11}$				
	$k_q^L(2662)$	$k_q^L(3130)$	$k_q^S(3130)$	$\frac{k_q^L(2662)}{k_q^L(3130)}$	$\frac{k_q^L(3130)}{k_q^S(3130)}$
Nitrogen	0.12 ± 0.01	0.35 ± 0.04	19 ± 18	0.34	0.018
Oxygen	0.12 ± 0.01	0.34 ± 0.07	16 ± 14	0.35	0.021
Carbon dioxide	0.27 ± 0.02	0.91 ± 0.13	59 ± 8	0.30	0.015
Carbon monoxide	0.17 ± 0.01	0.46 ± 0.14	30 ± 21	0.37	0.015
Argon	0.11 ± 0.01	0.27 ± 0.03	21 ± 11	0.41	0.013
Isobutane	0.45 ± 0.02	1.41 ± 0.46	70 ± 56	0.32	0.020
trans-2-Butene	0.69 ± 0.04[b]	1.68 ± 0.98	51 ± 60	0.41	0.033
Sulfur dioxide	0.38 ± 0.01	1.04 ± 0.02	76 ± 14	0.37	0.014
Nitric oxide	0.28 ± 0.02				
Methane	0.23 ± 0.02				
Benzene	0.80 ± 0.04				
Biacetyl	0.81 ± 0.05				

[a]Temperature, 25 ± 2°C; [b]in 2662 Å experiments, the cis-2-butene isomer was used.

REFERENCES AND NOTES

1. Present address, Chemistry Department, University of Alberta, Edmonton, Alberta.

2. Present address, Chemistry Department, University College, Dublin, Ireland.

3. I.H. Hillier and V.R. Saunders, Mol. Phys., 22, 193 (1971).

4. K.J. Chung, "Experimental and Theoretical Study of Sulfur Dioxide", Ph.D. Thesis, The Ohio State University, Columbus, Ohio, 1974.

5. D.D. Lindley, "Ad Initio SCF Studies on the Ground and Excited States of Sulfur Dioxide", Masters Thesis, The Ohio State University, Columbus, Ohio, 1976.

6. G. Herzberg, "Electronic Spectra and Electronic Structure of Polyatomic Molecules", D. Van Nostrand, Princeton, N.J., 1967, p. 605.

7. J.H. Clements, Phys. Rev., 47, 224 (1935).

8. N. Metropolis, Phys. Rev., 60, 295 (1941).

9. J.C.D. Brand and R. Nanes, J. Mol. Spectrosc., 46, 194 (1973).

10. R.N. Dixon and M. Halle, Chem. Phys. Lett., 22, 450 (1973).

11. Y. Hamada and A.J. Merer, Can. J. Phys., 52, 1443 (1974).

12. Y. Hamada and A.J. Merer, Can. J. Phys., 53, 2555 (1975).

13. J.C.D. Brand, J.L. Hardwick, D.R. Humphrey, Y. Hamada, and A.J. Merer, Can. J. Phys., 54, 186 (1976).

14. R.J. Shaw, J.E. Kent, and M.F. O'Dwyer, Chem. Phys., 8, 155 (1976).

15. R.J. Shaw, J.E. Kent, and M.F. O'Dwyer, Chem. Phys., 8, 165 (1976).

16. L.E. Brus and J.R. McDonald, J. Chem. Phys., 61, 97 (1974).

17. S. Butler and J.R. McDonald, Paper WC9, Thirty-First Symposium on Molecular Spectroscopy, The Ohio State University, 1976.

18. E. Cehelnik, C.W. Spicer, and J. Heicklen, J. Amer. Chem. Soc., 93, 5371 (1971).

19. L. Stockburger, III, S. Braslavsky, and J. Heicklen, J. Photochem., 2, 15 (1973/74).

20. E. Cehelnik, J. Heicklen, S. Braslavsky, L. Stockburger, III, and E. Mathias, J. Photochem., 2, 31 (1973/74).

21. A.M. Fatta, E. Mathias, J. Heicklen, L. Stockburger, III, and S. Braslavsky, J. Photochem., 2, 119 (1973/74).

22. J. Heicklen, "Atmospheric Chemistry", Academic Press, 1976, p. 334.

23. P.B. Sackett and J.T. Yardley, J. Chem. Phys., 57, 152 (1972).

24. H.W. Sidebottom, K. Otsuka, A. Horowitz, J.G. Calvert, B.R. Rabe, and E.K. Damon, Chem. Phys. Lett., 13, 337 (1972).

25. K. Otsuka and J.G. Calvert, J. Amer. Chem. Soc., 93, 2581 (1971).

26. S.J. Strickler, J.P. Vikesland, and H.D. Bier, J. Chem. Phys., 60, 664 (1974).

27. J.P. Briggs, R.B. Caton, and M.J. Smith, Can. J. Chem., 53, 2133 (1975).

28. S.W. Benson, "The Foundations of Chemical Kinetics", McGraw-Hill Co., 1960, pp. 128-130.

29. M. Bixon and J. Jortner, J. Chem. Phys., 50, 3284 (1969).

30. M.H. Hui and S.A. Rice, Chem. Phys. Lett., 17, 474 (1972).

31. H.D. Mettee, J. Chem. Phys., 49, 1784 (1968).

32. T.N. Rao, S.S. Collier, and J.G. Calvert, J. Amer. Chem. Soc., 91, 1609 (1969).

33. J.G. Calvert, Chem. Phys. Lett., 20, 484 (1973).

34. K.F. Freed and D.F. Heller, J. Chem. Phys., 61, 3942 (1974).

35. H.D. Mettee, J. Phys. Chem., 73, 1071 (1969).

36. A. Horowitz and J.G. Calvert, Int. J. Chem. Kinet., 4, 191 (1972).

37. H.W. Sidebottom, C.C. Badcock, J.G. Calvert, B.R. Rabe, and E.K. Damon, J. Amer. Chem. Soc., 93, 3121 (1971).

38. F.B. Wampler, K. Otsuka, J.G. Calvert, and E.K. Damon, Int. J. Chem. Kinet., 5, 669 (1973).

39. F.B. Wampler, J. Environ. Sci. Health, A11 (6), 397 (1976).

40. F.B. Wampler, Int. J. Chem. Kinet., 8, 687 (1976).

THE MECHANISM OF PHOTOCHEMICAL REACTIONS OF SO_2 WITH ISOBUTANE EXCITED AT 3130Å.

Introduction

The primary photophysical and photochemical processes in SO_2 excited into the first allowed singlet band (2500-3400 Å) and the forbidden band (3400-4000 Å) have been studied for about a decade. Since the OS-O bond dissociation energy is about 135 kcal/mole, corresponding to a wavelength smaller than 2180 Å,[1] any photochemically induced reactions of SO_2 in the excitation wavelength region 2500-4000 Å are the results of interactions with bound excited states of SO_2 molecules. Three emitting states of SO_2, one short-lived singlet and one long-lived singlet, presumably the $^1A_2$ and $^1B_1$ states,[2,3] and one triplet $SO_2(^3B_1)$,[4] have been observed in emission upon excitation into the region 2500-4000 Å.

Dainton and Ivin[5,6] studied the photolysis of SO_2 in the presence of several paraffinic and olefinic hydrocarbons. The principal product was the sulfinic acid. A slight decrease in reaction rate with increasing temperature was found between 15 and 100°C. Timmons[7] then reexamined the photochemical reactions of SO_2 with various alkanes. The negative temperature coefficient reported by Dainton and Ivin was confirmed, but the product analysis showed a number of important products. Since no evidence for the formation of alkyl radicals was found, he supported the insertion mechanism for the SO_2 + RH reactions, as suggested by Dainton and Ivin. He also argued that the great variety of products arise from thermal and/or photochemical decomposition of the sulfinic acid. Badcock, et al.,[8] presented arguments questioning this conclusion and suggested a primary reaction by excited SO_2 of H-atom abstraction in irradiated SO_2-RH mixtures. A quantitative analysis of products of the photochemical reactions of SO_2 with n-butane and isobutane was performed by Penzhorn, et al.[9,10] They concluded that the reaction of excited SO_2 molecules with alkane involves H-atom abstraction rather than insertion, and more than one triplet state of SO_2 molecules was thought to be involved in the reaction mechanism.

The photochemical reaction mechanism of SO_2-added gas mixtures is known to be complex. The results of these studies carried at low pressures ($P < 10$ Torr)[11,12] can be understood by invoking reactions of one singlet and one triplet state, presumably the $^1B_1$ and $^3B_1$ states. However, both the Heicklen and the Calvert research groups have concluded that the low pressure mechanism requires an expansion of some sort for the high pressure conditions ($P \geq 10$ Torr).[13-16] In addition to the previous states, one more unknown X state was suggested by Calvert and co-workers,[13,16] and three more states, designated as $SO_2^{\ddagger}$, $SO_2^{\ddagger *}$ and $SO_2^{\ddagger}$, were proposed by Heicklen and co-workers.[14,15,17-25] At the time of most of the previous studies of the photochemistry of SO_2 at high pressures, the pressure saturation effect of $SO_2(^3B_1)$ quenching[26-29] was unknown, the quenching rate constants determined at low pressures were applied incorrectly to the high pressure experiments. It is thus necessary to reexamine all the old kinetic reaction mechanisms of SO_2 photochemical reactions.

Penzhorn, et al.,[9,10] have shown that a good mass balance ($\geq$ 97%) between the rate of pressure drop and the rate of formation of the principal products is obtained in the photolysis of SO_2-isobutane mixtures. We thus carried out our studies on the SO_2-isobutane photoreaction by following the pressure drop during short irradiation periods (generally less than 3 minutes) at excitation wavelength 3130 Å. A new insight into the photochemical reaction mechanism of the SO_2-alkane system is given here.

Experimental

Light from a high pressure point source mercury lamp (HBO 500 W/2 L2) was filtered through the following solutions:[30] $NiSO_4$ (0.178 M, 5 cm), K_2CrO_4 (5.0×10^{-4} M, 5 cm), potassium biphthalate (0.024 M, 1 cm) and a Corning glass filter 7-54 (9863), 0.3 cm. A nearly uniform parallel beam through the cell was obtained utilizing a condensing lens and light stops. The incident light was monitored continuously during photolysis by reflecting a small fraction of the incident light from a quartz plate onto an RCA 935 phototube (S-5 cathode). Radiation exiting the reaction cell was attenuated with a uniform density filter and monitored with another RCA 935 phototube. The light intensity measured by both phototubes showed the stability of lamp to be about ± 5% during the experimental period. The reaction chamber was a 5 cm long, 4.5 cm diameter quartz cell. The light intensity was calibrated by potassium ferrioxalate actinometry.[31] The linearity of the response of the phototube with light intensity was also checked with actinometry. At SO_2 pressures of less than 50 Torr, the absorption followed the Beer-Lambert law with the decadic extinction coefficient, 1.59×10^{-3} $Torr^{-1}$ cm^{-1} ($0 \leq P \leq 15$ Torr). This checks reasonably well with the literature values of 1.60×10^{-3},[32] 1.57×10^{-3},[13] and 1.53×10^{-3} $Torr^{-1}$ cm^{-1},[33] for experiments at the same excitation wavelength.

A grease-free vacuum line was used in all the photolytic experiments. A mercury diffusion pump, separated from the main vacuum line by a liquid nitrogen trap, kept the system at a pressure of $5 \times 10^{-5} \sim 1.0 \times 10^{-6}$ Torr.

Matheson Co. isobutane and J.T. Baker Chem. Co. SO_2 (anhydrous) were used. Both gases were distilled from trap to trap at -196°C, retaining only the middle third, which was degassed many times. Before each run, the gases were degassed once again. Spectroquality benzene (Matheson Coleman and Bell) was degassed and distilled under vacuum, and the middle third was retained for use. These three gases were checked by mass spectrometry (Du Pont Model 21-491 B), and no impurity was observed. CO_2 (Matheson Co.) was also purified by vacuum distillation.

The photoreaction of SO_2 with isobutane was followed by means of the pressure drop in the reaction cell. The pressure was measured directly by three different Baratron capacitance manometers (MKS 310AHS-1, 310AHS-100, and 310BHS-1000), which were fused onto the reaction cell as closely as possible. In the medium pressure case ($1.2 < P < 120$ Torr), the pressure drop was quite linear with time during the irradiation period; i.e., the least squares fit of the pressure drop vs. time was almost exactly equal to the total pressure drop divided by the total irradiation time; see Figure 17. However, even at very short reaction times (1 ~ 3 minutes), scattered light

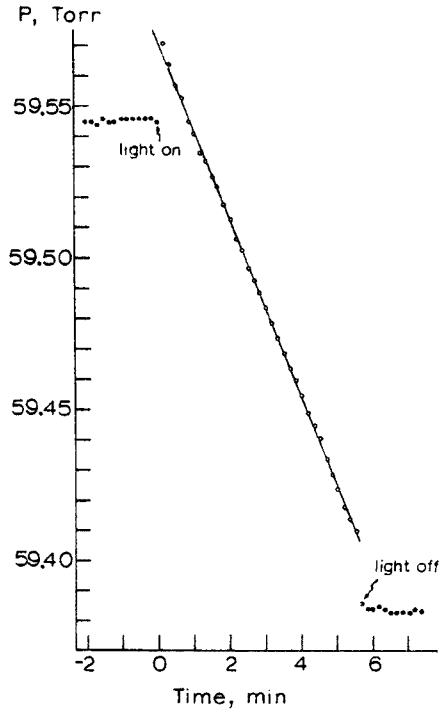

Figure 18. Example of the pressure variation in the 3130 Å photolysis of SO_2 (15.0 Torr) with isobutane (44.6 Torr).

in the cell was appreciable; see Figure 18. Since the pressure drop was quite linear with time, it was assumed that this scatter did not influence the absorption of light by SO_2, and the Beer-Lambert law was used to calculate the intensity of light absorbed. Light scatter was not an appreciable problem at low pressures ($P \leq 1.2$ Torr); see Figure 18. However, the pressure drop was not linear with time; see Figure 19. The reason for this non-linearity is not clear. To investigate the possibility that it was caused by interference of the product, the photolysis was carried out in two steps. After an initial radiation period, the contents of the cell were condensed in a liquid nitrogen trap and then allowed to warm to room temperature before radiation was continued. Removal of the solid and liquid products in this way indicated that the observed decrease in quantum yields was not due to the interference by these products. Because of the non-linearity of the data, only data taken during the first minute of irradiation (10 second interval) were utilized in the calculations of quantum yields. High pressure data ($P > 120$ Torr) were not reported because of the nonlinear pressure drop and the high magnitude of light scatter. Qualitatively, however, they showed a leveling-off of the quantum yield at high concentrations of isobutane ($P > 500$ Torr).

Blank experiments were carried out for each experiment to ensure that the pressure drop was due to reactions involving the isobutane.

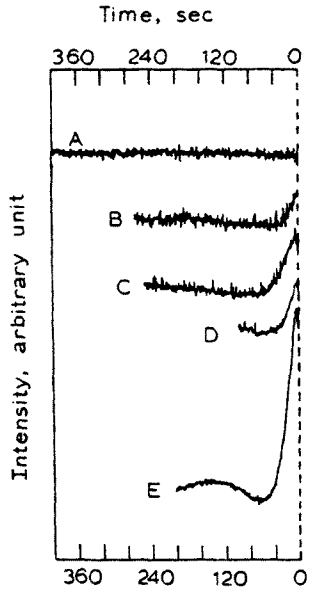

Figure 18. Light scattering observed in the photolysis; pressure of SO_2 and isobutane for curves A, B, C, D, and E are 0.196, 0.751; 2.50, 17.20; 2.50, 51.70; 14.99, 32.06; and 15.00, 707.7, respectively.

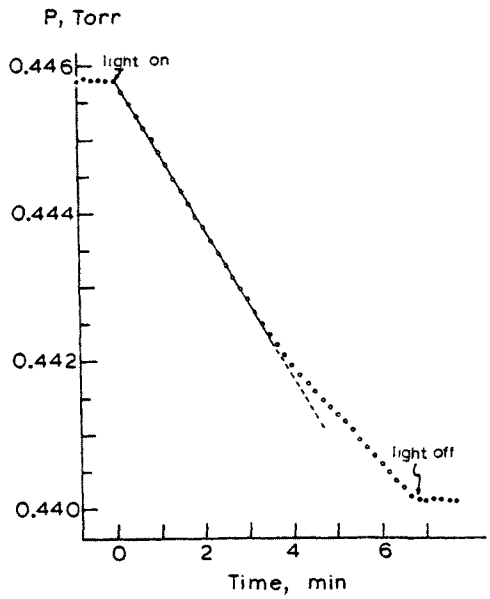

Figure 19. Example of the pressure variation in the 3130 Å photolysis of SO_2 (0.195 Torr) with isobutane (0.251 Torr).

In the medium pressure case, the gases in the cell after irradiation were analyzed by mass spectrometry. Within the maximum sensitivity obtainable (1-10 ppm), no gaseous products were detected. These results are contrary to those reported by Penzhorn, et al.[10]

Results and Discussion

Low Pressure Kinetics of Excited SO_2 Molecules--

Penzhorn, et al,[9] have shown that the photolysis of SO_2 with paraffins does not involve a chain mechanism under high pressure conditions. This is consistent with our observation that the quantum yield of product formation is independent of the light intensity; see Figure 20.

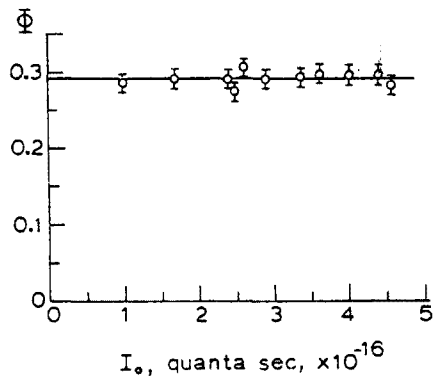

Figure 20. Plot of quantum yields as a function of light intensity; a test of the chain reaction mechanism; P_{SO_2} = 15.0 ± 0.2; $P_{isobutane}$ = 38.0 ± 0.3 Torr.

We have shown in our previous studies[3,34] that two excited singlet states, presumably the $^1A_2$ and $^1B_1$ states, can be reached at excitation wavelength 3130 Å. However, the kinetic data[3] and the quenching rate constants of $SO_2(^1A_2)$ and $SO_2(^1B_1)$ molecules[2,3] all indicate only the $SO_2(^1B_1)$ molecules are chemically important for steady state experiments. Furthermore, Butler and McDonald[35] have shown that the $SO_2(^1A_2)$ species are not the precursors of $SO_2(^3B_1)$ molecules. Therefore, for simplicity, we will not consider the $SO_2(^1A_2)$ molecules in the following discussion of kinetic scheme of SO_2.

The low pressure quantum yields for the SO_2-isobutane photolyses are tabulated in Tables 7 and 8. The reaction mechanism can be written as follows:

$$SO_2 + h\nu \rightarrow SO_2(^1B_1) \qquad (I)$$

$$SO_2(^1B_1) + SO_2 \rightarrow SO_2(^3B_1) + SO_2 \qquad (1a)$$

$$SO_4(^1B_1) + SO_2 \rightarrow (2SO_2) \qquad (1b)$$

$$SO_2(^1B_1) + \text{isobutane} \rightarrow \text{products} \qquad (2a)$$

TABLE 7. QUANTUM YIELDS FOR THE PHOTOLYSES OF SO_2 AND ISOBUTANE MIXTURES UNDER LOW PRESSURE CONDITIONS ($P < 1.2$ TORR)

$[SO_2]$, Torr	[RH], Torr	[RH]/$[SO_2]$	Φ	Φ_{calc} [a]
0.050	0.160	3.2	0.251	0.265
	0.258	5.16	0.236	0.287
	0.314	6.28	0.277	0.296
	0.405	8.10	0.313	0.302
	0.462	9.24	0.319	0.306
	0.515	10.3	0.313	0.308
	0.907	18.14	0.306	0.319
0.100	0.069	0.69	0.125	0.151
	0.096	0.96	0.161	0.179
	0.135	1.35	0.185	0.207
	0.231	2.31	0.240	0.246
	0.307	3.07	0.239	0.263
	0.423	4.23	0.257	0.279
	0.522	5.22	0.291	0.288
	0.535	5.35	0.286	0.289
	0.589	5.89	0.320	0.292
	0.591	5.91	0.291	0.293
	0.688	6.88	0.283	0.298
	0.734	7.34	0.309	0.300
	0.822	8.22	0.327	0.303
	0.881	8.81	0.335	0.305
	0.924	9.24	0.326	0.306
0.200	0.071	0.36	0.109	0.099
	0.161	0.81	0.158	0.164
	0.252	1.26	0.201	0.201
	0.297	1.48	0.212	0.214
	0.376	1.88	0.235	0.232
	0.404	2.02	0.201	0.237
	0.498	2.49	0.242	0.250
	0.500	2.50	0.243	0.250
	0.512	2.56	0.245	0.252
	0.526	2.63	0.252	0.254
	0.540	2.70	0.248	0.255
	0.612	3.06	0.245	0.263
	0.683	3.42	0.264	0.269
	0.814	4.07	0.267	0.277
0.300	0.111	0.37	0.102	0.102
	0.180	0.60	0.128	0.139
	0.273	0.91	0.162	0.174
	0.282	0.94	0.187	0.177
	0.430	1.43	0.211	0.211
	0.502	1.67	0.198	0.223
	0.632	2.11	0.231	0.240

[a] Φ_{calc} is calculated from relation (A) by assuming $k_{2b}/k_2 = 0.273$.

TABLE 8. QUANTUM YIELDS FOR THE PHOTOREACTION OF SO_2 WITH ISOBUTANE IN THE PRESENCE OF BENZENE UNDER LOW PRESSURE CONDITIONS

$[SO_2]$, Torr	[RH], Torr	$[C_6H_6]$, Torr	Φ
0.200	0.517	0.00000	0.248
0.199	0.515	0.00652	0.144
0.200	0.515	0.0118	0.118
0.200	0.513	0.0185	0.0901
0.200	0.516	0.0215	0.0875
0.200	0.512	0.0297	0.0779
0.200	0.518	0.0406	0.0744
0.200	0.517	0.0572	0.0644
0.200	0.524	0.0721	0.0592
0.200	0.514	0.0867	0.0553

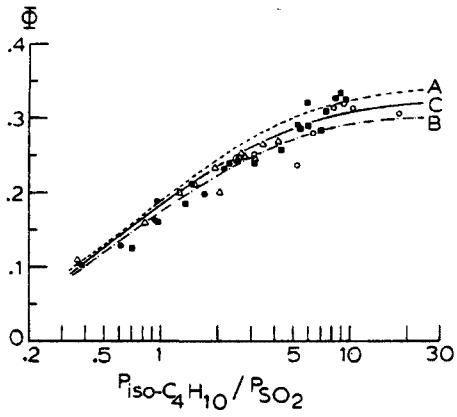

Figure 21. Plot of quantum yields as a function of [RH]/[SO_2] ratio. Experimental conditions: P_{SO_2} = 0.05 (○), 0.10 (■), 0.20 (Δ), and 0.30 Torr (●); curves A, B, and C are calculated from relation (A) by assuming k_{2b}/k_2 = 0.291, 0.255, and 0.273, respectively.

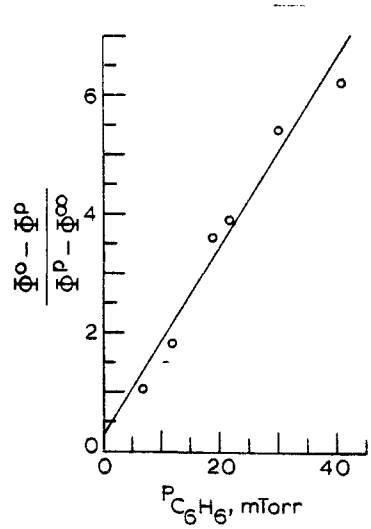

Figure 22. Plot of the function of the quantum yield, relation (C), versus the benzene pressure. Data are from the benzene-inhibited 3130 Å photolyses of SO_2-isobutane mixtures under low-pressure conditions.

$$SO_2(^1B_1) + \text{isobutane} \rightarrow SO_2(^3B_1) + \text{isobutane} \quad (2b)$$

$$SO_2(^1B_1) + \text{isobutane} \rightarrow (SO_2) + \text{isobutane} \quad (2c)$$

$$SO_2(^1B_1) \rightarrow SO_2 + h\nu_f \quad (3a)$$

$$SO_2(^1B_1) \rightarrow (SO_2) \quad (3b)$$

$$SO_2(^3B_1) + SO_2 \rightarrow SO_3 + SO \quad (4a)$$

$$SO_2(^3B_1) + SO_2 \rightarrow (2SO_2) \quad (4b)$$

$$SO_2(^3B_1) + \text{isobutane} \rightarrow \text{products} \quad (5a)$$

$$SO_2(^3B_1) + \text{isobutane} \rightarrow (SO_2) + \text{isobutane} \quad (5b)$$

$$SO_2(^3B_1) \rightarrow SO_2 + h\nu_p \quad (6a)$$

$$SO_2(^3B_1) \rightarrow (SO_2) \quad (6b)$$

where $(2SO_2)$ and (SO_2) symbolize $SO_2(X\ ^1A_1)$ or other long-lived or non-emitting product molecules, and "products" represents the various sulfinic or sulfonic (solid or liquid phase) products.[9,10] In the pressure range employed here, steps (3a), (3b), (6a), and (6b) are not important.[3,4] Using the steady state assumption, the above mechanism predicts:

$$\Phi = \frac{k_{2a}}{k_1\frac{[SO_2]}{[RH]} + k_2} + \frac{\left\{k_{1a}\frac{[SO_2]}{[RH]} + k_{2b}\right\}}{\left\{k_1\frac{[SO_2]}{[RH]} + k_2\right\}}\cdot\frac{k_{5a}}{\left\{k_4\frac{[SO_2]}{[RH]} + k_5\right\}} \quad (A)$$

$$= \Phi^S + \Phi^T \quad (B)$$

where Φ^S and Φ^T represent the quantum yields contributed from the excited singlet and triplet molecules, respectively; RH represents isobutane.

Relation (A) predicts the quantum yield Φ is a function of the $[SO_2]/[RH]$ ratio. Figure 21 shows that the experimental data do support this contention. Most of the rate constants in relation (A) have been determined previously: $k_1 = (1.04 \pm 0.02) \times 10^{11}$[3]; $k_2 = (1.41 \pm 0.46) \times 10^{11}$[3]; $k_4 = (4.21 \pm 0.12) \times 10^8$[4]; $k_5 = (8.74 \pm 0.17) \times 10^8$ $\ell.\ mole^{-1}\ sec^{-1}$ [36]. Since the quantum yields for this reaction are near unity, we then assume $k_{5a} \simeq k_5$. There are still three unknown variables, k_{2a}, k_{2b}, and k_{1a}.

An estimate of the extent of the singlet excited SO_2 involvement in the quantum yields in the photolysis of SO_2-isobutane mixtures -- The photolyses

of the SO_2-isobutane mixtures were inhibited by benzene addition in a series of runs at fixed pressures of SO_2 (0.200 ± 0.001) and isobutane (0.516 ± 0.007 Torr). These are summarized in Table 2. The rate constant for SO_2 ($^3B_1$) quenching by benzene is about 100 times that for isobutane.[36] Note in Table 2 the effectiveness of small quantities of benzene in quenching a large part of quantum yields; for these conditions Φ is reduced from 0.248 in the absence of benzene to 0.0744 for benzene pressures greater than about 0.0406 Torr. The concentration of the excited singlet fluorescence state of SO_2 could not have been altered significantly by the benzene addition (less than 10%), so that the benzene-inhibited quantum yields can be used to extract the contribution from the singlet state involved. The following step is added to the reaction mechanism:

$$SO_2(^3B_1) + C_6H_6 \rightarrow \text{nonradiative products} \qquad (7)$$

The total mechanism thus predicts

$$\frac{\Phi^0 - \Phi^p}{\Phi^p - \Phi^\infty} = \frac{k_7[C_6H_6]}{k_4[SO_2] + k_5[RH]} \qquad (C)$$

Here Φ^0, Φ^p and Φ^∞ refer to the measured quantum yields of products formed in the SO_2-isobutane-C_6H_6 mixtures with P_{SO_2} = 0.200, $P_{\text{isobutane}}$ = 0.516 Torr, and with benzene at 0, p Torr, and at a pressure which gives nearly complete triplet quenching, respectively. Relation (C) is tested with the experimental data in Figure 22. The best value of Φ^∞ extrapolated from the data of Table 8 is 0.0465. From the slope of Figure 22 (158 ± 33 $Torr^{-1}$) together with the measured rate constants k_4 and k_5, we estimate the quenching rate constant of $SO_2(^3B_1)$ for C_6H_6, k_7, to be (8.5 ± 1.8) x 10^{10} ℓ. $mole^{-1}$ sec^{-1}. This checks reasonably well with the values determined previously in the direct $SO_2(^3B_1)$ lifetime studies: (8.1 ± 0.7) x 10^{10}[37]; (8.8 ± 0.8) x 10^{10} ℓ. $mole^{-1}$ sec^{-1} [36].

From the value of Φ^∞ = 0.0465, relation (A), and the previously reported rate constants for k_1 and k_2, we estimate k_{2a} = 8.4 x 10^9 ℓ. $mole^{-1}$ sec^{-1}. This rate constant has not been extimated previously. Although Badcock, et al.,[8] assumed that the triplet molecules of SO_2 are alone responsible for the photochemistry observed in SO_2-hydrocarbon mixture photolyses in both the first allowed and the "forbidden" absorption bands of SO_2, the present work shows that the contribution from the singlet excited SO_2 molecules, although small, is not negligible, at least for the SO_2-isobutane system.

An estimate of the intersystem crossing ratios for excited SO_2 singlet induced by collisions with SO_2 and isobutane --Relation (A) can be rearranged to the more convenient form of (D):

$$(\Phi - \Phi^S)(0.738\,\frac{[SO_2]}{[RH]} + 1)(0.482 + \frac{[RH]}{[SO_2]}) = \frac{k_{1a}}{k_2} + (\frac{k_{2b}}{k_2})\,\frac{[RH]}{[SO_2]} \qquad (D)$$

where $\Phi^S = (12.3\,[SO_2]/[RH] + 16.7)^{-1}$ (E)

Relation (D) has been tested in Figure 23, where the term on the left side of relation (D) was plotted versus the ratio $[RH]/[SO_2]$. A very good linear relationship between the variables is seen. From the slope of Figure 23 we estimate: $k_{2b}/k_2 = 0.291 \pm 0.011$. In order to optimize the sensitivity of the quantum yields to $[SO_2]$ and improve the accuracy of the intercept, which determines the intersystem crossing ratio for SO_2, the data for $[RH]/[SO_2] > 5$ were discarded. A least squares fit of these data gives a intercept of 0.107 ± 0.027. Together with the previously reported rate constants k_1 and k_2, k_{1a}/k_1 is extimated to be 0.145 ± 0.037. This checks reasonably well with the various literature values: 0.21 ± 0.04 [32]; 0.12 ± 0.01 [38]; 0.20 ± 0.05 [38]; 0.14 ± 0.02 [39]; 0.14 ± 0.01 [39]. In this case the slope is somewhat smaller, 0.255 ± 0.012, than that determined from total sets of data, 0.291 ± 0.011. The theoretically calculated quantum yields with the above reported rate constants were plotted in Figure 21 as curves A, B, and C with $k_{2b}/k_2 = 0.291$, 0.255, and an averaged value 0.273, respectively. It is seen that the averaged value of $k_{2b}/k_2 = 0.273 \pm 0.018$ gives the best fit to the experimental data. Therefore, in the following discussion we will assume $k_{2b}/k_2 = 0.273 \pm 0.018$. No estimates of this ratio have been reported previously. The apparently higher intersystem crossing ratio for isobutane, 0.273 ± 0.018, is not surprising in view of the comparison with that for alkenes previously reported at 3130 Å: 0.51 ± 0.10 (cis-2-pentene) [37]; 0.62 ± 0.12 (trans-2-pentene) [38]; 0.85 ± 0.37 (cis and trans-2-butene) [32]; and 0.62 ± 0.05 (cis-C_5H_8) [39].

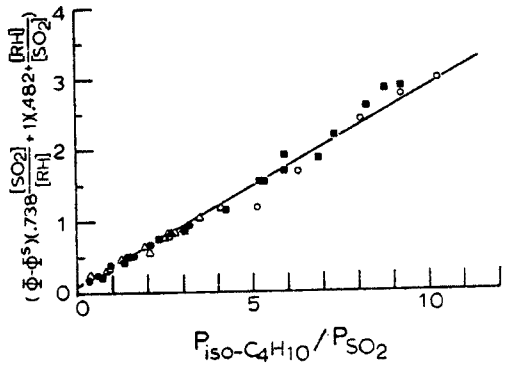

Figure 23. Plot of the function of the left-hand term in relation (D) as a function of the $[SO_2]/[\text{isobutane}]$ ratio.

Kinetics of Excited SO_2 Molecules at High Pressures--

The quantum yields of the product formation for the photolyses of SO_2-isobutane mixtures in the absence or presence of C_6H_6 or CO_2 under medium pressure conditions ($1 \leq P \leq 120$ Torr) are reported in Tables 9, 10 and 11. In these Tables the initial pressure jump of the system after irradiation (see Figure 1) and the rate of light scattering (see later discussion) are also reported.

Thermal effect on the initial pressure jump-- Dainton and Ivin[6] first found that on irradiation of any mixture containing SO_2 a small but very reproducible initial pressure rise was always observed during the first seconds of the irradiation. This has been shown in Figure 7; it is apparently due to the conversion of the absorbed light into heat. Dainton and Ivin also found a smooth, almost linear, relation between the pressure jump and the subsequent rate of pressure fall for given pressures of reactions, independent of the method of variation of the incident light intensity and wavelength. However, no theoretical argument to explain this effect was given by them. We have found that this thermal effect is a very interesting and useful phenomenon; it not only affords us a useful method to calibrate internally the absorbed light intensity in the system, but also gives us a new way to determine various physical properties such as thermal conductivities and concentrations of the reactants in the system. A detailed analysis is given elsewhere,[34] and only a brief description of some of the results will be given here to illustrate these observations.

It can be shown that for a pure SO_2 system the initial pressure jump, P_j, is related to the pressure of SO_2, P, and the absorbed light intensity, I_a, by

$$P_j = \gamma P I_a = \gamma P I_o (I_a/I_o) \qquad (F)$$

where $\gamma = \theta/T_o \underline{S} \delta$; θ is a proportionality constant which relates the rate of heat generation to the rate of absorbed light intensity; δ is the "heat transfer coefficient" per unit area;[40] T_o is the temperature of the wall; $\underline{S}$ is the total area of the wall; I_o is the incident light intensity. Relation (F) is tested by experimental data in Figure 24. An experimental $\gamma = (2.3 \pm 0.3) \times 10^{-19}$ sec/quanta is obtained. This checks reasonably well with the theoretically calculated γ value, 1.7×10^{-19} sec/quanta.[34]

In the presence of added gases it can be shown that

$$P_j = (\gamma_1 P_1 + \gamma_2 P_2 + \gamma_3 P_3)\, I_o\, (1 - 10^{-0.00903 P_1 + 0.0014\, P_2/P_1}) \qquad (G)$$

$$(P_1 \leq 15 \text{ Torr})$$

where $\gamma_i \equiv \theta/(T_o \underline{S} \delta_i)$; P_1, P_2, and P_3 are the initial partial pressures of SO_2, isobutane, and C_6H_6 or CO_2, respectively. A good check of relation (G) with experimental data in Tables 9, 10, and 11 is obtained. Theoretically, $\gamma_i/\gamma_j = \delta_j/\delta_i = \Lambda_j/\Lambda_i$, where Λ_i is the thermal conductivity of gas $\underline{i}$.

TABLE 9. QUANTUM YIELDS FOR THE PHOTOLYSES OF SO_2-ISOBUTANE MIXTURES UNDER MEDIUM PRESSURE CONDITIONS (P < 120 TORR

$[SO_2]$, Torr	[RH], Torr	Φ	P_j,[a] mTorr	R_{scat}, x 10^3	$\Delta P/\Delta t$ mTorr/sec
2.50	12.36	0.42	4.7	5.03	0.400
	15.59	0.322	3.9	-	-
	17.20	0.348	5.3	5.10	0.433
	19.24	0.379	7.2	-	-
	22.39	0.361	7.6	5.40	0.479
	22.93	0.375	5.0	-	-
	24.50	0.394	7.1	6.45	0.507
	24.71	0.446	7.0	5.78	0.463
	26.66	0.369	8.4	-	-
	27.48	0.409	8.9	7.73	0.538
	29.90	0.336	7.7	-	-
	30.10	0.423	8.9	6.53	0.513
	32.61	0.376	11.4	5.78	0.381
	34.72	0.379	9.6	4.95	0.429
	35.97	0.381	10.8	6.60	0.412
	36.15	0.371	12.3	5.48	0.466
	37.44	0.479	9.8	-	-
	38.83	0.387	11.6	7.42	0.539
	41.70	0.358	11.8	8.48	0.498
	44.55	0.366	12.4	-	-
	46.53	0.379	13.0	7.95	0.526
	50.47	0.392	14.5	8.48	0.540
	51.67	0.398	14.8	-	-
	51.70	0.418	15.0	7.58	0.556
	61.79	0.389	16.6	-	-
	66.76	0.385	18.4	8.4	0.563
	70.71	0.517	20.0	-	-
	87.93	0.484	22.7	8.70	0.682
4.98	4.90	0.171	6.0	1.58	0.350
5.00	9.77	0.234	6.0	-	-
5.07	16.11	0.271	-	6.60	0.558
5.00	18.89	0.283	8.6	7.50	0.569
4.99	24.02	0.325	12.3	2.78	0.557
5.00	29.86	0.346	15.5	7.73	0.685
5.00	39.09	0.371	26	8.02	0.667
4.98	45.33	0.385	23	8.02	0.644
5.00	51.14	0.388	27	8.70	0.795
5.00	53.25	0.394	-	7.50	0.637
5.00	58.06	0.411	31	7.20	0.851
5.00	58.26	0.398	32	7.35	0.696
4.99	66.06	0.414	34	9.75	0.835
4.98	66.74	0.405	-	7.05	0.679
5.00	73.25	0.418	35	-	-
4.97	76.79	0.432	40	6.98	0.679
5.01	79.36	0.431	-	-	-

(Continued)

TABLE 9. (Continued)

$[SO_2]$, Torr	[RH], Torr	Φ	P_j,[a] mTorr	R_{scat}, x 10^3	$\Delta P/\Delta t$, mTorr/sec
5.00	79.90	0.442	39	8.55	0.878
5.00	87.53	0.462	37	9.60	0.912
5.00	89.48	0.462	44	9.52	0.854
5.00	97.70	0.488	45	8.32	0.789
4.98	102.27	0.499	46	11.32	0.829
5.00	102.13	0.453	-	-	-
4.99	109.31	0.530	53	8.48	0.955
9.99	9.86	0.191	19.7	8.7	0.742
10.00	15.43	0.234	24.4	11.55	0.909
10.00	21.62	0.269	29.5	13.12	0.997
10.00	25.07	0.287	33.2	15.15	1.10
10.00	34.94	0.323	43	16.80	1.25
10.00	39.40	0.323	45	16.95	1.15
10.00	45.19	0.346	49.3	18.45	1.35
9.99	49.24	0.367	52.7	18.52	1.34
9.99	55.01	0.365	57	19.12	1.42
10.00	58.57	0.381	61.6	18.38	1.53
9.99	58.64	0.383	60.6	21.52	1.54
9.99	64.61	0.394	61.7	22.88	1.62
10.00	69.86	0.397	64.1	19.28	1.57
10.00	70.69	0.381	66.5	19.42	1.48
9.99	73.97	0.42	75	19.95	1.61
10.00	79.67	0.399	75.8	19.72	1.51
10.00	81.24	0.399	74.4	21.75	1.54
10.00	89.41	0.444	80.6	19.12	1.76
10.00	96.35	0.438	83.6	21.30	1.75
10.00	102.16	0.428	82.8	20.4	1.55
15.00	14.85	0.208	41	11.1	1.08
15.00	19.91	0.240	-	14.2	1.25
15.00	27.22	0.258	55	16.2	1.34
14.99	32.06	0.288	58.6	19.1	1.50
15.00	40.15	0.313	70	15.6	1.62
14.99	45.51	0.322	73	22.8	1.71
15.00	53.27	0.341	81.3	23.4	1.78
14.98	59.46	0.358	87	22.3	1.90
15.01	66.88	0.363	88	24.1	1.89
14.93	76.78	0.366	100	24.1	1.91
14.94	85.25	0.378	108	24.4	1.98
15.00	95.15	0.405	113	27.2	2.16
14.94	100.69	0.394	121	26.3	2.04

[a] The numbers reported here have been normalized to I_o = 3.07 x 10^{16} quanta/sec.

Experimentally we found that γ_1/γ_i = 1.99, 1.20, and 1.64 for isobutane, C_6H_6, and CO_2, respectively. Thermal conductivity data[41] show that Λ_i/Λ_1 = 1.77, 1.19, and 1.71 for isobutane, C_6H_6, and CO_2, respectively.

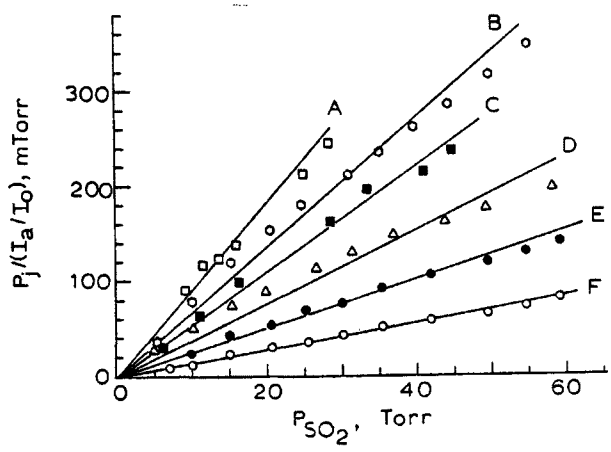

Figure 24. Plot of $P_j/(I_a/I_o)$ as function of P_{SO_2}. The I_o values for lines A,B,C,D,E, and F are 3.79, 3.16, 2.26, 1.58, 1.13, and 0.69 x 10^{-16} quanta/sec, respectively.

Evaluation of the high pressure photoreaction mechanism of SO_2-- The deviation of the phosphorescence lifetimes of $SO_2(^3B_1)$ molecules from the simple Stern-Volmer quenching relation in experiments at high pressures (P - 10-760 Torr) was recently reported by Rudolph and Strickler,[26,27] Su, et al.,[28] and Calvert.[29] This phenomenon has been described elsewhere and need not be considered in detail here. We have shown that the results of the photolyses of SO_2-isobutane mixtures carried out at low pressures ($P \leq 1.2$ Torr) can be understood by invoking reactions of one singlet and one triplet state, presumably the $^1B_1$ and $^3B_1$ state. However, the quantum yields of products from SO_2 photoexcited in isobutane mixtures at high pressures ($P > 10$ Torr), are much higher than those anticipated from the low pressure mechanism; this is shown in Figure 25. The dashed line in Figure 25 is calculated from relation (A) of the low pressure mechanism with the rate constants reported previously except $k_4 = 2.6 \times 10^3 + 2.0 \times 10^4/\{1 + 0.0133P_{SO_2}$ (Torr)$\}$ Torr^{-1} sec^{-1} was used to take into account the known saturation effect.[28] This phenomenon has been found also in many other photolysis systems of SO_2-added gas mixtures.[13-25] In addition to the previous low pressure steps, one more unknown X state was suggested by the Calvert group[13,16,32], and three more states designated as SO_2^*, SO_2^{**}, and SO_2 were proposed by the Heicklen research group.[14,15,17-25] In our view the high pressure mechanism of Heicklen has some serious shortcomings. First, there is no correspondence between the observed kinetic properties of the SO_2^* state suggested by Heicklen, et al., and the Stern-Volmer quenching parameters determined either by Brus and McDonald[2] or by us.[3] Second, the produced fractions, α, β, and γ, for the designated $SO_2(^3B_1)$, SO_2^*, and SO_2 excited molecules, defined by Heicklen and co-workers, are assumed to be

three constants at a given excitation wavelength. The intersystem crossing ratios from $SO_2(^1B_1)$ to $SO_2(^3B_1)$ for various foreign gases are known to be different.[41] Thus, it seems unlikely that the α value will be a constant in the presence of a mixture of different added gases within a wide pressure range (10^{-4}-10^3 Torr). The β and γ values determined by Heicklen, et al., are always different for different systems at the same excitation wavelength. For example, the γ value was determined to be 0.019 by Kelly, et al.,[21] but 0.092 by Partymiller and Heicklen.[25] Furthermore, Su and Calvert[29] have reexamined the data from the photochemical reactions carried out in the presence of high pressures of CO[42] and C_2H_2[22]. The postulate of Kelly, et al.,[22] that the photolysis of SO_2-C_2H_2-added gas mixtures excited within the $SO_2(^3B_1) \leftarrow SO_2(\tilde{X}\ ^1A_1)$ band involves the reactions of three different excited states of SO_2, namely the $SO_2(^3B_1)$, SO_2^* and SO_2^{**} states, appears to be incorrect. We feel that the Heicklen mechanism is essentially an empirical equation used to fit the experimental data; in our opinion it is not based upon a realistic photochemical reaction mechanism. Therefore, we have not used the Heicklen mechanism in our further discussions on the SO_2-isobutane photolysis system.

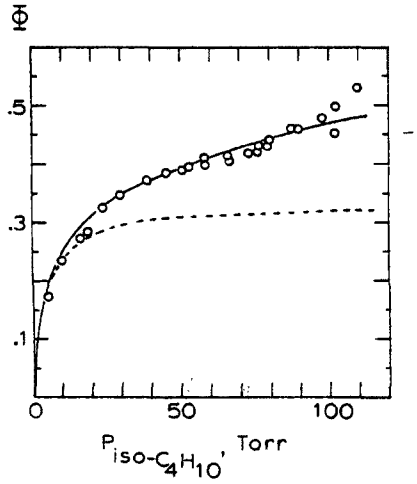

Figure 25. Plot of quantum yields as a function of $P_{isobutane}$; P_{SO_2} = 5.0 Torr. Dashed curve - calculated from relation (A); solid curve - calculated from relation (H).

In applying Calvert's photoreaction mechanism of SO_2 to the high pressure conditions, one should also consider the saturation effect on the phosphorescence lifetime of the $SO_2(^3B_1)$ molecules. Now we are ready to rationalize the data of the high pressure photolyses of SO_2-isobutane mixtures.

Photolyses of SO_2-isobutane mixtures at high pressures: In addition to the reaction mechanism from (I) to (6b) suggested before, the following steps should be considered:

$$SO_2(^1B_1) + SO_2 \rightarrow X + SO_2 \qquad (1c)$$

$$SO_2(^1B_1) + \text{isobutane} \rightarrow X + \text{isobutane} \quad (2d)$$

$$SO_2(^1B_1) + M \rightarrow SO_2(^3B_1) + M \quad (8a)$$

$$SO_2(^1B_1) + M \rightarrow X + M \quad (8b)$$

$$SO_2(^1B_1) + M \rightarrow (SO_2) + M \quad (8c)$$

$$X + SO_2 \rightarrow SO_2(^3B_1) + SO_2 \quad (9a)$$

$$X + SO_2 \rightarrow (2SO_2) \quad (9b)$$

$$X + \text{isobutane} \rightarrow SO_2(^3B_1) + \text{isobutane} \quad (10a)$$

$$X + \text{isobutane} \rightarrow (SO_2) + \text{isobutane} \quad (10b)$$

$$X + M \rightarrow SO_2(^3B_1) + M \quad (11a)$$

$$X + M \rightarrow (SO_2) + M \quad (11b)$$

$$X \rightarrow (SO_2) \quad (12)$$

$$SO_2(^3B_1) + M \rightarrow (SO_2) + M \quad (13)$$

Using the steady state approximation, the following relation can be derived:

$$\Phi = \frac{k_{2a}[RH]}{(k_1[SO_2] + k_2[RH] + k_8[M])} + \frac{k_{5a}[RH]}{(k_4[SO_2] + k_5[RH] + k_{13}[M])} \left\{ \right.$$

$$\frac{(k_{1a}[SO_2] + k_{2b}[RH] + k_{8a}[M])}{(k_1[SO_2] + k_2[RH] + k_8[M])} +$$

$$\left. \frac{(k_{1c}[SO_2] + k_{2d}[RH] + k_{8b}[M])(k_{9a}[SO_2] + k_{10a}[RH] + k_{11a}[M])}{(k_1[SO_2] + k_2[RH] + k_8[M])(k_{12} + k_9[SO_2] + k_{10}[RH] + k_{11}[M])} \right\} \quad (H)$$

In our present experiments M represents the CO_2 molecule. All the rate constants concerning the X state are unknown. Obviously, relation (H) is very complicated and cannot be tested adequately with the very limited data now available. However, in the absence of CO_2 as quenching gas, a reasonably good fit to the data in Table 9 was obtained by using a curve-fitting method. The results are shown in Figures 25 (solid curve) and 26 (all curves). The ratios of rate constants used for these fits were: $k_9/k_{12} = 0.053$, $k_{10}/k_{12} = 0.0067$, $k_{9a}/k_9 = 0.005$, $k_{10a}/k_{10} = 0.7$, $k_{1c}/k_1 = 0.136$, $k_{2d}/k_2 = 0.65$ [all from this work], and $k_4 = 2.6 \times 10^3 + 2.0 \times 10^4/\{1 + 0.0133[SO_2]\}$ $Torr^{-1}$ sec^{-1} [28]. All the other rate constants (or ratios) have been reported previsouly in our discussion of the low pressure mechanism.

TABLE 10. QUANTUM YIELDS FOR THE PHOTOLYSES OF SO_2-ISOBUTANE-C_6H_6 MIXTURES UNDER MEDIUM PRESSURE CONDITIONS (P < 120 TORR)

	$[C_6H_6]$, Torr	Φ	P_j,[a] mTorr	R_{scat}	$\Delta P/\Delta t$, mTorr/sec
I)[b]	0.000	0.411	31	8.25	0.851
	0.000	0.398	32	6.68	0.696
	0.022	0.386	28	6.82	0.666
	0.054	0.362	31	6.45	0.700
	0.101	0.340	31	8.02	0.618
	0.153	0.313	27	8.18	0.624
	0.247	0.283	32	4.05	0.451
	0.359	0.251	27	5.10	0.409
	0.450	0.239	30	4.88	0.486
	0.545	0.247	28	5.32	0.499
	0.551	0.226	31	5.62	0.450
	0.653	0.222	29	4.20	0.446
	0.800	0.201	32	3.75	0.408
	0.997	0.181	31	3.60	0.361
	1.202	0.173	31	3.00	0.318
	1.400	0.176	31	3.38	0.375
	1.600	0.145	28	2.92	0.302
	1.800	0.142	28	3.22	0.285
	1.960	0.121	30	2.25	0.250
	2.197	0.127	30	2.78	0.260
	2.387	0.113	30	3.45	0.238
	3.130	0.111	32	2.40	0.234
	3.727	0.090	35	1.80	0.178
	4.492	0.094	33	1.50	0.187
	4.989	0.092	35	1.50	0.190
II)[b]	0.000	0.383	60	20.1	1.54
	0.000	0.381	62	19.1	1.54
	0.152	0.304	59	17.8	1.24
	0.447	0.234	59	12.9	0.941
	0.719	0.215	61	9.52	0.830
	0.841	0.194	59	9.52	0.764
	1.127	0.178	63	8.55	0.696
	1.219	0.177	63	6.98	0.695
	1.474	0.163	62	6.38	0.613
	1.536	0.168	64	7.88	0.658
	1.917	0.134	60	5.18	0.531
	2.461	0.128	66	5.32	0.506
	3.001	0.109	64	4.28	0.434
	3.860	0.099	62	34.5	0.401
	4.611	0.094	64	3.68	0.372

[a] The numbers reported here have been normalized to $I_o = 3.07 \times 10^{16}$ quanta/sec.

[b] Experimental conditions for part I and II are: $P_{SO_2} = 5.02 \pm 0.13$, 10.00 ± 0.01; $P_{isobutane} = 58.31 \pm 0.58$, 58.36 ± 0.51 Torr; respectively.

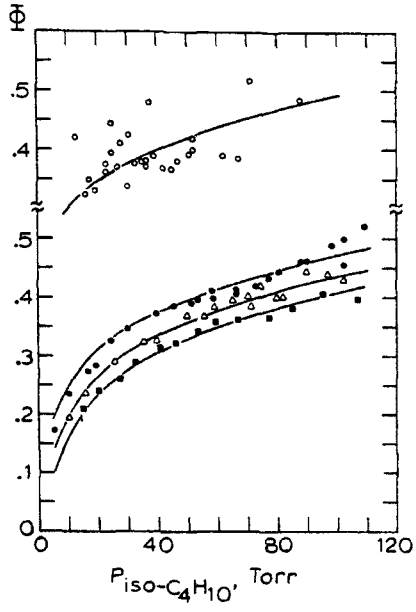

Figure 26. Plot of quantum yields as a function of $P_{isobutane}$. P_{SO_2} = 2.5 (○), 5.0 (●), 10.0 (Δ), and 15.0 Torr (■). Solid curves are calculated from relation (H).

The photolyses of the SO_2-isobutane mixtures were inhibited by C_6H_6 addition in a series of runs at fixed pressures of SO_2 and isobutane. These have been summarized in Table 10. Again it can be seen that the effectiveness of small quantities of C_6H_6 in quenching a large part of quantum yields. For our experimental condition the concentration of the excited singlet fluorescence state of SO_2 could not have been altered significantly by the C_6H_6 addition (less than 10%). The effect of addition of a small amount of C_6H_6 on the X state is not clear. We will assume that the C_6H_6-inhibited quantum yields can be tested simply to extract the contribution from the singlet state involved.[13] Thus by adding the reaction step 7, we predict relation (C) in the low pressure case can also be applied to the high pressure case. This is tested in Figure 27. Relation (H) predicts Φ^o and Φ_∞ to be 0.410 (0.373) and 0.056(0.053), respectively, for the case of P_{SO_2} = 5.02 ± 0.13 (10.00 ± 0.01) and $P_{isobutane}$ = 58.3 ± 0.6 (58.4 ± 0.5) Torr. As we have argued in the low pressure case, the two slopes of Figure 27, 1.86 ± 0.17 and 1.52 ± 0.10 $Torr^{-1}$, together with the previously reported values of k_4, k_5, P_{SO_2}, and $P_{isobutane}$, give k_7 = (9.9 ± 0.9) x 10^{10} and 8.3 ± 0.6) x 10^{10} ℓ. $mole^{-1}$ sec^{-1}, respectively. Within the error limit, these values are in reasonable accord with the low pressure value, (8.5 ± 1.8) x 10^{10}, and the literature values derived from lifetime studies: (8.1 ± 0.7) x 10^{10} ℓ. $mole^{-1}$ sec^{-1} [36].

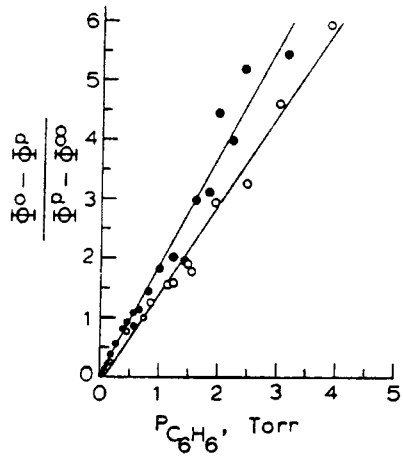

Figure 27. Plot of the function of quantum yield, relation (C), versus benzene pressure. Pressure of SO_2 and isobutane, respectively, are 5.0, 58.3 (●); and 10.0, 58.4 Torr (○).

The quantum yield data for the photolyses of SO_2-isobutane-CO_2 mixtures have been given in Table **11**. Several rate constants were determined previously: $k_8 = (4.9 \pm 0.7) \times 10^6$ [3], $k_4 = 2.6 \times 10^3 + 2.0 \times 10^4/\{1 + 0.0133P_{SO_2} + 0.0045P_{CO_2}\}$ [28], $k_{13} = 6.76 \times 10^3/\{1 + 0.0133P_{SO_2} + 0.0045P_{CO_2}\}$ $Torr^{-1}$ sec^{-1} [28]. Here, for convenience, P_{SO_2} and P_{CO_2} are in units of Torr. Three more unknown parameters in relation (H), k_{8a}, k_{11a}, and k_{11b}, need to be determined. Again, relation (H) is too complicated to be tested adequately by the limited data now available. Figure 28. shows that a very good fit can be obtained by assuming $k_{8a}/k_8 = 0.05$, $k_{8b}/k_8 = 0.5$, $k_{11}/k_{12} = 0.025$ $Torr^{-1}$, and $k_{11a}/k_{11} = 0.64$. Of course, these are not unique solutions. However, the fit in Figure 28. indicates the relation (H) can be used to rationalize all the data in this work.

The intersystem crossing ratio for CO_2, $k_{8a}/k_8 = 0.05$, determined from this work checks fairly well with the previously reported values: 0.052 ± 0.014 (2662 Å);[41] 0.052 (3130 Å).[32] $k_{8b}/k_8 = 0.5$ determined in this work is of comparable magnitude to that determined by Demerjian and Calvert,[32] 0.76 ± 0.11. However, the $k_{11}/k_{12} = 0.025$ $Torr^{-1}$ estimated here is a factor of 5.6 higher than that reported previously [Ref. 32], 0.0045 $Torr^{-1}$. Since the saturation effect of the phosphorescence lifetimes of the $SO_2(^3B_1)$ molecules had not been discovered and was not considered in the previous data treatment,[32] the values derived in the previous work at high pressures must be incorrect.

TABLE 11. QUANTUM YIELDS FOR THE PHOTOLYSES OF SO_2-ISOBUTANE-CO_2 MIXTURES UNDER MEDIUM PRESSURE CONDITIONS ($P < 120$ TORR)

$[CO_2]$, Torr	Φ	P_j,[b] mTorr	R_{scat}, x 10^3	$\Delta P/\Delta t$, mTorr/sec
0.00	0.269	29	13.72	1.00
5.089	0.264	35	12.75	1.02
7.745	0.259	38	13.95	0.993
8.076	0.251	40	12.08	0.964
11.30	0.259	42	10.8	0.951
19.18	0.246	46	13.7	0.943
23.55	0.242	50	13.0	0.887
26.75	0.251	57	13.3	0.959
30.94	0.243	55	11.8	0.904
35.19	0.235	62	11.2	0.878
37.94	0.242	62	11.4	0.913
41.52	0.244	64	10.8	0.927
46.41	0.232	71	11.7	0.888
53.57	0.227	-	11.4	0.859
57.98	0.222	81	12.4	0.839
58.76	0.226	81	11.0	0.855
66.46	0.224	84	11.7	0.823

[a] Experimental conditions are: P_{SO_2} = 10.00 ± 0.01; $P_{isobutane}$ = 21.58 ± 0.17 Torr.

[b] The numbers reported here have been normalized to $I_o = 3.07 \times 10^{16}$ quanta/sec.

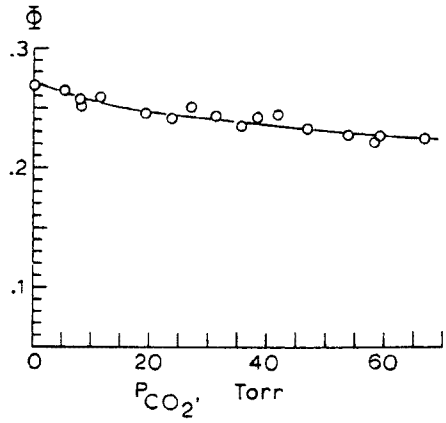

Figure 28. Plot of quantum yields as a function of the CO_2 pressure. The curve is calculated from relation (H).

The nature of the X species -- The nature of the ill-defined X species remains uncertain. Presumably it could be an excited nonemitting singlet or a triplet state of SO_2, one of its unstable isomers S-O-O or cyclic SO_2, or a high energy vibronic state of the ground electronic state. The structure of the phosphorescence spectrum of SO_2 at high pressures (250 Torr) was examined recently by Rudolph and Strickler.[27] The shape and position of the spectrum were identical to those observed for emission from the $^3B_1$ state at low pressures. Thus the X species does not emit significantly for $\lambda <$ 6500 Å. It cannot be the $^1A_2$ or $^1B_1$ state because the kinetic properties of this species show no correlation with those observed in our previous studies of these states.[3,34] It cannot be the $^3A_2$ or $^3B_2$ state either, because both theoretical arguments[43] and experimental evidence[4,44,45] indicate that the efficient unimolecular radiationless process such as step 12 are impossible. Therefore, we feel that the X state may be one of the isomers (S-O-O, or cyclic SO_2) or a high energy vibronic state of the ground electronic state of the SO_2 molecule. Obviously, more studies on this state under high pressure conditions are needed to further characterize this species.

Light scattering and aerosol formation -- Although no appreciable oily product was visible in the photolyses carried out here, the solid and liquid products, presumably the sulfinic and sulfonic acids,[9,10] were capable of being followed by the scattered light observed at the rear phototube in the optical train. As has been shown previously in Figure 8, the scattering was not appreciable under the low pressure conditions, but it could be measured quite reproducibly under the high pressure conditions. The scattering had about a 5-10 sec induction period and then started to increase for about 40-60 sec. It then reached the maximum value and fluctuated slowly around the maximum. The rate of increase of the scattering, R_{scat}, reported in Tables 9, 10, and 11 is defined to be the initial rate of increase of intensity of scattered light divided by the initial transmitted light intensity. The R_{scat} was plotted versus the rate of pressure fall, $\Delta P/\Delta t$, in Figure 29. A roughly linear relationship was found. This indicates that

the initial increase of scattered light is a result of the formation of the product molecules. About 40-60 sec after the homogeneous nucleation[46] starts the new particle production ceases. The particles already present grow by condensation mainly (there is some growth by coagulation) and decrease in number through this process.[46] The observed scattered light must depend on both the particle size and particle number. The condensation and coagulation thus cause a slow fluctuation of the scattering around the maximum value.

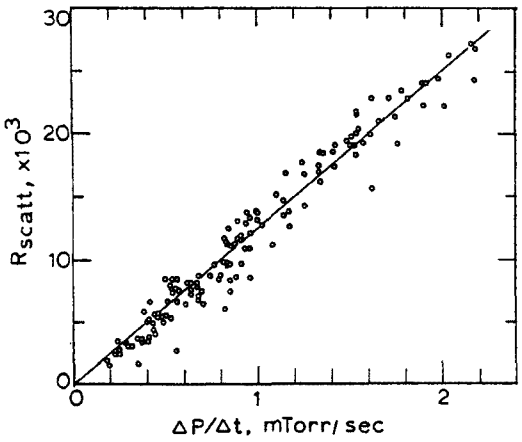

Figure 29. Plot of the rate of increase of initial light scattering R_{scat}, as a function of the rate of pressure drop.

Instead of measuring the scattered light, Penzhorn, et al.,[9] measured the aerosol mass concentration as a function of time for the photolyses of SO_2-n-butane mixtures. A good correlation between the product and aerosol formation was found. The detailed kinetic studies of the particle formation processes for the photolyses of SO_2-C_2H_2 and SO_2-allene had been reported by Luria, et al.[47,48] They found that initially as the reaction mixture was irradiated there was an induction period of about 45 sec, before which particles with size larger than 25 Å in diameter were not produced, although CO was produced immediately. Nucleation occured suddenly, particles were produced for a few sec, and then particle production ceased. The induction period of about 45 sec in their experiments is about the time of reaching maximum scattering in our experiments. Since large particles (diameter > 25 Å) were not formed during the first 45 sec, the total number of small particle then increased linearly with the time (because the rate of reaction is constant). Thus a linear relationship between R_{scat} and $\Delta P/\Delta t$ found in Figure 29 is not unexpected.

REFERENCES

1. J.G. Calvert and J.N. Pitts, Jr., "Photochemistry", John Wiley and Sons, Inc., New York, 1966, p. 209.

2. L.E. Brus and J.R. McDonald, J. Chem. Phys., 61, 97 (1974).

3. F. Su, J.W. Bottenheim, H.W. Sidebottom, J.G. Calvert, and E.K. Damon, Int. J. Chem. Kinet, in press.

4. F. Su, J.W. Bottenheim, D.L. Thorsell, J.G. Calvert, and E.K. Damon, Chem. Phys. Lett., in press.

5. F.S. Dainton and K.J. Ivin, Trans. Faraday Soc., 46, 374 (1950).

6. F.S. Dainton and K.J. Ivin, Trans. Faraday Soc., 46, 382 (1950).

7. R.B. Timmons, Photochem. Photobiol., 12, 219 (1970).

8. C.C. Badcock, H.W. Sidebottom, J.G. Calvert, G.W. Reinhardt, and E.K. Damon, J. Amer. Chem. Soc., 93, 3115 (1971).

9. R.D. Penzhorn, W.G. Filby, K. Gunther, L. Stieglitz, Int. J. Chem. Kinet., Symposium No. 1, 611 (1975).

10. R.D. Penzhorn, et al., Conference at Atmonton, 1975.

11. A. Horowitz and J.G. Calvert, Int. J. Chem. Kinet., 4, 175 (1972).

12. A. Horowitz and J.G. Calvert, Int. J. Chem. Kinet., 4, 191 (1972).

13. F.B. Wampler, A. Horowitz, and J.G. Calvert, J. Amer. Chem. Soc., 94, 5523 (1972).

14. E. Cehelnik, C.W. Spicer, and J. Heicklen, J. Amer. Chem. Soc., 93, 5371 (1971).

15. E. Cehelnik, J. Heicklen, S. Braslavsky, L. Stockburger III, and E. Mathias, J. Photochem., 2, 31 (1973/74).

16. A. Horowitz and J.G. Calvert, Int. J. Chem. Kinet., 5, 243 (1973).

17. S.E. Braslavsky and J. Heicklen, J. Amer. Chem. Soc., 94, 4864 (1972).

18. L. Stockburger, III, S. Braslavsky, and J. Heicklen, J. Photochem., 2, 15 (1973/74).

19. A.M. Fatta, E. Mathias, J. Heicklen, L. Stockburger, III, and S. Braslavsky, J. Photochem., 2, 119 (1973/74).

20. M. Luria and J. Heicklen, Can. J. Chem., 52, 3451 (1974).

21. N. Kelly, J.F. Meagher, and J. Heicklen, J. Photochem., 5, 355 (1976).

22. N. Kelly, J.F. Meagher, and J. Heicklen, J. Photochem., 6, 157 (1976/77).

23. K. Partymiller, J.F. Meagher, and J. Heicklen, J. Photochem., 6, 405 (1977).

24. N. Kelly and J. Heicklen, J. Photochem., 7, 123 (1977).

25. K. Partymiller and J. Heicklen, J. Photochem., in press.

26. R.N. Rudolph and S.J. Strickler, J. Amer. Chem. Soc., 99, 3871 (1977).

27. R.N. Rudolph and S.J. Strickler, paper to be published; we thank the authors for a preprint of this work.

28. F. Su, F.B. Wampler, J.W. Bottenheim, D.L. Thorsell, J.G. Calvert, and E.K. Damon, Chem. Phys. Lett., in press.

29. F. Su and J.G. Calvert, Chem. Phys. Lett., in press.

30. J.G. Calvert and J.N. Pitts, Jr., "Photochemistry", John Wiley and Sons, Inc., New York, 1965, p. 732.

31. J.G. Calvert and J.N. Pitts, Jr., "Photochemistry", John Wiley and Sons, Inc., New York, 1965, pp. 783-786.

32. K.L. Demerjian and J.G. Calvert, Int. J. Chem. Kinet., 7, 45 (1975).

33. K.J. Chung, "Experimental and Theoretical Study of Sulfur Dioxide", Ph.D. Thesis, The Ohio State University, Columbus, Ohio, 1974.

34. F. Su, "A Study on the Photochemistry of Sulfur Dioxide", Ph.D. Thesis, The Ohio State University, Columbus, Ohio, 1977.

35. Private communication with Dr. J.R. McDonald.

36. F.B. Wampler, K. Otsuka, J.G. Calvert, and E.K. Damon, Int. J. Chem. Kinet., 5, 669 (1973).

37. H.W. Sidebottom, C.C. Badcock, J.G. Calvert, B.B. Rabe, and E.K. Damon, J. Amer. Chem. Soc., 93, 3121 (1971).

38. F.B. Wampler, Int. J. Chem. Kinet., 8, 945 (1976).

39. F.B. Wampler, Int. J. Chem. Kinet., 8, 183 (1976).

40. M.F.R. Mulcahy, "Gas Kinetics", John Wiley and Sons, Inc., N.Y., 1973, pp. 214-219.

41. The thermal conductivities of SO_2, isobutane, CO_2, and C_6H_6 at 25°C are estimated to be 22.15, 39.2, 37.9, and 26.3 cal $cm^{-2}sec^{-1}$ $(^{o}C\ cm^{-1})^{-1}$, x 10^{6}; Handbook of Thermodynamic Tables and Charts, Kuzman Raenjevic, McGraw-Hill Book Comp., 1976, pp. 303-306.

42. G.E. Jackson and J.G. Calvert, J. Amer. Chem. Soc., 93, 2593 (1971).

43. M. Bixon and J. Jortner, J. Chem. Phys., 50, 3284 (1969).

44. M.H. Hui and S.A. Rice, Chem. Phys. Lett., 17, 474 (1972).

45. H.D. Mettee, J. Chem. Phys., 49, 1784 (1968).

46. J. Heicklen and M. Luria, Int. J. Chem. Kinet., Symposium No. 1, 567 (1975).

47. M. Luria, R.G. dePena, and J. Heicklen, J. Phys. Chem., 78, 325 (1974).

48. M. Luria, K.J. Olszyna, R.G. dePena, and J. Heicklen, J. Aerosol Sci., 5, 435 (1974).

A KINETIC FLASH SPECTROSCOPIC STUDY OF THE CH_3O_2-CH_3O_2 and CH_3O_2-SO_2 REACTIONS.

Introduction

The alkylperoxy radicals, RO_2, are a dominant reactive species generated within the sunlight-irradiated, NO_x-RH-polluted troposphere, and as such, they are of special interest to the atmospheric chemist. Computer simulations of the chemistry of the lower atmosphere suggest that organic peroxy radicals are important in the oxidation of NO and possibly other impurity species such as SO_2.[1-3] However there are very few direct determinations of the rate constants for the gas phase reactions of the RO_2 radicals, and the suggested role of their significance in the chemistry of the polluted troposphere has been inferred largely from "reasonable" kinetic speculation.

In this work we report the first results of a kinetic flash spectroscopic study of some of the reactions of the simplest alkyl peroxy radical, CH_3O_2. A first estimate of the rate constant for the CH_3O_2-SO_2 reaction is presented.

Experimental

The CH_3O_2 radicals were generated by the flash photolysis of azomethane-oxygen mixtures. The azomethane was prepared by the HgO oxidation of the symmetrical dimethyl hydrazine (Merck) by the method of Renaud and Leitch;[4] it was purified, degassed, and dried by repeated vacuum distillation at low temperatures. The SO_2 reactant gas (Matheson, anhydrous) was also further purified by vacuum distillation in the vacuum line.

The xenon flash lamp and multiple pass cell employed in these experiments was similar to that developed at the Physics Division of the National Research Council (Canada) and was constructed from drawings provided by them. The flash lamp, constructed of Vycor, operated at 20 kj per flash with a width at half maximum intensity of about 50 μsec. It paralleled the quartz reaction vessel (220 cm in length, 6.3 cm i.d.) but was separated from it by a Pyrex-plate filter (0.5 cm thickness) which transmitted only light of $\lambda > 2900$ Å. This wavelength range of the exciting light caused negligable excitation of SO_2 or CH_3O_2 product of the flashed azomethane-SO_2-O_2 mixture. A white surfaced (Kodak 6080 paint) reflector surrounded the flash lamp and cell. The cell housed a multiple reflection, White optical system which was usually adjusted for a path length in the range of 800-1600 cm in most of this work. The actual effective path length of the analytical beam was determined at each wavelength used for analysis by employing acetone vapor as the calibration gas. The ultraviolet and visible spectrum of the flash products was recorded photographically in a few experiments using a 0.65 m Hilger spectrograph and a small argon flash lamp which was fired with delay times varied from 0.6 to 2.0 msec following the large photochemical flash. In all kinetic experiments a continuous, 450 w point source xenon arc was employed together with a Jarrell Ash monochromator equipped with an RCA 1P-28 photomultiplier-oscilloscope combination. In most experiments a wavelength of 265 nm was selected from the

analytical beam to follow CH_3O_2. Absorption due to reactants Me_2N_2 and SO_2 and the possible secondary product radical HO_2 were minimized with this wavelength choice. The oscilloscope trace was photographed, and a kinetic analysis of the measured trace was made using computer techniques described in the next section.

The number of methyl radicals formed per flash, and the CH_3O_2 radicals formed ultimately in the Me_2N_2-O_2 mixtures, were extimated from the nitrogen yield from the flash photolysis of pure azomethane in the cell. The measured pressure increase following the flash was not a good monitor of the extent of azomethane decay since a small temperature increase (1-2°C) occurred slowly following the flash, largely as a result of the dissipation of the residual heat generated from the flash lamp itself following the discharge. The amount of nitrogen formed was determined both by volume measurement and by gas chromatography (Varian 5100TC) using He carrier gas and molecular sieve columns. These measurements showed that 0.29% of the azomethane was decomposed per flash for the usual charging voltage employed.

The gaseous mixtures of Me_2N_2-O_2, Me_2N_2-O_2-N_2, and Me_2N_2-O_2-SO_2 was prepared using a capacitance manometer (Baratron) and other calibrated pressure gauges (Wallace and Tiernan). Uniform mixing of the components was ensured through the operation of a mechanical,glass, circulating pump which was attached in series with the cell.

The flash photolysis of the Me_2N_2-O_2-SO_2 mixtures with the P_{SO_2} above 0.5 Torr, resulted in aerosol formation following the flash, and the resultant light scatter prevented quantitative measurements of the CH_3O_2 decay for these conditions. Thus all Me_2N_2-O_2-SO_2 mixture studies were carried out at SO_2 pressures below 0.2 Torr.

Results and Discussion

The Ultraviolet Absorption Spectrum of the CH_3O_2 Radical -

The methylperoxy radical was generated in the filtered ($\lambda > 290$ nm), flash photolysis of azomethane-oxygen mixtures through the reactions (1) and (2):

$$CH_3NNCH_3 + h\nu \rightarrow 2CH_3 + N_2 \qquad (1)$$

$$CH_3 + O_2 \ (+M) \rightarrow CH_3O_2 \ (+M) \qquad (2)$$

For our conditions of high O_2 concentration, less than 1% of the CH_3 radicals formed ethane in reaction (3):

$$2CH_3 \rightarrow C_2H_6 \qquad (3)$$

The temperature of the flash mixture remained essentially constant (23 ± 2°C) during the flash photolysis period.

The extinction coefficient of CH_3O_2 at 265 nm was determined in an extensive series of experiments utilizing mixtures of azomethane (1-5 Torr) in 50 Torr of O_2. The absorbance of CH_3O_2 was followed as a function of time ($\underline{A}_t$), and an extrapolation of these data to the initial absorbance $\underline{A}_o$ was made using the linear function, $\underline{A}_t^{-1} = \underline{A}_o^{-1} + (2k/\epsilon\underline{l})t$. Here 2k is the experimentally observed second order rate constant for CH_3O_2 decay, $\underline{l}$ is the effective path length of the analytical beam at 265 nm, and ϵ is the extinction coefficient for CH_3O_2 at 265 nm $\{\epsilon = [\log_{10}(I_o/I)]/[CH_3O_2]\underline{l}\}$. The $\underline{A}_o$ measurements derived from a series of 17 different flash experiments are plotted versus azomethane pressure in Figure12. The observed linear relationship between the variables is consistent with the limiting form of the Beer-Lambert absorption law and the small fractions of the incident flash lamp light absorbed by the azomethane for our conditions. The slope of this plot (equal in theory to $2\underline{f}\underline{l}/760 \times 0.0821 \times T$), the measured fraction of the azomethane photo-dissociated per flash ($\underline{f} = 0.0029$), and the measured effective path length of the analytical beam ($\underline{l} = 633$ cm, acetone standard), gave $\epsilon(265\text{ nm}) = 530 \pm 27$ l/mole-cm for CH_3O_2. Extinction coefficients at several wavelengths were derived in a similar fashion from less extensive data and are summarized in Figure 13 where they may be compared with other recent estimates of ϵ. The general broadband structure of the CH_3O_2 absorption reported previously[5,6] is confirmed. The absolute values of ϵ are most consistent with those reported by Hochanadel, et al.,[6] where the experimental method was very similar to that employed here. We find $\lambda_{max} = 235$ with $\epsilon \simeq 870$ l/mole-cm. The estimates of Parkes, et al.[5] are somewhat higher than ours at most wavelengths; they were derived by molecular modulation spectroscopy in a less direct fashion from photolyses at much lower intensities and radical concentrations.

The Rate Constant for the CH_3O_2-CH_3O_2 Reaction --

Most of our kinetic studies were carried out using the wavelength 265 nm for the analytical beam to follow CH_3O_2 decay. Plots of the reciprocal of the measured absorbance versus time were linear over a large portion of the time period measured. However small positive deviations from linearity were always observed at long times. The linear portion of the decay curves gave extimates of the ratio $2k_4'/\epsilon\underline{l}$, from which values of k_4', the apparent second order rate constant for CH_3O_2 decay, were derived. These are summarized in Table 30 for experiments over a

$$2CH_3O_2 \rightarrow \text{Products} \qquad (4)$$

range of azomethane, oxygen, and added nitrogen gas pressures. There appears to be no significant trend in the observed rate constant for the runs with $P_{O_2} = 50$ Torr and with a ten-fold variation in azomethane pressure or with 645 Torr of added nitrogen gas. In experiments at the lowest gas pressures, 5 Torr of azomethane and 20 Torr of O_2, values of k_4, appear to be somewhat higher, $(3.08 \pm 0.17) \times 10^8$, than those observed in similar mixtures at higher gas pressures. The origin of this effect is not clear. It is possible that it arises from non-thermally equilibrated radicals present in

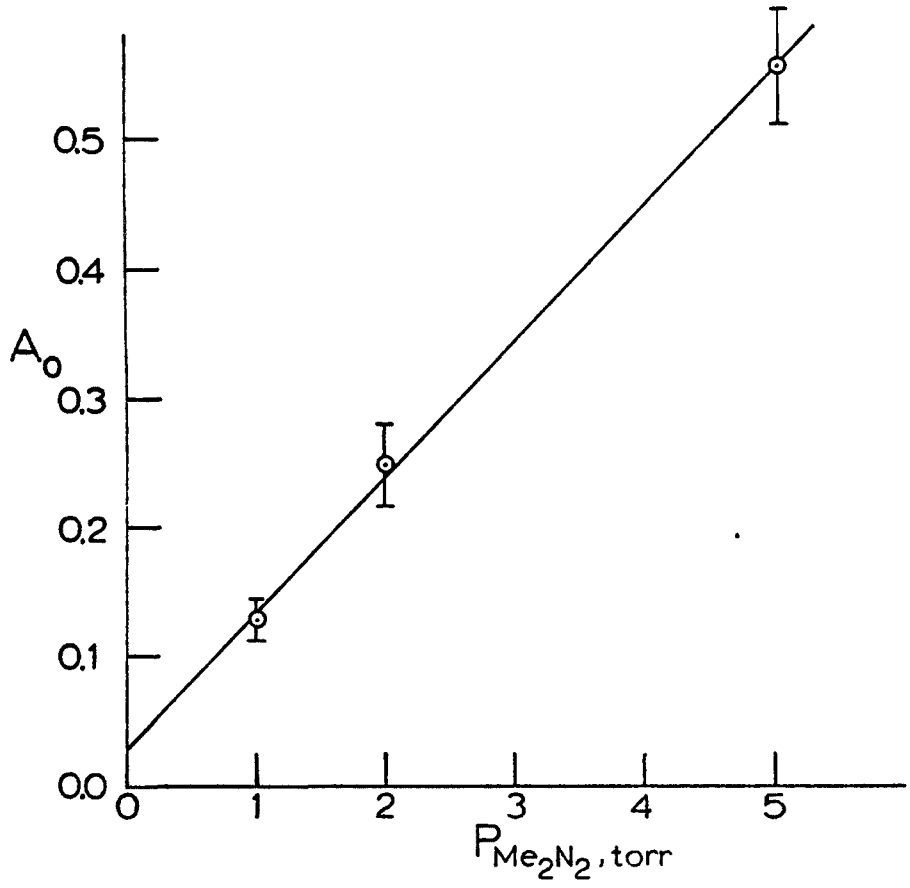

Figure 12. The measured initial absorbance of CH_3O_2 at 265 nm versus azomethane pressure used in the flash photolysis of Me_2N_2-O_2 (50 Torr) mixtures; path length, 633 cm.

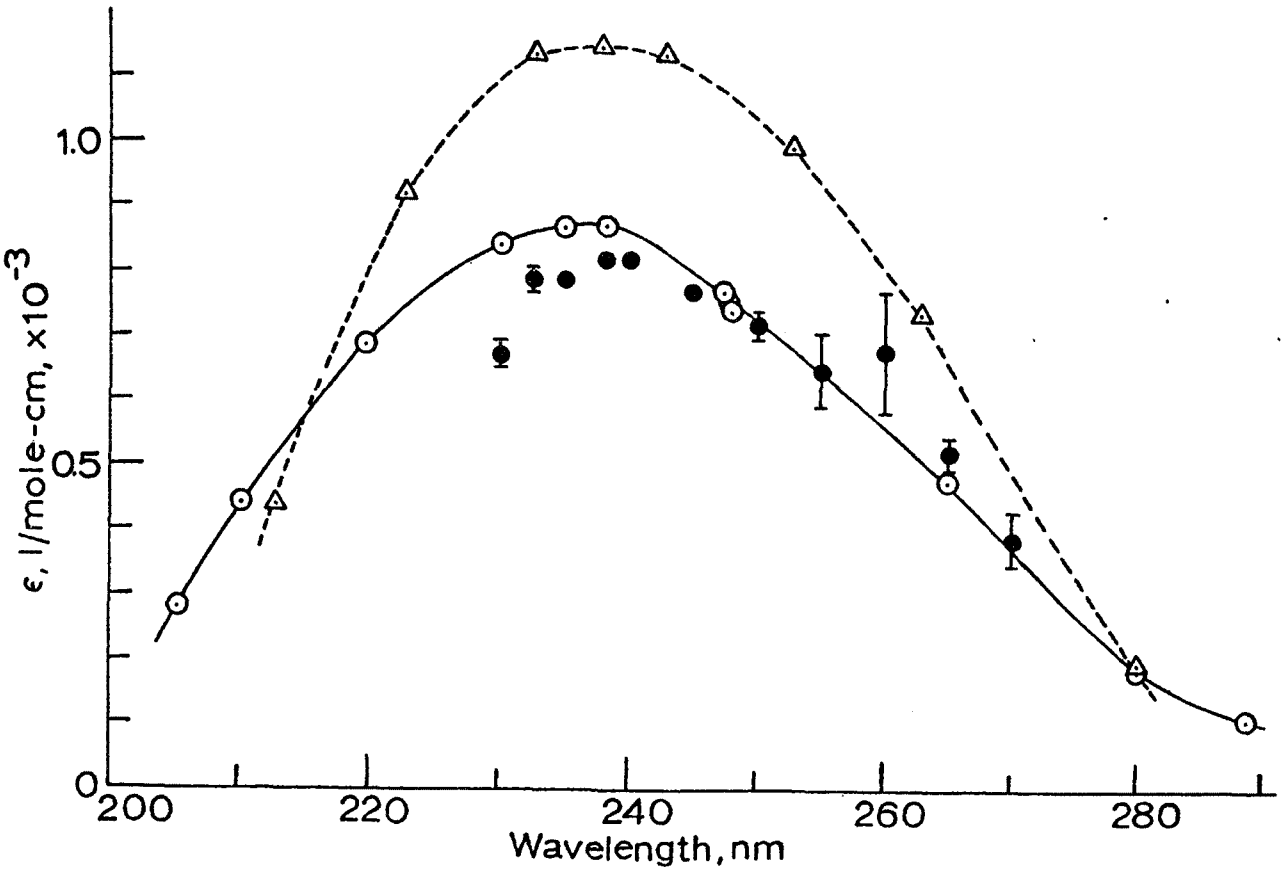

Figure 13. The gas phase extinction coefficients of CH_3O_2 as a function of wavelength, $\epsilon = \log_{10}(I_o/I)/l[CH_3O_2]$; data are from this work (closed circles); Parkes, et al.[5] (triangles); and Hochanadel, et al.[6] (open circles).

TABLE 12. ESTIMATES OF THE APPARENT RATE CONSTANT FOR THE REACTION 4, $2CH_3O_2$ PRODUCTS (4), DERIVED IN THE FLASH PHOTOLYSIS OF AZOMETHANE-O_2-N_2-MIXTURES[a]

$P_{Me_2N_2}$, torr	k_4, l/mole-sec, x 10^{-8}		$P_{Me_2N_2}$, torr	k_4, l/mole-sec, x 10^{-8}	
1.0	2.38		5.0[b]	3.24	
1.0	2.62		5.0[b]	2.97	3.08 ± 0.17
1.0	2.56	2.50 ± 0.16	5.0[b]	3.21	
1.0	2.28		5.0[b]	2.89	
1.0	2.64		5.0[c]	2.60	
2.0	2.49	2.45 ± 0.06	5.0[c]	2.40	
2.0	2.40		5.0[c]	2.14	2.36 ± 0.18
5.1	2.03		5.0[c]	2.24	
5.1	2.52		5.0[c]	2.40	
5.1	2.47		10.0	2.79	
5.1	2.10		10.0	2.72	
5.1	2.70		10.0	2.96	
5.1	2.88	2.53 ± 0.31	10.0	2.59	2.63 ± 0.25
5.1	2.36		10.0	2.31	
5.1	2.76		10.0	2.29	
5.1	2.65		10.0	2.74	
5.1	2.36				
5.1	3.00				

[a] P_{O_2} = 50 torr except for runs labeled b; temperature, 23 ± 3°C; CH_3O_2 absorbance followed at 265 nm.

[b] P_{O_2} = 20 torr.

[c] P_{O_2} = 50 torr, P_{N_2} = 645 torr.

the system at the lowest total pressure. However this seems unlikely to us, since a filtered flash was employed in this work and "hot" radical effects arising from either azomethane photolysis within its second absorption region ($\lambda < 2100$ Å) or from absorption by the CH_3O_2 primary product were eliminated here. There is no significant difference between k_4, estimates derived from the the experiments for which the total pressure of O_2 and added nitrogen ranged from 50 to 695 Torr. The average of the k_4, values from these experiments provides our best extimates of the apparent second order rate constant for CH_3O_2 loss: $k_{4'} = (2.5 \pm 0.3) \times 10^8$ l/mole-sec (23 ± 2^oC). This is in good agreement with the estimates of Hochanadel, et al.,[6] $k_{4'} = (2.3 \pm 0.3) \times 10^8$ l/mole-sec (22 ± 2^oC), Parkes, et al.,[5a] $k_{4'} = (1.3\text{-}2.6) \times 10^8$, and Parkes,[5b] $k_{4'} = (2.8 \pm 0.7) \times 10^8$ l/mole-sec (room temperature). In view of the differences in the absolute values of the extinction coefficients employed by each group of workers, it is somewhat surprising that the agreement between the results is this good.

Deviation from linearity of the plot of the reciprocal of the CH_3O_2 absorbance versus time was observed in this work at long times; this effect is also evident in the data of Figure 4 by Hochanadel, et al.[6] It seems unlikely to us that the effect is attributable to product interference or instrumental artifacts. It is conceivable that at long times where $[CH_3O_2]$ is low, reactions other than the bimolecular decay reaction (4) may occur. The possibility that the effect results from the reaction, $CH_3O_2 + CH_2O \rightarrow CH_3O_2H + HCO$, is not favored for several reasons. First, the magnitude of the deviation as seen in successive flashes of a given azomethane-O_2 mixture, is the same within the experimental error; one would expect about twice the deviation with the second flash if the reaction with CH_2O were the origin of the effect. Second, even if one assigns the rate constant for the CH_3O_2-CH_2O reaction at the unreasonably high value of 10^7 *l*/mole-sec, simulations show that this reaction could account for only a small part of the total effect seen. It appears to be more likely to us that the reaction (5) may lead to the effect:

$$CH_3O_2 + CH_3NNCH_3 \rightarrow \text{Product (A)} \qquad (5)$$

If we accept the mechanism of CH_3O_2 decay through reactions (4) and (5), then we expect the CH_3O_2 absorbance at time t, $\underline{A}_t$, to be given by relation (6):

$$\left[\ln \frac{1}{\underline{A}_t} + \frac{2k_{4'}}{\epsilon l}\left(\frac{1}{\underline{b}}\right)\right] = \ln\left[\frac{2k_{4'}}{\epsilon l}\left(\frac{1}{\underline{b}}\right) + \frac{1}{\underline{A}_o}\right] - \underline{b}t \qquad (6)$$

where $\underline{b} = [Me_2N_2]k_5$. Estimates of k_5, were derived from the data using relation (6). The function $2k_{4'}/\underline{\epsilon l}$ was determined from the slope of the linear portion of the $\underline{A}^{-1}$ versus time curve. An initial choice of $\underline{b}$ was made, and the term on the left of (6) was calculated for various times. The slope of the least squares fit of the plot of this term versus time was used to derive a new estimate of $\underline{b}$, and successive iterations of this procedure gave

the final "best" estimate of $\underline{b}$. From such procedures we derived the value for the rate constant for the apparent first order loss of CH_3O_2, k_5 = $(1.6 \pm 0.6) \times 10^5$ l/mole-sec. Further evidence for this reaction is presented in the next section.

Although the present data fit reasonably well the simple reaction scheme outlined, one should question whether the observed second order rate constant k_4, really applies to the bimolecular CH_3O_2 reaction 4 alone. The question arises since reactive CH_3O radicals are formed a fraction of the time, and ultimately HO_2 radicals are generated from these as well. Both radicals can remove CH_3O_2 in theory. It has been suggested by Heicklen and co-workers[7] that reaction (4) has three active product channels:

$$2CH_3O_2 \rightarrow 2CH_3O + O_2 \qquad (4a)$$

$$\rightarrow CH_2O + CH_3OH + O_2 \qquad (4b)$$

$$\rightarrow CH_3OOCH_3 + O_2 \qquad (4c)$$

They concluded that at 25°C about 43, 50, and 7% of the reaction occurs in (4a), (4b), and (4c), respectively. From studies of the products of the CD_3O_2 reactions they found 22, 60, and 18% of the reaction occurred by the steps analogous to (4a), (4b), and (4c), respectively. Parkes[5b] has estimated that $k_{4a}/(k_{4a} + k_{4b} + k_{4c}) \simeq 0.34$. Thus the reactive CH_3O radicals may be generated in 33 ± 10% of the reactive collisions between CH_3O radicals. It is necessary to investigate to what extent the subsequent CH_3O reactions may influence the estimates of k_4 in our system.

We expect the additional reactions (7-15) to occur following reaction (4a):

$$CH_3O + CH_3O_2 \rightarrow CH_2O + CH_3O_2H \qquad (7)$$

$$CH_3O + O_2 \rightarrow HO_2 + CH_2O \qquad (8)$$

$$CH_3O + CH_3O \rightarrow CH_3OH + CH_2O \qquad (9)$$

$$\rightarrow CH_3OOCH_3 \qquad (10)$$

$$CH_3O_2 + HO_2 \rightarrow CH_3O_2H + O_2 \qquad (11)$$

$$CH_3O + HO_2 \rightarrow CH_3OH + O_2 \qquad (12)$$

$$HO_2 + HO_2 \rightarrow H_2O_2 + O_2 \qquad (13)$$

$$CH_3O + MeN_2 \rightarrow \text{Product (B)} \qquad (14)$$

$$CH_3O_2 + \text{Product A (or B)} \rightarrow \text{Stable Products} \qquad (15)$$

The largest effect on the k_4 that we can expect from the occurrence of this sequence results for the peculiar circumstance that following CH_3O formation in reaction (4a), an additional CH_3O radical is always destroyed in either reaction 7 or 11. For this condition the measured second order rate constant k_4 for CH_3O decay may be greater than the true k_4 by a factor of 1.33 ± 0.10. We may estimate more accurately the magnitude of the effect expected using a computer simulation of the more complete reaction sequence. We have employed the following reasonable rate constant choices (l/mole-sec): $k_7 = (0.20)(k_4k_9)^{1/2} = 3.9 \times 10^8$ [7]; $k_9 = 1.5 \times 10^{10}$; $k_8 = 3.7 \times 10^5$ [8]; $k_{10} = 4.0 \times 10^9$ * ; $k_{11} = 1.0 \times 10^8$ or 4.6×10^8 + ; $k_{12} = 1.8 \times 10^{10}$ by analogy with the rate constant for the reaction $Cl + HO_2 \rightarrow HCl + O_2$ [12]; $k_{13} = 2.0 \times 10^9$ [13,14]; $k_{14} = 1.1 \times 10^5$, consistent with that suggested for the analogous reactions;[15] $k_5 = 8.2 \times 10^4$ (this work). In our simulations we have assumed further that each radical product of reactions (5) and (14) reacts at a non-limiting rate to remove another CH_3O_2 radical in (15) with $k_{15} = 1.0 \times 10^7$. The magnitude of k_4 was altered in the simulations so that the apparent second order rate constant for CH_3O_2 removal was equal to that observed experimentally ($k_4 = 2.5 \times 10^8$ l/mole-sec). Using the low and high extimates for k_{11} (1.0×10^8, 4.6×10^8), the simulations give $k_4 = 2.3 \times 10^8$ and 2.2×10^8, respectively. It is not clear which of these estimates is the more correct. In view of the low quantum yields of alkyl hydroperoxides seen in the recent RO_2 study of Alcock and Mile,[16] the lower estimate of k_{11} may be more nearly correct, and the apparent second order rate constant k_4 for CH_3O_2 loss may be only slightly larger than the true k_4. Thus we conclude $2.5 \times 10^8 \geq k_4 \geq 2.3 \times 10^8$ l/mole-sec. This conclusion is also consistent with the findings of Parkes [5b] that the observed values for k_4 are independent of the pressure of O_2 from 0.1 to 760 Torr in his experiments at relatively low intensities and 1 atm total pressure. Since the fraction of CH_3O radicals which would react by (8) would change greatly over this range of O_2 pressures, either CH_3O_2 loss in (7) and (11) is

---

*Estimated from the measured rate constant for the reverse of reaction (10) by Barker, et al.[8] and the appropriate equilibrium constant for $2CH_3O$ CH_3OOCH_3 estimated from ΔH^o data of Batt, et al.,[9] and S^o estimates of Benson.[10]

+These two estimates represent the range of values based upon the observed $R_{CH_3O_2H}/R_{CH_2O}$ ratios in experiments at high [O_2] in the study of Dever and Calvert,[11] 0.10, and Weaver, et al.,[7] 0.41, and a steady state treatment of the radical concentrations.

relatively unimportant, or the decrease in the rate of (7) in experiments at increasing [O_2] which must accompany the increased importance of the removal of CH_3O radicals by (8), must be accompanied by a completely compensating increase in the rate of the HO_2 reaction (11) with CH_3O_2. It seems more likely to us that the former expectation is more nearly correct. In any case the analysis points to the conclusion that our extimate of k_4 is an upper limit to the true k_4 value.

Estimate of the rate constant for the CH_3O_2-SO_2 reaction--

When SO_2 is present in the flash photolyzed azomethane-O_2 mixture the additional reaction of CH_3O_2 with SO_2 may occur:

$$CH_3O_2 + SO_2 \rightarrow \text{Product} \qquad (16)$$

Indeed in the SO_2 -containing mixtures we observed a suppression of the CH_3O_2 signal seen in otherwise identical runs but in the absence of SO_2. The study of this system by optical methods is limited to a very small range of added SO_2 concentrations since a light-scattering aerosol develops in experiments at pressures of SO_2 above about 0.2 Torr. Utilizing the simple reaction mechanism (1), (2), (4), (5), and (16) we expect the observed CH_3O_2 absorbance ($\underline{A}_t$) at time t to be given by relation (17):

$$\ln\left[\frac{1}{A_t} + \frac{2k_4'}{\epsilon l}\left(\frac{1}{b+c}\right)\right] = \ln\left[\frac{1}{\underline{A}_o} + \frac{2k_4'}{\epsilon l}\left(\frac{1}{b+c}\right)\right] + (\underline{b}+\underline{c})t \qquad (17)$$

Here $\underline{c} = [SO_2]k_{16}$, and $\underline{b} = [Me_2N_2]\,k_5'$. In a series of runs at constant [Me_2N_2], the value of $\underline{b} + \underline{c}$ was obtained, as in deriving $\underline{b}$ in relation (6), by an iterative Gaussian least squares treatment. These data are summarized in Table 13. A plot of $\underline{b} + \underline{c}$ versus P_{SO_2} should in theory be a straight line with slope = k_{16} and intercept = k_5 [Me_2N_2]. Such a plot, given in Figure 32, shows the expected linear dependence between the variables within the experimental error. From this we derive for the apparent second order rate constant for CH_3O_2 removal by SO_2, $k_{16}' = (6.4 \pm 1.4) \times 10^6$ l/mole-sec, and by azomethane, $k_5' = (1.8 \pm 0.2) \times 10^5$ l/mole-sec. The latter value is in reasonable accord with that derived from the azomethane-oxygen experiments described in the previous section ($k_5' = (1.6 \pm 0.6) \times 10^5$ l/mole-sec). If the reaction (5) involves the addition of CH_3O_2 to the N=N bond, then it is likely that a second CH_3O_2 radical will add by analogy with the observed tetramethyl hydrazine formation in the case of CH_3 addition to azomethane.[17] Thus we would estimate the true value of $k_5 \simeq k_5'/2 \simeq (8 \pm 3) \times 10^4$ l/mole-sec. There is no other estimate of this rate constant, and the rather indirect method which we have employed to derive k_5 here requires that it be accepted with considerable reservation. The rate constant for the analogous reaction of CH_3 addition to azomethane is somewhat smaller than k_5 at room temperature, 1.1×10^3 l/mole-sec.[17] Our estimate of k_5 is in line with the rough extimate for the analogous CH_3O_2 addition reaction with C_3H_6 for which $k \simeq 3 \times 10^4$ l/mole-sec.[1]

TABLE 13. RATE DATA FOR THE REACTION, CH_3O_2 + SO_2 PRODUCTS (16) and CH_3O_2 + Me_2N_2 PRODUCTS (5), DERIVED FROM THE FLASH PHOTOLYSIS OF AZOMETHANE-O_2-SO_2 MIXTURES[a]

p_{SO_2}, torr	$k_{16}[SO_2] + k_5[Me_2N_2]$, sec^{-1}	
0.122	80.6 ± 6.9	86.9 ± 5.5
	89.2 ± 4.2	
	90.9 ± 7.1	
0.10	68.5 ± 3.1	80.3 ± 19.0
	91.1 ± 7.6	
	67.2 ± 2.9	
	108.6 ± 8.4	
	65.9 ± 4.9	
0.080	58.0 ± 4.2	64.6 ± 7.5
	73.6 ± 4.3	
	73.8 ± 4.4	
	68.8 ± 5.6	
	61.3 ± 1.5	
	54.7 ± 1.2	
	62.7 ± 2.7	
	71.7 ± 2.7	
	57.0 ± 1.9	
0.060	55.4 ± 4.2	74.8 ± 17.1
	88.0 ± 2.7	
	80.9 ± 8.8	
0.040	68.2 ± 3.0	60.6 ± 7.8
	60.9 ± 2.6	
	52.6 ± 3.8	
0.020	53.4 ± 5.1	48.9 ± 6.4
	44.3 ± 4.4	

[a] $p_{Me_2N_2}$ = 5.0 torr; p_{O_2} = 50 torr; temperature, 23 ± 2°C; CH_3O_2 absorbance followed at 265 nm.

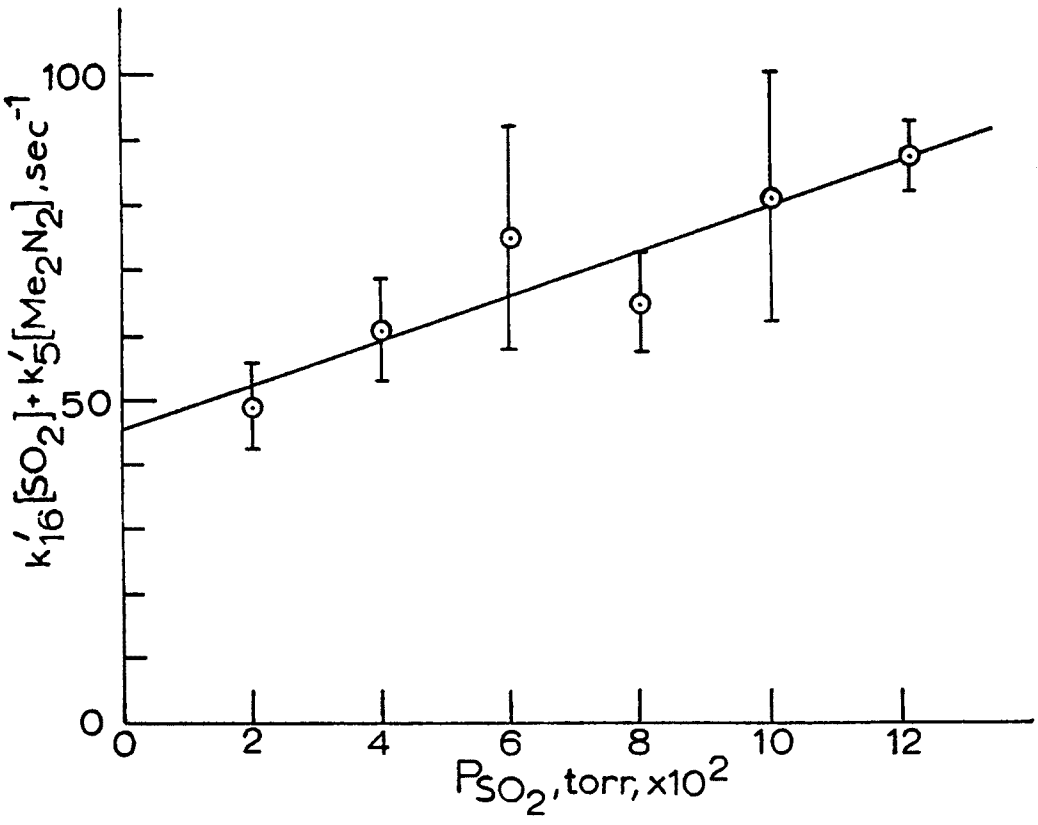

Figure 32. Plot of the rate constant function, $k'_{16}[SO_2] + k_{5'}[Me_2N_2]$ versus P_{SO_2}; data of Table II for flash experiments using $P_{Me_2N_2}$ = 5.0 Torr and P_{O_2} = 50 Torr; temperature, 23 ± 2°C.

The products of the reaction (16) have not been defined, but the measured, apparent rate constant for this reaction must represent a maximum, $k_{16} \leq (6.4 \pm 1.4) \times 10^6$ l/mole-sec. The reaction channels of reaction (16) may involve either O-atom transfer from CH_3O_2 (16a) or the addition of CH_3O_2 to SO_2 (16b):

$$CH_3O_2 + SO_2 \rightarrow CH_3O + SO_3 \qquad (16a)$$

$$\rightarrow CH_3O_2SO_2 \qquad (16b)$$

If (16a) is the major pathway, then the addition of the CH_3O product species to SO_2 may compete successfully with the reaction (8) and the other normal fates of this radical. If this occurs then there is a high probability that a second CH_3O_2 radical will be removed by reaction with the $CH_3OSO_2O_2$ species which may form subsequently. If (16b) is the major route then the initial $CH_3O_2SO_2$ radical, or the $CH_3O_2SO_2O_2$ species formed from it, may also react with an additional CH_3O_2 species in a non-rate limiting step. Hence it is likely that the true rate constant k_{16} is about one-half the measured apparent rate constant k_{16} . We suggest that the best present estimate of the rate constant for the elementary step (16) is: $(3.2 \pm 0.7) \times 10^6 \leq k_{16} \leq (6.4 \pm 1.4) \times 10^6$ l/mole-sec, and the lower estimate is probably most nearly correct.

This is the first reported estimate of k_{16}. It is interesting to compare it with that for the analogous reaction (17) studied by Payne, et al.:[18]

$$HO_2 + SO_2 \rightarrow HO + SO_3 \qquad (17)$$

They found $k_{17}/k_{13}^{1/2} = 11.8 \pm 1.7$ $(1/\text{mole-sec})^{1/2}$. Taking $k_{13} = 2.0 \times 10^9$ [13,14], $k_{17} \simeq 5.2 \times 10^5$ l/mole-sec. If we make the reasonable estimate that the differences in the entropies of activation for these reactions, $\Delta S_{16} - \Delta S_{17} \simeq 0.8$ eu, then the observed ratio of rate constants, $k_{17}/k_{16} \simeq 0.15$, corresponds to an activation energy difference, $E_{17} - E_{16} \simeq 1.4$ kcal/mole. This is a seemingly realistic result in view of the difference between the enthalpy changes for the two reactions: $\Delta H_{17} - \Delta H_{16} \cong 7.6$ kcal/mole. The measurable reactivity of the CH_3O_2 radical with SO_2 observed here is not typical of the other alkyperoxy radicals for which kinetic data are available. In additional studies in our laboratories, Whitbeck, et al.,[19] flash photolyzed 2,2'-azoisobutane-oxygen mixtures with and without SO_2. In this case there was no detectable effect of SO_2 addition on the very slow, second order $(CH_3)_3CO_2$ radical decay. It was estimated that $k_{18} \leq 4.4 \times 10^2$ l/mole-sec.

$$(CH_3)_3CO_2 + SO_2 \rightarrow (CH_3)_3CO + SO_3 \qquad (18a)$$

$$\rightarrow (CH_3)_3CO_2SO_2 \qquad (18b)$$

Calvert, et al.,[3] have concluded from a kinetic evaluation of the published kinetic data that the acetylperoxy radical is similarly unreactive toward SO_2 with $k_{19} \leq 7.8 \times 10^2$ l/mole-sec.

$$CH_3COO_2 + SO_2 \rightarrow CH_3CO_2 + SO_3 \quad (19a)$$

$$\rightarrow CH_3COO_2SO_2 \quad (19b)$$

Cox and Derwent[20] came to a similar conclusion in studies of peroxyacetyl nitrate and SO_2 mixtures; they suggested $k_{19} \leq 4.2 \times 10^2$ l/mole-sec. From computer simulations of the SO_2 oxidation in the sunlight-irradiated, NO_x-RH-polluted troposphere, Calvert, et al.,[3] concluded that the contribution to SO_2 oxidation from the branched peroxyalkyl and the acylperoxy radicals was negligible.

The results of the present work suggests that the reaction (16) of the CH_3O_2 radical may result in a significant rate of SO_2 oxidation in the highly polluted troposphere. Using the present estimate of k_{16} Calvert, et al.,[3] found that the contributions of SO_2 oxidation by HO, HO_2, and CH_3O_2 were about equal, and these accounted for a large fraction of the 4%/hr maximum rate of SO_2 oxidation observed in computer simulations. However the rates of oxidation of SO_2 within a reasonable clean troposphere were found to depend largely on the rate of HO-radical attack on SO_2.[3]

In view of the present results we suggest that the reaction (16) be included in the future quantitative considerations of the chemistry of the sunlight-irradiated, NO_x-RH-polluted troposphere, with $k_{16} \simeq 3.2 \times 10^6$ l/mole-sec.

REFERENCES

1. K.L. Demerjian, J.A. Kerr, and J.G. Calvert, Adv. Environ. Sci. Technol., 4, 1 (1974).

2. J.G. Calvert and R.D. McQuigg, Int. J. Chem. Kinet., Symp. 1, 113 (1975).

3. J.G. Calvert, F. Su, J.W. Bottenheim, and O.P. Strausz, "Mechanism of the Homogenous Oxidation of Sulfur Dioxide in the Troposphere", Proceedings Internation Symposium on Sulfur in the Atmosphere, Sept. 17-14, 1977, Dubrovnik, Yugoslavia, Atm. Environ., 12, 375 (1978).

4. R. Renaud and L.C. Leitch, Can. J. Chem., 32, 545 (1954).

5. (a) D.A. Parkes, D.M. Paul, C.P. Quinn, and R.C. Robson, Chem. Phys. Lett., 23, 425 (1973), (b) D.A. Parkes, Int. J. Chem. Kinet., 9, 451 (1977).

6. C.J. Hochanadel, J.A. Ghormley, J.W. Boyle, and P.J. Ogren, J. Phys. Chem., 81, 3 (1977).

7. J. Weaver, R. Shortridge, J. Meagher, and J. Heicklen, J. Photochem., 4, 109 (1975).

8. J.R. Barker, S.W. Benson, and D.M. Golden, Int. J. Chem. Kinet., 9, 31 (1977).

9. L. Batt, R.D. McCulloch, and R.T. Milne, Int. J. Chem. Kinet., Symp. 1, 441 (1975); L. Batt and R.T. Milne, Int. J. Chem. Kinet., 6, 945 (1974).

10. S.W. Benson, "Thermochemical Kinetics". 2nd Ed., Wiley, N.Y. 1976.

11. D.F. Dever and J.G. Calvert, J. Amer. Chem. Soc., 84, 1362 (1962).

12. M.T. Leu and W.B. Demore, Chem. Phys. Lett., 41, 121 (1976).

13. T.T. Paukert and H.S. Johnston, J. Chem. Phys., 56, 2824 (1972).

14. E.J. Hamilton, Jr., J. Chem. Phys., 63, 3682 (1975).

15. P. Gray, R. Shaw, and J.C.J. Thynne, Prog. Reaction Kinet., 4, 63 (1967).

16. W.G. Alcock and B. Mile, Comb. Flame, 24 125 (1975).

17. J.A. Kerr and J.G. Calvert, J. Phys. Chem., 69, 1022 (1965).

18. W.A. Payne, L.J. Stief, and D.D. Davis, J. Amer. Chem. Soc., 95, 7614 (1973).

19. M.R. Whitbeck, J.W. Bottenheim, S.Z. Levine, and J.G. Calvert, "A Kinetic Study of the CH_3O_2 and the $(CH_3)_3CO_2$ Radical Reactions by Kinetic Flash Spectroscopy", Abstracts 12th Informal Conference on Photochemistry, U.S. Bureau of Standards, Gaithersberg, Md., July, 1976, pp K1-1 to K1-5.

20. R.A. Cox and R.G. Derwent, "Laboratory Measurements of Free Radical Reactions Involving SO_2", paper presented at COST 61A Technical Symposium, Ispra, Nov. 15-17, 1976.

MECHANISM OF THE HOMOGENEOUS OXIDATION OF SULFUR DIOXIDE IN THE TROPOSPHERE

Introduction

The day has arrived when it is possible to include more than an empirically assigned, first order rate constant for SO_2 conversion to "sulfate" in our atmospheric transport and conversion models for SO_2. Atmospheric scientists have shown a new interest in the quantitative evaluation of the significance of the possible paths which convert SO_2 to its oxidation products, SO_3, H_2SO_4, NH_4HSO_4, $(NH_4)_2SO_4$, etc. It is now generally recognized that the development of scientifically sound and lasting strategy for "sulfate" aerosol control requires that we understand the nature of the various atmospheric reactants which oxidize SO_2, the chemical nature of the products formed in its reactions, the rates at which these reactions will occur in a given atmosphere, as well as the physical processes which transport these gases and aerosols about the atmosphere and those which remove them from it. Our group is engaged in the study of the kinetics and mechanisms of the elementary gas phase reactions which can lead to the homogeneous chemical transformation of SO_2 within the troposphere. The understanding of the homogeneous chemistry of SO_2 appears at first sight to be one of the simplest of the several important tasks faced by atmospheric scientists. The evaluation of the mechanisms and rates of the heterogeneous paths of SO_2 oxidation within the troposphere, the significance of surface removal processes, and the transport and diffusion processes are less amenable to laboratory study. However as we shall see in our discussions, there are as many unsolved problems as there are well defined areas of knowledge related to the homogeneous atmospheric chemistry of SO_2.

In any case the time is right to pause and take note of those aspects of the problem which appear to be well understood, as well as to reconsider some of the apparently conflicting observations, the unexplained results, and the alternative hypotheses which are so common in this area of research. The state of this science has improved greatly in recent years, and some new and definitive conclusions can be formulated from the wealth of existing information. In many cases where confusion remains, at least in our minds, we will offer our speculation on the possible resolutions. We hope that our prejudices will be readily distinguished from the experimental facts we quote and that they will serve to stimulate the reader to an active participation in the future solution to some of the many problems which remain unresolved.

We begin this study with an evaluation of the possible atmospheric reactions of the electronically excited SO_2 molecules. Next we consider the various possible reactions of the ground state SO_2 molecule with the reactive atmospheric components. From this we derive a set of our "preferred" values for the rate constants of the various elementary reactions. In the final section we attempt to evaluate the relative importance of the various homogeneous SO_2 conversion modes in the several major types of gaseous atmospheres which we encounter within the troposphere: the "clean" troposphere; the NO_x-hydrocarbon-CO-aldehyde-polluted regions of the troposphere; and finally the gaseous mixtures peculiar to the stack gas plumes.

Tropospheric Reaction of Electronically Excited Sulfur Dioxide

The Nature of the Reactive States in SO_2 Photochemistry--

The photochemistry of sulfur dioxide excited within the lower atmosphere provides in principle several reaction pathways which may lead to the oxidation or other transformation of SO_2. There has been general agreement in recent years that several other paths of SO_2 oxidation are probably much more rapid than those involving the excited states of SO_2. However this consensus was reached on the basis of a very limited body of information, and a new quantitative look at the reactions of excited SO_2 is in order. Some new insight into the rates and mechanisms of these reactions is possible from the results of recent studies.

Sulfur dioxide absorbs light within the ultraviolet region of the solar radiation incident within the troposphere. Its two near-ultraviolet absorption bands can be seen in Figure 33. The dashed curve represents the wavelength dependence of the relative quanta $cm^{-2}s^{-1}$ of the solar actinic flux incident near sea level at the solar zenith angle of 40^{o}(Peterson, 1976). The regions of overlap of these curves show that the absorption of solar energy by SO_2 in the troposphere occurs within the long wavelength tail of the relatively strong "allowed" band of SO_2 (2900-3300 Å) as well as within the much weaker "forbidden" band in the 3400-4000 Å region. Only when SO_2 is photoexcited at wavelengths less than 2180 Å is photodissociation of SO_2 energetically possible, $SO_2 + h\nu(\lambda < 2180\ Å) \rightarrow O(^3P) + SO(^3\Sigma^-)$. Thus solar radiation absorbed by SO_2 within the troposphere leads to non-dissociative, excited states of SO_2, and it is the nature of these states and their chemical reactions which concerns us here.

It is clear that excitation within the "forbidden" band of SO_2 leads to the population of the $SO_2(^3B_1)$ molecule, reaction I (Brand et al., 1970; Merer, 1963; Su et al., 1977a):

$$SO_2(X\ ^1A_1) + h\nu(3400 < \lambda < 4000\ Å) \rightarrow SO_2(^3B_1) \qquad (I)$$

Excitation of SO_2 within its first allowed absorption band leads to the generation of two emitting singlet species (Brus and McDonald, 1974; Su et al., 1977b), a very short-lived state which may be the $SO_2(^1A_2)$ species, and a long-lived state which is probably the $SO_2(^1B_1)$ molecule:

$$SO_2(X\ ^1A_1) + h\nu(2400 < \lambda < 3300\ Å) \rightarrow SO_2(^1A_2) \qquad (II)$$

$$\rightarrow SO_2(^1B_1) \qquad (III)$$

Collisional perturbation of these singlet states results in an additional efficient pathway for the formation of the $SO_2(^3B_1)$ species:

$$SO_2(^1A_2, ^1B_1) + M \rightarrow SO_2(^3B_1) + M \qquad (1)$$

In addition to these optically detectable or emitting states of SO_2, indirect chemical and physical evidence has led to the conclusion by some workers that two other non-emitting triplet states, presumably $SO_2(^3A_2)$ and $SO_2(^3B_2)$, are important in the photochemistry of SO_2. For example, see Cehelnik et al.

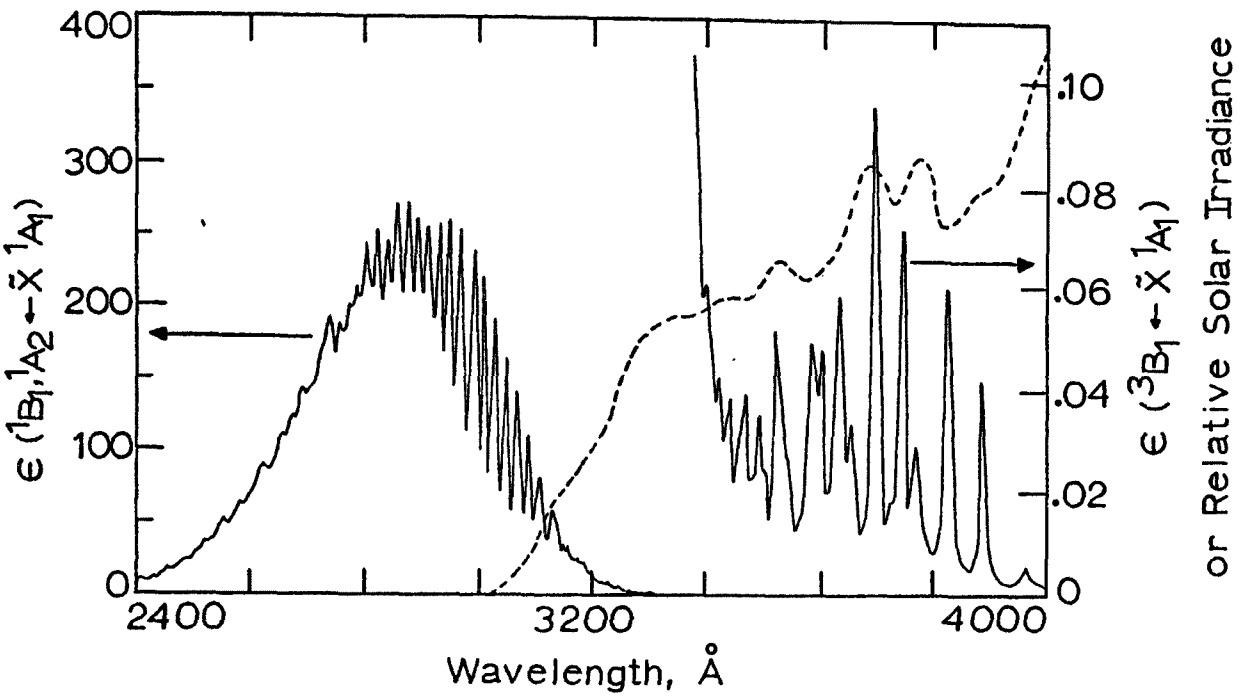

Figure 33. Comparison of the extinction coefficients of SO_2 within the first allowed band (left), the "forbidden" band (right), and a typical wavelength distribution of the flux of solar quanta (relative) at ground level (dashed curve).

(1971) and Kelley et al. (1976/77) and the references therein. However recent observations of Rudolph and Strickler (1977), Su et al. (1977c), and Su and Calvert (1977a) open to serious question this conclusion. It has been observed that the phosphorescent lifetime of the $SO_2(^3B_1)$ molecules at atmospheric pressure deviates markedly from the simple Stern-Volmer behavior characteristic of the low pressure regime. The lifetime of the $SO_2(^3B_1)$ molecule is about 2.4 times longer in one atmosphere of air than extrapolation of the low pressure quenching rate data would suggest. The phenomenon was first observed and rationalized by Rudolph and Strickler (1977) in terms of the saturation of the triplet-quenching at high pressures, an expectation of the recent theory of Freed (1976). A consideration of the details is not in order here, but a qualitative picture will suffice. The rate of triplet molecule quenching to ground state becomes independent of added gas pressure when the nearly degenerate rotational sublevels of the different singlet vibronic levels of the ground electronic state have collision-induced broadening which exceeds their spacings, so that the rovibronic manifold becomes an effective quasicontinuum. In the case of SO_2 this saturation occurs at pressures above about 100 Torr of added nitrogen gas. On the other hand, the chemical quenching of $SO_2(^3B_1)$ molecules follows second order kinetics as expected from theory, and for these cases, the low pressure bimolecular rate constants are applicable even at 1 atmosphere pressure. Su and Calvert (1977a) have reevaluated the previous high pressure studies of SO_2-CO and SO_2-C_2H_2 mixture photolyses with SO_2 excitation within the "forbidden" band. They have found that a simple mechanism involving only a single excited state of $SO_2(^3B_1)$ species, and the newly discovered saturation-quenching effect explain well all of the experimental data. Thus the postulate of Kelly et al. (1976/77) that the photolysis of SO_2-C_2H_2-added gas mixtures within the "forbidden" band involves the reactions of three different excited states of SO_2 appears to be incorrect.

When SO_2 in the atmosphere is excited within the first allowed band, it is unlikely that the newly formed $SO_2(^1B_1)$ and $SO_2(^1A_2)$ species will live to react with impurity molecules, since they are quenched by collisions with the major atmospheric gases so very efficiently (Su et al. 1977b). The possible chemical interaction of the excited singlet states with O_2 may occur in principle to generate an SO_4 excited triplet species or SO_3 and $O(^3P)$ in the reactions: $SO_2(^1A_2,^1B_1) + O_2(^3\Sigma_g^-) \rightarrow SO_4$ (or $SO_3 + O(^3P)$). However the near equality of the rates of quenching of each of the singlet states by the potentially reactive oxygen molecule and the "unreactive" nitrogen molecule argues against this possibility (Su et al., 1977b). The hypothetical energy transfer reaction, $SO_2(^1A_2,^1B_1) + O_2(^3\Sigma_g^-) \rightarrow SO_2(x\ ^1A_1) + O_2(^1\Delta_g,^1\Sigma_g^+)$, is spin forbidden and is probably unimportant also (Davidson et al., 1972/73). However the quenching does form the reactive $SO_2(^3B_1)$ molecule. Ground state molecules and conceivably some other unreactive or reactive species are formed in reaction 2.

$$SO_2(^1A_2,^1B_1) + M \rightarrow SO_2(X\ ^1A_1) + M \text{ (or other products)} \qquad (2)$$

Important for our considerations here is the intersystem crossing ratio, $k_1/(k_1 + k_2)$; this is the fraction of the originally excited singlet species

which form the reactive $SO_2(^3B_1)$ molecules. This fraction has been measured for various M species in experiments at relatively low pressures and rather short wavelengths of SO_2 excitation at 2650, 2662, and 2875 Å (Horowitz and Calvert, 1972a,b; Wampler et al., 1973a). In view of the recent saturation quenching effect observed with $SO_2(^3B_1)$, it may be inaccurate to use these low pressure data for our estimates for SO_2 in one atmosphere of air. The density of the vibronic states of the electronically excited singlet and triplet states of SO_2 are significantly less than that of the ground state SO_2 molecule at energies in the vibronic manifold equivalent to the excitation of the $SO_2(^3B_1)$ or the $SO_2(^1B_1, ^1A_2)$ states. As a result one would expect that the rate constants for the reaction 1 would not pressure saturate at as low a pressure as the rate constant for the reactions 2 and 3:

$$SO_2(^3B_1) + M \rightarrow SO_2(x\ ^1A_1) + M \qquad (3)$$

This may lead to an increase in the fraction of the singlets which are transformed into triplets when higher pressures of the quenching gases are employed in the photochemical experiments. Although there is now no direct experimental evidence of the saturation effect in singlet quenching, the possibility exists, and one must exercise caution in the use of the low pressure values for $k_1/k_1 + k_2$) to estimate $SO_2(^3B_1)$ formation rates in air at 1 atm. Furthermore recent observations of Su and Calvert (1977b) suggest that there is an increased efficiency of intersystem crossing for SO_2 singlet excitation at the longer wavelengths. Thus the extimates of $k_1/(k_1 + k_2)$ from the experiments in the 2650 to 2875 Å range are probably inappropriate for SO_2 excited singlets populated at the relatively long wavelengths present in the solar spectrum within the troposphere ($\lambda > 3000$ Å). Both the effects outlined would lead to the more efficient generation of $SO_2(^3B_1)$ on excitation of SO_2 at the long wavelength region of the first excited singlet band than would be anticipated from the low pressure, short wavelength data. In view of this discussion we should accept with great reservations the postulate of the participation of other reactive states of SO_2 to explain the "excess" triplet observed in singlet excited SO_2-containing systems at high pressures and long wavelength excitation.

The evidence at hand today appears to support the original contension of Okuda et al. (1969), that the $SO_2(^3B_1)$ molecule is the major photochemically active species formed in the photoexcitation of SO_2 even within the first allowed singlet absorption band at high pressures. Thus if we assume an average intersystem crossing ratio of 0.10 for M = SO_2 in Okuda's experiments, an effective first order rate constant for $SO_2(^3B_1)$ quenching to ground state of $1.5 \times 10^6 s^{-1}$ for 730 Torr of SO_2 (Su et al., 1977c), bimolecular chemical rate constant for reaction 4, $k_4 = 7.0 \times 10^{14}$ cm^3 molec^{-1}s^{-1} (Chung et al., 1975), $\Phi_{SO_3} = 0.026$ from the singlet excited SO_2, we derive the observed

$$SO_2(^3B_1) + SO_2 \rightarrow SO_3 + SO(^3\Sigma^-) \qquad (4)$$

value of $\Phi_{SO_3} = 0.08$ reported by Okuda et al. (1969).

We may update the earlier estimates of the rate of $SO_2(^3B_1)$ generation in the lower atmosphere (Sidebottom et al., 1972; Penzhorn et al., 1974a) utilizing all of the current data and alternative "reasonable" estimates of the effective intersystem crossing ratio. These data are shown in Table 14. The calculations have been made for two cases: (1) We have chosen the experimental values for the intersystem crossing ratio $k_1/(k_1 + k_2)$ determined by Wampler et al. (1973) from experiments at low pressures of added atmospheric gases; i.e., we assume that there are no pressure saturation or wavelength effects on the intersystem crossing ratio; see section A of Table 14. (2) In section B of the Table we have taken the intersystem crossing ratio as 0.11 at 1 atm for all of the atmospheric gases; i.e., we have assumed that pressure saturation effects and the longer solar wavelengths populating the excited singlet SO_2 resulted in an increase in the ratio observed at low pressures. It can be seen from the data of Table 14 that the maximum rate of excitation of $SO_2(^3B_1)$ for a solar zenith angle of 0^o (in a clean lower troposphere at 100% relative humidity) ranges from 4.7% hr^{-1} in the first case to 12.9% hr^{-1} in the second case.

The Nature and Rate of the $SO_2(^3B_1)$-O_2 Quenching Reaction--

Obviously the rate of excitation of $SO_2(^3B_1)$ does not alone establish the maximum rate of SO_2 photoreaction since quenching by the unreactive gases such as N_2, Ar, CO_2, and H_2O leads to no net chemical change. However there are several types of reactive species in the atmosphere which are of special interest as possible reactants with $SO_2(^3B_1)$ molecules. The first of these reactants is oxygen. Table 15 summarizes the estimated fractions of $SO_2(^3B_1)$ which will be quenched by the various atmospheric components; we have used the newly determined, pressure saturation quenching data in deriving these estimates. It should be noted that the quenching of $SO_2(^3B_1)$ by O_2 does not pressure saturate, as does that by N_2, Ar, CO_2, and other chemically unreactive gases. This points to some type of chemical action which accompanies this quenching action. The rate constant for the quenching of $SO_2(^3B_1)$ by O_2, $k = 1.6 \times 10^{-13} cm^3\ molec^{-1} s^{-1}$, is very similar to that observed for N_2, $k = 1.4 \times 10^{-13} cm^3\ molec^{-1} s^{-1}$ (Sidebottom et al., 1972). We have argued previously that this might indicate a physical, non-chemical, quenching of $SO_2(^3B_1)$ by O_2 as well as N_2. However if this were the case then, contrary to the fact, the saturation of $SO_2(^3B_1)$ quenching by O_2 would be seen at high O_2 pressures. From the data of Tables 14 and 15 we can estimate that the maximum rate of $SO_2(^3B_1)$-O_2 chemical interaction in air at 50% relative humidity (25^oC) and solar zenith angle of 40^o, will range from 1.8% hr^{-1} with mechanism A and 3.4% hr^{-1} with mechanism B of Table 14. Obviously these rates are very significant if chemical changes in SO_2 do result from the interaction.

We have considered previously several possible chemical changes which could occur in theory as $SO_2(^3B_1)$ is quenched by O_2 (Sidebottom et al., 1972). Ozone formation from excited $SO_2(^3B_1)$-O_2 interactions is possible through two reaction routes:

TABLE 14. ESTIMATED RATES OF $SO_2(^3B_1)$ GENERATION BY SOLAR RADIATION IN THE LOWER TROPOSPHERE*

Solar zenith angle, °	Rate by I† / Rate by II,1			Total rate of $SO_2(^3B_1)$ generation, % hr^{-1}		
rH:	0%	50%	100%	0%	50%	100%
A. Intersystem crossing ratios from the low pressure experiments at 2662 Å of Wampler et al. (1973); no singlet quenching saturation is assumed.§						
0	0.093	0.085	0.078	4.03	4.36	4.72
20	0.099	0.090	0.083	3. 4	3.96	4.28
40	0.125	0.113	0.104	2.59	2.84	3.06
60	0.243	0.220	0.203	1.04	1.15	1.22
80	0.569	0.515	0.475	0.18	0.18	0.18
B. Intersystem crossing ratios for all gases assumed to be 0.11 at 1 atm pressure.						
0		0.0273		12.9		
20		0.0289		11.7		
40		0.0365		8.2		
60		0.0710		3.1		
80		0.166		0.43		

*Percentage of singlet SO_2 quenching by the various atmospheric components at 25°C and 1 atm of air were estimated using k_{N_2}/k_{SO_2}= 0.326; k_{O_2}/k_{SO_2} = 0.321; k_{Ar}/k_{SO_2} = 0.275 (Su et al., 1977b); k_{H_2O}/k_{SO_2} = 1.2 (Mettee, 1969); Rates of direct excitation of $SO_2(^3B_1)$ and $SO_2(^1A_2, ^1B_1)$ are from Sidebottom et al. (1972).

†These rates refer to the reaction I and II followed by 1 of the text; the ratio gives the relative population of $SO_2(^3B_1)$ through absorption in the forbidden band to that for the first allowed band.

§The values used are: $k_1/(k_1 + k_2)$ = 0.033 (M = N_2); 0.030 (M = O_2); 0.025 (M = Ar); 0.09 (M= H_2O); 0.095 (M = SO_2).

TABLE 15. PERCENTAGE OF $SO_2(^3B_1)$-QUENCHING BY VARIOUS ATMOSPHERIC GASES IN AIR AT 25°C and 1 atm

Component	Percentage of $SO_2(^3B_1)$-quenching		
rH:	0%	50%	100%
Nitrogen	55.5	45.7	38.8
Oxygen	44.1	41.7	39.9
Argon	0.4	0.3	0.3
Water	0	12.2	21.1

$$SO_2(^3B_1) + O_2(^3\Sigma_g^-) \rightarrow SO_4(\text{cyclic}); \quad \Delta H \cong -79 \text{ kcal mole}^{-1} \qquad (5)$$

$$SO_4(\text{cyclic}) + O_2 \rightarrow SO_3 + O_3; \quad \Delta H \cong 15 \text{ kcal mole}^{-1} \qquad (6)$$

$$SO_2(^3B_1) + O_2(^3\Sigma_g^-) \rightarrow SO_3 + O(^3P); \quad \Delta H = -38 \text{ kcal mole}^{-1} \qquad (7)$$

$$O + O_2 \ (+M) \rightarrow O_3 \ (+M) \qquad (8)$$

Presumably the singlet SO_4(cyclic) species could be formed in 5 and stabilized by collisions. However even when vibrationally equilibrated, this species is rather unstable with respect to decomposition into SO_2 and O_2 (ΔH = 5 kcal mole^{-1}). A vibrationally rich SO_4 species initially formed in 5 could in principle react in 6, but the thermally stabilized SO_4 cannot react significantly to generate O_3 and SO_3 in reaction 6 at atmospheric temperatures, since this reaction is about 15 kcal mole^{-1} endothermic. See the following section for a more in depth consideration of possible roles of the SO_4 intermediate in atmospheric chemistry. Reaction 7 is energetically possible, but we would expect it to be slow since it involves an electron spin inversion. Indeed there is a great deal of experimental evidence which suggests the relative inefficiency of these reactions in pure air. Thus the photooxidation of dilute mixtures of SO_2 in oxygen leads to very small quantum yields of SO_2 oxidation to SO_3 or H_2SO_4. In those previous SO_2 photooxidation studies where a relatively large fraction of the gaseous mixture was SO_2 (Hall, 1953; Sethi, 1971; Allen et al., 1972a,b), it has been shown by Chung et al. (1975) that the quantum yield of SO_3 can be accounted for in large part through reactions 4 and 9:

$$SO_2(^3B_1) + SO_2 \rightarrow SO_3 + SO(^3\Sigma^-) \qquad (4)$$

$$SO + SO_3 \rightarrow 2SO_2 \qquad (9)$$

Relative large quantum yields of SO_3 formation in SO_2-rich mixtures are observed at short irradiation times (Skotnicki, 1975) or in flow systems in

which SO_3 is removed quickly and the reverse of reaction 9 is unimportant (Chung et al., 1975). In steady state photolyses in static systems, the rapid build up of the relatively low levels of SO_3 and SO is followed largely by reformation of SO_2 in 9. Much of the SO_3 (or H_2SO_4) which was formed in previous studies of the solar ultraviolet-irradiated SO_2-O_2 or SO_2-clean air mixtures probably was derived from the reaction 4 and bears no relation to the occurrence of the theoretically possible photooxidation steps 5 and 6 or 7 and 8. Several studies show that there is a small, but not insignificant rate of SO_3 (H_2SO_4) formation in very dilute SO_2-air mixtures; thus for typical solar intensities at ground level in clean air, the following SO_2 oxidation rates (at low [SO_2]) were estimated experimentally (% hr^{-1}): 0.65 (Cox and Penkett, 1970); 0.02-0.04 (Cox, 1972, 1973); < 0.1 (Junge, 1972); 0.7 (Kasahara and Takahashi, 1976); 0.000 (Friend et al., 1973).

Altwicker (1976) reported recently that the generation of small amounts of O_3 occurs in dilute SO_2-containing purified air samples irradiated in sunlight; for example, 1-3 pphm more ozone was developed in a pure air mixture with SO_2(3 ppm) after 40 min irradiation than was formed in the irradiation of a similar SO_2-free sample of purified air (0.6-1.0 pphm). His observations are interesting and in qualitative accord with the occurrence of the reaction sequences 5 and 6 and/or 7 and 8 at the rate of about 0.7% hr^{-1} or less. However further more detailed studies of the ozone formation in SO_2-air mixtures must be carried out before meaningful conclusions concerning the mechanism of O_3 generation in Altwicker's experiment can be established. However with the exception of Friend's observation, all of the present studies show a small, but not negligible, rate of the direct photooxidation of SO_2 occurs in pure air. Since it is so difficult to obtain pure air samples which have no small impurities of NO_x, O_3, RH, etc., one should not give great weight to the photooxidation experiments as proof of reactions 5 and 6 and/or 7 and 8 occurring. We conclude that the present data are consistent with an upper limit for the rate constants, $k_5 + k_7 = 3 \times 10^{-15} cm^3 molec^{-1} s^{-1}$.

At most a few percent of the $SO_2(^3B_1)$ quenching collisions with O_2 lead to SO_3. Thus some other "chemical" result must account for most of the quenching. Some further clues about this interaction can be had in consideration of the nature of the oxygen product formed in this process and the seemingly similar organic triplet molecule quenching by oxygen. It appears to us that the major chemical result of $SO_2(^3B_1)$-O_2 quenching encounters is likely energy transfer to generate excited singlet-O_2 species:

$$SO_2(^3B_1) + O_2(\ \Sigma_g^-) \rightarrow SO_2(X\ ^1A_1) + O_2(^1\Sigma_g^+) \qquad (10a)$$

$$\rightarrow SO_2(X\ ^1A_1) + O_2(^1\Delta_g) \qquad (10b)$$

The studies of the Abrahamson group (Davidson and Abrahamson, 1972; Davidson et al., 1972/73) have shown convincingly that reaction 10a occurs. The fraction of the reaction which leads to the alternative singlet states of O_2 is not now known. However the experimental data are not inconsistent with $k_{10a} + k_{10b} \cong 1.6 \times 10^{-13}$ $cm^3 molec^{-1} s^{-1}$, near the total quenching rate

constant for $SO_2(^3B_1)$ reacting with O_2. Support for this view is added from a comparison of these data with those obtained from organic triplet molecule quenching by O_2; in this case the analogous energy transfer reactions occur efficiently. In Figure 34 is shown a plot of the logarithm of the rate constants for the quenching of a series of organic triplet molecule by oxygen versus the energy difference between the first excited triplet and ground state of the various molecules ($E_{T_1} - E_{S_0}$). Data shown as open squares are from studies in benzene solvent; open circles are from hexane solutions (Patterson et al., 1970; Gijzeman et al., 1973a). Since these reactions at high $E_{T_1} - E_{S_0}$ values are not diffusion controlled, and non-polar solvents were employed, a comparison with gas phase rate constants should be meaningful. It is seen from the positions of the closed circles that our gas phase rate constant data for O_2-quenching of triplets of SO_2 and $(CH_3CO)_2$ follow well the trend observed with the other triplet molecules (Horowitz and Calvert, 1972; Sidebottom et al., 1972). Thus it seems most reasonable that the same triplet energy transfer mechanism invoked for organic triplet $M(T_1)$ quenching by O_2

$$M(T_1) + O_2(^3\Sigma_g^-) \rightarrow M(S_0) + O_2(^1\Sigma_g^+, {}^1\Delta_g) \qquad (11)$$

is descriptive of that for $SO_2(^3B_1)$ as well (Kawaoka et al., 1967; Kearns, 1971; Gijzeman and Kaufman, 1973; Gijzeman, 1974).

In summary the present data are consistent with singlet oxygen formation as the major result of $SO_2(^3B_1)$ quenching by O_2 ($k_{10a} + k_{10b} \cong 1.6 \times 10^{-13}$ cm^3 $molec^{-1}s^{-1}$), and the oxidation of SO_2 to SO_3 results at most a small fraction of the quenching collisions ($k_5 + k_7 = 3 \times 10^{15}$ cm^3 $molec^{-1}s^{-1}$).

The Nature and Rates of the $SO_2(^3B_1)$-Chemical Quenching Reactions with the Common Atmospheric Contaminants--

The extensive rate data related to $SO_2(^3B_1)$ quenching reactions points to some potentially significant chemical reactants with $SO_2(^3B_1)$ among the common air pollutants. Thus the very large rate constant for the quenching of the triplets with NO (1.2×10^{-10}cm $molec^{-1}s^{-1}$; Sidebottom, 1972) suggests come important chemistry at first sight. Although the possible reaction, $SO_2(^3B_1) + NO \quad SO(^3\Sigma^-) + NO_2$ is exothermic by 15 kcal $mole^{-1}$, there is no evidence that this chemical change or any other of significance occurs. N Nitric oxide has been found to quench efficiently the triplet excited states of many molecules. The lowest excited electronic state of NO, a $^4\pi$ state, lies 35,000 cm^{-1} above the ground state, so energy transfer from $SO_2(^3B_1)$ 25,766 cm^{-1} above $SO_2(X\ ^1A_1)$, is not a possible quenching mechanism here. However theoretical studies show that intersystem crossing of an excited triplet molecule ($^3M^*$) to its ground state (^1M) may be catalyzed by its interaction with nitric oxide (Gijzeman et al., 1973):

$$NO(^2\Pi) + {}^3M^* \rightarrow {}^2(M\text{-}NO) \rightarrow NO(^2\Pi) + {}^1M \qquad (12)$$

Gijzeman et al. (1973b) have observed a correlation between the magnitude of the rate constant for triplet molecule quenching by NO and the triplet-

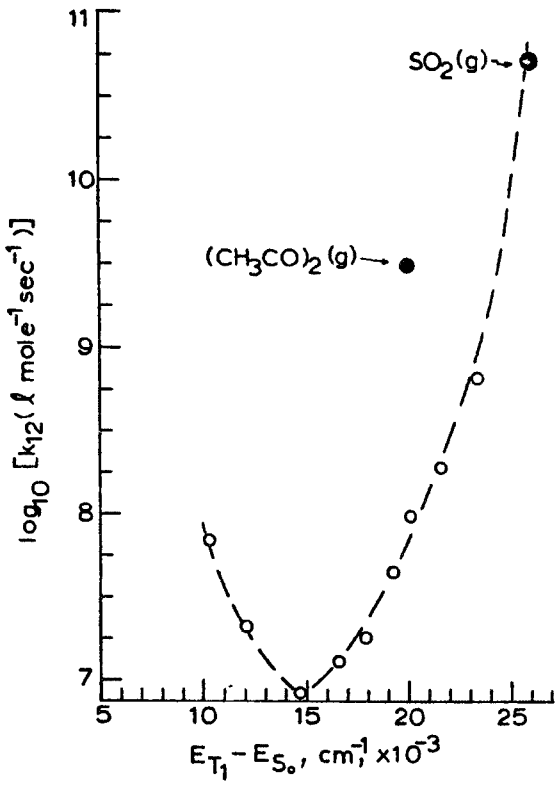

Figure 34. Relation between the rate constants for the triplet-quenching reaction with oxygen and the energy separation between the first excited triplet and the ground state of a series of molecules: aromatic triplets measured in hexane solution (squares), benzene solution (open circles) from Patterson et al. (1970) and Gijzeman et al. (1973a); $(CH_3CO)_2$ and SO_2 data from gas phase measurements (Horowitz and Calvert, 1972; Sidebottom et al., 1972).

ground state energy difference of the molecules; see Figure 35. The open circles are data from hexane solution studies of a variety of organic triplet molecules. They have suggested a theory which can rationalize this correlation in terms of reaction 12. Observe the magnitude of the quenching rate constant increases dramatically with $E_{T_1} - E_{S_0}$ value for energy separations greater than 1.5×10^4 cm^{-1}. This trend is just the opposite to that observed in Figure 2 and the O_2-quenching of triplets where the mechanism is electronic energy transfer to O_2. Our data from the gas phase studies of the quenching of SO_2 and biacetyl triplet molecules by NO are plotted in Figure 35 as closed circles. It is seen that these molecules follow the same trend observed for the organic triplet molecules. Thus it is probable that the net effect of of $SO_2(^3B_1)$ quenching by NO can be represented simply by reaction 13; no interesting net chemistry is expected here.

$$SO_2(^3B_1) + NO(^2\Pi) \rightarrow {}^2(SO_2\text{-}NO) \rightarrow SO_2(x\ ^1A_1) + NO(^2\Pi) \qquad (13)$$

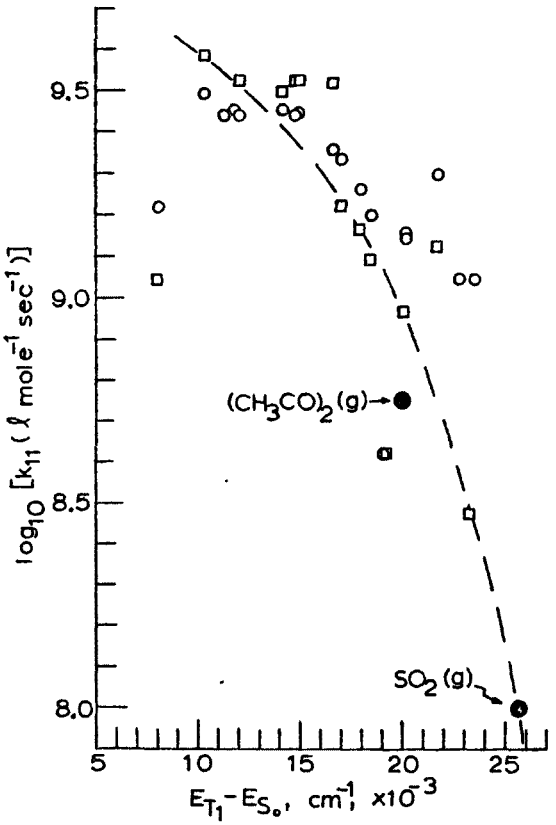

Figure 35. Relation between the rate constant for the triplet-quenching reaction with nitric oxide and the energy separation between the first excited triplet and the ground state of a series of molecules; aromatic triplets measured in hexane solutions (open circles) from Gijzeman et al. (1973b); $(CH_3CO)_2$ and SO_2 data from gas phase measurements (Horowitz and Calvert, 1972; Sidebottom et al., 1972).

Other potential atmospheric reactants with $SO_2(^3B_1)$ are SO_2, CO, C_2H_2, alkenes, and alkanes. The quenching rate constants for the "chemical" part of the reactions of $SO_2(^3B_1)$ with some representative impurity molecules and atmospheric components are summarized in Table 16. The $SO_2(^3B_1)$ can act as an oxidizing agent to form CO_2 from CO in reaction 14 (Cehelnik et al., 1971, 1974/74; Kelly et al., 1976/77; Jackson and Calvert, 1971; Wampler et al., 1972). Through some undefined intermediate product, CO is formed from C_2H_2 in reaction 15 (Kelly et al., 1976). The alkenes quench $SO_2(^3B_1)$ at rates which approach the collision frequency (Sidebottom et al., 1971; Wampler et al., 1973b). The quenching act appears to be the formation of a transient species resulting from the addition of SO_2 to the double bond of the alkene, reaction 16. This transient allows rotation about the bond, and its rapid dissociation leads to the cis-trans isomers of the alkene as the only net chemical effect of the quenching (Demerjian et al., 1974). Although light scattering aerosol is formed in the irradiated SO_2-alkene systems,

TABLE 16. THE $SO_2(^3B_1)$ "chemical" QUENCHING RATE CONSTANTS FOR VARIOUS ATMOSPHERIC COMPONENTS AND IMPURITY SPECIES IN THE OVERALL REACTIONS SHOWN

Reactant	Reaction		k, $cm^3 molec^{-1} s^{-1}$	Reference
Oxygen	(5,6)	$SO_2(^3B_1) + O_2 \rightarrow SO_4 \xrightarrow{O_2} SO_3 + O_3$	$<3 \times 10^{-15}$	See the text.
	(7)	$SO_2(^3B_1) + O_2 \rightarrow SO_3 + O(^3P)$		
	(10)	$SO_2(^3B_1) + O_2 \rightarrow SO_2 + O_2(^1\Delta_g^+, ^1\Sigma_g)$	$\sim 1.6 \times 10^{-13}$	Sidebottom et al.(1972)
Sulfur dioxide	(4)	$SO_2(^3B_1) + SO_2 \rightarrow SO_3 + SO(^3\Sigma^-)$	7.0×10^{-14}	Chung et al.(1975)
Nitric oxide	(13)	$SO_2(^3B_1) + NO(^2\Pi) \rightarrow {}^2(SO_2\text{-}NO) \rightarrow SO_2 + NO(^2\Pi)$	1.3×10^{-10}	Sidebottom et al.(1972)
Carbon monoxide	(14)	$SO_2(^3B_1) + CO \rightarrow SO(^3\Sigma^-) + CO_2$	4.3×10^{-15}	Jackson and Calvert(1971), Su and Calvert(1977a)
Acetylene	(15)	$SO_2(^3B_1) + C_2H_2 \rightarrow (?) \rightarrow CO + \text{other products}$	2.7×10^{-12}	Kelley et al.(1976), Su and Calvert(1977a)
cis-2-Butene	(16)	$SO_2(^3B_1) + \text{cis-}C_4H_8 \rightarrow {}^3(SO_2\text{-}C_4H_8) \rightarrow \text{trans-}C_4H_8$ / $\rightarrow \text{cis-}C_4H_8$	2.2×10^{-10}	Sidebottom et al.(1971), Demerjian and Calvert(1974)
Isobutane	(17)	$SO_2(^3B_1) + \text{iso-}C_4H_{10} \rightarrow HOSO + C_4H_9$	1.4×10^{-12}	Wampler et al.(1972), Badcock et al.(1971), Su and Calvert(1977b)

its formation appears to correlate best with the extent of SO_2 molecule quenching of $SO_2(^3B_1)$; it is thought to be SO_3 (or ultimately H_2SO_4) which causes the scattering observed following reaction 4 in the system. So although the alkenes quench $SO_2(^3B_1)$ with very high efficiency, the net trivial chemistry which results from this process is apparently of no importance to the removal or the chemical transformation of SO_2 in the atmosphere.

The alkanes quench $SO_2(^3B_1)$ reasonably effectively, and the magnitude of the quenching rate constant increases with decreasing strength of the C-H bonds and the increasing number of C-H bonds in the hydrocarbon (Badcock et al., 1971; Wampler et al., 1973b). The quenching act has been related to an H-atom abstraction by the $SO_2(^3B_1)$ molecule (Badcock et al., 1971; Penzhorn et al., 1975). Thus in the case of isobutane-SO_2 mixture photolysis, the measured chemical rate of quenching of $SO_2(^3B_1)$ to form sulfinic acids and other complex products is very nearly equal to the rate of $SO_2(^3B_1)$-isobutane quenching as measured by lifetime studies (Su and Calvert, 1977b).

$$SO_2(^3B_1) + \text{iso-}C_4H_{10} \rightarrow HOSO + C_4H_9 \qquad (17)$$

The enthalpy change which accompanies reaction 17 is about -22 kcal mole^{-1}, not very different from that for the analogous HO-radical reaction with isobutane (-26.6 kcal mole^{-1}). If the abstraction of an H-atom occurs by $SO_2(^3B_1)$-alkane interaction in the atmosphere, the ultimate result of the quenching likely will not be the formation of sulfinic acids or other products characteristic of the laboratory studies of SO_2-RH mixtures. Thus the HOSO and R radicals formed in the quenching reaction 18 will probably react with O_2, the dominant reactive species in the air. The HOSO radical may combine with oxygen and ultimately form SO_3 or H_2SO_4 by a reaction sequence such as the following:

$$SO_2(^3B_1) + RH \xrightarrow{(a)} HOSO + R \qquad (18)$$

$$HOSO + O_2 \rightleftharpoons HOSCO \xrightarrow{(b)} HO + SO_3$$

$$HOSCO \xrightarrow{(c)} HOS(=O)(=O)-O \xrightarrow{(+RH)} H_2SO_4 \qquad (d)$$

The overall enthalpy change for steps a and b above is about -25 kcal mole^{-1}; $\Delta H_c \cong -65$; $\Delta H_d \cong 40$ kcal mole^{-1}. Thus path d will not occur. It seems less likely to us that the HOSO will react with O_2 in the less exothermic step, $HOSO + O_2 \rightarrow SO_2 + HO_2$; $\Delta H \cong -6$ kcal mole^{-1}. The radical R formed in 18 will give RO_2, RO, aldehydes, etc., in subsequent reactions in the atmosphere. In view of these considerations, net photooxidation of SO_2 could result from the quenching of $SO_2(^3B_1)$ by alkanes.

The predicted rates of the various "chemical" quenching reactions of $SO_2(^3B_1)$ by impurity molecules in the atmosphere have been estimated for typical solar intensities encountered near ground level for a solar zenith

angle of about 40°. See Table 17. The hypothetical atmosphere contains 1 ppm of the different impurity molecules. Various amounts of SO_2 are chosen which range from 500 ppm, common to fresh stack gas emissions, to 0.05 ppm which is more representative of the levels of SO_2 present in ambient polluted air. The rates (ppm hr^{-1}) of all of the reactions shown are very slow. Even under the most favorable conditions which one might choose to enhance the importance of these reactions, the rates are far below those which we extimate for the reactions of HO, HO_2, etc., with these impurities and SO_2 in the lower troposphere.

From our considerations we may conclude that the major chemical effect of SO_2 photooxidation by sunlight within the polluted atmosphere is the generation of $O_2(^1\Sigma_g^+)$ and $O_2(^1\Delta_g)$ through reactions 10a and 10b; see Table 17. Although the expected rates are relatively large, the rates of this reaction are about 1/20th of those expected from excited NO_2 reactions with O_2 when NO_2 and SO_2 are at comparable levels (Jones and Bayes, 1971; Frankiewicz and Berry, 1972; Demerjian et al, 1974). The available data do support as well the occurrence of a slow, but not insignificant rate of SO_2 photo-oxidation, presumably through reactions 5 and 6 or 7 and 8. The maximum rates for these reactions correspond to less than 0.04% hr^{-1} (See Table17). The observed rates of SO_2 oxidation in air are much higher than this. Obviously the oxidation of SO_2 by reactions other than those involving photo-excited SO_2 molecules must be important within the troposphere. We shall consider these in the remaining sections of this study.

Reactions of Ground State SO_2 with Reactive Molecules and Transient Species in the Troposphere

Many reactive species present in the lower atmosphere are potentially important reactants for SO_2. A number of reviews have appeared in recent years in which the significance of the various reaction pathways for SO_2 conversion in the atmosphere has been estimated (Calvert and McQuigg, 1975; Davis and Klauber, 1975; Sander and Seinfeld, 1976; Bottenheim and Strausz, 1977; Levy et al., 1976). Some significant new rate data related to these systems have become available recently, and it is timely for us to re-evaluate the various potentially important SO_2 reaction pathways. The increasing use of these chemical reaction mechanisms in atmospheric models makes a careful, continuing reassessment of the kinetics and rate constant data related to these reactions of special value. We have summarized the thermochemistry of several reactions of interest in Table 18. Most of the reactions shown are exothermic, and from these energy considerations alone, they warrent our attention, since they could occur at significant rates at the temperatures of the troposphere. Also listed in Table 18 are our recommended values for the various rate constants. Each is expressed as an apparent second order rate constant which should be applicable for the pressures of the lower atmosphere near 25°C. In this section we will consider in some detail the data upon which each of these estimates were based.

The Reactions of $O_2(^1\Delta_g)$ and $O_2(^1\Sigma_g^+)$ with SO_2--

TABLE 17. THE THEORETICAL RATE OF REACTION (ppm hr^{-1}) OF SO_2 ($^3B_1$) REACTIONS WITH VARIOUS IMPURITY SPECIES AND O_2 IN A HYPOTHETICAL SUNLIGHT-IRRADIATED LOWER TROPOSPHERE*

Reactant molecule	Reaction No.		Initial [SO_2], ppm 500	50	5	0.5	0.05
NO	13	A†	3.1×10^{-2}	3.1×10^{-3}	3.1×10^{-4}	3.1×10^{-5}	3.1×10^{-6}
		B†	8.9×10^{-2}	8.9×10^{-3}	8.9×10^{-4}	8.9×10^{-5}	8.9×10^{-6}
CO	14	A	9.9×10^{-7}	9.9×10^{-8}	9.9×10^{-9}	9.9×10^{-10}	9.9×10^{-11}
		B	2.9×10^{-6}	2.9×10^{-7}	2.9×10^{-8}	2.9×10^{-9}	2.9×10^{-10}
C_2H_2	15	A	6.1×10^{-4}	6.1×10^{-5}	6.1×10^{-6}	6.1×10^{-7}	6.1×10^{-8}
		B	1.8×10^{-3}	1.8×10^{-4}	1.8×10^{-5}	1.8×10^{-6}	1.8×10^{-7}
cis-2-C_4H_8	16	A	5.0×10^{-2}	5.0×10^{-3}	5.0×10^{-4}	5.0×10^{-5}	5.0×10^{-6}
		B	1.5×10^{-1}	1.5×10^{-2}	1.5×10^{-3}	1.5×10^{-4}	1.5×10^{-5}
iso-C_4H_8	17	A	3.4×10^{-4}	3.4×10^{-5}	3.4×10^{-6}	3.4×10^{-7}	3.4×10^{-8}
		B	9.7×10^{-4}	9.7×10^{-5}	9.7×10^{-6}	9.7×10^{-7}	9.7×10^{-8}
SO_2	4	A	8.1×10^{-3}	8.1×10^{-5}	8.1×10^{-7}	8.1×10^{-9}	8.1×10^{-11}
		B	2.4×10^{-2}	2.4×10^{-4}	2.4×10^{-6}	2.4×10^{-8}	2.4×10^{-10}
O_2§	10	A	<9.0	$<9.0 \times 10^{-1}$	$<9.0 \times 10^{-2}$	$<9.0 \times 10^{-3}$	$<9.0 \times 10^{-4}$
		B	<17.0	<1.7	$<1.7 \times 10^{-1}$	$<1.7 \times 10^{-2}$	$<1.7 \times 10^{-3}$
	5,6,7	A	$<1.0 \times 10^{-1}$	$<1.0 \times 10^{-2}$	$<1.0 \times 10^{-3}$	$<1.0 \times 10^{-4}$	$<1.0 \times 10^{-5}$
		B	$<1.9 \times 10^{-1}$	$<1.9 \times 10^{-2}$	$<1.9 \times 10^{-3}$	$<1.9 \times 10^{-4}$	$<1.9 \times 10^{-5}$

*Calculated for a solar zenith angle of 40°, near sea level, 25°C, 1 atm, 50% relative humidity, and 1 ppm of the specific impurity molecule present; in the case of SO_2 impurity, the column heads represent the amount present.

†Values in rows labeled A were calculated for the case A in Table 1 and 50% relative humidity; values in rows labeled B were calculated for case B in Table 1.

§Oxygen is assumed to be present in each case at 156.7 Torr (air at 50% relative humidity, 25°C).

TABLE 18. ENTHALPY CHANGES AND RECOMMENDED RATE CONSTANTS FOR POTENTIALLY IMPORTANT REACTIONS OF GROUND STATE SO_2 and SO_3 MOLECULES IN THE LOWER TROPOSPHERE

Reaction	$-\Delta H°$,* kcal mole^{-1}(25°C)	k,† cm^{3}molec^{-1}s^{-1}
(19) $O_2(^1\Delta_g) + SO_2 \rightarrow SO_4$(biradical);$SO_4$(cyclic)	∿25;∿28	
(20) $O_2(^1\Delta_g) + SO_2 \rightarrow SO_3 + O(^3P)$	-13.4	$(3.9 \pm 0.9) \times 10^{-20}$
(21) $O_2(^1\Delta_g) + SO_2 \rightarrow O_2(^3\Sigma_g^-) + SO_2$	22.5	
(22) $O_2(^1\Sigma_g^+) + SO_2 \rightarrow SO_4$(biradical);$SO_4$(cyclic)	∿40;∿43	
(23) $O_2(^1\Sigma_g^+) + SO_2 \rightarrow SO_3 + O(^3P)$	1.7	6.6×10^{-16}
(24) $O_2(^1\Sigma_g^+) + SO_2 \rightarrow SO_2 + O_2(^1\Delta_g)$	15.1	
(25) $O(^3P) + SO_2$ (+M) $\rightarrow SO_3$ (+M)	83.3	$(5.7 \pm 0.5) \times 10^{-14}$
(26) $O_3 + SO_2 \rightarrow O_2 + SO_3$	57.8	$<8 \times 10^{-24}$
(27) $NO_2 + SO_2 \rightarrow NO + SO_3$	10.0	8.8×10^{-30}
(28) $NO_3 + SO_2 \rightarrow NO_2 + SO_3$	32.8	$<7 \times 10^{-21}$
(29) $ONOO + SO_2 \rightarrow NO_2 + SO_3$	∿30	$<7 \times 10^{-21}$
(30) $N_2O_5 + SO_2 \rightarrow N_2O_4 + SO_3$	24.6	$<4 \times 10^{-23}$
(31) $HO_2 + SO_2 \rightarrow HO + SO_3$	19.3	$>(8.7 \pm 1.3) \times 10^{-16}$
(32) $HO_2 + SO_2$ (+M) $\rightarrow HO_2SO_2$ (+M)	∿7	
(33) $CH_3O_2 + SO_2 \rightarrow CH_3O + SO_3$	∿27	$(5.3 \pm 2.5) \times 10^{-15}$
(34) $CH_3O_2 + SO_2 \rightarrow CH_3O_2SO_2$	∿31	
(35) $(CH_3)_3CO_2 + SO_2 \rightarrow (CH_3)_3CO + SO_3$	∿26	$<7.3 \times 10^{-19}$
(36) $(CH_3)_3CO_2 + SO_2 \rightarrow (CH_3)_3CO_2SO_2$	∿30	
(37) $CH_3COO_2 + SO_2 \rightarrow CH_3CO_2 + SO_3$	∿33	$<1.3 \times 10^{-18}$
(38) $CH_3COO_2 + SO_2 \rightarrow CH_3COO_2SO_2$	∿37	
(39) $HO + SO_2$ (+M) $\rightarrow HOSO_2$ (+M)	∿37	$(1.1 \pm 0.3) \times 10^{-12}$
(40) $CH_3O + SO_2$ (+M) $\rightarrow CH_3OSO_2$ (+M)	∿24	$\sim 6 \times 10^{-15}$
(41) 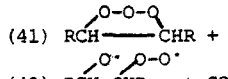 $+ SO_2 \rightarrow 2RCHO + SO_3$	∿89	----------
(42) 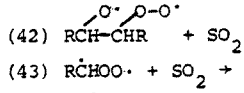 $+ SO_2 \rightarrow 2RCHO + SO_3$	∿103	----------
(43) $R\dot{C}HOO\cdot + SO_2 \rightarrow RCHO + SO_3$	∿98	$\frac{k_{43a}}{k_{43}} \cong 6 \times 10^{-5}$
(43a) $R\dot{C}HOO\cdot + H_2O \rightarrow RCOOH + H_2O$	∿147	
(44) 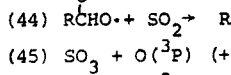 $+ SO_2 \rightarrow RCHO + SO_3$	∿52	----------
(45) $SO_3 + O(^3P)$ (+M) $\rightarrow SO_4$(biradical);SO_4(cyclic)	∿38;∿41	$\sim 7 \times 10^{-13}$
(46) $SO_3 + O(^3P)$ (+M) $\rightarrow SO_2 + O_2$	35.9	
(47) $SO_3 + H_2O \rightarrow H_2SO_4$	24.6	$(9.1 \pm 2.0) \times 10^{-13}$

*Enthalpy change estimates were derived from the data of Benson(1976,1977), O'Neal

The quenching reactions of $O_2(^1\Delta_g)$ and $O_2(^1\Sigma_g^+)$, reactions 19 through 24, have been studied quantitatively in recent years. Penzhorn et al. (1974) estimated the total quenching rate constant for $O_2(^1\Delta_g)$ by SO_2, $k_{19} + k_{20} + k_{21} = (3.9 \pm 0.9) \times 10^{-20} cm^3 molec^{-1} s^{-1}$.

$$O_2(^1\Delta_g) + SO_2 \quad SO_4(\text{biradical}; SO_4(\text{cyclic}) \tag{19}$$

$$O_2(^1\Delta_g) + SO_2 \rightarrow SO_3 + O(^3P) \tag{20}$$

$$O_2(^1\Delta_g) + SO_2 \rightarrow O_2(^3\Sigma_g^-) + SO_2 \tag{21}$$

The endothermicity and spin inversion of the possible reaction 20 excludes it from further consideration. The possible formation of the transient SO_4 species in reaction 19 may account for at least a portion of the total quenching reaction observed. Although many researchers have invoked the intermediate SO_4 in their considerations of SO_2 photooxidation since this suggestion was first made by Blacet (1952), only recently has any rather direct evidence for the existence of the SO_4 intermediate species been observed. The infrared kinetic studies of the $O(^3P)$-SO_3 reaction in the gas phase by Daubendiek and Calvert (1972, 1977) gave strong indirect evidence that the SO_4 intermediate was involved in the formation of transient molecules S_3O_9 and S_3O_8 observed in their system. Kugel and Taube (1975) have prepared an SO_4 species in CO_2(s) and Ar(s) matrices at 78° and 15°K, respectively, through the action of O-atoms on SO_3. It is probably significant that Kugel and Taube saw no SO_4 formation when SO_2 was irradiated with 2537 Å in an O_2 matrix at 15°K. Presumably $O_2(^1\Delta_g, {}^1\Sigma_g^+)$ would be formed by interaction of the adjacent partners, $SO_2(^3B_1)$-O_2 under these circumstances, and reactions such as 19 or 22 could then occur. Neither of these reactions appear to be important, and the mechanism of deactivation of $O_2(^1\Delta_g)$ by SO_2 remains unclear. It probably involves no chemical change in the SO_2 molecule, but only electronic relaxation occurs as in 21. In any case for the usual steady state levels of $O_2(^1\Delta_g)$, about 10^8 molec cm^{-3}, which we might anticipate in a typical polluted urban atmosphere (Demerjian et al., 1974), the maximum rate of quenching by SO_2 amounts to an insignificant, 1.4×10^{-6}% hr^{-1}.

Kear and Abrahamson (1974/75) determined the rate constant for the quenching of $O_2(^1\Sigma_g^+)$ by SO_2 to be: $k_{22} + k_{23} + k_{24} = 6.6 \times 10^{-16} cm^3$ $molec^{-1}$ s^{-1}.

$$O_2(^1\Sigma_g^+) + SO_2 \rightarrow SO_4(\text{biradical}); SO_4(\text{cyclic}) \tag{22}$$

$$O_2(^1\Sigma_g^+) + SO_2 \rightarrow SO_3 + O(^3P) \tag{23}$$

$$O_2(^1\Sigma_g^+) + SO_2 \rightarrow SO_2 + O_2(^1\Delta_g) \tag{24}$$

The rate of $O_2(^1\Sigma_g^+)$ attack on SO_2 in the lower atmosphere must be very low also, about 1.4×10^{-7}% hr^{-1}, for typical values of $[O_2(^1\Sigma_g^+)] = 6 \times 10^2$ molec cm^{-3} (Demerjian et al., 1974). Thus we can conclude that the rate of singlet oxygen reactions with SO_2 in the lower atmosphere is insignificant, and we may confidently neglect them in our further considerations.

The Reaction of $O(^3P)$ with SO_2 --

The earlier kinetic work on the reaction 25 has been reviewed by Schofield (1973), Hampson and Garvin (1975), and Westenberg and deHaas (1975a).

$$O(^3P) + SO_2 \ (+M) \rightarrow SO_3 \ (+M) \qquad (25)$$

From the data available in 1973 Schofield's choice of constants gave $k_{25} = (1.3 \pm 1.3) \times 10^{-13}$ cm^3 $molec^{-1}s^{-1}$ for the apparent second order constant at 1 atm of N_2 (25°C). Hampson and Garvin picked the value of Davis et al. (1974a) as their preferred rate constant: $k_{25} = 2.0 \times 10^{-14}$ cm^3 $molec^{-1}s^{-1}$ (1 atm N_2, 25°C). Westenberg and deHaas (1975a) have concluded, however, that most of the earlier estimates of k_{25} which were based upon $O(^3P)$ disappearance rate are too high by a factor of two. Their recent findings show that the reaction, $SO_3 + O(^3P) \rightarrow SO_2 + O_2$, is so very fast that a second O-atom loss is expected to occur almost every time the reaction 25 occurs for the conditions employed in many of the studies. From their extimates, $k_{25} = (4.9 \pm 0.2) \times 10^{-14}$ cm^3 $molec^{-1}s^{-1}$ for M = N_2 at 1 atm, 25°C. The only studies of k_{25} with O_2 as the third body come from the work of Mulcahy et al. (1967); correcting their estimate for the occurrence of reaction 46, in accord with the Westenberg and deHaas suggestion, we derive $k_{25} = (9.2 \pm 1.7) \times 10^{14}$ for M = O_2 (1 atm, 25°C). Combining the best estimates for M = N_2 and M = O_2, we derive, $k_{25} = (5.7 \pm 0.5) \times 10^{-14}$ cm^3 $molec^{-1}s^{-1}$, M = air (1 atm, 25°C). The estimate which we have chosen is in reasonable accord with that observed by Atkinson and Pitts (1974) using N_2O as the third body: $k_{25} = 7.6 \times 10^{-14}$ cm^3 $molec^{-1}s^{-1}$ at 1 atm, 25°C; the greater number of internal degrees of freedom of N_2O than for N_2 and O_2 would result in a somewhat higher value of k_{25} for M = N_2O. Our present estimate is considerably higher than that of Davis et al. (1974) with M = N_2; the peculiarly high efficiency of SO_2 as M which was found by Davis et al. may have resulted from an overcorrection for the contribution of the reaction, $O(^3P) + SO_2 + SO_2 \rightarrow SO_3 + SO_2$, to the total rate measured in the N_2-SO_2 mixtures.

Our estimate of k_{25} coupled with a fairly normal $[O(^3P)]$ for a sunlight-irradiated, NO_x-polluted, lower troposphere, 2×10^5 molec cm^{-3}, the anticipated oxidation rate for SO_2 by reaction 25 is about 1.2×10^{-2}% hr^{-1}. Thus we expect reaction 25 to be relatively unimportant for the conditions normally encountered in the lower troposphere. We should retain this

reaction in our simulations, however, since it is important, at least in theory, during the early stages of stack gas dilution.

The O_3-SO_2 Reaction--

In view of the great exothermicity of reaction 26, it is surprising slow; the upper limit on its rate constant has been set by Davis et al. (1974b) as $k_{26} < 10^{-22}$ and by Daubendiek and Calvert (1975) as $k_{26} < 8 \times 10^{-24} cm^3$ molec^{-1}s^{-1}.

$$O_3 + SO_2 \rightarrow SO_3 + O_2 \qquad (26)$$

Using our upper limit estimate of k_{26} and an $[O_3] = 5 \times 10^{12}$ molec cm^{-3}, typical of photochemical smog in a highly polluted atmosphere, it can be shown that the SO_2 oxidation rate through reaction 26 will be less than 1.4×10^{-5} % hr^{-1}, truly unimportant for our further consideration.

The Reactions of the Oxides of Nitrogen with SO_2--

The extrapolation of the high temperature rate data for the NO_2-SO_2 reaction 27 from Boreskov and Illarionov (1940) leads to the estimate, $k_{27} = 8.8 \times 10^{-30}$ cm^3 molec^{-1}s^{-1} for 25°C.

$$NO_2 + SO_2 \rightarrow NO + SO_3 \qquad (27)$$

Data of Daubendiek and Calvert (1975) and Davis and Klauber (1975) give $k_{28} < 7 \times 10^{-21}$ and about 10^{-21}, respectively; these workers also report $k_{30} < 4 \times 10^{-23}$ and about $10^{-23} cm^3$ molec^{-1}s^{-1}, respectively.

$$NO_3 + SO_2 \rightarrow NO_2 + SO_3 \qquad (28)$$

$$N_2O_5 + SO_2 \rightarrow N_2O_4 + SO_3 \qquad (30)$$

For typical concentrations of NO_2 (5×10^{12} molec cm^{-3}; 0.20 ppm), the concentrations of NO_3 and N_2O_5 which are expected in heavy photochemical smog are about 2.5×10^7 and 2.5×10^9 molec cm^{-3}, respectively. Thus the rates of attack on SO_2 by NO_2, NO_3, and N_2O_5 should be of the order of: 1.6×10^{-11}, 6.3×10^{-8}, and 3.6×10^{-8}% hr^{-1}. The suggestion of the probable importance of NO_3 in atmospheric reactions of smog regularly reappears (Stephens and Price, 1972; Wilson et al., 1972; Louw et al., 1973). However it seems unlikely that these reactions can be an important source for oxidation oxidation of SO_2 during the daylight hours. Hov et al. (1977) have made an important point for consideration here; during the nighttime hours the chemistry of NO_3 may become significant since its major formation reaction ($NO_2 + O_3 \rightarrow NO_3 + O_2$) is not strongly reduced in rate at night, while the rate of its major loss reaction during the day ($NO_3 + NO \rightarrow 2NO_2$) is lowered at night due to the decline in the [NO]. However the rates of attack on SO_2 should remain relatively unimportant even under these conditions.

The possible reactant ONOO, the intermediate species formed by the $NO-O_2$ bimolecular interaction, is presumably in equilibrium with NO and O_2 in air:

$$NO + O_2 \rightleftarrows ONOO \qquad (48)$$

From the data of Benson (1976) we may estimate that the [ONOO]/[NO] ratio in air at 1 atm and 25°C is about 0.029. If the rate constant for reaction 29 is near equal to that for the analogous reaction 28 of the symmetrical NO_3 species which it parallels in enthalpy change, then for the [NO] = 5×10^{12}, [ONOO] = 1.5×10^{11} molec cm^{-3}, and the extimated SO_2 oxidation rate by reaction 29 will be less than 3.8×10^{-4}% hr^{-1}.

$$ONOO + SO_2 \rightarrow NO_2 + SO_3 \qquad (29)$$

In summary, current data rule out the significant contribution of all of the oxides of nitrogen (NO_2, NO_3, ONOO, N_2O_5) to the oxidation of SO_2 within the lower troposphere.

The HO_2-SO_2 Reactions--

The study of Payne et al. (1973) provides the only experimental estimate of reaction 31 of which we are aware. It was based upon a photochemical competitive, $^{18}O_2$-labeling technique in which rate measurements of reaction 31 versus reaction 49 were made:

$$HO_2 + SO_2 \rightarrow HO + SO_3 \qquad (31)$$

$$2HO_2 \rightarrow H_2O_2 + O_2 \qquad (49)$$

They derived the estimate $k_{31}/k_{49}^{1/2} = (4.8 \pm 0.7) \times 10^{-10}$ $(cm^3 molec^{-1} s^{-1})^{1/2}$; taking the then preferred value of $k_{49} = 3.3 \times 10^{-12}$ cm^3 $molec^{-1} s^{-1}$ (Baulch et al., 1972), they extimated $k_{31} = (8.7 \pm 1.3) \times 10^{-16}$ cm^3 $molec^{-1} s^{-1}$. The error limits shown are those inherent in the measurement of the rate constant ratio alone. The uncertainty in k_{49} is an additional source of error. Thus Hampson and Garvin chose $k_{49} = 5.6 \times 10^{-12}$ at 25°C from a review of the rate data available in 1975, while Lloyd (1974) chose $k_{49} = 3.2 \times 10^{-12}$ cm^3 $molec^{-1}$ s^{-1} at 25° in his evaluation. A brief review of the estimates of k_{49} is important here in that this value determines our k_{31} estimate through the measured ratio, $k_{31}/k_{49}^{1/2}$.

The first extimate of k_{49} was made by Foner and Hudson (1962); they found $k_{49} \cong 3 \times 10^{-12}$ $cm^3 molec^{-1} s^{-1}$ in a fast-flow, mass spectrometric method of HO_2 detection. The later measurements of Paukert and Johnston (1972) and Hockanadel et al. (1972), based upon ultraviolet detection of HO_2, gave $k_{49} = 3.65 \times 10^{-12}$ and 9.58×10^{-12} $cm^3 molec^{-1} s^{-1}$, respectively,

at 25°C. Hamilton (1975) noted that the major difference between the reactant systems employed by Paukert and Johnston and Hochanadel et al. was the presence of H_2O vapor (21 Torr) in the latter work; no H_2O was present in the former study. He reinvestigated the reaction 49 using varied amounts of H_2O vapor in a 1.5 MeV electron pulsed gaseous mixture of H_2 (2 atm) and O_2 (5 Torr). He followed HO_2 by uv-absorption spectroscopy. Indeed he found that the k_{49} was sensitive to the pressure of H_2O vapor present; using Paukert and Johnston's absorption coefficient for HO_2 for experiments at $P_{H_2O} = 0$, he derived a value, $k_{49} = 3.15 \times 10^{-12}$ $cm^3 molec^{-1} s^{-1}$, in excellent agreement with that of Paukert and Johnston. In experiments with added water the k_{49}/ϵ_{HO_2} values derived were near equivalent to those of Hochanadel et al. In view of these results Hamilton and Naleway (1976) have proposed that a complex between water and HO_2 radicals forms in the H_2O-containing mixtures:

$$HO_2 + H_2O \rightleftarrows HO_2 \cdot H_2O \qquad (50)$$

The apparent increase in rate constant for reaction 49 with increasing H_2O seemed to result from the occurrence of the more rapid reaction 51 in addition to 49:

$$HO_2 + HO_2 \cdot H_2O \rightarrow H_2O_2 + O_2 + H_2O \qquad (51)$$

They estimated the thermodynamic properties of the $HO_2 \cdot H_2O$ species theoretically, and noted that the ratio $[HO_2 \cdot H_2O]/[HO_2]$ was equal to about 0.037 in air at 100% relative humidity (25°C). About 3.5% and 1.8% of the HO_2 radicals in the atmosphere at 100 and 50% relative humidity, respectively, are in the complex at 25°C. The observations of Hamilton and Naleway introduce a new and probably significant complication into the already horrendous problems of the atmospheric scientist who desires to simulate the rates of chemical changes in the troposphere. If the interpretation of Hamilton and Naleway is correct as outlined, then modelers should employ a value of k_{49} which varies with the humidity as well as the temperature. We have used the estimates of Hamilton and Naleway to calculate the fraction of the HO_2 which will be in the form of the complex for various humidities and temperatures; see Figure 36. Although the amount of H_2O in the air at a given relative humidity rises exponentially as the temperature is increased, the stability of the complex decreases somewhat with increasing temperature. The net result seen in Figure 36 is that there is small increase in the fraction with increasing temperature (constant relative humidity). Although about 1% of the HO_2 is expected to be complexed with H_2O at 0°C and 50% relative humidity, about 4.5% is complexed at 40°C and 100% relative humidity. The immediate significance of these observations for our purposes is the effect on the choice of value for k_{49} which should be used with the data of Payne et al. in deriving k_{31}. Note that 20 Torr of H_2O vapor was employed in all of the experiments of Payne et al., and it may be more appropriate to use the higher value for the rate constant $k_{49}(9.6 \times 10^{-12}$ cm^3 $molec^{-1} s^{-1})$ in estimating k_{31}. Thus the rate constant k_{31} may be as high as 1.5×10^{-15} cm^3 $molec^{-1} s^{-1}$. Although we have chosen

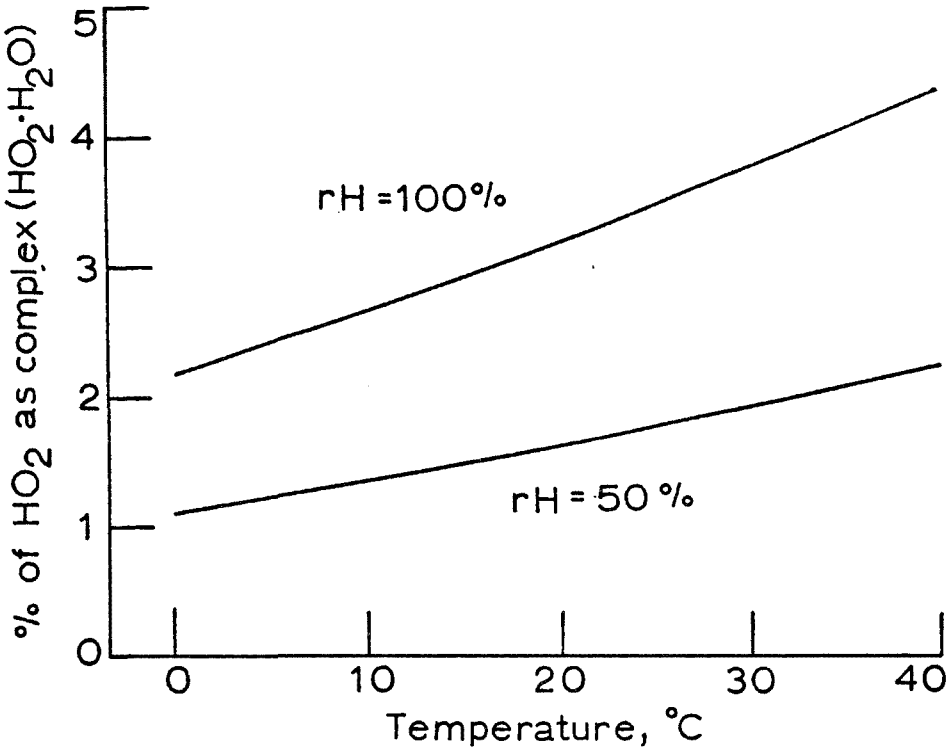

Figure 36. The theoretical percentage of HO_2 in the gas phase which is complexed with H_2O vapor as a function of the temperature and relative humidity; estimated using the thermodynamic data from Hamilton and Naleway (1976).

the lower value in our summary of Table 18, we have shown it as a lower limit which must be increased if further experimentation proves the Hamilton and Naleway hypothesis correct.

A typical $[HO_2]$ expected in a sunlight-irradiated region of the lower atmosphere which is highly polluted is about 6×10^9 molec cm^{-3} (Demerjian et al., 1974). This will lead to a rate of SO_2 oxidation through reaction 31 of about 1.9% hr^{-1}. The $[HO_2]$ for a fairly clean atmosphere may be lower by a factor of 10 or so, and the rates of conversion of SO_2 by 31 will be reduced correspondingly. However it is seen that this reaction can be a major source of SO_2 conversion in the atmosphere, and it must be included in our further considerations.

Reaction 32 which results in HO_2 addition to SO_2 has not been observed experimentally and only speculation on its possible significance can be made at this time.

$$HO_2 + SO_2 \ (+M) \rightarrow HO_2SO_2 \ (+M) \qquad (32)$$

Calvert and McQuigg (1975) have estimated by analogy with similar reactions that $k_{32} = 10^{-16}$ cm^3 molec^{-1}s^{-1}. If this magnitude is correct, then reaction 32 will result in only a few tenths of a percent conversion hr^{-1} for the highly polluted atmosphere, conditions which favor it. Benson's enthalpy estimates (1977) suggest that the intermediate adduct HO_2SO_2 formed in 32 will not be stable at 25°, since the decomposition reaction, HO_2SO_2 HO + SO_3 will be energetically favorable (ΔH = -12 kcal mole^{-1}). Thus the net effect of the occurrence of reaction 32 in the experiments of Payne et al. (1973) may be the formation of HO and SO_3, hence their estimate probably refers to the rate constant sum, $k_{31} + k_{32}$.

The CH_3O_2-SO_2 Reaction--

The first preliminary estimates of reactions 33 and 34 have been reported recently by Whitbeck et al. (1976).

$$CH_3O_2 + SO_2 \rightarrow CH_3O + SO_3 \qquad (33)$$

$$CH_3O_2 + SO_2 \rightarrow CH_3O_2SO_2 \qquad (34)$$

They observed the kinetics of the decay of CH_3O_2 spectroscopically following its generation in flash photolyzed mixtures of azomethane and oxygen, and azomethane, oxygen, and sulfur dioxide. The range of initial concentrations of SO_2 which could be employed was very limited ($P_{SO_2} < 0.3$ Torr), since the products of the reaction formed an aerosol which interferred with the optical measurements for experiments at high SO_2 pressures. The rate constant estimate, independent of the absolute extinction coefficient for CH_3O_2, gave $k_{33} + k_{34} \cong (5.3 \pm 2.5) \times 10^{-15}$ cm^3 molec^{-1}s^{-1}. If $k_{33} > k_{34}$ then the magnitude of this estimate is in reasonable accord with that for the analogous reaction 31. Taking the difference in entropies of activation for reactions 31 and 34 as 0.8 eu, then the ratio of the observed rate constants $k_{31}/k_{33} = 0.16$ corresponds to an activation energy difference, $E_{31} - E_{33} \cong 1.3$ kcal mole^{-1}, not unreasonable in view of the differences in enthalpy between these reactions: $\Delta H_{31} - \Delta H_{33} = 7.6$ kcal mole^{-1}.

The CH_3O_2 radical is probably the most abundant of the many organic peroxy radicals in the atmosphere. In a highly polluted atmosphere it is expected to be present at about 10^9 molec cm^{-3} (Demerjian et al., 1974), and the oxidation of SO_2 may occur through 33 and 34 by a rate as large as 2% hr^{-1}. In the fairly clean troposphere, rates of 1 x 10^{-2}% hr^{-1} are expected (Crutzen and Fishman, 1977). Obviously we do want to include these reactions in our further considerations.

It is not possible to determine the extent to which each of the reactions 33 and 34 occur from the existing data, but thermochemical arguments favor the reaction 33; thus the $CH_3O_2SO_2$ intermediate formed in 34 may decompose readily into CH_3O and SO_3 after a short delay.

The Tert-butylperoxy Radical-SO_2 Reaction--

Whitbeck et al. (1976) have studied the tert-$C_4H_9O_2$ decay kinetics by flash photolysis of $(CH_3)_3CN{=}NC(CH_3)_3$ mixtures with pure oxygen and in mixtures with O_2 and SO_2. In this case the reactivity of the radicals toward SO_2 was sufficiently low so that aerosol formation was not a serious problem at short times. At long times (one minute) aerosol appeared. This was attributed to the subsequent addition of $(CH_3)_3CO$ radicals to SO_2 following their generation in the major $C_3H_9O_2$ loss reaction in this system: $2C_3H_9O_2 \rightarrow 2C_3H_9O + O_2$. No difference in the decay rate of the tert-$C_3H_9O_2$ radicals could be detected in runs with added SO_2 (0.2 Torr), so in this case only an upper limit can be set for the rate constants: $k_{35} + k_{36} < 7.3 \times 10^{-19}$ cm^3 molec^{-1}s^{-1}.

$$(CH_3)_3CO_2 + SO_2 \rightarrow (CH_3)_3CO + SO_3 \qquad (35)$$

$$(CH_3)_3CO_2 + SO_2 \rightarrow (CH_3)_3CO_2SO_2 \qquad (36)$$

This value is smaller than the estimate of $k_{33} + k_{34}$ by a factor of 10^{-4}; thus we conclude that reactions 35 and 36, as well as those of the other highly hindered tert-alkylperoxy radicals, will be unimportant in the atmospheric conversion of SO_2. The very marked difference in reactivity of the tert-$C_4H_9O_2$ and the CH_3O_2 radicals noted here with SO_2, is also seen in the RO_2-RO_2 reactions of these species: $2t\text{-}C_4H_9O_2 \rightarrow 2t\text{-}C_4H_9O + O_2$; $2CH_3O_2 \rightarrow 2CH_3O$ (or $CH_2O + CH_3OH$) $+ O_2$. The rate constant of the former is 10^{-4} to 10^{-5}-times that of the latter (Parkes et al., 1973; Parkes, 1974; Whitbeck et al., 1976).

The Acetylperoxy Radical-SO_2 Reactions--

The peroxyacyl radicals are significant participants in photochemical smog formation. Some of them formed in the polluted atmosphere react with NO_2 to form the peroxyacyl nitrates:

$$RCOO_2 + NO_2 \rightarrow RCOO_2NO_2 \qquad (52)$$

The possible significance of these radicals in SO_2 oxidation has not been studied directly, but there is some information related to the reactions 37 and 38 which we can extract from existing published kinetic data:

$$CH_3COO_2 + SO_2 \rightarrow CH_3CO_2 + SO_3 \qquad (37)$$

$$CH_3COO_2 + SO_2 \rightarrow CH_3COO_2SO_2 \qquad (38)$$

Heicklen (1976) has quoted unpublished data of Shortridge which presumably gives evidence that the peroxyacetyl radical reacts readily with SO_2 in reaction 37. He found SO_2 addition to photolyzed mixtures of CH_3CHO and O_2 did not affect the rate of acetaldehyde oxidation, although SO_2 was removed and an aerosol formed. It is not clear how this evidence proves uniquely the occurrence of reaction 37, since many other chain carriers such as HO, HO_2, CH_3O, CH_3O_2, etc., will be present and may also oxidize SO_2 without terminating the chains.

Perhaps somewhat more definitive results related to the reactions 37 and 38 were reported by Pate et al. (1976). They observed the rate of reaction of peroxyacetyl nitrate (PAN) with many compounds including SO_2. The apparent bimolecular rate constant at 296°K for the PAN-SO_2 reaction was found to be less than 1.35×10^{-23} cm^3 molec^{-1}s^{-1}. However it has been rather well established that PAN is in equilibrium with CH_3COO_2 and NO_2, and we can estimate from the data of Pate et al. rate information related to reactions 37 and 38. The data from the Pitts group and those from Hendry and Kenley (1977) clearly demonstrate the dynamic character of the PAN present in gaseous mixtures:

$$CH_3COO_2NO_2 \rightarrow CH_3COO_2 + NO_2 \qquad (53)$$

$$CH_3COO_2 + NO_2 \rightarrow CH_3COO_2NO_2 \qquad (54)$$

Hendry and Kenley have estimated the rate constant k_{53} as a function of temperature. For 23°C, the temperature of the experiments of Pate et al, $k_{53} = 2.65 \times 10^{-4}s^{-1}$. Taking their theoretical estimate of $k_{54} = 1.04 \times 10^{-12}$ cm^3 molec^{-1}s^{-1}, we may estimate the $[CH_3COO_2]$ at equilibrium:

$$[CH_3COO_2]_{eq} = \frac{[CH_3COO_2NO_2](2.6 \times 10^8)}{[NO_2]} \text{ molec cm}^{-3} \qquad (55)$$

It seems reasonable to attribute any reaction of PAN to that of the CH_3COO_2 radicals in equilibrium with it. Thus the observed rate constant (k_{exp}) may be related to the rate constant sum, $k_{37} + k_{38}$, by relation 56:

$$(k_{37} + k_{38})[CH_3COO_2][SO_2] = k_{exp}[PAN][SO_2] \qquad (56)$$

Estimating $[CH_3COO_2]$ from the equilibrium data and relation 55 gives: $k_{37} + k_{38} = k_{exp}[NO_2]/2.55 \times 10^8$ cm^3 molec^{-1}s^{-1}. It is not reported what levels of NO_2 were present in the experiments of Pate et al., but it is likely that no more than 1 ppm (2.5×10^{13} molec cm^{-3}) was present on the average. With this estimate the data of Pate et al. lead to a value of $k_{37} + k_{38} < 1.3 \times 10^{-18}$ cm^3 mole^{-1}s^{-1}. For the theoretically estimated levels of the peroxyacetyl radicals expected to be present in heavy photochemical smog ($\sim 2 \times 10^8$ molec cm^{-3}), the new rate constant estimate suggests a maximum rate of oxidation of SO_2 through 37 and 38 of about 1×10^{-4}% hr^{-1}. We conclude that the oxidation of SO_2 by CH_3COO_2 radicals, and peroxacyl radicals in general, is negligible for the usual atmospheric conditions. The results of Fox and Wright (1977) can also be interpreted to support this conclusion. They carried out sunlight-irradiated smog chamber experiments using dilute mixtures of C_3H_6 and NO_x in air and matched mixtures of these compounds but with SO_2 added (0.75 ppm). They observed that SO_2 addition did not inhibit significantly the formation of PAN; the peak concentration was not lowered appreciably. The rate of [PAN] increase with time, if altered at all by

SO_2 addition, was somewhat more rapid in the SO_2-containing system. Thus in our opinion all of the definitive evidence at hand point to the unimportance of the reactions 37 and 38 in the tropospheric conversion of SO_2.

The HO-SO_2 Addition Reaction--

The kinetics of free radical addition to SO_2 have been observed for a number of free radical species; thus H-atoms (Halstead and Jenkins, 1968), CH_3-radicals (Good and Thynne, 1967a; Calvert et al., 1971; James et al., 1973), C_2H_5-radicals (Good and Thynne, 1967b), fluoroethyl radicals, $CH_2^{18}FCH_2$ (Milstein et al., 1974), cyclohexyl and other radicals formed during recoil tritium reactions with cyclohexene (Fee et al., 1972), all react with reasonably large rate constants which approach those of the analogous reactions with oxygen in some cases. Of course the H-atoms and alkyl radicals formed in the troposphere do not live to encounter SO_2 present at low impurity concentrations. They react with oxygen largely, to form alkylperoxy radicals and ultimately alkoxy radicals, HO_2, and other free radicals and molecular products. As we have seen in our earlier discussions, the additions of some alkylperoxy and acylperoxy radicals (reactions 36 and 38) to SO_2 appear to be rather slow reactions, while those of HO_2 and CH_3O_2 additions remain unevaluated. Much of the important homogeneous chemistry of the impurity molecules within the troposphere is dominated by the reactions of the ubiquitous radical pair, HO and HO_2. Indeed it appears that the homogeneous SO_2 removal paths also depend largely on the reactions of these radicals. In particular the HO-addition to SO_2, reaction 39, seems to be the most important of the several homogeneous reaction paths of SO_2 in the troposphere for many different atmospheric conditions.

$$HO + SO_2 \ (+M) \rightarrow HOSO_2 \ (+M) \qquad (39)$$

There has been a significant and productive effort of several research groups to determine the rate constant for this seemingly important reaction. It was apparently first suggested by McAndrew and Wheeler (1962) as one of the reactions necessary to rationalize the effect of SO_2 on radical chain terminations in propane-air flames. Following the suggestions of Fair and Thrush (1969), the McAndrew and Wheeler rate constant estimations can be used to derive a third order rate constant, $k_{39} = 1.1 \times 10^{31}$ cm^6 molec^{-2}s^{-1} at 2080°K. Many of the estimates of k_{39} were obtained in competive rate studies using the HO reaction with CO as a reference.

$$HO + CO \rightarrow H + CO_2 \qquad (57)$$

With this technique Davis et al. (1973) reported a third order rate constant $k_{39} \cong 3 \times 10^{-31}$ cm^6 molec^{-2}s^{-1} with M = H_2O. In similar experiments Payne et al. (1973) found $k_{39} = 1.5 \times 10^{-31}$ cm^6 molec^{-2}s^{-1} using the Stuhl and Niki (1972) estimate of the rate constant for reaction 57. Cox (1974/75, 1975) also carried out competitive SO_2-CO reaction studies by photolyzing HONO in air at 1 atm pressure; they found $k_{39} = (6.0 \pm 0.8) \times 10^{-13}$ cm^3 molec^{-1}s^{-1} in air at 1 atm, using $k_{57} = 1.5 \times 10^{-13}$ cm^3 molec^{-1}s^{-1} as

recommended by Baulch and Drysdale (1974). The Castleman group (Wood et al., 1974) also have made rather extensive competitive rate studies of 39 in experiments which have extended over a number of years. They photolyzed H_2O in a mixture of SO_2, CO, and H_2O in N_2 carrier gas. Their first work gave $k_{39} = 3.8 \times 10^{-13}$ cm^3 $mole^{-1}s^{-1}$ for the high pressure limit. They recognized early the probable importance of this reaction in SO_2 conversion in the atmosphere (Castleman et al., 1974; Wood et al., 1975). In a later similar study (Castleman et al., 1975), they found a pseudo-second order rate constant at 1 atm of N_2, $k_{39} = 6.0 \times 10^{-13}$, taking $k_{57} = 1.4 \times 10^{-13}$ cm^3 $molec^{-1}s^{-1}$ (Hampson and Garvin, 1975). In the most recent report of this group, Castleman and Tang (1976/77) extended their competitive rate study from 20 to 1000 Torr of added N_2 gas. Again accepting k_{57}, they calculated: $k_{35} = 6.0 \times 10^{-13}$ cm^3 $molec^{-1}s^{-1}$. In experiments at low pressures carried out over a range of temperatures from 24 to -20°C, they estimated $E_{35} = -2.8$ kcal $mole^{-1}$.

Some more direct measurements of k_{39} have been made by flash photolysis HO-resonance fluorescence techniques. Using this method Davis and Schiff (1974) reported the reaction 39 to be in the high pressure fall off region above ~10 Torr of He. At 500 Torr of added helium, the effective bimolecular rate constant was reported to be: 2.5×10^{-13} (2.5×10^{-3} shown, must be in error) cm^3 $molec^{-1}s^{-1}$, and the low pressure value of the third order rate constant, $k_{39} = 2 \times 10^{-32}$ cm^6 $molec^{-2}s^{-1}$ with He = M (work of Davis and Schiff quoted in Payne et al., 1973). In further experiments Davis (1974b) reported preliminary values for the effective bimolecular rate constants for k_{39}: with He as M, values varied from 0.87×10^{-13} at 50 Torr to 2.7×10^{-13} at 500 Torr; for M = Ar, 1.37×10^{-13} at 50 Torr to 3.7×10^{-13} at 500 Torr; for M = N_2, 0.80×10^{-13} at 5 Torr to 2.4×10^{-13} cm^3 $molec^{-1}s^{-1}$ at 20 Torr. Harris and Wayne (1975) studied reaction 39 using the HO-resonance technique but in a discharge flow system at low pressures. They derived the third order rate constants: $k_{39} = (4.5 \pm 1.5) \times 10^{-31}$ with M = Ar, and $k_{39} = (7.2 \pm 2.6) \times 10^{-31}$ cm^6 $molec^{-2}s^{-1}$ with M = N_2. Atkinson et al. (1976) also utilized H_2O flash photolysis with HO-resonance spectroscopy to determine k_{39} over a wide range of argon pressures. The estimated second order rate constant for 25°C and 1 atm (M = Ar) was: $k_{39} = (6.7 \pm 0.7) \times 10^{-13}$, with the high pressure limit (extrapolated) of 8.3×10^{-13} cm^3 $molec^{-1}$ s^{-1}. Gordon and Mulac (1975) employed pulsed radiolysis and absorption spectroscopy to follow the HO radical at 3087 Å; in $H_2O(g)$ at 1 atm and 435°K; they obtained $k_{39} = 1.8 \times 10^{-12}$ cm^3 $molec^{-1}s^{-1}$.

Recently Sie et al. (1976) and Cox et al. (1976) have presented strong evidence that the rate constant for the reaction 57, used as a reference value in many competitive studies of reaction 39, was pressure sensitive. Both groups of workers concluded that the rate constant k_{57} was very much larger at 1 atm total gas pressure than had been assumed in view of the

earlier low pressure data. A unique test of the pressure dependence of k_{57} was not possible in the work of Cox et al. (1976), since their experiments were carried out at a fixed pressure of 1 atm (largely air). However they found the ratio k_{57}/k_{58} to be about twice that observed by other experimentalists who used much lower pressures of reactants and added gas; they suggested the phyothesis of a pressure dependent k_{57} seemed most compatible with their results.

$$HO + H_2 \rightarrow H_2O + H \qquad (58)$$

In the work of Sie et al. (1976) the pressure of added gas (H_2, He, SF_6) was varied from 20 to 774 Torr with an observed increase in k_{57}/k_{58} with pressure by over a factor of two in the case of added H_2 or SF_6. Chan et al. (1977) confirmed the conclusions of these workers. They reported from competitive HO rate studies with dilute mixtures of CO and iso-C_4H_{10} in air, that the rate constant ratio k_{57}/k_{59} was about a factor of two higher in experiments at 700 Torr of air than in runs with 100 Torr in air.

$$HO + \text{iso-}C_4H_{10} \rightarrow C_4H_9 + H_2O \qquad (59)$$

There is no reason to believe the pressure dependence observed by these workers resulted from the normal bimolecular H-atom abstraction reactions 58 and 59; it is reasonable to assume that these rate constants remain at their low pressure values: $k_{58} = 7.0 \times 10^{-15}$, (Cox et al., 1976); $k_{59} = 2.34 \times 10^{-12}$ cm^3 molec^{-1}s^{-1} (Greiner, 1970). Accepting this seemingly plausible premise, we have derived estimates from the various competitive experiments for k_{57} and have plotted these together with the data from the direct measurements at low pressures in Figure 37. Excluding the one very divergent point of Sie et al (1976) at 570 Torr of added SF_6, the general increase of the rate constant k_{57} with increasing pressure of H_2, N_2, O_2, and SF_6 seems clear. Obviously values of the HO-SO_2 reaction rate constants from the data at the higher pressures based upon the low pressure value of k_{57} must be corrected to take into account the pressure sensitive character of k_{57}. Thus the estimates of k_{39} by Davis et al. (1973), Payne et al. (1973), Cox (1975), Castleman et al. (1975), and Castleman and Tang (1976/77) should be corrected. We have made such a correction to the extensive and seemingly accurate data set of Castleman and Tang, using the values corresponding to those of the dashed curve given in Figure37 for k_{59}. The apparent second order rate constant derived in this fashion are plotted versus the reciprocal of the pressure of N_2 in Figure38 (triangles). Also plotted here are the values of k_{39}^{-1} determined more directly by resonance fluorescence of HO in experiments at various pressures of Ar; the open circles are data from Atkinson et al (1976) and the closed circles are data from Davis (1974b). The two sets of data from the direct HO-measurements do not check very well at low pressures but appear to reach about the same value at high pressures. The data of Atkinson et al. give k_{39} (M = Ar, 1

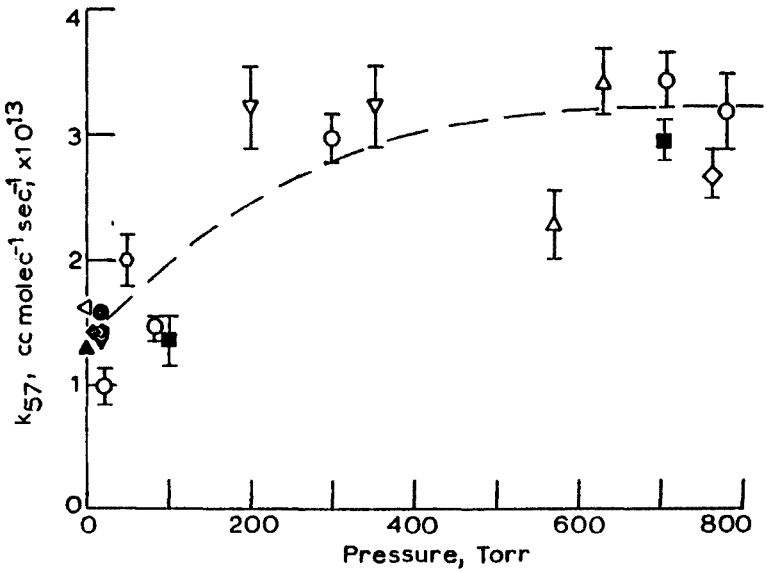

Figure 37. The variation of the apparent second order rate constant for the reaction 57, HO + CO (M) → H + CO_2 (+M), with pressure of added gases; data for H_2, Sie et al., 1976 (open circles); air, Cox, 1975 (diamond), Chan et al. 1977 (closed squares); SF_6, Sie et al, 1976 (open triangles), Overend et al., 1974, and Paraskevopoulos, 1976 (inverted triangles); He, Paraskevopoulos, 1976 (hexagons); low pressure points shown: Stuhl and Niki, 1972 (inverted closed triangle); Greiner, 1967 (closed diamond); Mulcahy and Smith, 1971 (on-end triangle); Davis et al., 1974c (open diamond); Westenberg and deHaas, 1973 (closed triangle); Smith and Zellner, 1973 (closed hexagon).

atm) = (6.7 ± 0.7) x 10^{-13} and a high pressure limit of 8.3 x 10^{-13} cm^3 $molec^{-1}s^{-1}$. Since Ar is somewhat less efficient as a third body than N_2 and O_2, the latter number is probably the best estimate from the Atkinson et al. data which is applicable to air at 1 atm. The Davis (1974b) data are less abundant, but the extrapolated upper limit to k_{39} for M = Ar is compatible with this estimate as well. The Davis data for k_{39} using M = N_2 consisted of only 3 points (not shown in Figure 37) at low pressures (P < 40 Torr), so the value obtained by extrapolation of these data to 1 atm N_2 ($k_{39} \cong 9 \times 10^{-13}$) cannot be very accurate. We will take as the best estimate of the Davis group the number quoted by Davis and Klauber (1975) for the bimolecular rate constant in the troposphere, $k_{39} \cong 8 \times 10^{-13}$ cm^3 $molec^{-1}$ s^{-1}. The Castleman and Tang (1976/77) corrected estimates (using our

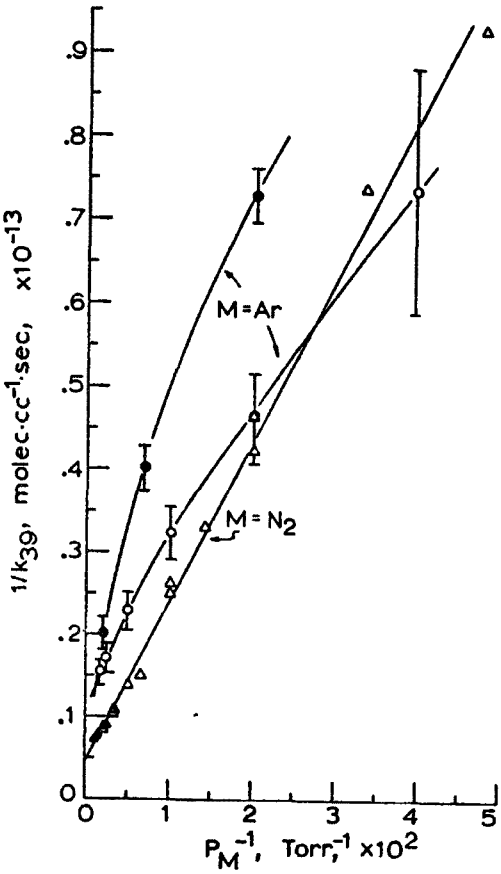

Figure 38. Plot of the reciprocal of the apparent second order rate constant for the reaction 39, HO + SO_2 (+M) → $HOSO_2$ (+M), versus the reciprocal of the pressure of added gas (M); estimates for M = N_2 were calculated from the data of Castleman and Tang (1976/77) using corrected values for k_{57} (triangles); for M = Ar data are from Atkinson et al., 1976 (open circles) and Davis, 1974b (closed circles).

preferred choice for k_{57} = 3.0 x 10^{-13} cm^3 $molec^{-1}s^{-1}$, Chan et al., 1977) gives k_{39} = 1.4 x 10^{-12} cm^3 $molec^{-1}s^{-1}$ for M = N_2 (1 atm, 24°C). The Cox (1975) extimate corrected to our preferred choice for k_{57} gives k_{39} = (1.2 ± 0.2) x 10^{-12} cm^3 $molec^{-1}s^{-1}$. We feel the best current choice for k_{39} in the lower troposphere (1 atm air, 25°C) is derived from an average of the results of the four most extensive studies at the highest pressures, i.e., the data of Davis (1974b), Atkinson et al. (1976), and the corrected data of Cox (1975), and Castleman and Tang (1976/77). We suggest the value: k_{39} = (1.1 ± 0.3) x 10^{-12} cm^3 $molec^{-1}s^{-1}$ which is given in Table 18.

The typical [HO] which is anticipated theoretically in the highly polluted (NO_x, RH, SO_2), sunlight-irradiated, lower atmosphere, is about 7 x 10^6 molec cm^{-3} (Calvert and McQuigg, 1975). That expected for a relatively clean atmosphere in the midday summer sun in the midlatitudes of the northern hemisphere, is somewhat lower, typically 1 x 10^6 molec cm^{-3} (Crutzen and Fishman, 1977). Using these estimates we predict that SO_2 removal by reaction with HO in 39 may be as high as 2.7% hr^{-1} in the dirty atmosphere and typically 0.4% hr^{-1} in the clean troposphere. Our evaluation certainly confirms the current view of atmospheric chemists that reaction 39 is a very important factor in the homogeneous oxidation of SO_2 in the atmosphere.

The Fate of the $HOSO_2$ Product of Reaction 39--

The $HOSO_2$ species formed as reaction 39 occurs is not a stable product, but it is a free radical which will react further to form final products. Calvert and McQuigg (1975), Davis and Klauber (1975), and Benson (1977) have speculated on the subsequent events expected following the formation of $HOSO_2$. It is important to review these possible steps in light of recent information concerning them.

	ΔH, kcal $mole^{-1}$	
$HO + SO_2$ (+M) $\rightarrow$ $HOSO_2$ (+M)	-37	(39)
$HOSO_2 + O_2 \rightarrow HOSO_2OO$	-16	(60)
$HOSO_2OO + NO \rightarrow HOSO_2O + NO_2$	-25	(61)
$HOSO_2OO + NO_2 \rightleftharpoons HOSO_2OONO_2$	?	(62)
$HOSO_2OONO_2 \rightarrow HOSO_2O + NO_3$	?	(63)
$HOSO_2OO + NO_2 \rightarrow HOSO_2O + NO_3$	-2	(64)
$HOSO_2OO + HO_2 \rightarrow HOSO_2O_2H + O_2$	-43	(65)
$2HOSO_2OO \rightarrow 2HOSO_2O + O_2$	-22	(66)
$HOSO_2O + NO \rightarrow HOSO_2ONO$	-26	(67)
$HOSO_2ONO + h\nu \rightarrow HOSO_2O + NO$		(68)
$HOSO_2O + NO_2 \rightarrow HOSO_2ONO_2$	-22	(69)
$HOSO_2O + HO_2 \rightarrow HOSO_2OH + O_2$	-57	(70)
$HOSO_2O + C_3H_8 \rightarrow HOSO_2OH + iso\text{-}C_3H_7$	-10	(71)
$HOSO_2O + C_3H_6 \rightarrow HOSO_2OCH_2CHCH_3$	?	(72)
H_2SO_4 + aerosol (H_2O,NH_3,CH_2O,C_nH_{2n}..) $\rightarrow$ (growing aerosol)		(73)

$HOSO_2ONO_2$ + aerosol(H_2O) → aerosol(H_2SO_4,$HONO_2$..) (74)

$HOSO_2ONO$ + aerosol(H_2O) → aerosol(H_2SO_4, HONO..) (75)

The first step in the sequence of $HOSO_2$ reactions, reaction 60, should be the major fate of the $HOSO_2$ radical in the troposphere. It is exothermic by 16 kcal $mole^{-1}$. The alternative disproportionation reaction, $HOSO_2 + O_2$ $HO_2 + SO_3$, will be non-competitive with 60 since it is endothermic by about 8 kcal $mole^{-1}$. As with the HO_2 and RO_2 radicals, it is likely that the $HOSO_2OO$ radical will oxidize NO, reaction 61, or react with NO_2 in reaction 62, since NO and NO_2 impurity will be present with SO_2 in most of the impurity-laden air mixtures encountered. Reaction 61 is more exothermic (-25 kcal $mole^{-1}$) than the comparable, analogous, fast reaction, $RO_2 + NO$ $RO + NO_2$ (-17 kcal $mole^{-1}$). The coupling reaction 62 should be somewhat exothermic, and it forms in theory an inorganic analogue to peroxyacetyl nitrate (PAN) as suggested by Calvert and McQuigg (1975). This compound would be expected to be somewhat unstable toward decomposition, and reaction 62 is written as reversible. Benson (1977) has not reported estimates for $\Delta H_f(HOSO_2OONO_2)$, but he noted that both the adducts of the $HOSO_2OO$ radical with NO and NO_2 will not be stable; the reaction 64 with NO_2 to form $HOSO_2O$ and NO_3 is slightly exothermic. Disproportionation of the $HOSO_2OO$ radical may occur with the HO_2 radical in 65, or, in the absence of other radicals, it may react with another $HOSO_2OO$ radical in 66. It is unlikely that $HOSO_2OO$ will oxidize SO_2 at any significant rate: $HOSO_2OO + SO_2 \rightarrow HOSO_2O + SO_3$ (ΔH = -35 kcal $mole^{-1}$), in view of the slowness of the reaction 37 of near equal ΔH. If this is important, then rates of SO_2 oxidation estimated in this work are minimum rates.

The $HOSO_2O$ radical in this sequence is somewhat analogous to the HO radical. It may form sulfuric acid by abstracting a hydrogen from a hydrocarbon, aldehyde, or other H-containing species such as HO_2 in reactions 70 and 71. However the H-atom abstraction reaction of the HO-radical analogous to the typical reaction 71 is much more exothermic (ΔH = -25 kcal $mole^{-1}$) than reaction 71, so one may expect the rate constant for H-abstraction by $HOSO_2O$ to be somewhat smaller than the analogous HO reaction. The $HOSO_2O$ radical may add to alkenes and generate organic sulfate containing species in reaction 72. It may react with NO in reaction 67 and form the well known reactive reagent for nitrosation and oxidation of organic compounds and diazotization of amines, nitrosylsulfuric acid, $ONOSO_2OH$. It is interesting to observe that this compound is available now commercially (duPont) in a sulfuric acid solution. Nitrosylsulfuric acid may photolyze in sunlight in 68, react in aerosol solutions to hydrolyze to H_2SO_4 and HONO, or react with organic matter present in the H_2SO_4 -rich aerosol in 75. Alternatively the $HOSO_2O$ species may combine with NO_2 in 69 and form the nitrylsulfuric acid. In principle this compound could react on aerosols to hydrolyze to H_2SO_4 and $HONO_2$, or it may act to nitrate certain organic compounds present in the aerosol solution, reaction 74.

It seems probable to us that the reactions of the $HOSO_2O_2$ and $HOSO_2O$ radicals which are shown do occur in the atmosphere, and the reactive species formed in these reactions should be considered as prime candidates for the active forms of the "sulfate" aerosol of our urban atmospheres.

The assignment of rate constants for these reactions of the basis of our present knowledge is very speculative. However recognize that once the HO radical has added to SO_2, the reactions proceed to form sulfuric acid, peroxysulfuric acid, and other compounds which will eventually lead to sulfate and nitrate containing aerosols. If the aerosol is rich in unneutralized H_2SO_4, then much of the nitrate will be lost to the atmosphere as nitric acid.

Davis and Klauber (1975) and Davis et al. (1974d) have suggested an alternative reaction route for the $HOSO_2O$ radical which we should consider further here. This is the chain reaction sequence 76, 77, and 61 which can presumably pump NO to NO_2 as in the HO_2, HO cycle in smog.

$$HOSO_2O + O_2 \ (+M) \rightarrow HOSO_2O_3 \qquad (76)$$

$$HOSO_2O_3 + NO \rightarrow HOSO_2O_2 + NO_2 \qquad (77)$$

$$HOSO_2O_2 + NO \rightarrow HOSO_2O + NO_2 \qquad (61)$$

The reaction 76 is analogous to the reaction 78 involving the HO radical:

$$HO + O_2 \rightarrow HOOO \qquad (78)$$

Using Benson's (1976) estimates for $\Delta H_f(HO_3) \cong 60$ eu (1 atm, 25°C), we calculate that at equilibrium in the lower troposphere at 25° the ratio $[HOOO]/[HO] = 2.6 \times 10^{-19}$. The greater endothermicity of the reaction 76 compared to 78 will lead to a still lower ratio of $[HOSO_2O_3]/[HOSO_2O]$ in the lower troposphere. Thus it is improbable that the proposed reactions 76 and 77 occur in the atmosphere.

The observed O_3 -bulge which Davis and colleagues saw late in the transport of a stack gas plume does not require reaction 76 and 77 for explanation. The conventional reactions involving NO to NO_2 conversion chains of typical smog are the likely O_3 developing mechanism in a plume which is well diluted with the usual contaminants of polluted urban air.

The Methoxy Radical Addition to SO_2--

There are no kinetic data related to reaction 40 of which we are aware.

$$CH_3O + SO_2 \rightarrow CH_3OSO_2 \qquad (40)$$

Calvert and McQuigg (1975) have presented a very rough estimate: $k_{40} \cong 6 \times 10^{-15}$ cm^3 $molec^{-1}s^{-1}$, which was based upon comparisons with analogous reactions of other radicals. An experimental estimate should be made. In contrast to the CH_3O_2 and other alkyl peroxy radicals, the CH_3O radical and other alkoxy radicals are reactive toward molecular O_2; e.g., $CH_3O + O_2 \rightarrow CH_2O + HO_2$. Thus the steady state concentrations of CH_3O and other alkoxy radicals within a sunlight-irradiated, polluted, lower atmosphere are quite low, about 5×10^6 molec cm^3. Using this estimate the rate of SO_2 reaction in 40 should be about 0.01% hr^{-1}. This reaction seems to be an unimportant

loss mechanism for SO_2 in the atmosphere. However in view of the reactive nature of the potential alkylating agents which should form eventually following reaction 40, an experimental determination of the rate constants for alkoxy radical reactions with SO_2 should be made to allow an accurate assessment of the significance of this reaction.

The Oxidation of SO_2 by Products of the O_3 -alkene Reaction--

As we have seen in the preceeding section, the rate of oxidation of SO_2 by O_3 reaction 26, is negligibly slow at smbient air temperatures and at the low levels which are characteristic of O_3 and SO_2 impurities in the troposphere. However when a third reactant, an alkene is present in the O_3-SO_2-air mixture, a fairly rapid oxidation of SO_2 occurs even in the dark. This very significant observation was first reported in detail by Cox and Penkett (1971a,b). For their conditions the rate of removal of SO_2 was 3% hr^{-1} with the alkene cis-2-pentene and 0.4% hr^{-1} with propylene. They considered as a possible reactant in 43 the so-called "zwitterionic" species, or Criegee intermediate, RCHOO·, postulated by Criegee (1957) in his classical mechanism of the ozone-alkene reactions in solution:

$$O_3 + RCH{=}CHR \rightarrow RCH\overset{O\text{-}O\text{-}O}{\diagup\!\!\diagdown}CHR \qquad (79)$$

$$RCH\overset{O\text{-}O\text{-}O}{\diagup\!\!\diagdown}CHR \rightarrow RCHO + \dot{R}CHOO\cdot \qquad (80)$$

$$\dot{R}CHOO\cdot + SO_2 \rightarrow RCHO + SO_3 \qquad (43)$$

In a later more extensive study, Cox and Penkett (1972) also considered the original ozonide (molozonide) product of 79 as an alternative reactant in 41:

$$RCH\overset{O\text{-}O\text{-}O}{\diagup\!\!\diagdown}CHR + SO_2 \rightarrow 2RCHO + SO_3 \qquad (41)$$

The rate data from a series of different alkenes (cis-2-butene, cis-2-pentene, trans-2-butene, 2-methyl-1-pentene, and 1-hexene) were rationalized well by a simple mechanism in which an intermediate, presumably the original molozonide or the Criegee intermediate, oxidized SO_2 through the reaction series 79, 80, 43, and/or 41, or underwent decomposition, reaction at the wall, or some other fate unproductive to SO_2 oxidation. Although a strong inhibition of the SO_2 oxidation occurred with increased $[H_2O]$ in the reaction mixture, the effect of H_2O remained puzzling and unexplained by Cox and Penkett. Wilson et al. (1974) accepted a similar mechanism in their computer simulation of the Cox and Penkett O_3-alkene-SO_2-air results.

In the reaction schemes considered here for this system, two other reactive entities related to the molozonide and its products should be noted as well as potential reactants: the open form of the original molozonide (reaction 42), and the rearranged Criegee intermediate (reaction 44):

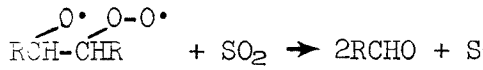

(42)

(43)

Other possible reactants for SO_2 in the alkene-O_3-SO_2-air system have been suggested. Demerjian et al (1974) speculated that the reactant diradical of 44 might be formed from the original Criegee intermediate by reaction with O_2:

(81)

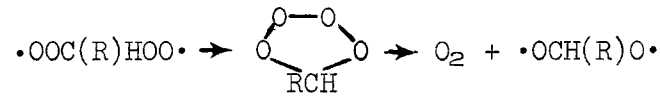

(82)

Alternatively O'Neal and Blumstein (1973) envisaged a rapid rearrangement of the Criegee intermediate through reaction sequence 83:

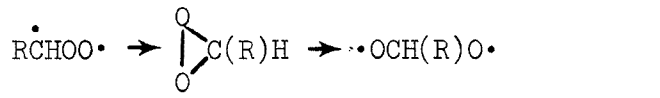

(83)

Thus at least four different reactants should be considered as potential SO_2 reactants in this system; note in Table 18 that all of the potential reactions 41-44 are considerably exothermic. However there is some uncertainty whether one needs to invoke any of these reactions to explain SO_2 oxidation. Demerjian et al. (1974) have argued that the $\cdot OCH(R)O\cdot$ radical will react readily with oxygen to generate other reactive species (RCO_2, HO_2, RO_2, etc.), and Calvert and McQuigg (1975) suggested that these may be responsible for the SO_2 oxidation observed in the alkene-O_3-SO_2 system.

The O_3-alkene reactions are very complex, and the simple Criegee mechanism cannot be the only route of fragmentation and rearrangement to products in the gas phase system. There is abundant evidence today that fragmentation of the ozonide formed with the simple alkenes in gas phase reactions creates highly excited free radicals including HO and carbonyl species (Kummer et al., 1971; Pitts et al., 1972; Finlayson et al., 1972; Atkinson et al., 1973). It is difficult to rationalize the formation of these highly excited species through the Criegee mechanism alone. O'Neal and Blumstein (1973) have suggested several alternative paths for decomposition of the original ozonide which can account better for some of the chemiluminescent products of the gas phase ozone-alkene reactions. Various modified forms of the O Neal and Blumstein mechanism have been adopted by various groups of modelers of smog chemistry; for example, see Whitten and Hogo, 1976; Sander and Seinfeld, 1976. However the extent and the nature of the fragmentation and rearrangement paths which are chosen must necessarily be rather arbitrary at this stage of our knowledge. Use of the

Benson (1976) thermochemical-kinetic considerations have been made by O'Neal and Blumstein (1973) and others to derive "best estimates" of the importance of the alternative paths of reaction of the ozonides. In most detailed modeling schemes involving SO_2 removal which are in use today, reactions such as 41, 42, 43, or 44 are not considered to be important, but the SO_2 oxidation in the alkene-O_3-SO_2 system is made to occur exclusively through partial fragmentation of the ozonide to various free radicals, followed by reactions 31-40 or Table 18 and their various analogues. For examples see Sander and Seinfeld, 1976; Walter et al., 1977.

However it appears to us that the ideas related to the mechanism of the gas phase O_3-alkene reactions must be modified again. Recent FTS-IR spectroscopic observations of the O_3-alkene-air systems have been made by Niki et al. (1977). They provide striking new evidence for the reasonable stability of many of the gas phase ozonides. Thus the role of reactions 41-44 should not be discarded. Hull et al. (1972) had observed through low temperature (-175 to -80°C) infrared studies in the condensed phase, the primary ozonides of C_3H_6, iso-C_4H_8, cis- and trans-2-C_4H_8, cyclopentene, cyclohexene, trimethylethylene, and tetramethylethylene; these decomposed to various products upon warming the frozen mixtures to room temperature. In 1959 Hanst et al. concluded from long-path infrared experiments that they observed ozonide formation from the gas phase reactions of O_3 with 1-hexene and 3-heptene but not from 1-pentene and the smaller alkenes. However the recent work of Niki et al. (1975) shows clearly that ozonide formation can be observed in the gas phase from olefins as small as propylene. In their work, Niki et al. reacted O_3 (5 ppm), cis-2-C_4H_8 (10 ppm), and CH_2O (10 ppm) in 700 Torr of air. The identified products (ppm) included: CO_2(1.9), CO, CH_4(0.66), CHO_2H(0.25), CH_3OH(0.4), CH_2CO, and, significantly propylene ozonide (0.88 ppm). Thus they presented unambiguous evidence that the Criegee intermediate $CH_3\dot{C}HOO\cdot$ (or conceivably the rearranged radical, $CH_3\overset{\dot{O}}{C}HO\cdot$) had a much longer lifetime in air than has been suggested in recent years by O'Neal and Blumstein (1973), Demerjian et al. (1974), and many others; it lived to react with the added CH_2O and formed propylene ozonide:

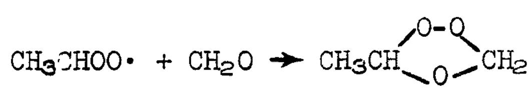
(84)

For the purposes of this review another most important observation was made by Niki et al. (1977); they found that addition of SO_2 at the 5 ppm level to the O_3, C_3H_6, CH_2O system quenched ozonide formation completely, and the SO_2 was consumed to an extent comparable to the ozonide yield observed in its absence. Furthermore the rearrangement of the $CH_3CHOO\cdot$ species to acetic acid was not observed in these experiments, although it is expected in the O'Neal and Blumstein considerations:

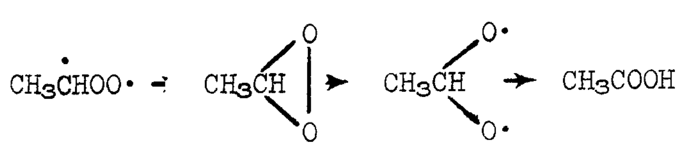
(85)

Niki (1977) has indicated to us that the ozonide yield is about 20% for all of the alkenes studied except C_2H_4 where no ozonide formation was detected. The "radical" product yield was less than 50%.

At this writing it is not clear what species we should invoke as the reactants in the O_3-alkene-SO_2 system, but Niki's work demonstrates that the Criegee intermediate is a strong candidate. Some reaction from various free radical fragmentation products may occur as well. With this apparent return to the original mechanism suggested by Cox and Penkett (1971a,b), it is instructive to reconsider the detailed results of Cox and Penkett (1972).

A major problem in the quantitative evaluation of the rates of reactions 41-44, is the lack of information related to the absolute rate constants of the intermediate, SO_2-oxidizing species. In the mixture of gases encountered in the polluted troposphere, NO is commonly present with SO_2. If the Criegee intermediate is formed by ozone-alkene interactions, then SO_2 must compete with NO (reaction 86) and other reactants as well in order to be oxidized by RCHOO·.

$$CH_3\dot{C}HOO\cdot + NO \rightarrow CH_3CHO + NO_2 \qquad (86a)$$

$$\text{or } CH_3\overset{O\cdot}{\overset{/}{C}}H\text{-}O\cdot + NO \rightarrow CH_3CHO + NO_2 \qquad (86b)$$

The enthalpy changes for these reactions ($\Delta H_{86a} \cong -97$; $\Delta H_{86b} \cong -51$ kcal mole^{-1}) may be compared to that for the oxidation of NO by O_3 ($\Delta H_{87} = -48$ kcal mole^{-1}), a reactive species which is very similar to the Criegee intermediate.

$$O_3 + NO \rightarrow O_2 + NO_2 \qquad (87)$$

It seems likely that $k_{86a} > k_{86b} \cong k_{87} = 1.6 \times 10^{-14}$ cm^3 molec^{-1}s^{-1} (Clyne et al., 1964), and a good competition with the possible SO_2 oxidation reactions must be provided by NO in the atmosphere. In the absence of an experimental basis for the evaluation of the inhibition of SO_2 oxidation by NO addition to the O_3-alkene-SO_2 system, it will be impossible to judge accurately the significance of reactions such as 43 and 44 in the atmosphere. It is interesting to note that ΔH_{44} is comparable to ΔH_{26}, and reaction 26 is immeasurably slow at room temperature. This evidence seems to favor the direct involvement of the Criegee intermediate and not the rearranged form, $RC\overset{O\cdot}{\underset{|}{H}}\text{-}O\cdot$ in SO_2 oxidation.

Let us adopt for the purposes of our considerations here an expanded version of the Cox and Penkett mechanism for the cis-2-butene, O_3, SO_2, H_2O, air system, and focus our attention on the Criegee intermediate as the major source of SO_2 oxidation in these experiments. The competitive reactions of the Criegee intermediate in the NO-free system may occur in principle with SO_2, the alkenes, ozone, oxygen, water, as well as the unimolecular decay to other products:

$$O_3 + \text{cis-2-}C_4H_8 \rightarrow (\text{molozonide}) \rightarrow CH_3\dot{C}HOO\cdot + CH_3CHO \quad (88)$$

$$\rightarrow (RCHO,\ RCO_2H,\ \text{etc.}) \quad (89)$$

$$CH_3\dot{C}HOO\cdot + SO_2 \rightarrow CH_3CHO + SO_3 \quad (90)$$

$$CH_3\dot{C}HOO\cdot + C_4H_8 \rightarrow CH_3CHO + C_4H_8O\ (\text{and other products}) \quad (91)$$

$$CH_3\dot{C}HOO\cdot + O_3 \rightarrow CH_3CHO + 2O_2 \quad (92)$$

$$CH_3\dot{C}HOO\cdot + O_2 \rightarrow CH_3\overset{\overset{O\cdot}{|}}{C}H\text{-}O\cdot \qquad (\text{other products}) \quad (93)$$

$$\rightarrow O_3 + CH_3CHO \quad (94)$$

$$CH_3\dot{C}HOO\cdot + H_2O \rightarrow CH_3COOH + H_2O \quad (95)$$

$$CH_3\dot{C}HOO\cdot \rightarrow (CH_3COOH)^{\ddagger} \rightarrow CH_4 + CO_2(CH_3OH,\ CO,\ \text{etc.}) \quad (96)$$

Each of these steps is energetically feasible, but the extent of the participation of each is unclear. Since the rate of O_3-alkene reaction and the rate of SO_2 oxidation in alkene-O_3-SO_2 mixtures was relatively unaffected by replacing the air with N_2 (0.2%) in the experiments of Cox and Penkett (1972), then reactions 93 and 94 are probably unimportant. Deviations of the O_3-alkene stiochiometry from 1 to 1 in reactant mixtures with excess of O_3 or excess of alkene, suggest that 91 and 92 may occur to some extent. The marked inhibition by H_2O which they observed is consistent with some reaction such as 95. One might speculate that H_2O catalyzes the rearrangement of $CH_3\dot{C}HOO\cdot$ to CH_3CO_2H by way of some complex between the Criegee intermediate and water:

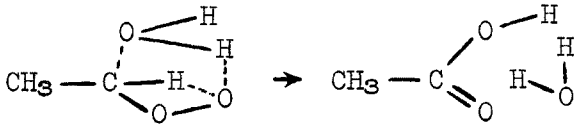

The Cox and Penkett data for cis-2-butene, SO_2, O_3, H_2O, air mixtures can be reconsidered in terms of these reactions. Following Cox and Penkett we may assume that the reactive Criegee intermediate achieves a steady state concentration. Let us assume further that SO_2 oxidation occurs only in reaction 90 and that $R_{92} \ll R_{88} + R_{89}$. Then we expect relation 97 to hold:

$$\frac{-R^o_{O_3}}{R^o_{SO_3}} = \left(\frac{k_{88} + k_{89}}{k_{88}}\right)\left(1 + \frac{1}{[SO_2]k_{90}}\left[k_{96} + [C_4H_9]k_{91} + [O_3]k_{92} + [H_2O]k_{95}\right]\right) \quad (97)$$

The rather limited data cannot provide a test of the functional form for each of the reactants in relation 97, but certain observations can be made. In the Cox and Penkett experiments the $[O_3]^o$ and $[C_4H_8]^o$ were held essentially constant at 0.5 and 1.0 ppm, respectively. For these conditions the form of the relation 97 simplifies to 98, where A and B are constants:

$$\frac{-R^o_{O_3}}{R^o_{SO_3}} = B + \left(\frac{B\{A + [H_2O]k_{95}\}}{k_{90}}\right) \frac{1}{[SO_2]} \qquad (98)$$

From relation 98 we expect a linear relation between $-R^o_{O_3}/R^o_{SO_3}$ and $1/[SO_2]$ for a series of runs made at constant $[H_2O]$. This was observed by Cox and Penkett, and such a plot has been redrawn from the original data; see Figure 39. Observe that the slope to intercept ratios for the linear plots at each $[H_2O]$ should give the quantity, $(A + [H_2O]k_{95})/k_{90}$, where $A = k_{96} + [C_4H_8]k_{91} + [O_3]k_{92}$. For runs at 76, 40 and 10% relative humidity, the slope/intercept ratios in Figure 39 are: 1.43 ± 0.26, 0.83 ± 0.21, and 0.30 ± 0.02 ppm. These are plotted versus $[H_2O]$ in Figure 40 and the expected linear dependence is seen. The intercept and slope in Figure 40 give $A/k_{90} \cong (6.1 \pm 0.3) \times 10^{-5}$, respectively. The kinetic treatment given here differs somewhat from that of Cox and Penkett in that we have attempted to include explicitly the reaction of H_2O with the intermediate. The data do suggest that the reaction with water is by far the dominant reaction of the intermediate; the ratio of rate of the reaction with water to that for all other reactions of the intermediate varies from about 4 for experiments at 40% relative humidity to about 8 at 76% relative humidity. This striking effect for water noted by Cox and Penkett suggests indirectly that RO_2, HO_2, HO, and other radical species which may be formed in the alkene-SO_2-O -H_2O air system are not the important oxidizing species present. Their reactivity toward H_2O is thought to be very low, and their concentrations will be altered insignificantly with H_2O increase.

There is one other rather thorough study of the alkene-O_3-SO_2-air system of which we are aware. McNelis (1974) made a kinetic study of the C_3H_6, O_3, SO_2, air system, and it is interesting to compare these results with those of Cox and Penkett. First it must be observed that McNelis did not vary the relative humidity over a wide range in his study so a quantitative test of the effect of H_2O is not possible. However he did observe in otherwise similar runs at 20% and 36% relative humidity, a conversion of 0.071 and 0.066 ppm SO_2/ppm O_3 consumed, respectively, the direction of the trend seen by Cox and Penkett. In retreating the McNelis data we have assumed that the reaction with H_2O is present and have used the same mechanism outlined for the butene studies. We recalculated the apparent second order rate constants for the O_3-C_3H_6 reaction from the McNelis data, using the conventional second order rate law and the observed data for $[O_3]$ and $[C_3H_6]$ versus time. The initial rate method used by McNelis seemed less accurate to us. The seemingly consistent set of data from the McNelis runs 26, 27, 31, 87, 88, 89, and 90 were used. The data gave $k_{95'}/k_{90'} \cong (7.4 \pm 1.5) \times 10^{-5}$ for the propylene data, in reasonable

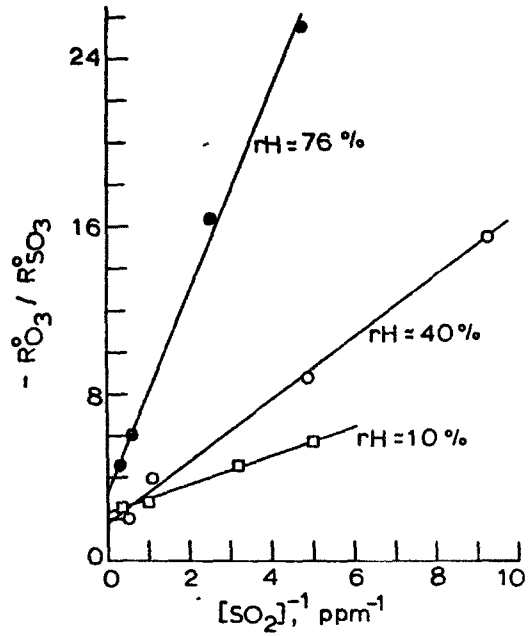

Figure 39. Plot of the ratio of rate of O_3 loss to rate of SO_3 formation versus $[SO_2]^{-1}$ for the data of Cox and Penkett (1972) from the dark reaction in cis-2-butene-SO_2-O_3-H_2O-air mixtures at various relative humidities (22°C).

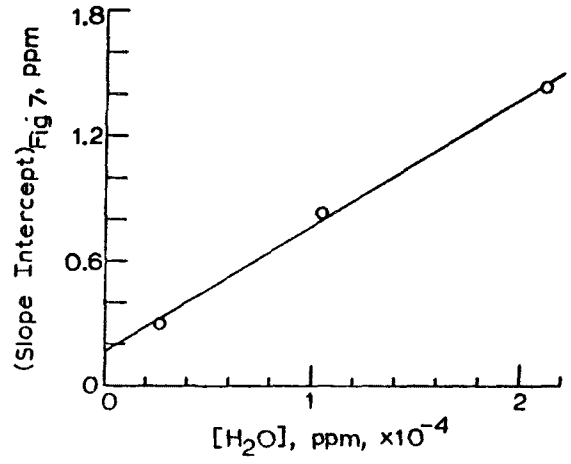

Figure 40. Plot of the ratio of slope/intercept for the plots of Figure 7 versus $[H_2O]$ derived from the data of Cox and Penkett (1972); the slope gives the k_{95}/k_{90} estimate used in this study.

accord with the estimate from the C_4H_8 data. Reactions 95' and 90' refer to the reactions of the species $\cdot CH_2OO\cdot$ as well as $CH_3CHOO\cdot$ which are both formed in the C_3H_6 system.

We can estimate the rate of SO_2 oxidation by the reactive intermediates formed in the O_3-alkene reactions using the data derived here. Taking a concentration of total alkenes = 0.10 ppm, $[O_3]$ = 0.15 ppm, and $[SO_2]$ = 0.05 ppm, typical of a highly polluted, sunlight-irradiated urban atmosphere, and using Niki's observation that about 20% of the O_3 molecules which react with alkene form the Criegee intermediate, we extimate that the rate of SO_2 oxidation, presumably through 43, will occur at about 0.23 and 0.12% hr^{-1} at 50 and 100% rH (25°C) when the reactivity of the alkene toward O_3 is typical of that for an alkene with a terminal double bond ($k \cong 1 \times 10^{-17}$ cm^3 $molec^{-1}s^{-1}$). In the unlikely event that 0.10 ppm of a highly reactive alkene such as cis-2-butene were present together with 0.15 ppm of ozone, then much higher rates of SO_2 oxidation would be expected. However we have neglected completely any loss reaction for the Criegee intermediate with NO in these considerations, so the rates estimated represent theoretical upper limits. Although these rates do not seem large in comparison with those expected for HO, HO_2, and CH_3O_2 reactions, they are not insignificant. The O_3-alkene reactions will continue to occur during the nighttime hours when both reactants are present, and the SO_2 oxidation from the products of this interaction will carry on as well; however, the rates are not expected to be large.

The SO_3 Reactions in the Atmosphere--

Reactions 45 and 46 have generally been neglected in kinetic simulations of the tropospheric chemistry of SO_2 and SO_3.

$$SO_3 + O(^3P)\ (+M) \rightarrow SO_4\ (+M) \qquad (45)$$

$$SO_3 + O(^3P)\ (+M) \rightarrow SO_2 + O_2\ (+M) \qquad (46)$$

Jacob and Winkler's 1972 estimate of the bimolecular rate constant for the SO_3-$O(^3P)$ reaction, $k_{45} + k_{46} \cong 5 \times 10^{-17}$ cm^3 $molec^{-1}s^{-1}$, justified this action. However more recently Daubendiek and Calvert (1973, 1977) and Westenberg and deHaas (1975b) have found that these reactions are very much faster than the earlier measurements suggested, and a new look at their potential role in the troposphere should be taken. Daubendiek and Calvert reported infrared kinetic studies from the O_3 photolysis ($\lambda > 590$ nm) in the presence of SO_3; they noted a rapid reaction (compared to $O + O_3 \rightarrow 2O_2$) which destroyed SO_3, but surprisingly, there was a delay in the SO_2 appearance which is expected if reaction 46 occurs. A metastable product absorbing at 6.78 μ was seen which decayed in the dark ($\tau_{1/2}$ = 280 s) to form SO_3 and SO_2. From the stoichiometry of the gases evolved the species appeared to be a mixture of S_3O_8 and S_3O_9. These seemed to form in the reaction between the SO_4 initial product of 45 and SO_2 and SO_3. The O-SO_3 reaction appeared to obey second order kinetics for pressures of SO_3 and O_3 above about 6 Torr. From the competitive rates of SO_3 and O_3 reactions with $O(^3P)$,

$$O(^3P) + O_3 \rightarrow 2O_2$$

they derived $k_{45} + k_{46} \cong 7 \times 10^{-13}$ cm^3 molec^{-1}s^{-1}, accepting $k_{99} = 8.5 \times 10^{-15}$ cm^3 molec^{-1}s^{-1} at 25°C (Hampson and Garvin, 1975).

Westenberg and deHaas (1975b) reported rate studies of the $O(^3P)$-SO_3 reaction using a discharge flow method with ESR detection of the $O(^3P)$. They found no evidence for an SO_4 intermediate for their conditions, but the fast overall reaction 46 seemed to occur with third order kinetics up to 7 Torr of He. They derived $k_{46} = 1.4 \times 10^{-31} e^{785/}$ cm^6 molec^{-2}s^{-1}(298-507°K). The third order nature of the reaction which they observed at low pressures suggests that an SO_4 intermediate is formed prior to rearrangement to their observed products, SO_2 and O_2. Indeed the results of both recent studies give strong independent evidence for the rapid occurrence of reactions 45 and 46; where the data do overlap in pressures employed, good agreement is found between the Daubendiek and Calvert and Westenberg and deHaas data. Both sets are consistent with the estimate: $k_{45} + k_{46} \cong 7 \times 10^{-13}$ cm^3 molec^{-1} s^{-1} in air at 1 atm and 25°C.

Consider the possible implications of these findings on the atmospheric chemistry of SO_2 and SO_3. Westenberg and deHaas (1975a) concluded from a consideration of the two reactions 25 and 46 alone, that the main effect of the presence of SO_2 on O in the atmosphere would be to catalyze its recombination with little or no net SO_3 formation.

$$O(^3P) + SO_2 \ (+M) \rightarrow SO_3 \ (+M) \qquad (25)$$

$$O(^3P) + SO_3 \ (+M) \rightarrow SO_2 + O_2 \ (+M) \qquad (46)$$

Thus using our present estimates of the rate constants for air at 1 atm, and assuming that SO_4 always forms $SO_2 + O_2$ ultimately, then we find $[SO_3]/[SO_2] = 0.08$ at the steady state. However there is no chance that a steady state of SO_3 and SO_2 will be established involving reactions 25 and 46 in the real atmosphere. The SO_3 molecule encounters with O-atoms will be very much less frequent than those with the abundant water molecule within the lower troposphere. Recent evidence of Castleman et al. (1975) confirmed the conclusion of Goodeve et al. (1934) that the overall reaction 47 is very fast; they estimated $k_{47} = (9.1 \pm 2.0) \times 10^{-13}$ cm^3 molec^{-1}s^{-1} from flow experience at low pressures. The rate constant estimate is surprisingly

$$SO_3 + H_2O \rightarrow H_2SO_4 \qquad (47)$$

large for such a complex rearrangement of reactant molecules that must accompany this reaction; the observation of the mass 98 product in the experiments of Castleman et al. may reflect the formation of an $SO_3 \cdot H_2O$ adduct which is a precursor to the final rearranged, stable product molecule, H_2SO_4. In any case the ultimate removal of SO_3 by its net reaction 47 with water is so very fast that the reaction of SO_3 with any other species in the moist lower atmosphere should be unimportant. We conclude from the evidence at hand that the usual assumption of modelers of the SO_2 conversion in the

troposphere, namely, that H_2SO_4 formation will always follow the generation of SO_3, appears to be sound.

Evaluation of the Relative Importance of the Homogeneous SO_2 Reactions with Various Reactive Species in the Troposphere

It is instructive to use the present evaluation of the SO_2 rate data to estimate in greater detail the rates of SO_2 homogeneous oxidation which we expect to occur in various clean and polluted regions of the troposphere. First let us consider the rate of oxidation of SO_2 which is anticipated for the relatively clean troposphere. The concentrations of the important species, HO, HO_2, and CH_3O_2 were estimated for various elevations within the troposphere of the northern hemisphere, and for various latitudes and seasons. If one considers the presence of SO_2 to be the ppb level or below in these atmospheres, it is a fair approximation to assume very little perturbation will occur in the estimated radical concentrations. Thus we can use the Crutzen and Fishman (1977) estimates to calculate the theoretical SO_2 conversion rates by reactions with HO, HO_2, and CH_3O_2 in the troposphere. Shown in Figure 41 are the rates averaged over all northern latitudes and the entire depth of the troposphere for each month of the year. Obviously the rate for the HO-radical reaction with SO_2, reaction 39, accounts for most of the oxidation; a significant fraction is also contributed by the HO_2-radical reaction 31 and a smaller amount from the CH_3O_2 species. The total average rate of SO_2 oxidation from these three most important homogeneous reactions varies from a low of 0.09% in January to a maximum of 0.2% hr^{-1} in July. Of course these rates are directly related to the solar irradiance, the temperature, and the atmospheric composition at the particular point within the troposphere. One can observe in Figure 42 the theoretical rates which are representative of the maximum values of the SO_2 oxidation by HO and HO_2 which occur near the 1200 hr averaged over each day in July. These are as high as 1.5% hr^{-1} at ground level and about 32° N latitude. The rate is somewhat lower at most latitudes as the elevation above sea level is increased. At 8 km a maximum rate of about 0.4% hr^{-1} is seen near 28° N latitude. At higher elevations (12 km) a small increase in rate can be observed. It is clear from these considerations that the rate of SO_2 homogeneous oxidation in the relatively clean troposphere can be very significant at certain time periods and positions within the troposphere.

Theoretical rates of SO_2 oxidation in parcels of highly polluted air are of special interest to us as well. Previous computer simulations of the reactions within a sunlight-irradiated, NO_x, RH, RCHO-polluted air mass have been made by Calvert and McQuigg (1975), Sander and Seinfeld (1976), and Graedel (1976). All workers agreed as to the importance of the HO- and HO_2-radical reaction rates with SO_2. For the simulated polluted atmosphere chosen by Calvert and McQuigg and for an older less accurate set of rate constants, a maximum SO_2 oxidation rate of 1.1% hr^{-1} was predicted in simulations carried out at a solar zenith angle of 40°. With a somewhat different choice of elementary reactions, rate constants, and initial reactants, Sander and Seinfeld predicted a maximum SO_2 homogeneous oxidation rate in their simulated polluted atmosphere of 4.5% hr^{-1}, with HO and HO_2 radicals again accounting for much of the reaction rate. Graedel's simulations employed the energetically unfavorable and unlikely chain

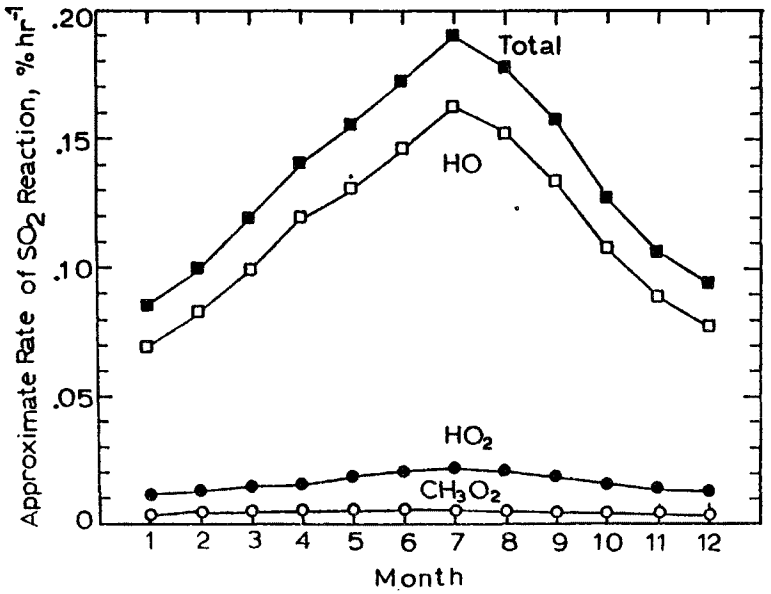

Figure 41. The theoretical monthly average of the rate (% hr^{-1}) of SO_2 oxidation within the northern atmosphere as a function of month of the year; rates are shown for the HO reaction 39, the HO_2 reaction 31, the CH_3O_2 reaction 33, and the total of these three rates; calculated using [HO], [HO_2], and [CH_3O_2] estimates of Crutzen and Fishman (1977).

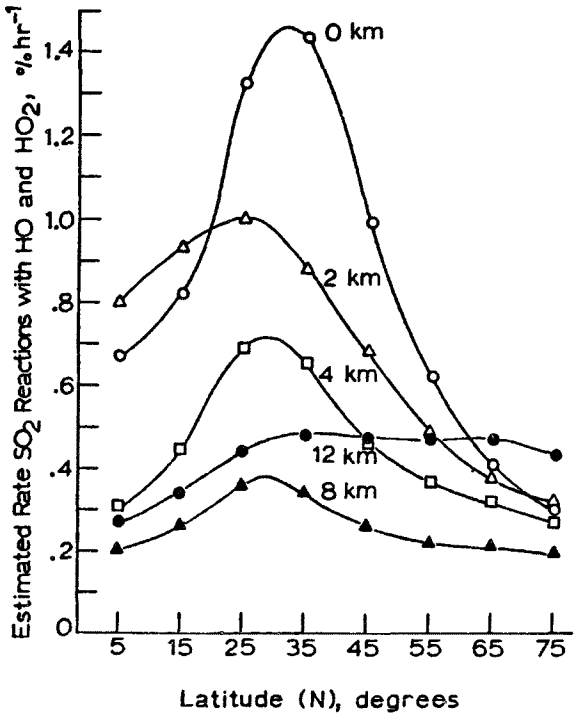

Figure 42. The theoretical rate (% hr^{-1}) of SO_2 oxidation by HO (reaction 39) and HO_2 (reaction 31) at various elevations within the troposphere and at various latitudes in the northern hemisphere; data are for the average rates for the 1200 hour in the month of July; calculated using the [HO] and [HO_2] estimates of Crutzen and Fishman (1977).

reaction sequence of Davis and Klauber (1975), so comparisons with his results are of questionable value. In Figure 43 is given an updated version of the Calvert and McQuigg simulations of SO_2 removal rates based upon the new data and the new rate constant choices presented in this study. The simulated atmosphere contained initially (ppm): [NO] = 0.15; [NO_2] = 0.05; [cis-2-C_4H_8] = 0.10; [CO] = 10; [CH_4] = 1.5; [CH_2O] = 0; [CH_3CHO] = 0; [SO_2] = 0.05; relative humidity, 50% (25°C); solar zenith angle, 40°; a stagnant air mass without dilution was considered to simulate the conditions of highest smog-forming potential. The O_3 concentration in this simulation rose to 0.15 ppm at the 120 min point of the irradiation at which time the alkene had decreased to 0.013 ppm. The length of the ordinate within each area of Figure 11 represents the theoretical % hr^{-1} of SO_2 oxidation by the radicals shown. Note that the total oxidation rate from the several species rises to over 4% hr^{-1} at about 60 min into the irradiation. There is one major difference between these results and those of the previous simulations. The newly estimated rate constant for the CH_3O_2-SO_2 reactions 33 and 34, has been included, and this reaction has added an additional increment to the SO_2 homogeneous oxidation rate expected in theory. It appears that about equal rates of oxidation of SO_2 occur in a highly polluted atmosphere through the reactions of the HO_2, CH_3O_2, and the HO species (reactions 31, 33, 39). We have picked conditions, a high concentration of very reactive alkene (trans-2-butene) and $k_{86} = 0$, which should accentuate the contribution of the Criegee intermediate. Even so the rates of SO_2 oxidation from reaction 43 are relatively small compared to the rates of the three major reacting species; the contribution from this reaction increases to a maximum of 0.25% hr^{-1} at about 60 min into the irradiation period. It is improbable that an actual polluted atmosphere would contain this much reactive alkene and that $k_{86} = 0$. Hence we conclude that the Criegee intermediate is probably never a major reactant for SO_2 oxidation in the highly polluted atmosphere, although during nighttime hours this reaction is likely the major homogeneous SO_2 oxidation mechanism which is operative.

There is one other major class of SO_2 polluted atmosphere which is of special interest to us. It is that contained in a stack plume from a power plant or other industrial combustion operation. These gaseous mixtures are of unique composition; the original effluent is oxygen-depleted and NO- and SO_2- rich. Because of the very high NO levels and the very low hydrocarbon and CO levels, the long oxidation chains which can lead to the reasonably rapid conversions of SO_2 to SO_3, H_2SO_4, etc., are suppressed during the first stages of the plume transport. The initial [NO_2]/[NO] ratio is very low so that the [O_3] generated through the reaction sequence 100, 101, and 87,

$$NO_2 + h\nu(\lambda < 4100\ \text{Å}) \rightarrow NO + O \qquad (100)$$

$$O + O_2\ (+M) \rightarrow O_3\ (+M) \qquad (101)$$

$$O_3 + NO \rightarrow NO_2 + O_2 \qquad (87)$$

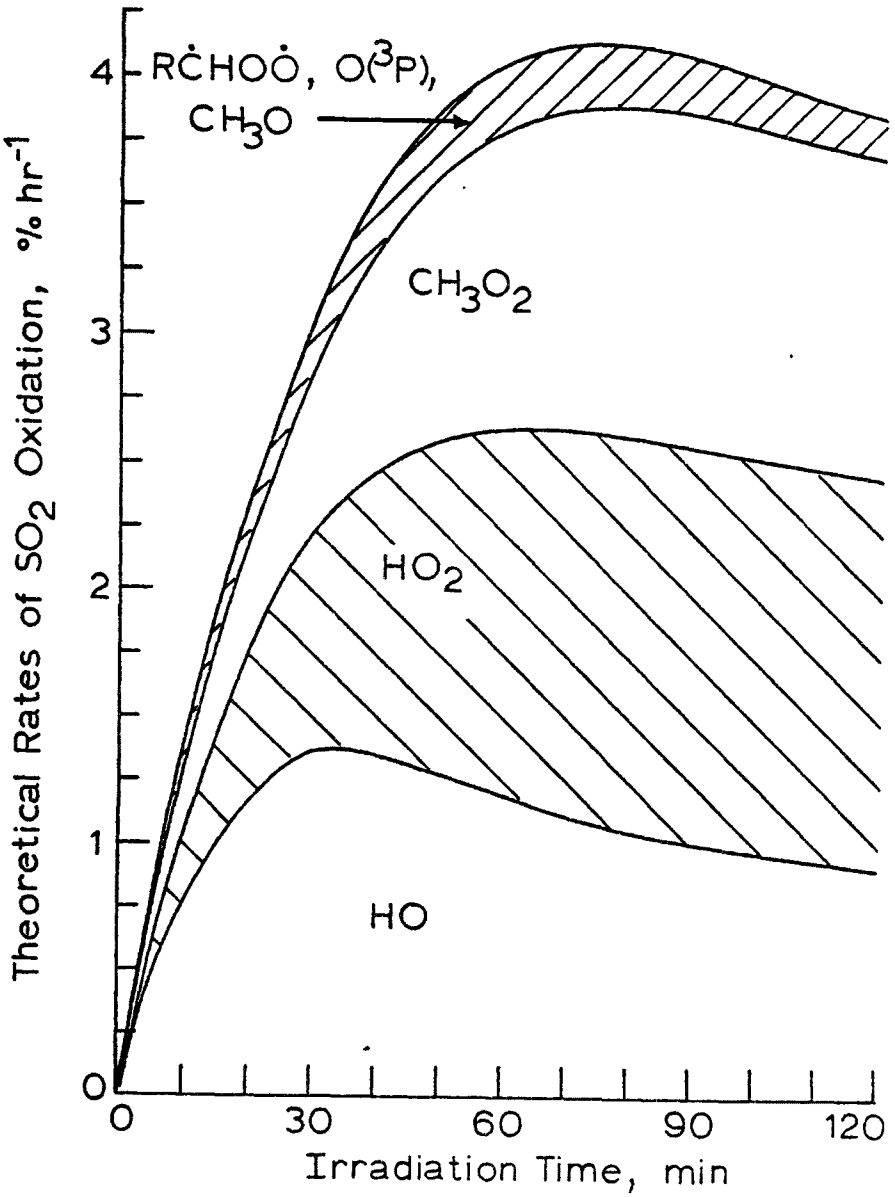

Figure 43. The theoretical rate of attack of various free radical species on SO_2 (% hr^{-1}) for a simulated sunlight-irradiated (solar zenith angle = 40°), polluted atmosphere; initial concentrations (ppm): [SO_2] = 0.05; [NO] = 0.15; [NO_2] = 0.05; [CO] = 10; [CH_4] = 1.5; [CH_2O] = 0; [CH_3CHO] = 0; relative humidity, 50%($25^{\circ}C$).

will be very much below the 0.04 ppm values observed in relatively clean ambient air. For the conditions present in the plume after a short mixing period, the O_3 should reach a photostationary state for which the $[O_3]$ will be related to the $[NO_2]/[NO]$ ratio, the apparent first order rate constant for the rate of photolysis of NO_2 in 100 (k_{100}), the rate limiting process for O_3 formation in 101, and the rate constant k_{87} for the dominant O_3 loss reaction 87.

$$[O_3] \cong [NO_2]\ k_{100}/[NO]\ k_{87} \qquad (102)$$

k_{100} is a function of the solar irradiance in the 4100 to 2900 Å region and a typical value for k_{100}/k_{87} is 0.02 ppm for the 1000 to 1400 time period (Calvert, 1976). Thus the ozone level will not reach the "clean air" background values within the plume until the $[NO_2]/[NO]$ ratio climbs to near 2. Actual plume data show significant depletion of the ambient ozone levels within the plume for very great distances. For examples see Davis et al. (1974d) and Wilson et al. (1976). Only after the plume gases have mixed with sufficient quantities of reactant hydrocarbons, aldehydes, CO, etc., present in the ambient air can extensive NO to NO_2 conversion be effected and O_3 levels climb. However there are at least two mechanisms which in theory can contribute to an initial burst of SO_2 oxidation involving the elementary reactions of Table 18.

The first of these involves the photolysis of NO_2 (reaction 100) early in the plume dilution when the $[O_2]$ is relatively low, $[SO_2]$ is high, and the fraction of O-atoms captured by SO_2 can be significant. NO_2 represents a small fraction of the plume gases released to the atmosphere. Additional NO_2 is formed as the ambient air mixes in with the NO-rich gases: $2NO + O_2 \rightarrow 2NO_2$. For these conditions the SO_2 in the plume gases can compete somewhat successfully with NO, NO_2, as well as O_2 for the O-atoms formed from NO_2 photolysis in 100:

$$NO_2 + h\nu \rightarrow O + NO \qquad (100)$$

$$O + O_2\ (+M) \rightarrow O_3\ (+M) \qquad (101)$$

$$O + NO_2 \rightarrow O_2 + NO \qquad (102)$$

$$O + NO_2\ (+M) \rightarrow NO_3\ (+M) \qquad (103)$$

$$O + NO\ (+M) \rightarrow NO_2\ (+M) \qquad (104)$$

$$O + SO_2\ (+M) \rightarrow SO_3\ (+M) \qquad (25)$$

The rates of SO_2 oxidation from reaction 25 alone in the sunlight-irradiated stack gases can be significant during the early stages of dilution. Thus if we assume stack gases to be at the concentrations: $[NO] = 500$, $[SO_2] = 500$, $[NO_2] = 20$; $[O_2] = 1 \times 10^5$ ppm, for midday sunlight we expect an instantaneous rate of SO_2 oxidation by 25 alone to be about 1.4% hr^{-1}. This rate will drop fairly quickly as further dilution occurs with

the transport of the plume. As the plume is further diluted by factors of 4, 8, 16, and 32, the instantaneous rates of SO_2 oxidation by reaction 25 are expected to fall to 0.43, 0.20, 0.10, and 0.05% hr^{-1}. A similar early peak in the rate of the homogeneous oxidation of SO_2 by reaction 39 is expected with the HO-radicals formed from the photolysis of HONO. The

$$HONO + h\nu(\lambda < 4000\ \text{Å}) \rightarrow HO + NO \qquad (105)$$

generation of HONO early in the dilution of stack plumes may occur in theory through the homogeneous reaction 106 (Chan et al., 1976) or through heterogeneous paths involving water condensation or particulate surfaces:

$$NO + NO_2 + H_2O \rightarrow 2HONO \qquad (106)$$

Thus the development of as much as 10 ppm of HONO within a short dilution period of certain stack effluents with very high NO, NO_2, and H_2O concentrations may occur. When HONO is at the 10 ppm level with $[SO_2] = 500$, $[NO] = 500$, $[NO] = 20$, $[CO] = 1$ ppm, the instantaneous rate of SO_2 oxidation by 39 is expected to be about 1.2% hr^{-1} in noonday sunlight. In this case O_2 is not a competitor for HO but the NO, NO_2, and CO are:

$$HO + SO_2\ (+M) \rightarrow HOSO_2\ (+M) \qquad (39)$$

$$HO + NO\ (+M) \rightarrow HONO\ (+M) \qquad (107)$$

$$HO + NO_2\ (+M) \rightarrow HONO_2\ (+M) \qquad (108)$$

$$HO + CO\ (+M) \rightarrow H + CO_2\ (+M) \qquad (109)$$

After dilution of the reaction mixture by a factor of ten with clean air, the rate of SO_2 oxidation by 106 again falls presipitously to 0.1% hr^{-1}.

Recently Miller (1977) has simulated the chemical rates of change within a stack plume; the only SO_2 removal mode which he included was reaction 39. It is interesting that he did observe a maximum rate of SO_2 oxidation (about 0.1% hr^{-1}) early in the dilution of the stack gases with either unpolluted or polluted air.

As we have seen one anticipates in theory that SO_2 may be oxidized at rates up to several percent per hour for a short period during the early stages of stack gas dilution through the occurrence of the homogeneous reactions 25 and 39 in a sunlight-irradiated plume. It is evident that the apparent order of SO_2 conversion will appear to be higher than first during the first stages of plume dilution. Such orders have been observed in stack plumes. They have been rationalized well in terms of heterogeneous reactions alone (Schwartz and Newman, 1977).

The homogeneous SO_2 conversion rates at long transport times are expected to increase as dilution of the stack gases with urban air containing hydrocarbons, aldehydes, ozone, etc., occurs, and the rapid chain reaction sequence familiar to smog chemistry take over. The SO_2 to sulfate conversion rates estimated in plumes at long transport times in the study of Wilson

et al. (1976) were observed to increase from about 1.5% hr^{-1} during the 0.7 to 1.5 hr transport time period (10-21 km path) to about 5% hr^{-1} after 2.3 to 3.2 hours of transport (32-45 km path). Gillani et al. (1977) observed in recent studies in the St. Louis area, maximum rates of SO_2 conversion to particulate sulfur of the order of 3% hr^{-1} in plumes with significant transport time and dilution. They also presented some significant evidence that homogeneous photochemical processes may be important in the SO_2 conversions observed.

From the considerations presented in the present study we conclude that the homogeneous oxidation of SO_2 in the troposphere does occur at rates which constitute a major fraction of the rates observed experimentally. It is the hope of the authors that the discussion and the data presented in this study will be useful to the atmospheric scientists in their continued development of more quantitative models of the tropospheric SO_2 oxidation and transport.

REFERENCES

E.R. Allen and J.E. Bonelli (1972b) The photooxidation of sulfur dioxide in urban atmospheres. Abstracts, 6th Informal Photochemistry Conference, Oklahoma State University, p. 6.1-6.2.

E.R. Allen, R.D. McQuigg, and R.D. Cadle (1972a) The photooxidation of gaseous sulfur dioxide in air. Chemosphere 1, 25-32.

E.R. Altwicker (1976) Ozone formation during sulfur dioxide irradiation. J. Environ. Sci. Health A11, 439-443.

R. Atkinson, B.J. Finlayson and J.N. Pitts, Jr. (1973) Photoionization mass spectrometer studies of gas phase ozone-olefin reactions. J. Amer. Chem. Soc. 95, 7592-7599.

R. Atkinson, R.A. Perry and J.N. Pitts, Jr. (1976) Rate constants for the reactions of the OH radical with NO_2 (M = Ar and N_2) and SO_2 (M = Ar). J. Chem. Phys. 65, 306-310.

R. Atkinson and J.N. Pitts, Jr. (1974) Rate constants for the reaction of $O(^3P)$ atoms with SO_2 (M = N_2O) over the temperature range 299-392 K. Chem. Phys. Letters 29, 28-30.

C.C. Badcock, H.W. Sidebottom, J.G. Calvert, G.W. Reinhardt, and E.K. Damon (1971) Mechanism of the photolysis of sulfur dioxide-paraffin hydrocarbon mixtures. J. Amer. Chem. Soc. 93, 3115-3121.

D.L. Baulch and D.D. Drysdale (1974) An evaluation of the rate data for the reaction CO + OH → CO_2 + H. Combust. Flame 23, 215-225.

D.L. Baulch, D.D. Drysdale, and A.C. Lloyd (1972) Evaluated kinetic data for high temperature reactions, Vol. 1, Butterworths, London.

S.W. Benson (1976) Thermochemical kinetics, Second Edition, John Wiley & Sons, Inc., New York, pp 1-320.

S.W. Benson (1977) Thermochemistry and kinetics of sulfur containing molecules and radicals. Preprint of a paper to appear in Chem. Revs.

F.E. Blacet (1952) Photochemistry in the lower atmosphere. Ind. Eng. Chem. 44, 1339-1346.

G.K. Boreskov and V.V. Illarionov (1940) J. Phys. Chem. Moscow 14, 1428; quoted in Kondratiev V.N. (1970) Rate constants of gas-phase reactions, Science Publishing House, Moscow, p. 233.

J.W. Bottenheim and O.P. Strausz (1977) Review of pollutant transformation processes relevant to the Alberta oil sands area and proposals for further studies. Teport to Atmospheric Environment Service, Dept. Supply and Services Canada, Contract No. OSU 76-00169, from Hydrocarbon Research Center, University Alberta, Edmonton, Alberta, Canada, T6G 2G2.

J.C.D. Brand, C. diLauro, and V.T. Jones (1970) Structure of the $^3B_1$ state of sulfur dioxide. J. Amer. Chem. Soc. 92, 6095-6096.

L.E. Brus, and J.R. McDonald (1974) Time-resolved fluorescence kinetics and $^1B_1(^1\Delta_g)$ vibronic structure in tunable ultraviolet laser excited SO_2 vapor. J. Chem. Phys. 61, 97-105.

J.G. Calvert (1976) Test of the theory of ozone generation in Los Angeles atmosphere. Environ. Sci. Technol. 10, 248-256.

J.G. Calvert and R.D. McQuigg (1975) The computer simulation of the rates and mechanisms of photochemical Smog formation. Int. J. Chem. Kinet. Symp. 1, 113-154.

J.G. Calvert, D.H. Slater, and J.W. Gall (1971) The methyl radical-sulfur dioxide reaction. In Chemical Reactions in Urban Atmospheres, Tuesday C.S., editor, American Elsevier Publishing Co., pp. 133-158.

A.W. Castleman, Jr., H.R. Munkelwitz, and B. Manowitz (1974) Isotopic studies of the sulfur component of the stratospheric aerosol layer. Tellus 26, 222-234.

A.W. Castleman, Jr. and I.N. Tang (1976/77) Kinetics of the association reaction of SO_2 with the hydroxyl radical. J. Photochem. 6, 349-354.

E. Cehelnik, J. Heicklen, S. Braslavsky, L. Stockburger III, and E. Mathias (1973/74) Photolysis of SO_2 in the presence of foreign gases. IV. Wavelength and temperature effects with CO. J. Photochem. 2, 31-48.

E. Cehelnik, C.W. Spicer, and J. Heicklen (1971) Photolysis of sulfur dioxide in the presence of foreign gases. I. Carbon monoxide and perfluoroethylene. J. Amer. Chem. Soc. 93, 5371-5380.

W.H. Chan, R.J. Nordstrom, J.G. Calvert, and J.H. Shaw (1976) Kinetic study of HONO formation and decay reactions in gaseous mixtures of HONO, NO, NO_2, H_2O, and N_2. Environ. Sci. Technol. 10, 674-682.

W.H. Chan, W.M. Uselman, J.G. Calvert, and J.H. Shaw (1977) The pressure dependence of the rate constant for the reaction: $HO + CO \rightarrow H + CO_2$. Chem. Phys. Letters 45, 240-244.

K. Chung, J.G. Calvert and J.W. Bottenheim (1975) The photochemistry of sulfur dioxide excited within its first allowed band at 3130Å and the "forbidden" band (3700-4000Å). Int. J. Chem. Kinet. 7, 161-182.

M.A.A. Clyne, B.A. Thrush and R.P. Wayne (1964) Kinetics of the chemiluminescent reaction between nitric oxide and ozone. Trans. Faraday Soc. 60, 359-370.

R.A. Cox (1972) Quantum yields for the photooxidation of sulfur dioxide in the first allowed absorption region. J. Phys. Chem. 76, 814-820.

R.A. Cox (1973) Some experimental observations of aerosol formation in the photooxidation of sulfur dioxide. Aerosol. Sci. 4, 473-483.

R.A. Cox (1974/75) The photolysis of nitrous acid in the presence of carbon monoxide and sulfur dioxide. J. Photochem. 3, 291-304.

R.A. Cox (1975) The photolysis of gaseous nitrous acid -- A technique for obtaining kinetic data in atmospheric photooxidation reactions. Int. J. Chem. Kinet. Symp. 1, 379-398.

R.A. Cox and S.A. Penkett (1970) The photooxidation of sulfur dioxide in sunlight. Atm. Environ. 4, 425-433.

R.A. Cox and S.A. Penkett (1971a) Oxidation of atmospheric SO_2 by products of the ozone-olefin reaction. Nature 230, 321-322.

R.A. Cox and S.A. Penkett (1971b) Photooxidation of atmospheric SO_2. Nature 229, 486-488.

R.A. Cox and S.A. Penkett (1972) Aerosol formation from sulfur dioxide in the presence of ozone and olefinic hydrocarbons. J. Chem. Soc. Faraday Trans. I 68, 1735-1753.

R. Criegee (1957) The course of ozonization of unsaturated compounds. Record Chem. Progr. 18, 111-120.

P.J. Crutzen and J. Fishman (1977) Average concentrations of OH in the northern hemisphere troposphere, and the budgets of CH_4, CO, and H_2. Geophys. Res. Letters, submitted for publication May, 1977; in a private communication to one of the authors, computer readouts of [OH], [HO_2], and [CH_3O_2] were provided.

R.L. Daubendiek and J.G. Calvert (1973) A photochemical study involving SO_2, O_2, SO_3 and O_3. Abstracts 165th National Meeting of the Amer Chem. Soc., Dallas, Texas, Physical Section, paper #19.

R.L. Daubendiek and J.G. Calvert (1975) A study of the N_2O_5-SO_2-O_3 reaction system. Environ. Letters 8, 103-116.

R.L. Daubendiek and J.G. Calvert (1977) An infrared study of the O + SO_3 reaction. Paper in preparation.

J.A. Davidson and E.W. Abrahamson (1972) The SO_2 photosensitized production of $O_2(^1\Sigma_g+)$. Photochem. Photobiol. 15, 403-405.

J.A. Davidson, K.E. Kear and E.W. Abrahamson (1972/73) The photosensitized production and quenching of $O_2(^1\Sigma_g^+)$. J. Photochem. 1, 307-316.

D.D. Davis (1974a) A kinetics review of atmospheric reactions involving H_x O_y compounds. Can. J. Chem. 52, 1405-1414.

D.D. Davis (1974b) Absolute rate constants for elementary reactions of atmospheric importance: results from the University of Maryland s gas kinetics 1974; quoted in Hampson and Garvin (1975), p. 55.

D.D. Davis, S. Fischer, and R. Schiff (1974c) Flash photolysis reasonance fluorescence kinetics study: temperature dependence of the reactions OH + $CO \rightarrow CO_2$ + H and OH + $CH_4 \rightarrow H_3O$ + CH_3. J. Phys. Chem. 61, 2213-2219.

D.D. Davis and G. Klauber (1975) Atmospheric gas phase oxidation mechanisms for the molecule SO_2. Int. J. Chem Kinet. Symp. 1, 543-556.

D.D. Davis, J. Prusazcyk, M. Dwyer and P. Kim (1974b) A stop-flow time-of-flight mass spectrometer kinetics study. Reaction of ozone with nitrogen dioxide and sulfur dioxide. J. Phys. Chem. 78, 1775-1779.

D.D. Davis and R. Schiff (1974); unpublished work quoted in D.D. Davis (1974a).

D.D. Davis, R. Schiff and S. Fischer (1974a); unpublished work quoted in D.D. Davis (1974a).

D.D. Davis, G. Smith, and G. Klauber (1974d) Trace gas analysis of power plant plumes via aircraft measurement: O_3, NO_x, SO_2 chemistry. Science 186, 733-736.

K.L. Demerjian, J.G. Calvert and D.L. Thorsell (1974) A kinetic study of the chemistry of the $SO_2(^3B_1)$ reactions with cis- and trans-2-butene. Int. J. Chem. Kinet. 6, 829-848.

K.L. Demerjian, J.A. Kerr and J.G. Calvert (1974) The mechanism of photochemical smog formation. Adv. Environ. Sci. Technol. 4, 1-262.

E.S. Domalski (1971) Thermochemical properties of peroxyacetyl (PAN) and peroxybenzoyl nitrate (PBN) Environ. Sci. Technol. 5, 443-444.

R.W. Fair and B.A. Thrush (1969) Reaction between hydrogen atoms and sulfur dioxide. Trans Faraday Soc. 65, 1550-1570.

D.S. Fee, S.S. Markowitz and J.K. Garland (1972) Sulfur dioxide as a radical scavenger in alkene systems. Radiochim. Acta 17, 135-138.

B.J. Finlayson, J.N. Pitts Jr. and R. Atkinson (1974) Low pressure gas phase ozone-olefin reactions. Chemiluminescence, kinetics and mechanisms. J. Amer. Chem. Soc. 96, 5356-5367.

S.N. Foner and R.L. Hudson (1962) Mass spectrometry of inorganic free radicals. Advan. Chem. Ser. 36, 34-49.

D.L. Fox and R.S. Wright (1977) Photochemical smog mechanisms-HC-NO_x-SO_2 systems. Paper presented at the 4th International Clean Air Congress, May 16-20, Tokyo, Japan; the authors are grateful for a preprint of this paper.

T. Frankiewicz and R.S. Berry (1972) Singlet molecular oxygen production from photoexcited NO_2. Environ. Sci. Technol. 6, 365-366.

K. F. Freed (1976) Theory of collision induced intersystem crossing. J. Chem. Phys. 64, 1604-1611.

J.P. Friend, R. Leifer and M. Trichon (1973) On the formation of stratospheric aerosols. J. Atm. Sciences 30, 465-479.

O.L.J. Gijzeman (1974) Interaction between oxygen and aromatic molecules. J. Chem. Soc. Faraday Trans. II 70, 1143-1152.

O.L.J. Gijzeman and F. Kaufman (1973) Oxygen quenching of aromatic triplet states in solution. Part 2. J. Chem. Soc., Faraday Trans. II 69, 721-726.

O.L.J. Gijzeman, F. Kaufman and G. Porter (1973a) Oxygen quenching of aromatic triplet states in solution. Part 1. J. Chem. Soc., Faraday Trans. II 69, 708-720.

O.L.J. Gijzeman, Kaufman F., and Porter G. (1973b) Quenching of aromatic triplet states in solution by nitric oxide and other free radicals. J. Chem. Soc. Faraday Trans. II 69, 727-737.

N.V. Gillani, R.B. Jusar, J.D. Husar and D.E. Patterson (1977) Project MISTT: Kinetics of particulate sulfur formation in a power plant plume out to 300 km. Paper in International Symposium on "Sulfur in the Atmosphere", Dubrovnik, Yugoslavia, Sept. 7-14, 1977; the authors are grateful for a preprint of this.

A. Good and J.C.J. Thynne (1967a) Reaction of free radicals with sulfur dioxide. Part 1-Methyl radicals. Trans. Faraday Soc. 63, 2708-2719.

A. Good and J.C.J. Thynne (1967b) Reaction of free radicals with sulfur dioxide. Part 2-Ethyl radicals. Trans. Faraday Soc. 63, 2720-2727.

S. Gordon and W.A. Mulac (1975) Reaction of the $OH(X^2\Pi)$ radical produced by the pulse radiolysis of water vapor. Int. J. Chem. Kinet. Symp. 1, 289-299.

T.E. Graedel (1976) Sulfur dioxide, sulfate aerosol, and urban ozone. Geophys. Res. Letters 3, 181-184.

R. Greiner (1967) Hydroxyl-radical kinetics by kinetic spectroscopy. I. Reactions with H_2, CO, and CH_4 at 300°K. J. Chem. Phys. 46, 2795-2799.

T.C. Hall (1953) Photochemical studies of nitrogen dioxide and sulfur dioxide. Ph.D. Thesis, University of California, Los Angeles.

C.J. Halstead and D.R. Jenkins (1969) Sulfur dioxide-catalyzed recombination of radicals in premixed fuel-rich hydrogen + oxygen + nitrogen flames. Trans. Faraday Soc. 65, 3013-3022.

E.J. Hamilton Jr. (1975) Water vapor dependence of the kinetics of the self-reaction of HO_2 in the gas phase. J. Chem. Phys. 63, 3682-3683.

E.J. Hamilton Jr. and C.A. Naleway (1976) Theoretical calculation of strong complex formation by the HO_2 radical: $HO_2 \cdot H_2O$ and $HO_2 \cdot NH_3$. J. Phys. Chem. 80, 2037-2040.

R.F. Hampson and D. Garvin (1975) Chemical kinetic and photochemical data for modeling atmospheric chemistry. U.S. National Bureau Standards Technical Note 866, U.S. Government Printing Office, 1-113.

P.L. Hanst, E.R. Stephens, W.E. Scott and R.C. Doerr (1959) Atmospheric ozone-olefin reactions. Paper presented before Division of Petroleum Chemistry, 136th National Meeting American Chemical Society, Atlantic City, Sept. 13, paper #28, p. 7R.

G.W. Harris and R.P. Wayne (1975) Reaction of hydroxyl radicals with NO, NO_2 and SO_2. J. Chem. Soc. Faraday I 71, 610-617.

J. Heicklen (1976) Atmospheric Chemistry, Academic Press, New York, pp. 343-344.

D.G. Hendry and R.A. Kenley (1977) Generation of peroxy radicals from peroxy nitrates (RO_2NO_2). Decomposition of peroxyacyl nitrates. J. Amer. Chem. Soc. 99, 3198-3199.

C.J. Hochanadel, J.A. Ghormley and P.J. Ogren (1972) Absorption spectrum and reaction kinetics of the HO_2 radical in the gas phase. J. Chem. Phys. 56, 4426-4432.

A. Horowitz A. and J.G. Calvert (1972a) The SO_2-sensitized phosphorescence of biacetyl in photolyses at 2650 and 2875Å; the intersystem crossing ratio in sulfur dioxide. Int. J. Chem. Kinet. 4, 175-189.

A. Horowitz and J.G. Calvert (1972b) A study of the intersystem crossing reaction induced in gaseous sulfur dioxide molecules by collisions with nitrogen and cyclohexane at 27°. Int. J. Chem. Kinet. 4, 191-205.

A. Horowitz and J.G. Calvert (1972c) Emission studies of the mechanism of gaseous biacetyl photolysis at 3450, 3650, 3880 and 4380Å and 28°C. Int. J. Chem. Kinet. 4, 207-227.

O. Hov, I.S.A. Isaken and E. Hesstvedt (1977) Diurnal variations of ozone and other pollutants in an urban area. Report No. 24, Institutt for Geofysikk, Universitetet i Oslo, Jan., 1977.

L.A. Hull, I.C. Hisatsune and J. Heicklen (1972) Low-temperature infrared studies of simple alkene-ozone reactions. J. Amer. Chem. Soc. 94, 4856-4864.

G.E. Jackson and J.G. Calvert (1971) The triplet sulfur dioxide-carbon monoxide reaction exited within the $SO_2(^1A_1) \rightarrow SO_2(^3B_1)$ "forbidden" band. J. Amer. Chem. Soc. 93, 2593-2599.

A. Jacob and C.A. Winkler (1972) Kinetics of the reaction of oxygen atoms and nitrogen atoms with sulfur trioxide. J. Chem. Soc. Faraday Trans. I 68, 2077-2082.

F.C. James, J.A. Kerr and J.P. Simons (1973) Direct measurement of the rate of reaction of the methyl radical with sulfur dioxide. J. Chem. Soc. Faraday Trans. I 69, 2124-2129.

I.T.N. Jones and K.D. Bayes (1971) Energy transfer from electronically excited NO_2. Chem Phys. Letters 11, 163-166.

C.E. Junge (1972) The cycle of atmospheric gases-natural and man made. Quart. J. Roy. Meteor. Soc. 98, 711-729.

M. Kasahara and K. Takahashi (1976) Experimental studies on aerosol particle formation by sulfur dioxide. Atm. Environ. 10, 475-486.

K. Kawaoka, A.U. Khan and D.R. Kearns (1967) Role of singlet excited states of molecular oxygen in the quenching of organic triplet states. J. Chem. Phys. 46, 1842-1853.

K. Kear and E.W. Abrahamson (1974/75) Electronic energy transfer in the gas phase: the quenching of $O_2(^1\Sigma_g^+)$. J. Photochem. 3, 409-416.

D.R. Kearns (1971) Physical and chemical properties of singlet molecular oxygen. Chem. Rev. 71, 395-427.

N. Kelly, J.F. Meagher and J. Heicklen (1976/77) The photolysis of sulfur dioxide in the presence of foreign gases. VIII. Excitation of SO_2 at 3600-4100Å in the presence of acetylene. J. Photochem. 6, 157-172.

J.A. Kerr and M.J. Parsonage (1972) Evaluated kinetic data on gas phase reactions. Butterworths, University of Birmingham, England.

R. Kigel and H. Taube (1975) Infrared spectrum and structure of matrix-isolated sulfur tetroxide. J. Phys. Chem. 79, 2130-2135.

W.A. Kummer, J.N. Pitts Jr., and R.P. STeer (1971) The chemiluminescent reaction of ozone with olefins and organic sulfides. Envir. Sci. Technol. 5, 1045-1047.

A. Levy, D.R. Drewes and J.M. Hales (1976) SO_2 oxidation in plumes: a review and assessment of relevant mechanistic and rate studies. Report EPA-450/3-76-022 prepared for the U.S. Environmental Protection Agency, Office of Air Quality Planning and Standards, Contract No. 68-02-1982 by Battelle Pacific Northwest Laboratories, Richland, Washington 19352.

A.C. Lloyd 1974) Evaluated and estimated kinetic data for gas phase reactions of the hydroperoxyl radical. Int. J. Chem. Kinet. 6, 169-228.

R. Louw, J. vanHam and H. Nieboer (1973) Nitrogen trioxide: key intermediate in the chemistry of polluted air? J. Air Pollut. Control Ass. 23, 716.

R. McAndrew and R. Wheeler (1962) The recombination of atomic hydrogen in propane flame gases. J. Phys. Chem. 66, 229-232.

D.N. McNelis (1974) Aerosol formation from gas-phase reactions of ozone and olefin in the presence of sulfur dioxide. Final report 650/4-74-034 to the Environmental Protection Agency, Research Triangle Park, North Carolina, for program element 21 AKB, ROAP 38, August, 1974.

A.J. Merer (1963) Rotational analysis of bands of the 3800Å system of SO_2. Discussions Faraday Soc. 35, 127-136.

H.D. Mettee (1969) Foreign gas quenching of sulfur dioxide vapor emission. J. Chem. Phys. 73, 1071-1076.

D.F. Miller (1977) Simulations of gas-phase reactions in power plant plumes. Preprint of a paper presented at 173rd National Meeting Amer. Chem. Soc., New Orleans, March, 1977.

R. Milstein, R.L. Williams and F.S. Rowland (1974) Relative reaction rates involving thermal fluorine-18 atoms and thermal fluoroethyl radicals with oxygen, nitric oxide, sulfur dioxide, nitrogen, carbon monoxide and hydrogen iodide. J. Phys. Chem. 78, 857-863.

M.F.R. Mulcahy, J.R. Steven and J.C. Ward (1967) The kinetics of reaction between oxygen atoms and sulfur dioxide; an investigation by electron spin resonance spectrometry. J. Phys. Chem. 71, 2124-2131.

M.F.R. Mulcahy and R.H. Smith (1971) Reactions of OH radicals in the H-NO_2 and H-NO_2-CO systems. J. Chem. Phys. 54, 5215-5221.

H. Niki (1977) Private communication to one of the authors.

H. Niki, P.D. Maker, C.M. Savage and L.P. Breitenbach (1975) Fourier transform spectroscopic studies of organic species participating in photochemical smog formation. Paper at International Conference on Environmental Sensing and Assessment, Las Vegas, Nevada, Sept. 14, 1975, Vol. 2, 24-4.

H. Niki, P.D. Maker, C.M. Savage and L.P. Breitenbach (1977) Fourier transform IR spectroscopic observations of propylene ozonide in the gas phase reaction of ozone-cis-butene-formaldehyde. Chem. Phys. Letters 46, 327-330.

S. Okuda, T.N. Rao, D.H. Slater and J.G. Calvert (1969) Identification of the photochemically active species in sulfur dioxide photolysis within the first allowed absorption band. J. Phys. Chem. 73, 4412-4415.

H.E. O'Neal and C. Blumstein (1973) A new mechanism for gas phase ozone-olefin reactions. Int. J. Chem Kinet. 5, 397-413.

R. Overend, G. Paraskevopoulos and R.J. Cvetanovic (1974) Hydroxyl radical rate measurement for simple species by flash photolysis kinetic spectroscopy. Paper 6-4, Abstracts 11th Informal Conference of Photochemistry, Vanderbilt University, Nashville, Tennessee, 248-252.

G. Paraskevopoulos (1976) Private communication to one of the authors.

D.A. Parkes (1974) The roles of alkylperoxy and alkoxy radicals in alkyl radical oxidation at room temperature. Paper presented at the 15th International Symposium on Combustion, Japan, 1974.

D.A. Parkes, D.M. Paul, C.P. Quinn and R.C. Robson (1973) The ultraviolet absorption by alkylperoxy radicals and their mutual reactions. Chem. Phys. Letters 23, 425-429.

C.T. Pate, R. Atkinson and J.N. Pitts, Jr. (1976) Rate constants for the gas phase reaction of peroxyacetyl nitrate with selected atmospheric constituents. J. Environ. Sci. Health--Environ. Sci. Eng. A11, 19-31.

L.K. Patterson, G. Porter and M.R. Topp (1970) Oxygen quenching of singlet and triplet states. Chem. Phys. Letters 7, 712-614.

T.T. Paukert and H.S. Johnston (1972) Spectra and kinetics of the hydroperoxyl free radical in the gas phase. J. Chem. Phys. 56, 2824-2838.

W.A. Payne, L.J. Stief and D.D. Davis (1973) A kinetics study of the reaction of HO_2 with SO_2 and NO. J. Amer. Chem. Soc. 95, 7614-7619.

R.D. Penzhorn, W.G. Filby, H. Gusten (1974a) Die photochemische abbaurate des schwefeldioxids in der unteren atmosphare mitteleuropas. Z. Naturforsch. 29a, 1449-1453.

R.D. Penzhorn, W.G. Filby, K. Gunther and L. Stieglitz (1975) The photoreaction of sulfur dioxide with hydrocarbons. II. Chemical and physical aspects of the formation of aerosols with butane. Int. J. Chem. Kinet. Symp. 1, 611-627.

R.D. Penzhorn, H. Gusten, U. Schurath and K.H. Becker (1974b) Quenching of singlet molecular oxygen by some atmospheric pollutants. Current Res. 10, 907-909.

J.T. Peterson (1976) Calculated actinic fluxes (290-700 nm) for air pollution photochemical applications. U.S. Environmental Protection Agency Report 600/4-76-025, p. 21.

J.N. Pitts, Jr., B.J. Finlayson, H. Akimoto, W.A. Kummer and R.P. Steer (1972) The chemiluminescent reactions of ozone with olefins and organic sulfides. Advan. Chem. Ser. 113, 246-254.

R.N. Rudolph and S.J. Strickler (1977) Direct measurement of the lifetimes of the $^3B_1$ state of SO_2 in air at atmospheric pressure. J. Amer. Chem. Soc. 99, 3871-3872.

S.P. Sander and J.H. Seinfeld (1976) Chemical kinetics of homogeneous atmospheric oxidation of sulfur dioxide. Environ. Sci. Technol. 10, 1114-1123.

K. Schofield (1973) Evaluated chemical rate constants for various gas phase reactions. J. Phys. Chem. Ref. Data 2, 25-77.

S.E. Schwartz and L. Newman (1977) Processes limiting the oxidation of sulfur dioxide in stack plumes. Manuscript of a paper to be submitted for publication.

H.W. Sidebottom, C.C. Badcock, J.G. Calvert, B.R. Rabe and E.K. Damon (1971) Mechanism of the photolysis of mixtures of sulfur dioxide with olefin and aromatic hydrocarbons. J. Amer. Chem. Soc. 93, 3121-3128.

H.W. Sidebottom, C.C. Badcock, J.G. Calvert, B.R. Rabe and E.K. Damon (1972a) Lifetime studies of the biacetyl excited singlet and triplet states in the gas phase at 25°. J. Amer. Chem. Soc. 94, 13-19.

H.W. Sidebottom, C.C. Badcock, G.E. Jackson, J.G. Calvert, G.W. Reinhardt, and E.K. Damon (1972b) Photooxidation of sulfur dioxide. Environ. Sci. Technol. 6, 72-79.

B.K.T. Sie, R. Simonaitis and J. Heicklen (1976) The reaction of OH with CO. Int. J. Chem. Kinet. 8, 85-98.

P.A. Skotnicki, A.G. Hopkins and C.W. Brown (1975) Time dependence of the quantum yields for the photooxidation of sulfur dioxide. J. Phys. Chem. 79, 2450-2452.

I.W.M. Smith and R. Zellner (1973) Rate measurements of reactions of OH by resonance absorption. Part 2. Reactions of OH with CO, C_2H_4, and C_2H_2 J. Chem. Soc. Faraday Trans. II 69, 1617-1627.

E.R. Stephens and M.A. Price (1972) Comparison of synthetic and smog aerosols. J. Colloid Interface Sci. 39, 272-286.

F. Stuhl and H. Niki (1972) Pulsed vacuum-uv photochemical study of OH with H_2, O_2, and CO using a resonance-fluorescence detection method. J. Chem. Phys. 57, 3671-3677.

F. Su and J.G. Calvert (1977a) The mechanism of the photochemical reactions of SO_2 with C_2H_2 and CO excited within the $SO_2(^3B_1) \leftarrow SO_2(x^1A_1)$ "forbidden" band. Chem. Phys. Letters, in press.

F. Su and J.G. Calvert (1977b), work in preparation for publication.

F. Su, J.W. Bottenheim, H.W. Sidebottom, J.G. Calvert and E.K. Damon (1977b) Kinetics of fluorescence decay of SO_2 excited in the 2662-3273Å region. Int. J. Chem. Kinet., in press.

F. Su, J.W. Bottenheim, D.L. Thorsell, J.G. Calvert and E.K. Damon (1977a) The efficiency of the phosphorescence decay of the isolated $SO_2(^3B_1)$ molecule. Chem. Phys. Letters, in press.

F. Su, R.B. Wampler, J.W. Bottenheim, D.L. Thorsell, J.G. Calvert and E.K. Damon (1977c) On the pressure saturation effect of the quenching of $SO_2(^3B_1)$ molecules. Chem. Phys. Letters, in press.

T.A. Walter, J.J. Bufalini and B.W. Gay, Jr. (1977) Mechanism for olefin-ozone reaction. Environ. Sci. Technol. 11, 382-386.

F.B. Wampler, J.G. Calvert and E.K. Damon (1973a) A study of the bimolecular intersystem crossing reaction induced in the first excited singlet of SO_2 by collsions with O_2 and other atmospheric gases. Int. J. Chem. Kinet. 5, 107-117.

F.B. Wampler, A. Horowitz and J.G. Calvert (1972) The mechanism of carbon dioxide formation in 3130Å-irradiated mixtures of sulfur dioxide and carbon monoxide. J. Amer. Chem. Soc. 94, 5523-5532.

F.B. Wampler, K. Otsuka, J.G. Calvert and E.K. Damon (1973b) The temperature dependence and the mechanism of $SO_2(^3B_1)$ quenching reactions. Int. J. Chem. Kinet. 5, 669-687.

A.A. Westenberg and N. deHaas (1973) Rates of CO + OH and H_2 + OH over an extended temperature range. J. Chem. Phys. 58, 4061-4065.

A.A. Westenberg and N. deHaas (1975a) Rate of the reaction O + SO_2 + M SO_3 + M. J. Chem. Phys. 63, 5411-5415.

A.A. Westenberg and N. deHaas (1975b) Rate of the O + SO_3 reaction. J. Chem. Phys. 62, 725-730.

M.R. Whitbeck, J.W. Bottenheim, S.Z. Levine and J.G. Calvert (1976) A kinetic study of the CH_3O_2 and $(CH_3)_3CO_2$ radical reactions by kinetic flash spectroscopy. Abstracts of 12th Informal Conference on Photochemistry, U.S. National Bureau of Standard, Gaithersberg, Maryland, July, 1976, pp K1-1 to K1-5.

G.Z. Whitten and H.H. Hogo (1976) Mathematical modeling of simulated photochemical smog. Final Report EF 76-126 by Systems Application Inc., to the U.S. Environmental Protection Agency, August, 1976.

W.E. Wilson, R.J. Charlson, R.B. Husar, K.T. Whitby and D. Blumenthal (1976) Sulfates in the atmosphere. Paper presented at 69th meeting of the Air Pollut. Control Ass., Portland, Oregon, June, 1976.

W.E. Wilson, M.C. Dodge, D.N. McNelis and J. Overton (1974) SO_2 oxidation mechanism in olefin-NO_x-SO_2 smog. Paper presented before Division of Environmental Chemistry, American Chemical Society, Los Angeles, April, 1974.

W.E. Wilson, A. Levy and D.B. Wimmer (1972) A study of sulfur dioxide in photochemical smog. II. Effect of sulfur dioxide on oxidant formation in photochemical smog. J. Air Pollut. Control Ass. 22, 27-32.

W.P. Wood, A.W. Castleman, Jr., and I.N. Tang (1974) Mechanisms of aerosol formation from SO_2. Paper presented at 67th annual meeting Air Pollut. Control Ass., Denver, Colorado, June 9-13, 1974.

W.P. Wood, A.W. Castleman, Jr., and I.N. Tang (1975) Mechanisms of aerosol formation from SO_2. J. Aerosol Sci. 6, 367-375.

SECTION 3

STUDIES RELATED TO FORMALDEHYDE REMOVAL MECHANISM IN THE ATMOSPHERE

QUANTUM EFFICIENCY OF THE PRIMARY PROCESSES IN CH_2O PHOTOLYSIS AT 3130Å AND 25°C

Introduction

Efforts to elucidate the mechanism of formaldehyde photolysis have increased greatly in recent years. The renewed interest in this system has been stimulated largely by two factors: (1) the high potential of formaldehyde for successful laser-photolysis, isotope separation; and (2) the need for the quantitative evaluation of the significance of CH_2O reactions in smog formation.[1] In this study our attention was focussed on the second area of interest. The extensive efforts of many research groups have defined many features of the formaldehyde photolysis mechanism,[2-34] but several qualitative and quantitative aspects are not fully understood today. It is well established that primary reactions 1 and 2 occur when formaldehyde is excited to the first excited singlet state.

$$CH_2O + h\nu \rightarrow H + HCO \qquad (1)$$

$$CH_2O + h\nu \rightarrow H_2 + CO \qquad (2)$$

Uncertainty remains about the detailed reaction paths through which these processes occur. McQuigg and Calvert[15] rationalized the wavelength dependence of ϕ_1/ϕ_2 in terms of a simple kinetic model which implied the occurrence of internal conversion of the original excited state to a vibrationally excited ground state reactant common to both decomposition modes. Some recent more quantitative experimental and theoretical studies also favor this interpretation;[20,22,30,32-34] others show the possible involvement of the lowest triplet excited state in the process 1.[20,22,32-34] All recent studies indicate that the dominant final products of formaldehyde photolysis are H_2 and CO, and their quantum yields suggest that $\phi_1 + \phi_2$ may be near unity at most wavelengths within the first absorption band ($^1A_2 \leftarrow x^1A_1$). The effects of radical scavengers such as iodine,[3] alkenes,[14] oxygen,[27] and nitric oxide[24,28] on these quantum yields, the relative chemiluminescence of excited HNO formed by H-atom capture by NO following process 1 in CH_2O-NO mixture photolyses,[29] and isotopic scrambling experiments with CH_2O, CD_2O, CHDO,[8,15,18,31] have all been used in the estimation of the ϕ_1/ϕ_2 ratio as a function of wavelength. It is generally accepted today that the importance of the free radical mode of decomposition, reaction 1, increases with decreasing wavelength used to excite the CH_2O. However, the absolute values reported for the primary quantum yields are widely divergent. Thus at 3130 Å previous estimates of ϕ_2 vary from 0.01[3] to 0.5.[15,27] The apparent disagreement between the quantum yields measured in the different studies may have resulted at least in part from different conditions employed, i.e.,

temperature, light intensity, etc., as well as unrecognized complexities in the reaction pathways in many of the CH_2O-radical scavenger studies and the subsequent misinterpretation of the results.

We initiated our present work as part of an effort to estimate the importance of CH_2O photolysis as a source of H-atoms in the atmosphere. We have carried out formaldehyde photolyses in the presence of several different, seemingly simple, H-atom and HCO-radical scavengers in order to define the best system for the accurate determination of ϕ_1 and ϕ_2. The varied results from the several systems which we have studied in this work provide a new and reliable set of self-consistent estimates of ϕ_1 and ϕ_2 for formaldehyde photolysis at 3130Å.

Experimental

Materials --

Formaldehyde was prepared from paraformaldehyde (Eastman) according to the procedures of Spence and Wild[35] and stored in a trap cooled to dry ice-acetone temperature. Isobutene (Phillips), trimethylsilane (PCR), and NO (Matheson) were purified by trap-to-trap distillation. The NO in the storage bulb was cooled to dry ice temperature before introduction to the cell to insure that any traces of NO_2 present in the NO would be trapped in the bulb.

Apparatus and Procedures --

The photolysis was carried out in a 500 cc, 34 cm long, cylindrical quartz cell which was joined to a grease-free vacuum line. Attached to the cell was a P7D Dynasciences pressure transducer which served to measure the pressures of the gases that were introduced into the cell and the pressure changes which occurred during the reaction. At pressures exceeding 14 Torr the pressure transducer was used as a null instrument in combination with a Wallace Tiernan pressure gauge. The light source was an Osram HBO 500 W high pressure mercury lamp from which the wavelength band near 3130Å was isolated by combination of chemical filters and a Corning 7-54 glass filter.[36] The intensity of the transmitted light was monitored with an RCA 935 photodiode mounted at the back of the cell. A series of uniform density filters were employed in one series of experiments in which the effect of the absorbed light intensity on the rates of the reaction was studied. Both potassium ferrioxalate and azomethane photolyses were used to establish the incident light intensity. With the latter compound, the fractions of the incident light absorbed by CH_2O and Me_2N_2 were kept about equal in successive runs. The quantum yield of CH_2O decomposition was found to be very reproducible, so standard formaldehyde photolyses were used also as a periodic check on the light intensity. The apparent average extinction coefficient of formaldehyde at 3, 8, and 12 Torr was found to be 7.05, 6.54 and 5.83 ℓ $mole^{-1}cm^{-1}$, respectively, for our conditions. The observed decrease of ϵ with pressure increase is not expected because of the large range of absorption coefficients of formaldehyde within the relatively wide excitation band isolated from the high pressure mercury lamp.

Formaldehyde was degassed before its introduction to the cell. At pressures up to 8 Torr practically no polymerization was observed; even at

the highest pressure employed (12 Torr) the pressure drop as a result of polymerization was negligible during the short irradiation times made possible by the use of the high intensity source. When other gases were added to formaldehyde prior to irradiation, the mixture was allowed to stand for 20 min to insure complete mixing. After photolysis, the gases were pulled through a glass bead-containing trap immersed in $N_2(l)$ and separated from CH_2O using a Toepler pump. The non-condensible gases H_2 and CO were transferred to a calibrated volume and the total pressure of the mixture measured. H_2 and CO were determined using a gas chromatograph (Varian 2700) equipped with a TC detector and 1/8th in x 12 ft column filled with NO-treated Molecular Sieve 5A held at 100°C. Nitrogen was used as the carrier gas when the concentrations were high, while at low CO concentrations, helium was used. H_2 and CO were the only non-condensible products (except for experiments with added NO), and therefore one of them could be directly determined and other by difference from the known total pressure. The results obtained with both direct product measurements and those by pressure change checked well with one another.

Results and Discussion

The Photolysis of Pure Formaldehyde --

The photolysis of formaldehyde at 3130Å was studied in a series of experiments at room temperature (25 ± 2°C) and over a range of pressures (1-12 Torr) and light intensities. The data, summarized in Table 19, confirm the previous observation of near equality of the quantum yields of carbon monoxide and hydrogen products; these results give $\Phi_{CO}/\Phi_{H_2} = 1.01 \pm 0.09(2\sigma)$. Furthermore the ratio of twice the pressure change (Δp) during the course of the p photolysis to the pressure (Δ) of the recovered noncondensable gases (H_2 and CO) is unity within the experimental error; the data of Table 19 give $2\Delta p/\Delta = 1.00 \pm 0.08(2)$. Thus we conclude that H_2 and CO are the only significant products of formaldehyde photolysis and the observed rate of pressure increase during an experiment is equal to the rate of CH_2O decomposition. Then for formaldehyde photolyses at low pressures for which the limiting form of Beer's law applies well, we anticipate that the total pressure p in the system with the initial formaldehyde pressure p_o should be described by the expression I:

$$\ln [(2p_o - p)/p_o] = -kt \qquad (I)$$

Indeed the results of an experiment at 2.49 Torr of CH_2O, plotted in Figure 44, show that this simple first order rate law describes the data well, at least over the first 30% of the reaction which was followed here.

In one series of experiments at 2.50 Torr of CH_2O, the rate of pressure increase was monitored using different incident light intensities. These data, shown in Figure 45, indicate that the rate of CH_2O decomposition is directly proportional to the incident light intensity, so that for our conditions the quantum yield of formaldehyde decomposition is intensity independent. This result is consistent with that observed by Sperling and Toby[19] in experiments at low intensities but differs from what they observed at the higher temperatures (80-120°C), higher pressures (up to 40 Torr), and at the highest intensities used in their experiments.

TABLE 14. EXPERIMENTAL DATA FROM THE PHOTOLYSIS OF FORMALDEHYDE AT 3130Å AND 25°C

P_{CH_2O}, Torr Initial	P_{CH_2O}, Torr Average	Irradiation time, sec	Quanta abs. /cell x 10^{-18}	$2\Delta p$, Torr x 10^{3}[b]	Δ, Torr x 10^{3}[c]	$2\Delta p/\Delta$	P_{H_2}, Torr x 10^{3}[d]	P_{CO}, Torr x 10^{3}[d]	Φ_{H_2}	Φ_{CO}	Φ_{CO}/Φ_{H_2}
1.044	1.015	900	(0.92)	118	117	1.01	59.8	(56.8)	a	a	0.95
1.033	1.011	900	(0.91)	127	120	1.06	59.7	(60.3)	a	a	1.01
1.037	1.008	900	(0.91)	118	116	1.02	60.1(56.5)	59.7(56.1)	a	a	0.99
1.036	1.007	900	(0.91)	118	121	0.98	64.8(55.9)	65.1(56.2)	a	a	1.01
1.036	1.002	900	(1.13)	137	137	1.00	71.3	(66.0)	a	a	0.93
1.035	1.004	900	(1.13)	125	141	0.89	70.9	(70.2)	a	a	0.99
1.006	0.975	1000	(0.99)	125	125	1.00	62.3	(62.5)	a	a	1.00
1.007	0.976	1000	(1.01)	123	124	0.99	59.8	(64.4)	a	a	1.08
1.007	0.975	1000	1.00	130	129	1.01	64.9	(64.0)	1.10	1.09	0.99
3.240	3.135	900	3.21	390	419	0.93	200	(219)	1.06	1.16	1.10
3.236	3.133	900	3.21	404	413	0.98	(211)	202	1.12	1.07	0.96
3.249	3.158	900	2.73	353	364	0.97	176 (179)	185 (187)	1.10	1.15	1.05
3.244	3.156	900	2.73	361	361	1.00	176 (195)	167 (185)	1.15	1.09	0.95
3.346	3.256	900	2.81	373	350	1.07	167 (182)	169 (183)	1.05	1.06	1.01
3.238	3.161	900	2.44	313	310	1.01	152 (159)	152 (159)	1.08	1.08	1.00
3.158	3.079	900	2.38	330	316	1.04	150 (166)	150 (165)	1.13	1.12	1.00
3.157	3.082	900	2.39	298	302	0.99	146	(156)	1.04	1.11	1.07
3.156	3.082	900	2.39	296	298	0.99	144	(154)	1.02	1.10	1.07
3.173	3.090	1000	2.63	328	330	0.99	(164)	167	1.05	1.08	1.02
3.187	3.094	1000	2.58	376	372	1.01	187	(185)	1.23	1.22	0.99
3.153	3.060	1000	2.86	375	371	1.01	(183)	189	1.08	1.12	1.03
8.268	8.169	450	2.96	396	396	1.00	199	(197)	1.14	1.13	0.99
8.400	8.302	450	3.00	404	391	1.03	195	(196)	1.10	1.11	1.01
8.303	8.221	450	2.53	344	328	1.05	161 (158)	170 (167)	1.07	1.13	1.05
8.303	8.193	600	3.23	460	442	1.04	215 (208)	234 (226)	1.11	1.21	1.09
8.030	7.924	600	3.34	403	423	0.95	207	(197)	1.05	1.00	0.95
8.438	8.311	700	4.07	499	510	0.98	247	(262)	1.03	1.09	1.06
8.072	7.960	600	3.59	445	448	0.99	227	(222)	1.07	1.05	0.98
8.008	7.895	600	3.42	449	449	1.00	226	(223)	1.12	1.11	0.99
8.062	7.954	600	3.39	435	434	1.00	215	(219)	1.08	1.10	1.02
8.062	7.949	600	3.49	456	451	1.01	(225)	226	1.09	1.10	1.00
8.060	7.952	600	3.23	417	420	0.99	(200)	221	1.05	1.16	1.11
12.10	11.95	600	4.71	572	601	0.95	307	(294)	1.10	1.05	0.96
12.12	11.97	600	4.72	568	596	0.95	305	(291)	1.10	1.05	0.95

[a]In these experiments ε could not be determined accurately, and quantum yields are not reliable. [b]Δp is the pressure change in the cell. [c]Δ is the pressure of noncondensables. [d]Yield by pressure difference (parentheses).

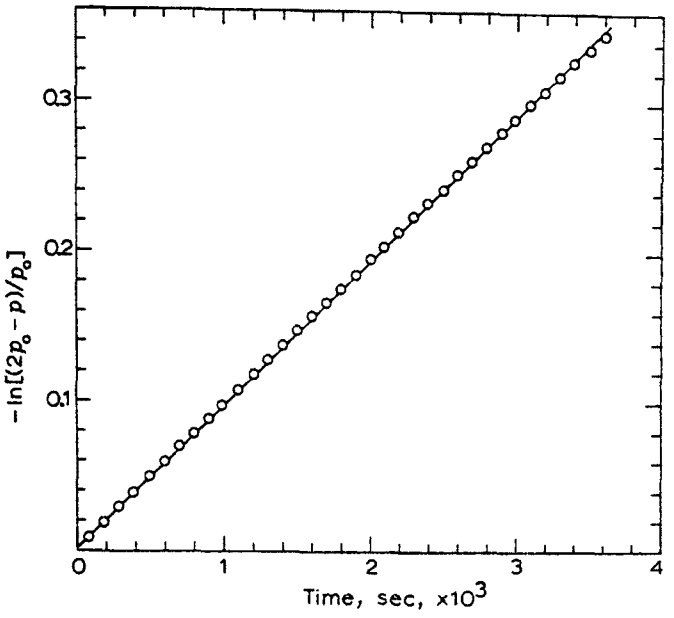

Figure 44. First-order plot of a function of the pressure in formaldehyde photodecomposition at 3130 Å. p_o = 2.488 Torr, temperature 25°C.

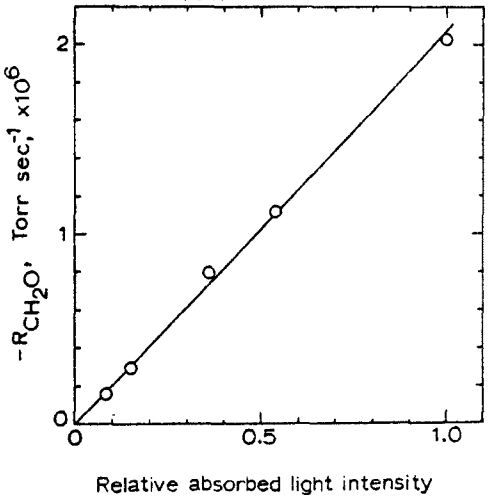

Figure 45. Effect of incident light intensity on the rate of formaldehyde photodecomposition at 3130 Å. P_{CH_2O} = 2.50 Torr, temperature 25°C.

Consider the present kinetic results in terms of the following simple reaction mechanism:

$$CH_2O + h\nu \rightarrow H + HCO \quad (1)$$

$$CH_2O + h\nu \rightarrow H_2 + CO \quad (2)$$

$$H + CH_2O \rightarrow H_2 + HCO \quad (3)$$

$$HCO + HCO \rightarrow CH_2O + CO \quad (4)$$

$$HCO + HCO \rightarrow H_2 + 2CO \quad (5)$$

$$HCO + HCO \rightarrow (HCO)_2 \quad (6)$$

$$HCO + M \rightarrow H + CO + M \quad (7)$$

$$H + HCO \rightarrow H_2 + CO \quad (8)$$

Since the present results show Φ_{CO}/Φ_{H_2} is unity within the experimental error, some restriction on the relative importance of these reactions is imposed. The occurrence of reaction 6 would lead to $\Phi_{H_2}/\Phi_{CO} > 1$, and a different pressure change during photolysis would be observed here. Thus it is likely that $k_6 < (k_5 + k_4)$, and reaction 6 can be neglected here. This conclusion is in accord with the findings of Khan, Norrish, and Porter[6] who also found no evidence of glyoxal formation following the flash photolysis of CH_3CHO.

Kinetic considerations show that reactions 7 and 8 are also unimportant here. Thus the present best estimates related to the thermochemistry of reaction 7 give $\Delta H_7^\circ \cong 17.5$ kcal mole^{-1}[Ref. 28,29,31,37-40] and $\Delta S_7^\circ \cong 20.9$ eu (25°C, 1 atm);[41] from these data we may estimate $k_7 = k_7/k_{-7} \cong 2.3 \times 10^{-10}$ mole ℓ^{-1} at 25°C. Taking the measured value of $k_{-7} = (4.0 \pm 0.6) \times 10^7\ \ell^2$ mole^{-2} sec^{-1} for M = H_2 at 25°C,[42] we estimate $k_7 \cong 9 \times 10^{-3}\ \ell$ mole^{-1} sec^{-1} at 25°C. From these data, the measured value of $k_4 + k_5 = 2.2 \times 10^{10}$ ℓ mole^{-1} sec^{-1} [Ref. 43], the measured absorbed light intensity in the experiments at 12 Torr of CH_2O, and the steady state assumption for [H] and [HCO], we calculate that the rate of HCO radical loss by dissociation in 7 to that in reactions 4 and 5 will be negligible: $R_7/2(R_4 + R_5) \cong 2 \times 10^{-7}$. Furthermore taking $k_3 = 2.8 \times 10^7\ \ell$mole^{-1} sec^{-1}, an average of the recent determinations,[44,46] and a reasonable estimate of $k_8 \cong 2 \times 10^{10}\ \ell$mole^{-1} sec^{-1}, the ratio of the rate of HCO loss in 8 compared to that in 4 and 5 is also very small: $R_3/2(R_4 + R_5) \cong 3 \times 10^{-4}$. Thus for our conditions, 1-5 appear to be the only reactions of H and HCO which will occur at significant rates; reactions 6,7, and 8 may be neglected in our further considerations here.

The results of Table 1 give the average values: $\Phi_{CO} = 1.09 \pm 0.09(2\sigma)$ and $\Phi_{H_2} = 1.10 \pm 0.09$. Clark has concluded from the results of his recent study[28] that $\Phi_{CO} = \Phi_{H_2} = 1.0$ at wavelengths near 3130 Å employed here, but the experimental error in his determinations is somewhat higher than that of the present work. Although our estimates of Φ_{H_2} and Φ_{CO} include unity within the 2σ error limits, the results of the CH_2O-Me_3SiH experiments suggest (See the next section.) that the true values are somewhat larger than unity as our average estimates do indicate. Formation of the photolysis products hydrogen and carbon monoxide in equal yields is consistent with the occurrence of both reactions 4 and 5. However in view of the unimportance of reaction 7 and chain reactions for our conditions, values of Φ_{H_2} and Φ_{CO} greater than unity suggest that reaction 5 as well as 4 must occur to some extent. If $\Phi_1 + \Phi_2 = 1.0$, as seems likely from other results in this study, then from the measured values of $\Phi_{H_2} = \Phi_{CO} = 1.10$ and the reaction sequence 1-5, we anticipate in theory that $\Phi_1 = 0.10(k_4 + k_5)/k_5$. Glicker and Stief[16] assumed that reaction 5 was the only fate of HCO radicals in their short wavelength CH_2O photolysis studies; i.e., $k_5/(k_4 + k_5) = 1.0$. If this were the case here, then our results would require $\Phi_1 = 0.10$ and $\Phi_2 = 0.90$. This conclusion is inconsistent with the results of all other studies of CH_2O photolysis at the 3130 Å region where estimated values of $\Phi_2 = 0.01$,[3] 0.17,[8] 0.48,[14] 0.5,[15] 0.2,[19] 0.45,[27] 0.58 (at 3172 Å)[28] and 0.37 (at 3140 Å),[29] and it is not considered realistic. Only if our actinometry were seriously in error and the actual Φ_{H_2} and Φ_{CO} values were much lower than we estimated could the hypothesis of Glicker and Stief lead to consistent Φ_2 values. It appears more likely to us that reaction 5 is not the sole fate of HCO radicals as they suggested, and in view of Clark's results and conclusions,[28] there must be some question as to whether reaction 5 occurs at all. In order to assess better the relative importance of reactions 4 and 5 and to define well the magnitude of the primary quantum yield sum, $\Phi_1 + \Phi_2$, we have carried out CH_2O photolyses in the presence of trimethylsilane.

Photolysis of Formaldehyde-Trimethylsilane Mixtures --

We reasoned that trimethylsilane would be an excellent trap for H-atoms and HCO radicals through the reactions 9 and 10, and conceivably the occurrence of the usual reactions 3, 4, and 5 of pure formaldehyde photolysis could be suppressed completely.

$$H + Me_3SiH \rightarrow H_2 + Me_3Si \quad (9)$$

$$HCO + Me_3SiH \rightarrow CH_2O + Me_3Si \quad (10)$$

$$Me_3Si + CH_2O \rightarrow Me_3SiH + HCO \quad (11)$$

$$2Me_3Si \rightarrow Me_3SiSiMe_3 \qquad (12)$$

However abstraction of H-atoms from CH_2O by Me_3Si radicals in reaction 11 may occur to some extent since $D(Me_3Si\text{-}H) \cong 89 \pm 4$ [Ref. 47] while $D(HCO\text{-}H) \cong 86.3 \pm 1.5$ kcal mole^{-1} [Refs. 28,29,31,37-40]. In Table 20 the results of CH_2O-Me_3SiH photolyses are summarized. Note that with added trimethylsilane the quantum yield of H_2 is lowered from the value of 1.10 characteristic of pure formaldehyde to unity within the experimental error [$\Phi_{H_2} = 1.00 \pm 0.08$ (2σ)], even at the lowest concentration of the silane added here. This is consistent with the occurrence of primary processes 1 and 2 with $\Phi_1 + \Phi_2 = 1.0$, followed by reactions 9, 10, and 12 alone. Presumably the extent of lowering of Φ_{H_2} reflects the contribution of hydrogen formation from reaction 5 which cannot occur under these conditions. These results support the "high" values of Φ_{CO} and Φ_{H_2} found here in the pure CH_2O runs, and place the quantum yield of H_2 formed by way of reaction 5 at about 0.10 for pure formaldehyde photolyses under our conditions.

However not all of the results of the CH_2O-Me_3SiH mixture photolyses are explicable in terms of the simple mechanism outlined above. The Φ_{CO} data and the pressure changes observed in the data of Table 20 cannot be explained using reactions 1-5 and 9-12 alone. If only these reactions occurred in this system then one would expect $\Phi_{CO} = \Phi_2$ and $\Phi_{H_2} - \Phi_{CO} = \Phi_1$; the change in pressure (Δp) observed in the system should be given by $\Delta p = P_{CO}$, since no pressure change should result from the occurrence of reaction 1 followed by 9, 10, and 12. It can be seen that the measured Δp in column 5 of Table 20 is not equal to P_{CO} in column 8; the observed pressure change is always smaller than that anticipated from the occurrence of only reactions 1, 2, and 9-12. Furthermore the imbalance of Δp and P_{CO} increases with increasing trimethylsilane concentration. In rationalizing these results additional reactions must be considered. The reaction sequence 1, 2, 9-12 together with the additional reactions 13-19 can qualitatively explain these results:

$$Me_3Si + CH_2O \rightarrow Me_3SiOCH_2 \qquad (13)$$

$$Me_3SiOCH_2 + CH_2O \rightarrow Me_3SiOCH_3 + HCO \qquad (14)$$

$$Me_3SiOCH_2 + Me_3SiH \quad Me_3SiOCH_3 + Me_3Si \qquad (15)$$

$$Me_3Si + HCO \rightarrow Me_3SiH + CO \qquad (16)$$

$$Me_3SiOCH_2 + HCO \rightarrow Me_3SiOCH_3 + CO \qquad (17)$$

$$2Me_3SiOCH_2 \rightarrow Me_3SiOCH_2CH_2OSiMe_3 \qquad (18)$$

$$Me_3Si + Me_3SiOCH_2 \rightarrow Me_3SiCH_2OSiMe_3 \qquad (19)$$

TABLE 20. EXPERIMENTAL DATA FROM THE PHOTOLYSIS OF FORMALDEHYDE IN THE PRESENCE OF TRIMETHYLSILANE[a]

P_{CH_2O}, Torr Initial	P_{CH_2O}, Torr Average	P_{Me_3SiH}, Torr	Quanta abs. /cell x 10^{-18}	Δp, Torr x 10^3[c]	Δ, Torr x 10^3[d]	P_{H_2}, Torr x 10^3[e]	P_{CO}, Torr x 10^3[e]	Φ_{H_2}	Φ_{CO}	Φ_{CO}/Φ_{H_2}
1.033	1.010	0.504	0.91	29	98.5	55.1	39.8	1.02[b]	0.74[b]	0.72
1.033	1.006	1.257	0.91	16	104.4	54.7	39.9	1.02[b]	0.75[b]	0.73
1.037	1.012	5.225	0.91	-22	94.5	54.4	40.1	1.01[b]	0.74[b]	0.73
3.252	3.175	0.487	2.71	85	282	154	139	0.96	0.87	0.91
3.205	3.137	1.143	2.43	21	247	135	95.2	0.95	0.67	0.70
3.228	3.148	1.249	2.69	57	283	159	122	1.01	0.77	0.76
3.234	3.165	4.730	2.33	0	245	139	94.1	1.01	0.69	0.69
3.033	2.958	7.266	2.42	50	263	151	113	1.06	0.79	0.75
3.187	3.006	8.668	2.57	--	267	166	105	1.07	0.68	0.63
3.187	3.058	28.5	2.50	--	260	151	109	1.03	0.74	0.72
8.263	8.239	4.275	3.59	33	356	199	173	0.94	0.82	0.87
8.292	8.241	4.422	3.59	-70	331	204	142	0.96	0.67	0.70

[a]Excitation at 3130 Å, temperature 25°C. [b]In experiments at 1 Torr pressure of CH_2O, Φ_{H_2} and Φ_{CO} were estimated relative to pure CH_2O photolysis with $\Phi_{CO} = \Phi_{H_2} = 1.10$. [c]$\Delta p$ is the pressure change in the cell. [d]Δ is the pressure of noncondensables. [e]Except for results marked with an asterisk, all values are from direct determinations.

The occurrence of reaction 13 is in accord with the smaller pressure increases, and the pressure decreases, which are observed in some of the experiments at high silane concentrations. Reaction 13, the addition of Me_3Si radicals to CH_2O, is not unprecedented, although we had not anticipated this happening. The addition reactions of silyl radicals to carbonyl compounds have been observed previously;[48] they seem to occur readily, presumably as a result of the high oxygen affinity of the silyl radicals.

Consider the effect of trimethylsilane addition to CH_2O on the CO formation in terms of this more complete mechanism. When Me_3SiH is added to CH_2O, reaction 9 takes over from reaction 3 as the main sink for H-atoms, and 10 presumably may compete with the bimolecular HCO loss reactions 4 and 5. However since HCO radicals can still be formed in reactions 11 and 14, this effect need not necessarily lead to a decrease in Φ_{CO}. The results of Table 20 show that the addition of even a small amount of Me_3SiH causes a marked decrease in Φ_{CO}, and the ratio Φ_{CO}/Φ_{H_2} approaches a constant value of about 0.7. Since Φ_{H_2} is practically constant at unity for these conditions, this result taken alone appears to favor $\Phi_2 \cong 0.7$. However an alternative interpretation is possible, and indeed it is likely. In the presence of Me_3SiH, CO is probably formed by reactions 2, 16, and 17 largely, since the radical concentrations $[Me_3Si]$ and $[Me_3SiOCH_2]$ are probably much larger than [HCO]. Hence reactions 4 and 5 are probably much less important. Thus for these conditions the seemingly constant value of Φ_{CO} observed at high $[Me_3SiH]$ may be a consequence of reasonably constant rates of 1, 16, and 17 which are achieved for these conditions. In this case the data require that $\Phi_2 < \Phi_{CO} = 0.7$. Obviously the mechanism of CO formation in the CH_2O-Me_3SiH system is very much more complex than we had anticipated, and we must resort to other less complicated kinetic systems to estimate Φ_2 accurately. The isobutene-CH_2O system seems to fulfill our needs.

Photolysis of Formaldehyde-Isobutene Mixtures--

The complete reaction sequence, in addition to reactions 1-5, which we would expect to describe the product formation in the CH_2O-isobutene system is as follows:

$$H + \underline{iso}\text{-}C_4H_8 \rightarrow \underline{tert}\text{-}C_4H_9 \qquad (20a)$$

$$H + \underline{iso}\text{-}C_4H_8 \rightarrow \underline{iso}\text{-}C_4H_9 \qquad (20b)$$

$$2C_4H_9 \rightarrow C_4H_{10} + C_4H_8 \qquad (21a)$$

$$2C_4H_9 \rightarrow C_8H_{18} \qquad (21b)$$

$$HCO + C_4H_9 \rightarrow C_4H_{10} + CO \qquad (22a)$$

$$HCO + C_4H_9 \rightarrow C_4H_9CHO \qquad (22b)$$

$$C_4H_9 + CH_2O \rightarrow C_4H_{10} + HCO \quad (23)$$

$$C_4H_9 + C_4H_8 \rightarrow C_8H_{17} \quad (24)$$

$$HCO + C_4H_8 \rightarrow C_4H_8CHO \quad (25)$$

$$HCO + C_4H_8 \rightarrow CO + C_4H_9 \quad (26)$$

The rate constant for H-atom addition to isobutene, $k_{20} = (1.5 \pm 0.5) \times 10^9$ ℓ mole^{-1}sec^{-1} [Ref. 49], is about 50-times larger than that for H-atom abstraction from CH_2O by H-atoms, reaction 3 [Ref. 44-46], so hydrogen formed in reaction 3 should be suppressed essentially completely by the addition of relatively small amounts of isobutene to CH_2O. This expectation is borne out by our experimental findings; see the data of Table 21. In experiments with added isobutene at each pressure of formaldehyde employed, the Φ_{H_2} is decreased to the same limiting value within the experimental error, 0.32 ± 0.03; we believe that these data provide our best estimate for Φ_2. In view of the results from the CH_2O-Me_3SiH experiments, $\Phi_1 + \Phi_2 = 1.0$, and hence $\Phi_1 = 0.68 \pm 0.03$. Using the estimate for Φ_1 and the relation which one anticipates in theory for pure CH_2O photolysis with reactions 1-5, $k_4/k_5 = (\Phi_1 - 0.10)/0.10$, we find $k_4/k_5 \cong 5.8$. Although the accuracy of this estimate is low, our results do suggest that reaction 5 does occur to a small extent in addition to the reaction 4.

A kinetic test of the mechanism of isobutene inhibition of H_2 formation in formaldehyde photolyses was made in experiments reported in Table 22. The P_{CH_2O} was kept as high as possible without inducing significant polymerization, and the irradiation times were as short as possible to insure that a wide range of Φ_{H_2} values could be covered by C_4H_8 additions without the significant depletion of the isobutene concentration during the irradiation time. These conditions were not met in the experiments of Table 21 at the lowest added isobutene pressures. Considering reactions 1 and 3 as the major sources of H_2 in the CH_2O-C_4H_8 photolyses, we expect Φ_{H_2} to be given by the approximate relation II:

$$\frac{\Phi_1}{\Phi_{H_2} - \Phi_2} - 1 = \frac{k_{20}[C_4H_8]}{k_3[CH_2O]} \quad (II)$$

In Figure 46 is shown a plot of the quantum yield function of relation II versus the ratio $[C_4H_8]/[CH_2O]$, taking $\Phi_1 = 0.683$ and $\Phi_2 = 0.317$, the average of the nine values derived from the experiments at the highest $[C_4H_8]/[CH_2O]$ ratios in Table 21 (marked with asterisks). A reasonably good linear relationship between the variables can be seen. The least squares treatment of the data gives $k_{20}/k_3 = 43 \pm 4(2\sigma)$ and an intercept

TABLE 21. EXPERIMENTAL DATA FROM THE PHOTOLYSIS OF FORMALDEHYDE IN THE PRESENCE OF ISOBUTENE[a]

P_{CH_2O}, Torr Initial	P_{CH_2O}, Torr Average	$P_{C_4H_8}$, Torr	Irradiation time, sec	Quanta abs./cell x 10^{-18}	$2\Delta p$, Torr x 10^3[b]	Δ, Torr x 10^3[c]	P_{H_2}, Torr x 10^3	P_{CO}, Torr x 10^3	Φ_{H_2}[d]	Φ_{CO}	Φ_{CO}/Φ_{H_2}[d]
0.959	0.943	5.185	900	1.01	10	63.3	19.5	46.2	0.327*	0.775	2.37*
0.998	0.981	5.185	900	1.05	10	68.0	20.3	47.7	0.327*	0.768	2.35*
3.193	3.156	0.067	600	2.16	108	171	80.0	90.5	0.629	0.711	1.13
3.198	3.139	0.067	600	2.15	95	157	73.0	83.8	0.577	0.662	1.15
3.191	3.137	0.214	900	3.22	78	218	79.6	138	0.420	0.729	1.74
3.194	3.139	0.207	900	3.22	102	200	79.6	143	0.419	0.751	1.79
3.203	3.152	0.517	900	3.23	56	203	66.3	140	0.348	0.733	2.11
3.207	3.150	0.506	900	3.23	70	205	64.8	140	0.340	0.735	2.16
3.176	3.127	1.004	900	3.21	64	198	64.8	133	0.343	0.702	2.05
3.194	3.144	1.004	900	3.22	--	199	62.4	137	0.328	0.718	2.19
3.186	3.151	3.537	900	2.43	41	141	40.9	100	0.286*	0.695	2.43*
3.185	3.137	5.188	900	3.22	48	192	62.0	130	0.327*	0.685	2.10*
3.217	3.171	5.211	900	3.20	44	186	56.0	130	0.297*	0.690	2.32*
8.265	8.200	0.259	500	3.30	172	272	108	163	0.558	0.840	1.51
8.268	8.210	0.519	500	3.30	30	234	80.4	153	0.413	0.788	1.31
8.242	8.185	1.141	500	3.29	72	228	74.9	153	0.386	0.787	2.04
8.272	8.219	3.095	500	3.30	--	212	67.1	145	0.344	0.744	2.16
8.248	8.202	10.37	450	2.97	--	186	54.8	131	0.313*	0.748	2.39*
8.228	8.176	10.37	500	3.29	52	207	62.5	144	0.322*	0.744	2.31*
12.12	12.04	1.145	600	4.44	--	312	107	205	0.415	0.796	1.92
12.10	12.02	2.408	600	4.68	--	308	101	207	0.366	0.756	2.05
12.09	11.85	10.10	600	4.36	--	219	85.4	206	0.325*	0.785	2.41*
11.83	11.76	30.25	600	4.49	--	291	86.3	208	0.326*	0.786	2.41*

[a]Excitation at 3130 Å, temperature 25°C. [b]Δp is the pressure change in the cell. [c]Δ is the pressure of non-condensables. [d]Experiments marked with asterisks are the runs at the highest $[C_4H_8]/[CH_2O]$ ratios which were used to derive the best estimates of the primary quantum yield ϕ_2 and the limiting Φ_{CO}/Φ_{H_2} ratio.

TABLE 22. THE RATES OF H_2 FORMATION IN FORMALDEHYDE PHOTOLYSES WITH SMALL AMOUNTS OF ADDED ISOBUTENE[a]

P_{CH_2O}, Torr	$P_{C_4H_8}$, Torr x 10^3	Irradiation time, sec	P_{H_2}, Torr x 10^3	Φ_{H_2}
13.1	101	34.8	16.6	0.866
12.0	204	75	28.8	0.767
12.0	299	75	24.9	0.663
12.0	402	75	22.6	0.602
12.0	604	75	20.0	0.553
12.0	994	75	17.7	0.471

[a]Excitation at 3130 Å, temperature 25°C.

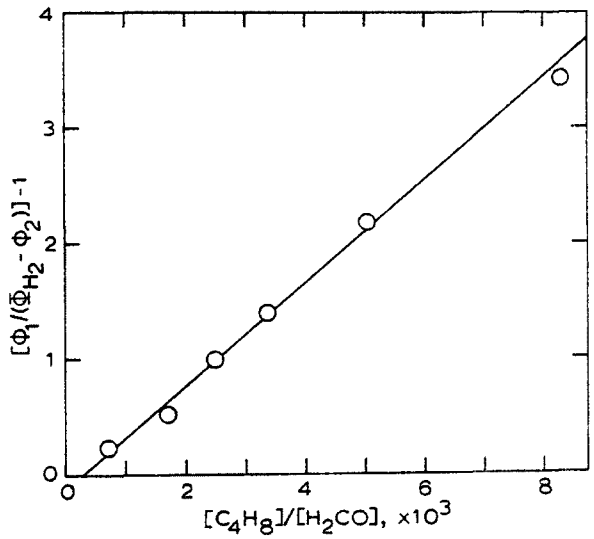

Figure 46. Plot of $[\Phi_{H_2} - \Phi_2] - 1$ versus $[C_4H_8]/[CH_2O]$. $\Phi_1 = 0.683$ and $\Phi_2 = 0.317$.

near zero (-0.12 ± 0.14), as anticipated from relation II. This k_{20}/k_3 estimate is in reasonable accord with that calculated from the ratio of the individual rate constants, $k_{20}/k_3 = 54 \pm 15(1\sigma)$,[44-46,49] and the result adds some credence to the mechanism choice, and the selection of the limiting Φ_{H_2} at high butene pressures as equal to Φ_2 appears justified.

Again in these C_4H_8-CH_2O mixture photolyses, as in the Me_3SiH-CH_2O mixture studies, the mechanism of the HCO destruction reactions and CO formation appear to be ill-defined. A consideration of the reactions other than H-atom removal will illustrate the unresolved problems. The structurally undesignated C_4H_9 radicals shown in the reaction series should be largely of the tert-butyl structure, since $k_{20a}/k_{20b} \cong 20$ [Ref. 49]. In view of the relative magnitude of D(tert-C_4H_9-H) ≅ 91 [Ref. 50] and D(HCO-H) ≅ 86 kcal $mole^{-1}$, the occurrence of 23 cannot be ruled out as an additional source of HCO radicals. Reactions 24 and 25 should be followed by H-atom transfer from formaldehyde, or addition to isobutene, thus leading to possible chain reactions; some of these may also generate HCO radicals. The pressure change in this system suggests that there may be short chains involving C_4H_8 polymerization reactions such as 24. There is obviously no chain involving CO formation. The reaction 26 has not been observed or considered previously to our knowledge, yet its occurrence here seems to be another reasonable source of CO. It is the analogue to the somewhat more exothermic, well studied reactions of HCO with NO and O_2: HCO + NO → HNO + CO, $\Delta H \cong -28$; $\Delta H_{26} \cong -21$ kcal $mole^{-1}$.

Note from the results in Table 21 that Φ_{CO}/Φ_{H_2} climbs from a value of 1.0 for pure CH_2O to a seemingly constant value of about 2.3 at high isobutene concentrations, independent of the $[CH_2O]$. Since Φ_{CO} is much larger than the Φ_2 we have estimated from the Φ_{H_2} values at high $[C_4H_8]$, reaction 25 cannot be very important. It can be seen from the quantum yield data that a decrease in Φ_{CO} occurs significantly even at very low pressures of added isobutene. We believe that this rapid onset of the attenuation of CO reflects not only the decrease in reaction 3 as a source of HCO but the suppression of the bimolecular reactions 4 and 5 which dominate CO formation in the uninhibited CH_2O photolysis; the incomplete suppression points to new sources of CO. If the tert-butyl radical concentration is considerably higher than that of the HCO radical, presumably through the significant occurrence of reaction 26, the reaction 22a as well as 26 may become major HCO loss steps. From the rate constants $k_{21} = 9.3 \times 10^9$ [Ref. 51] and $k_4 + k_5 = 2.2 \times 10^{10}$ [Ref. 43], the approximate value of $k_{22} \cong 2[k_{21}(k_4 + k_5)]^{1/2} = 2.9 \times 10^{10}$ ℓ $mole^{-1}sec^{-1}$, can be estimated. From this it can be shown that the $[HCO]/[C_4H_9]$ ratio must be lowered below 0.066, presumably through the HCO radical removal reactions 25 and 26, before 90% of the HCO loss will occur by reactions other than 4 and 5. It appears to be unrealistic to assume that C_4H_8 addition and C_4H_9 radicals do not perturb the HCO radical concentrations at all in the CH_2O photolyses; thus if HCO were removed only

in reactions 4 and 5 even in the presence of isobutene, we expect $\Phi_1 = 2(1 - \Phi H_2)/\{1 + [k_4/(k_4 + k_5)]\}$ and $\Phi_1 = 2(1 - \Phi_{CO})/\{[k_4/(k_4 + k_5)]\}$; using measured values of $\Phi_{CO} = 0.74$ and $\Phi_{H_2} = 0$ for the isobutene-CH_2O experiments we would estimate $\Phi_1 = 0.84$; $\Phi_2 = 0.16$, and $k_4/k_5 = 1.6$. These values are untenable in terms of the other results reported previously and determined by other methods in this work. We conclude that reactions 4 and 5 are probably unimportant loss reactions for HCO radicals and CO formation in the CH_2O-C_4H_8 experiments, but the relative contribution of the reactions 22a and 26 to CO formation remains unclear.

Further confirmation of the conclusions concerning Φ_1 and Φ_2 formulated here can be had from the results of the CH_2O-NO experiments described in the next section.

Photolysis of Formaldehyde-Nitric Oxide Mixtures

As a further test of the Φ_1 and Φ_2 estimates derived from the CH_2O-C_4H_8 system experiments, CH_2O was photolyzed in the presence of nitric oxide; these data are summarized in Table 23. Note that the addition of NO to CH_2O results in an increase in Φ_{CO} and a decrease in Φ_{H_2}. Formation of N_2 was also observed with yields which increased with NO concentration. No attempt at the quantitative determination of this product was made. These observations are in line with the results of other photolytic studies of Strausz and Gunning,[12] Tadasa et al.,[24] Harger and Lee,[52] and Clark;[28] however in the latter study an increase in Φ_{CO} was observed only for excitation at 2991 Å but not for the longer wavelengths.

In order to rationalize the major features of these results consider the simple reaction scheme 26-28:

$$H + NO\ (+NO) \rightarrow HNO\ (+NO) \qquad (26a)$$

$$H + NO\ (+CH_2O) \rightarrow HNO\ (+CH_2O) \qquad (26b)$$

$$HCO + NO \rightarrow HNO + CO \qquad (27)$$

$$2HNO \rightarrow H_2O + N_2O \qquad (28)$$

Obviously this sequence is incomplete since it does not involve NO_2 formation which occurs in experiments at high NO.[12,24] The results of Table 23 show that with the addition of the smallest amount of NO, Φ_{CO} reaches its maximum value while ΦH_2 is only slightly reduced. This suggests that at low NO concentrations, the following reaction rate inequalities must exist: $R_{27} > R_4 + R_5$ and $R_3 > R_{26}$. Indeed, taking the measured values of $k_4 + k_5$ [Ref. 43] and $k_{27} = 5.2 \times 10^9$ ℓ mole^{-1}sec^{-1} [Ref. 53] it can be shown that at the absorbed light intensities of the present work (1.1×10^{16} quanta ℓ^{-1} sec^{-1} at 8 Torr of CH_2O), practically all of the formyl radicals will react

TABLE 23. EXPERIMENTAL DATA FROM THE PHOTOLYSIS OF FORMALDEHYDE IN THE PRESENCE OF NITRIC OXIDE[a]

P_{CH_2O}, Torr		P_{NO}, Torr	Irradiation time, sec	Quanta abs./ cell x 10^{-18}	P_{H_2}, Torr x 10^3	P_{CO}, Torr x 10^3	Φ_{H_2}	Φ_{CO}
Initial	Average							
1.007	0.987	20.1	1000	1.04	24.4	---	0.398	----
3.131	3.038	5.89	1000	2.79	137	---	0.825	----
3.220	3.127	5.86	1000	2.83	-----	257	-----	1.54
3.043	2.950	8.12	1000	2.67	107	---	0.663	----
3.230	3.137	12.1	1000	3.02	79.5	---	0.464	----
3.148	3.055	16.1	1000	2.97	-----	225	-----	1.28
3.139	3.046	20.6	1000	2.87	84.5	---	0.508	----
3.061	2.968	38.1	1000	2.80	53.1	---	0.327	----
3.286	3.194	60.0	1000	3.00	-----	219	-----	1.24
8.075	7.969	0.405	600	3.37	177	---	0.881	----
8.021	7.911	1.025	600	3.34	178	---	0.902	----
8.019	7.910	1.865	600	3.38	-----	313	-----	1.57
8.010	7.899	1.919	600	3.37	173	---	0.863	----
8.079	7.969	3.034	600	3.32	153	---	0.780	----
8.023	7.913	4.610	600	3.29	151	---	0.778	----
8.018	7.908	6.418	600	3.32	144	---	0.736	----
8.031	7.926	6.398	600	3.32	-----	295	-----	1.51
8.048	7.938	15.2	600	3.27	107	---	0.550	----
8.055	7.946	15.3	600	3.18	-----	284	-----	1.51
8.001	7.891	27.6	600	3.25	90.9	---	0.474	----
8.021	7.912	32.6	600	3.17	-----	262	-----	1.40
8.396	8.286	70.0	600	3.14	61.3	---	0.331	----
8.060	7.948	103	600	3.30	70.3	---	0.361	----

[a]Excitation at 3130 Å, temperature 25°C.

with NO in experiments with $P_{CH_2O} = 8$ and $P_{NO} = 0.5$ Torr. The extent of the H-atom removal reactions 26a and 26b is more difficult to assess since values for k_{26} with M = CH_2O and NO are not known. However $k_{26c} = 2.2 \times 10^{10}$ $\ell^2 mole^{-2} sec^{-1}$ [Refs. 53,54] with 1 atm of H_2:

$$H + NO\ (+H_2) \rightarrow HNO\ (+H_2) \qquad (26c)$$

Assuming $k_{26b} \leq 10 k_{26c}$, it can be shown that Φ_{H_2} will be reduced by less than 14% for experiments at CH_2O and NO pressures as before. Thus the NO-CH_2O experiments provide a unique system in that NO quenches the HCO radicals efficiently but affects the H-atoms very little in experiments at low NO and total gas pressures.

According to the reaction scheme outlined above, at high NO concentrations all of the H atoms will be scavenged and the Φ_{H_2} will be reduced to Φ_2. As expected the lowest values of Φ_{H_2} of 0.327 and 0.331 at formaldehyde pressures of 3 and 8 Torr, respectively, are very close to Φ_2 as determined in the CH_2O-C_4H_8 system, $\Phi_2 = 0.32 \pm 0.03$. At a formaldehyde pressure of 1 Torr, Φ_{H_2} is reduced by the addition of 20 Torr of NO, but only to a value of 0.398; this probably reflects the difference in the rate constants, $k_{26b} > k_{26a}$, and the less efficient quenching of H-atoms for the low pressure conditions. The average of the two determinations at 8 and 3 Torr of CH_2O and at the highest added NO pressures gives $\Phi_{H_2} = 0.34$. This compares well with $\Phi_{H_2} = 0.31$ reported by Clark from experiments at 3172 Å using $P_{CH_2O} = 10$ and $P_{NO} = 50$ Torr.[28]

In terms of the mechanism 1-3 and 26-28 outlined above, the relation III should describe Φ_1 in experiments at low NO concentrations:

$$\Phi_{CO} - \Phi_{H_2} = \Phi_1 \qquad (III)$$

This expectation appears to be qualitatively correct; using it we estimate $\Phi_1 = 0.724$ (3 Torr CH_2O) and 0.717 (8 Torr CH_2O); this should be compared with $\Phi_1 = 0.68$ from the isobutene experiments. However, it can be seen from an inspection of the data at both 3 and 8 Torr of CH_2O that $\Phi_{CO} - \Phi_{H_2}$ increases as NO increases. A similar observation was made by Clark.[28] There are several possible explanations of these results. First, Φ_1 could change as the result of a perturbation of the distribution between the precursors of molecules and radical products. Houston and Moore[22] have observed that addition of NO to formaldehyde photolyzed at 3055 Å increased the rate of formation of vibrationally excited CO (v = 1). They rationalized this effect assuming that collisions with NO enhanced the molecular mode of formaldehyde decomposition. Following this line of argument we would expect $\Phi_{CO} - \Phi_{H_2}$ to decrease with increasing NO concentration; however the reverse

effect is observed. Careful examination of the assumptions made in the derivation of expression III points to an alternative explanation for this effect. The equality between $\Phi_{CO} - \Phi_{H_2}$ and Φ_1 is based upon the simple reaction scheme which requires that for each H-atom lost through the reaction 26, a formyl radical and therefore a molecule of CO will not form. It is possible that this assumption does not hold at high NO concentrations. Under these conditions both N_2 and NO_2 are formed, and the simple reaction scheme used in the derivation of expression III cannot account for this. Conceivably one of the intermediates involved in the reaction sequence that leads to the N_2 and NO_2 might be a free radical that abstracts hydrogen from formaldehyde. In this case a decrease in Φ_{H_2} would not be accompanied by a concurrent decrease in Φ_{CO}.

REFERENCES

1. a) J.G. Calvert, J.A. Kerr, K.L. Demerjian, and R.D. McQuigg, Science, 175, 751 (1972); b) K.L. Demerjian, J.A. Kerr, and J.G. Calvert, Advan. Environ. Sci. Technol., 4, 1 (1974).

2. R.G.W. Norrish and F.W. Kirkbride, J. Chem. Soc., 1932, 1518.

3. E. Gorin, J. Chem. Phys., 7, 256 (1939).

4. E.I. Akeroyd and R.G.W. Norrish, J. Chem. Soc., 1936, 890.

5. F.E. Blacet and W.J. Blaedel, J. Amer. Chem. Soc., 62, 3374 (1940).

6. M.A. Khan, R.G.W. Norrish and G. Porter, Proc Roy. Soc., (London), A219, 312 (1953).

7. J.G. Calvert and E.W.R. Steacie, J. Chem. Phys., 19, 1176 (1951).

8. R. Klein and L.J. Schoen, J. Chem. Phys., 24, 1094 (1956).

9. E.C.A. Horner, and D.W.G. Style, Trans. Faraday Soc., 50, 1197 (1954)

10. J.F. McKellar and R.G.W. Norrish, Proc. Roy. Soc., (London), A254, 147 (1960).

11. A.G. Harrison and F.P. Lossing, Can. J. Chem., 38, 544 (1960).

12. O.P. Strausz and H.E. Gunning, Trans. Faraday Soc., 60, 347 (1964)

13. M. Venugopalan and K.O. Kutschke, Can. J. Chem., 42, 2451 (1964).

14. B.A. DeGraff and J.G. Calvert, J. Amer. Chem. Soc., 89, 2247 (1967).

15. R.D. McQuigg and J.G. Calvert, J. Amer. Chem Soc., 91, 1590 (1969).

16. S. Glicker and L.J. Stief, J. Chem. Phys., 54, 2852 (1971).

17. E.S. Yeung and C.B. Moore, App. Phys. Lett., 21, 109 (1972).

18. E.S. Yeung and C.B. Moore, J. Chem. Phys., 58, 3988 (1973).

19. H.P. Sperling and S. Toby, Can. J. Chem., 51, 471 (1973).

20. R.G. Miller and E.K.C. Lee, Chem. Phys. Lett., 27, 475 (1974).

21. E.S. Yeung and C.B. Moore, J. Chem. Phys., 60, 2139 (1974).

22. P.L. Houston and C.B. Moore, J. Chem. Phys., 65, 757 (1976).

23. R.S. Lewis and E.K.C. Lee, unpublished work which is referenced in Lewis, et al., ref. 29.

24. K. Tadasa, N. Imai and T. Inaba, Bull. Chem. Soc. Japan, 49, 1758 (1976).

25. T.L. Osif and J. Heicklen, J. Phys. Chem., 80, 1526 (1976).

26. R.G. Miller and E.K.C. Lee, Chem. Phys. Lett., 33, 104 (1975).

27. T.L. Osif, Ph.D. Thesis, "The Reactions of $O(^1D)$ and OH with CH_3OH, the Oxidation of HCO Radicals, and the Photochemical Oxidation of Formaldehyde", Pennsylvania State University, August, 1976.

28. J.H. Clark, Ph.D. Thesis, "Laser Photochemistry and Isotope Separation in Formaldehyde", University of California, Berkeley, 1976.

29. R.S. Lewis, K.Y. Tang, and E.K.C. Lee, J. Chem. Phys., 65, 2910 (1976).

30. K.Y. Tang, P.W. Fairchild, and E.K.C. Lee, J. Chem. Phys., 66, 3303 (1977).

31. J. Marling, J. Chem. Phys., 66, 4200 (1977).

32. W.H. Fink, J. Amer. Chem. Soc., 94, 1073, 1078 (1972).

33. D.M. Hayes and K. Morokuma, Chem. Phys. Lett., 12, 539 (1972).

34. R.L. Jaffe, D.M. Hayes, and K. Morokuma, J. Chem. Phys., 60, 5108 (1974).

35. R. Spence and W. Wild, J. Chem. Soc., 1935, 338.

36. J.G. Calvert and J.N. Pitts, Jr., "Photochemistry", John Wiley and Sons, New York, 1966, p. 732.

37. P. Warneck, Z. Naturforsch., 26A, 2047 (1971).

38. E. Murad and M.G. Inghram, J. Chem. Phys., 41, 404 (1964).

39. R. Walsh and S.W. Benson, J. Amer. Chem. Soc., 88, 4570 (1966).

40. A. Horowitz and J.G. Calvert, work in preparation for publication.

41. JANAF Thermodynamic Tables, 2nd Edition, U.S. Department of Commerce, N.B.S., 1971.

42. T. Hikida, J.A. Eyre, and L.M. Dorfman, J. Chem. Phys., 54, 3422 (1971).

43. a) M.J. YeeQuee and J.C.Y. Thynne, Trans. Faraday Soc., 63, 1656 (1967); b) Ibid, Ber. Bunsenges. Phys. Chem., 72, 211 (1968).

44. W.R. Brennen, I.D. Gay, G.P. Glass, and H. Niki, J. Chem. Phys., 43, 2569 (1965).

45. A.A. Westenberg and N. deHaas, J. Phys. Chem., 76, 2213 (1972).

46. B.A. Ridley, J.A. Davenport, L.J. Stief, and K.H. Welge, J. Chem. Phys., 57, 520 (1972).

47. a) I.M.T. Davidson and A.B. Howard, J. Chem. Soc. Chem. Comm., 323 (1973); b) P. Potzinger, A. Ritter, and J. Krause, Z. Naturforsch., 30A, 347 1975); c) R. Walsh and J.M. Wells, J. Chem. Soc. Faraday I, 72, 100 (1976).

48. J. Cooper, A. Hudson, and R.A. Jackson, J. Chem. Soc., Perkin Trans. II, 1973, 1933.

49. J.A. Kerr and M.J. Parsonage, "Evaluated Kinetic Data on Gas Phase Addition Reactions", Butterworth, London, 1972, p. 32; we have averaged the six independent estimates shown here which were derived from the experiments at the low pressures comparable to those employed in this work.

50. "Handbook of Chemistry and Physics" 50th Edition, R.C. West editor, The Chemical Rubber Company, Cleveland, 1969, p. F-165.

51. D.A. Parkes and C.P. Quinn, J. Chem. Soc., Faraday Trans. I, 72, 1952 (1976).

52. R.A. Harger and E.K.C. Lee, Abstracts, 173rd American Chemical Society Meeting, New Orleans, La., March 20-25, 1977.

53. I. Tanaka, private communication of the results of Dr. Shibuya, Ph.D. Thesis, Tokyo Institute of Technology, Tokyo, Japan, 1976.

54. J.J. Ahumada, J.V. Michael and D.T. Osborne, J. Chem. Phys., 57, 3736 (1972).

55. R. Atkinson and R.J. Cvetanovic, Can. J. Chem., 51, 370 (1973).

THE WAVELENGTH DEPENDENCE OF THE QUANTUM EFFICIENCIES OF THE PRIMARY PROCESSES IN CH_2O PHOTOLYSIS AT 25°C

Introduction

The absorption of solar radiation by formaldehyde vapor present in the polluted atmosphere results in its photodissociation by the primary processes (1) and (2):

$$CH_2O + h\nu \rightarrow H + HCO \quad (1)$$

$$CH_2O + h\nu \rightarrow H_2 + CO \quad (2)$$

The H and HCO radicals formed in (1) react with oxygen in the air to generate HO_2 and $HCOO_2$ radicals:

$$H + O_2 + M \rightarrow HO_2 + M \quad (3)$$

$$HCO + O_2 + M \rightarrow HCOO_2 + M \quad (4)$$

$$HCO + O_2 \rightarrow HO_2 + CO \quad (5)$$

Thus CH_2O photolysis in the atmosphere may be a significant source of the hydroperoxy and peroxyformyl radicals; both radicals may be of significance in photochemical smog formation and in other atmospheric reactions.[1-7] Previous estimates of the rates of processes (1) and (2) in the lower atmosphere[4-6] were based upon the primary quantum yield versus wavelength data of McQuigg and Calvert[7] which were determined by a very indirect and necessarily imprecise method. The wavelength dependence of Φ_1 and Φ_2 has been estimated in several studies which have extended over nearly a forty year period.[7-15] In many of these studies CH_2O photolyses were made with added radical scavengers (alkenes, NO, I_2) and the limiting values of Φ_{H_2} and Φ_{CO} at high scavenger concentrations were used to derive estimates of Φ_1 and Φ_2. However the published estimates of these quantities are so widely divergent that trends in Φ_1 with λ are not well defined; see Figure 47. However if one examines the trend of Φ_1 with λ within each set of the several recent results (Calvert and McQuigg,[7] triangles; Lewis, et al.,[12] closed circles; Clark,[14] closed squares), it is clear that the value of Φ_1 increases with decreasing wavelength of the absorbed light. However the large divergence between Φ_1 estimates of the different groups points to the critical need for a further accurate definition of the Φ_1 values as a function of λ.

The wavelength dependence of Φ_1 can in principle be used to establish the wavelength of the onset of the process (1). If the dissociation originates from the vibrationally excited ground state of the CH_2O molecule, as seems likely, then the threshold wavelength may be related to the bond

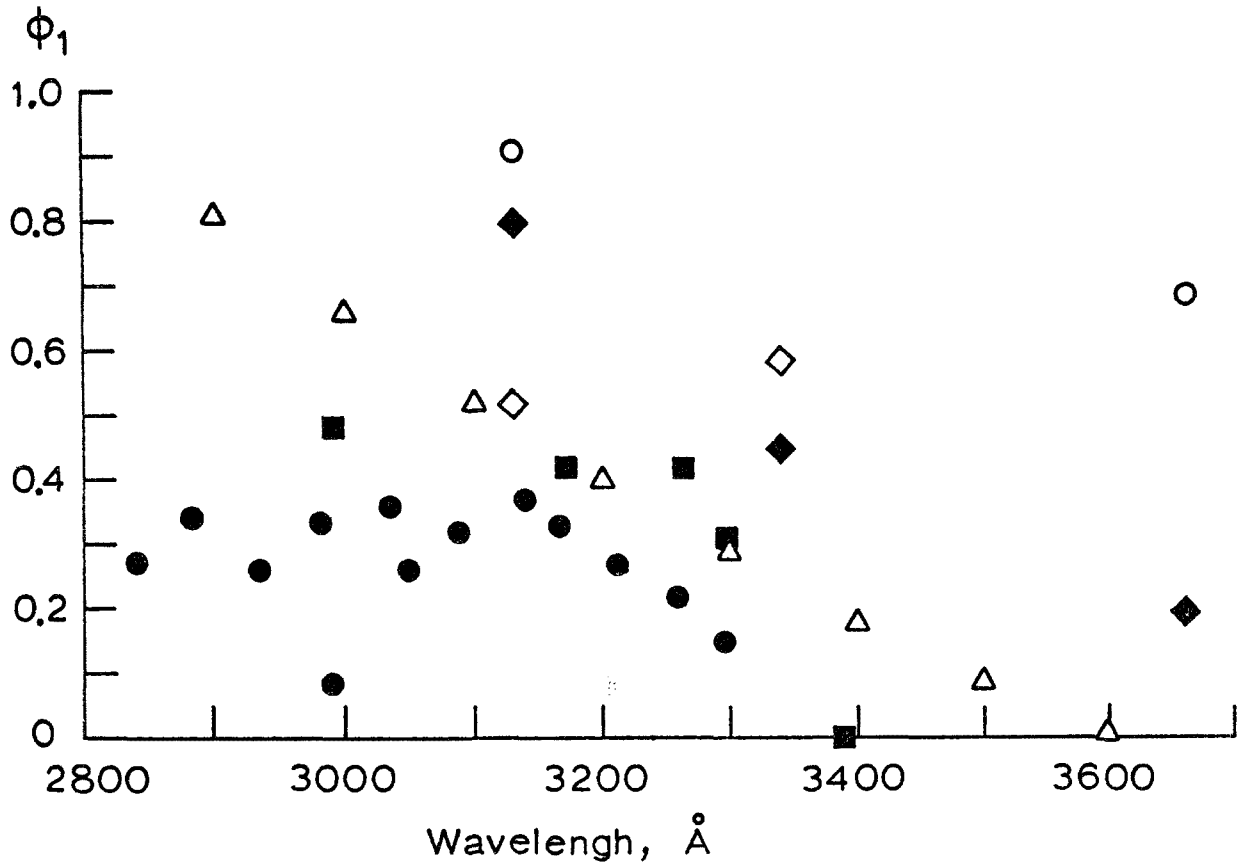

Figure 47. The previously published estimates of the primary quantum yield of the free radical-forming process (1) in CH_2O photolysis: $CH_2O + h\nu$ $H + HCO$ (1); data are from the following studies: Gorin,[8] open circles; DeGraff and Calvert,[10] open diamonds; McQuigg and Calvert,[7] open triangles; Sperling and Toby,[11] closed diamonds; Lewis, Tang, and Lee,[12] closed circles; Clark,[14] closed squares.

dissociation energy, D(H-CHO). Recent studies[12,14,15] suggest strongly that the threshold for photodissociation of CH_2O is near 3400 Å; the energy at this wavelength (84 kcal $mole^{-1}$) is in reasonable agreement with the D(H-CHO) estimates based upon kinetic[16] and photoionization experiments.[17] On the other hand results of several earlier studies[7,9,11,18] indicated that the free radical process (1) in CH_2O photolysis can occur at wavelengths considerably longer than 3400 Å. A new unambiguous determination of the threshold wavelength for (1) is required to settle this issue.

In a recent study of the 3130 Å photolysis of CH_2O at 25°C, we have found that Φ_1 and Φ_2 can be determined relatively simply using isobutene as an H-atom scavenger.[19] We have applied this technique in the present study to provide seemingly reliable new estimates of Φ_1 and Φ_2 at selected wavelengths from 2890 to 3380 Å. It has been possible to derive a new estimate of D(H-CHO) from these data. Also we have used them to estimate the rate of H and HCO generation from CH_2O photolysis in the lower atmosphere.

Experimental

The experimental setup and the method of gas chromatographic analysis were the same as that used in the previous work.[19] In order to isolate the different wavelengths from the high pressure mercury arc (Osram HBO 500W), we used a high intensity grating monochromator (Schoeffel GM 250). This had a grating with 2365 grooves mm^{-1} that gave reciprocal linear dispersion of of 16.5 Å per 1 mm slitwidth. The monochromator was calibrated with the 3132 and 3342 Å lines of the mercury arc with the monochromator set at 0.25 mm (hbw, 4.1 Å). The amount of scattered light at wavelengths longer than 3380 Å did not exceed 0.2%, and in most cases, it was considerably smaller as determined by introducing a WG-385 filter (cut off, ~ 3650 Å) between the monochromator and the photodiode (RCA 935) placed at the back of the cell.

For the non-monochromatic source employed here, the "effective" excitation band is determined by the wavelength distribution of the absorbed light; this is controlled by the emission spectrum of the source on which a near Gaussian intensity distribution is superimposed by the slit of the monochromator, and by the absorption spectrum of CH_2O. Taking these factors into account we have calculated the effective bands for the different monochromator settings used in this work. In general for the 33 Å hbw experiments, about 90% of the absorbed light fell within the $\lambda_{eff} \pm 33$ Å range; we define the "effective" wavelength here as that wavelength at which the absorbed light intensity versus wavelength plot could be divided into two parts of equal area. As a result of the presence of strong mercury lines at 2968, 3023, 3132, and 3342 Å and the fine structure of the CH_2O absorption spectrum, some of the band profiles obtained for the 50 and 66 Å hbw experiments showed long, and at times, intense tails that extended well beyond the $\lambda_0 \pm$ hbw region. However even in these cases λ_{eff} was probably not displaced greatly from λ_0 as indicated by the agreement between the experimental results at the same λ but with different hbw values.

Azomethane was used for actinometry taking $\Phi_{N_2} = 1.00$. In addition, in order to ensure an accurate determination of the quantum yields, each run with added isobutene was preceded by a run with pure CH_2O at the pressure employed in the CH_2O-isobutene photolyses. In all experiments the temperature was near 25°C, and the P_{CH_2O} was 10 Torr. Polymerization of the CH_2O was negligible for these conditions. The conversion of CH_2O into CO and H_2 did not exceed 2% in any experiment.

Results

The photolysis of CH_2O mixtures with isobutene was studied over the wavelength range from 2890 to 3380 Å, and the results of these experiments are summarized in Table 24. At 3380 Å the addition of either 1 Torr of O_2 or 25 Torr of NO to 10 Torr of CH_2O, did not have any significant effect of Φ_{H_2}. In addition the effect of CO_2 addition on hydrogen formation was examined both in the absence and presence of isobutene. The results of these experiments are given in Table 25.

Discussion

The Wavelength Dependence of the Quantum Yields of the Primary Photodissociation Processes in Formaldehyde --

Previous studies have shown that the photolysis of pure formaldehyde at 25°C results in the formation of hydrogen and carbon monoxide via reactions (1), (2), (6)-(8):

$$CH_2O + h\nu \quad H + HCO \tag{1}$$

$$CH_2O + h\nu \rightarrow H_2 + CO \tag{2}$$

$$H + CH_2O \rightarrow H_2 + HCO \tag{6}$$

$$2HCO \rightarrow H_2CO + CO \tag{7}$$

$$2HCO \rightarrow H_2 + 2CO \tag{8}$$

In our previous CH_2O study at 3130 Å and 25°C,[19] we found that isobutene was an effective scavenger for H-atoms, and when sufficient isobutene was added, Φ_{H_2} was reduced to a value which corresponded to Φ_2 through the occurrence of reaction (9):

$$H + \text{iso-}C_4H_8 \rightarrow C_4H_9 \tag{9}$$

In view of the simplicity of this system, we have adopted the same approach to Φ_1 and Φ_2 determination in the present study. The absolute value of Φ_{H_2} was determined in experiments with pure CH_2O at 25°C and at several wavelengths over the range important for the lower atmosphere photochemistry of CH_2O: 2930, 3130, 3150, 3335, and 3380 Å. With the exception of the runs at 3130 Å and 3380 Å, the data confirm the view that the quantum yield of the product H_2 is unity within the experimental error.[14] The results

TABLE 24. THE EFFECT OF ISOBUTENE ON HYDROGEN FORMATION IN THE PHOTOLYSIS OF FORMALDEHYDE AT 25°C AND WITH EXCITATION AT 2890 TO 3380Å

Wavelength (λ_{eff})[b], Å	hbw, Å	$\Phi^{\circ}_{H_2}$[c]	$\Phi^{i}_{H_2}/\Phi^{\circ}_{H_2}$[d]
2890	66	----	0.313
2894 (2894)	33	----	0.303
2930	66	1.02	0.275
2970 (2975)	41	----	0.278
3030 (3032)	33	----	0.255
3130 (3137)	33	1.12	0.280
3150	33	1.06	-----
3175	50	----	0.322
3195 (3180)	33	----	0.457
3230	41	----	0.491
3250	50	1.01	0.549
3270 (3271)	33	----	0.571
3300 (3297)	33	----	0.677
3300	50	----	0.660
3335	33	1.0	0.792
3340 (3338)	17	----	0.889
3360	66	----	0.946
3380 (3385)	33	----	1.03
3380	66	0.75	1.03

[a]Isobutene is present in all experiments at 10-14 Torr. [b]The effective wavelength given here is that λ which divides the absorbed light intensity versus wavelength plot into two parts of equal area. [c]No isobutene present; P_{CH_2O} = 10 Torr. [d]Ratio of quantum yields of H_2 in CH_2O (10 Torr)-isobutene (10-14 Torr) mixtures to that for H_2 in pure CH_2O (10 Torr).

TABLE 25. THE EFFECT OF CO_2 ON HYDROGEN FORMATION IN THE PHOTOLYSIS OF FORMALDEHYDE AT 25°C[a]

Wavelength, Å	(hbw)	$P_{iso\text{-}C_4H_8}$, Torr	P_{CO_2}, Torr	$\Phi_{H_2}/\Phi^{\circ}_{H_2}$ [b]
2890	(66)	10	0	0.313
2890	(66)	10	250	0.319
2930	(66)	10	0	0.275
2930	(66)	10	350	0.280
3130	(33)	0	400	0.996
3300	(50)	0	305	0.905
3300	(50)	14	0	0.660
3300	(50)	14	315	0.582
3300	(50)	14	320	0.546
3360	(66)	0	295	0.761
3380	(66)	0	154	0.910
3380	(66)	0	200	0.810
3380	(66)	0	276	0.757
3380	(66)	0	330	0.606

[a] P_{CH_2O} = 10 Torr in each run. [b] The quantum yield ratio is Φ_{H_2} from the run at the added CO_2 pressure shown to that for pure CH_2O photolysis at this wavelength and P_{CH_2O} = 10 Torr.

from the experiment at 3130 Å and those which we reported previously for this wavelength region,[19] give estimates of Φ_{H_2} somewhat higher than unity. This was interpreted in our previous work as suggesting the occurrence of reaction (8) with $k_7/k_8 \cong 5.8$. In view of the present results at the four other short wavelengths studied, we now feel that it is likely that $\Phi_{H_2} \cong 1.0$ over the entire range from 3335 to 2890 Å. Thus as Clark has suggested,[14] reactions (6) and (7) are probably the dominant fates of the H and HCO radicals in pure CH_2O photolysis at 25°C. We have estimated previously that $k_9/k_6 \cong 43$, so that in our present experiments employing P_{CH_2O} = 10 Torr, and $P_{C_4H_{10}}$ = 10-14 Torr, about 98% of the hydrogen atoms formed in (1) will be scavenged by isobutene. Thus the primary quantum yield (Φ_1) of the free radical process (1) can be estimated reliably from our results using the relation (10):

$$\Phi_1 = \Phi^o_{H_2}\left[1 - \frac{\Phi^i_{H_2}}{\Phi^o_{H_2}}\right]\left[1 + \frac{P_{CH_2O}}{43P_{C_4H_8}}\right] \qquad (10)$$

Here $\Phi^o_{H_2}$ and $\Phi^i_{H_2}$ are the quantum yields of H_2 in pure formaldehyde photolyses and in CH_2O-isobutene mixture photolyses, respectively. The Φ_1 values estimated in this fashion are given in Table 26.

Inspection of the results of Table 26 shows that the onset of formaldehyde photodissociation in primary process (1) is at 3370 ± 10 Å. This corresponds to an H-CHO bond dissociation energy of 84.8 ± 0.3 kcal mole^{-1}, in reasonable accord with the other recent estimates of the photodissociation limit: $\lambda_D > 3300$ Å, D(H-CHO) $\leq$ 87 kcal mole^{-1} [Ref. 12], and $\lambda_D \cong 3392$ Å, D(H-CHO) $\cong$ 84 kcal mole^{-1} [Ref. 14]. The limit which was estimated for CHDO dissociation is λ_D = 3250 ± 50 Å, D(H-CDO) = 88 ± 1.4 kcal mole^{-1} [Ref. 15]. Our present estimate of D(H-CHO) is somewhat lower than, but in accord with the kinetic estimate of D(H-CHO) = 87 ± 1 kcal mole^{-1} [Ref. 16] and the photoionization value of D(H-CHO) = 88.0 ± 1.6 kcal mole^{-1} [Ref. 17].

Our data show that for CH_2O photolyses from 3380 to 3130 Å, Φ_1 increases rapidly until it levels off at about 3130 Å. The general features of the λ dependence of Φ_1 are in agreement with the observations made in recent studies of Lewis, et al.,[12] Marling,[15] and Clark[14] using very different methods. The results of these studies are also given in Table III for comparison. In the case of the study by Marling, CHDO photolyses were made, and the relative yields of H_2, D_2, and HD were measured in photolyses using either monochromatic laser radiation or a high pressure mercury arc-monochromator combination with a hbw of 30 Å. In this system H_2 and D_2 could be formed only in free radical reactions following (1), while HD could be generated from both the molecular and free radical decomposition

TABLE 26. THE WAVELENGTH DEPENDENCE OF THE PRIMARY QUANTUM EFFICIENCY OF THE PHOTODECOMPOSITION OF FORMALDEHYDE INTO H AND HCO (Φ_1)

λ, Å	Quantum yield of primary process (1), ϕ_1					
	This work	Marling [15][a]	Lewis, et al.[12][a]		Clark [14][b]	
			Original	Normalized	Low NO	High NO
2840			0.27	0.57		
2882			0.34	0.72		
2890	0.701					
2894	0.711					
2930	0.740					
2934			0.26	0.55		
2970	0.737					
2982			0.33	0.70		
2991					0.48	0.70
3030	0.760					
3035			0.36	0.76		
3040		0.760				
3050			0.26	0.55		
3088			0.32	0.68		
3130	0.735					
3140		0.760	0.37	0.78		
3166			0.33	0.70		
3172					0.42	0.69
3175	0.692					
3180		0.636				
3195	0.554					
3210			0.27	0.57		
3230	0.519					
3250	0.460	0.456				
3260		0.442	0.22	0.46		
3264					0.42	0.48
3270	0.438					
3296			0.15	0.32		
3298					0.31	0.38
3300	0.330					
3310		0.097				
3324		0.097				
3335	0.212					
3340	0.113					
3360	0.048					
3378		0.111				
3380	0.00					
3392					-0.03	0.01

[a]Normalized at 3040 Å to give $\phi_1 = 0.76$. [b]Experiments with low NO, assuming $\Phi_{CO} - \Phi_{H_2} = \phi_1$ as in the original work; experiments with high NO, assuming $\Phi_{H_2} = \phi_2$ and taking $\phi_1 + \phi_2 = 1$ for $\lambda \leq 3300$ Å and $\phi_1 + \phi_2 = 0.75$ at 3392 Å.

modes of CHDO. Accordingly the lower limit of Φ_1 should be given by the fraction $(H_2 + D_2)/(H_2 + D_2 + HD)$, provided that $\Phi_1 + \Phi_2 = 1$. Furthermore as Marling noted, this ratio should be proportional to Φ_1 values. We may use our data to determine the proportionality factor. At short wavelengths the difference between Φ_1 in CH_2O and CHDO should be small, so we have assigned our experimental value of $\Phi_1 = 0.76$ at 3030 Å to his ratio of 0.55 measured at 3040 Å. The Φ_1 versus λ results of Marling normalized in this fashion check reasonably well with those which we have estimated in this work. Compare the Φ_1 values so derived from the Marling data (squares) with ours (closed circles) in Figure 48. In view of the isotopic difference between the CH_2O and CHDO molecules, we would not expect a more exact correspondence between the two sets of data.

Our results may be compared as well with those of Clark[14] who employed a tunable laser to photolyze CH_2O with NO added as a HCO-radical and H-atom scavenger. He estimated Φ_{H_2} and Φ_{CO} in experiments with both large and small amounts of added NO. In the runs at low added NO, Clark assumed that $\Phi_1 = \Phi_{CO} - \Phi_{H_2}$. However in his experiments with 3392 Å excitation and with large amounts of added NO, Φ_{H_2} decreased to a value significantly below the value of Φ_2 expected from the relation $\Phi_2 = 1 - \Phi_1$ and his Φ_1 estimate obtained in experiments with small amounts of added NO. This effect was attributed to the enhanced CH_2O decomposition by (1) when large NO amounts were present. However, our results are not in accord with this interpretation. Our photodissociation limit of 3370 ± 10 Å obtained with the added isobutene experiments, suggests that there is an energy deficiency for $CH_2O \rightarrow H + HCO$ in experiments with excitation wavelengths as long as 3392 Å, so collisional perturbations should not enhance the dissociation. Furthermore, we find no significant reduction of Φ_{H_2} with NO addition and with CH_2O excitation at 3380 Å; the quantum yield of H_2 (0.75) in the absence of NO is lowered only slightly ($\Phi_{H_2} = 0.73$) by the addition of 25 Torr of NO. Therefore it seems more likely to us that Clark's Φ_{H_2} values at high [NO] are more appropriate estimates of Φ_2 than those derived from the low [NO] data. Indeed, the Φ_1 values estimated from Clark s results with this assumption are in excellent agreement with those reported in this work; see Table 26 and the plot in Figure 48 (open circles).

Lewis, Tang, and Lee[12] photolyzed CH_2O-NO mixtures at low pressures using a tunable laser (~1 Å hbw). In a very unique experiment they measured the intensity of the chemiluminescence from the excited HNO molecules formed in the reaction, $H + NO \rightarrow HNO$, following process (1). Their method gave relative values of Φ_1 which were then converted to absolute values taking $\Phi_1 = 0.36$ at 3035 Å. The reference value was obtained in another set of experiments in which the low pressure photolysis of CH_2O-1-butene mixtures was studied. The vibrationally-rich C_4H_9 radicals, which resulted

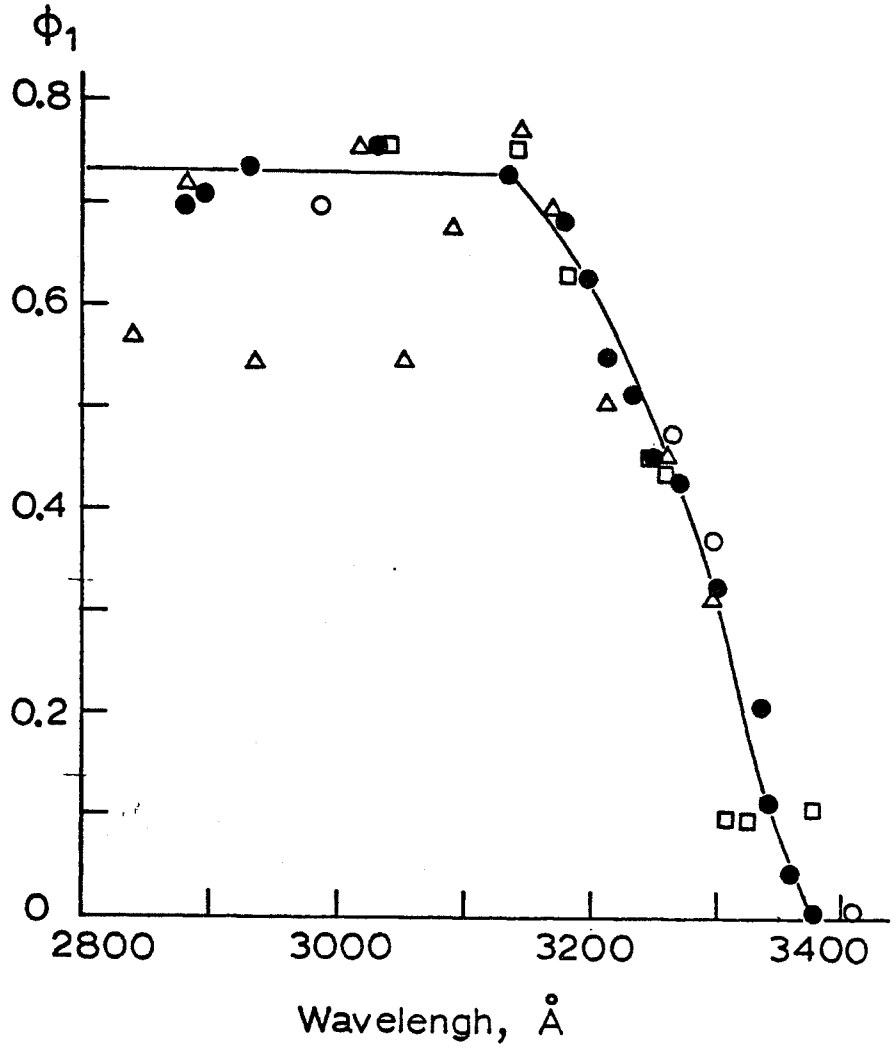

Figure 48. The wavelength dependence of the primary quantum yield Φ_1 of the free radical-forming process (1) in CH_2O photolysis: $CH_2O + h\nu \rightarrow H + HCO$ (1); estimates shown are from experiments at room temperature: this work, closed circles; Lewis, Tang, and Lee,[12] triangles (Φ_1 reference at 3065 Å was adjusted to our estimates); Marling,[15] squares (from H_2, D_2, HD product ratio data from CHDO photolyses normalized to our value of $\Phi_1 = 0.76$ at 3030 Å; Clark,[14] open circles (estimates derived from the high NO experiments).

from H-atom capture by 1-butene following process (1), were monitored through their fragmentation to C_3H_6 (and CH_3) [Ref. 20]. It can be seen in Table III that the trend in our results parallels that observed by Lewis, et al.,[12] but our absolute values are significantly higher than those of Lewis, et al., at each wavelength. The origin of the difference appears to be related to the choice of Φ_1 value by Lewis et al., for the standard at 3035 Å. Since the details of the CH_2O-1-butene study have not yet appeared, it is difficult to judge the wisdom of their choice. If we accept our estimate of Φ_1 at 3030 Å as the standard to adjust the relative Φ_1 data of Lewis, et al., at 3035 Å, then our data and those of Lewis, et al., agree well over a wide range of wavelengths; in Figure 48 compare our data (closed circles) with those of Lewis, et al. (triangles). Thus the seemingly logical adjustments of the data outlined here lead to a set of self consistent estimates of Φ_1 and its variation with λ. The data from our study and all of the recent studies carried out at room temperature,[12,14,15] define the same Φ_1 versus λ function within the experimental error of the determinations; see Figure 48 All the data support the conclusion that there is a much more rapid initial rise in Φ_1 with decreasing λ for excitations below 3400 Å than had been suggested from previous studies using less definitive methods of Φ_1 determination.[7-11] Furthermore the plateau in Φ_1 values which occurs well below unity, appears to be well documented from all of the recent results. For excitation at wavelengths less than 3100 Å, the decomposition of the excited formaldehyde by processes (1) and (2) appears to occur in a nearly constant ratio of about 3/1, independent of the excitation energy.

The absence of a CO_2 effect on Φ_{H_2} in the photolysis of CH_2O-isobutene mixtures at 2890 and 2930 Å (see Table 25.), indicates that the theoretically possible formation of "hot" hydrogen atoms that cannot be quenched by isobutene is unimportant in this system. If this were the case then the addition of the large amount of CO_2 to the CH_2O-C_4H_8 mixture photolysis should have resulted in a decrease in Φ_{H_2} for these conditions; no such effect is seen experimentally.

A further test of the mechanism of CH_2O photolysis at 3380 Å was made in this work. We observed in another recent study of CH_2O-O_2 mixture photolyses at 3130 Å that H_2 is formed in an unexpected, long-chain process which appears to be initiated by HO_2 radical interactions with CH_2O. Quantum yields as high as $\Phi_{H_2} = 6$ were observed in these experiments at 25°C.[21] In the present study we added 1 Torr of O_2 to CH_2O (10 Torr) in photolyses at 3380 Å and observed no increase in Φ_{H_2} which characterized the H-atom chain in the experiments at 3130 Å. This confirms our conclusion based upon the CH_2O-C_4H_8 and CH_2O-NO photolyses that there is very little, if any, dissociation of CH_2O into free radicals when it is excited at 3380 Å.

The Effect of CO_2 Addition on the Photodissociation of Formaldehyde --
If one is to extrapolate our findings regarding Φ_1 and Φ_2 variation with

λ to estimate the rates of processes (1) and (2) in the lower atmosphere, then the possibility of quenching of the excited CH_2O molecules by air at 1 atm must be evaluated. All present evidence suggests that decomposition in processes (1) and (2) proceeds via a highly vibrationally excited ground state molecule;[22] hence relaxation of the excited molecule before decomposition is a real possibility at pressures of the lower atmosphere. The addition of a representative atmospheric gas such as nitrogen in these experiments was precluded by the analytical methods which we employed, so CO_2 gas was added to determine the possible significance of the relaxation processes. CO_2 is somewhat more efficient than the diatomic gases N_2 and O_2 in energy relaxation processes; thus it is 2.4-times more efficient than O_2 and N_2 in the relaxation of excited singlet SO_2 [Ref. 23]. Thus about 300 Torr of CO_2 should provide roughly the equivalent relaxation medium for CH_2O as 1 atm of air. Our results from experiments with CH_2O and CH_2O-isobutene mixture photolyses with added CO_2 are summarized in Table 25. It can be seen that in experiments at 2890, 2930, and 3130 Å, there is no significant lowering of the Φ_{H_2} with CO_2 additions of up to 400 Torr. Thus we can conclude that the quantum efficiencies of primary processes (1) and (2) are not sensitive to added CO_2 gas pressures equivalent to 1 atm of air for CH_2O excitations at 3130 Å or shorter wavelengths. However the data from experiments with excitation at 3300 Å show a small quenching of hydrogen with CO_2 addition. The Φ_{H_2} value estimated in CH_2O-isobutene mixtures in the absence of CO_2 is 0.660; this is lowered somewhat (Φ_{H_2} = 0.582, P_{CO_2} = 315; 0.546, P_{CO_2} = 320 Torr) in runs with added CO_2. It is important to establish whether any concurrent reduction in Φ_1 occurred for these experiments. We can attempt this comparing the data from the pure CH_2O and CH_2O-CO_2 runs at 3300 Å. The Φ_{H_2} values from these two runs show that $\Phi_1 + \Phi_2$ is lowered from 1.0 to 0.905 on adding 305 Torr of CO_2. From the experiments with added isobutene and CO_2-isobutene we would expect a lowering by a fraction of $(0.564 \pm 0.018)/0.660 = 0.85 \pm 0.03$ if both Φ_1 and Φ_2 were quenched equally by CO_2 addition; the lowering of Φ_{H_2} to $0.34 + (0.564 \pm 0.018) = 0.904 \pm 0.018$ would occur if only Φ_2 were affected significantly by CO_2 addition. Obviously the experimental value observed here, 0.905, suggests that the latter alternative is correct. Although the accuracy of our data does not allow a firm conclusion, the present data suggest that the effect of added CO_2 on Φ_{H_2} in CH_2O photolyses at 3300 Å is largely on the quenching of primary process (2); Φ_1 appears to be affected very little, if any, by the addition of 320 Torr of added CO_2, at least for the vibronic bands of CH_2O populated by CH_2O excitation at 3300 Å.

A much more pronounced quenching of Φ_{H_2} by added CO_2 was observed in experiments at 3380 Å. Here the quantum yield of hydrogen formation is well below unity even in the absence of added CO_2 (Φ_{H_2} = 0.75). The ratio of this Φ_{H_2} to that observed with added CO_2 decreased regularly from 0.91 to 0.61 as 154 to 330 Torr of CO_2 was added. Our observations here are in accord

with the effects of added CO_2 on CH_2O quantum yields observed by Sperling and Toby[11] in their experiments at 3130 and 3340 Å and 160°C. Our quenching data do not fit well a simple one excited state quenching mechanism of the Stern-Volmer type. It seems likely to us that a multistep mechanism of deactivation of the vibrationally excited CH_2O must be operative with dissociation rates which increase markedly with increasing vibrational excitation of the CH_2O. Only the molecular primary process occurs at 3380 Å, and it is apparent from these data that the efficiency of fragmentation by this mode can be lowered significantly at the pressures of the lower atmosphere for excitation of CH_2O at wavelengths longer than 3380 Å.

Estimation of the Rate of Formaldehyde Photolysis in the Lower Atmosphere--

We may use the primary quantum yield data derived in this study together with the CH_2O extinction data of McQuigg and Calvert[7] and the recent actinic irradiance data of Peterson,[24] to derive new estimates of k_1, the apparent first order rate constant for the sunlight-initiated, free radical-forming primary process (1) for CH_2O in the lower atmosphere. The standard procedures outlined by Leighton[25] were applied in our calculations; the ϵ and Φ_1 values were averaged over wavelength intervals of 50 Å. No correction was necessary for the quenching of the 1 atm of air on the primary quantum yields of process (1), since quenching of Φ_{H_2} became important in the experiments with added CO_2 only at the wavelengths were Φ_1 was unimportant. The k_1 values so derived are summarized in Table 27 for typical conditions near ground level and at various solar zenith angles. These estimates were made using Peterson's data calculated assuming no reflection from the earth's surface. They should be increased by the factor $1 + \underline{a}$ where $\underline{a}$ is the fraction of the solar ultraviolet light (2900-3700 Å) which is reflected from the surface of the earth at the point of interest.

Because of the strong dependence of Φ_2 on the presence of added gas for CH_2O excited at the longer wavelengths ($\lambda > 3360$ Å), and the undetermined efficiency of N_2 and O_2 on this process, no attempt was made to estimate rate constants for the photodecomposition of CH_2O in sunlight which occurs by process (2). We did estimate the rate constant for light absorption by CH_2O in lower atmosphere (k_a), and these data are also presented in Table 27. This constant can be used as an upper limit to the apparent first order rate constant for the total rate of CH_2O photodecomposition by processes (1) and (2) in sunlight. Because of the stated uncertainties in the extent of air quenching of process (2) in CH_2O excited at the long wavelengths, $k_2 < k_a - k_1$. The present estimates of k_1 and k_a are shown graphically in Figure 49 for various solar zenith angles. These estimates are, on the average, about 15% lower than those derived by our group previously from less accurate Φ_1 and solar irradiance data.[3,25]

It is clear that H-atoms formed in process (1) will react almost exclusively in the lower atmosphere to form HO_2 radicals in reaction (3). The fraction of the HCO radicals which will react by the two paths (4) and (5)

TABLE 27. ESTIMATED APPARENT FIRST ORDER RATE CONSTANTS FOR SUNLIGHT ABSORPTION BY CH_2O (k_a) AND FOR PHOTODECOMPOSITION BY REACTION (1), $CH_2O + h\nu \rightarrow H + HCO$ (1), IN SUNLIGHT IN THE LOWER ATMOSPHERE (k_1)[a]

Solar Zenith Angle, deg	0	10	20	30	40	50	60	70	78	86
k_a, $min^{-1} \times 10^3$[b]	7.74	7.62	7.38	6.90	6.18	5.14	3.80	2.19	0.96	0.21
k_1, $min^{-1} \times 10^3$	2.31	2.22	2.17	1.98	1.71	1.35	0.92	0.46	0.17	0.028

[a]The actinic irradiance was taken from the estimates of Peterson [24] for conditions of zero ground reflectivity. [b]These values represent an upper limit to the specific rates of the total decomposition of formaldehyde by both primary processes (1) and (2); uncertainties in the extent of the collisional quenching of excited CH_2O at the wavelengths greater than 3350 Å where only reaction (2) is important, require $k_2 \leq k_a - k_1$.

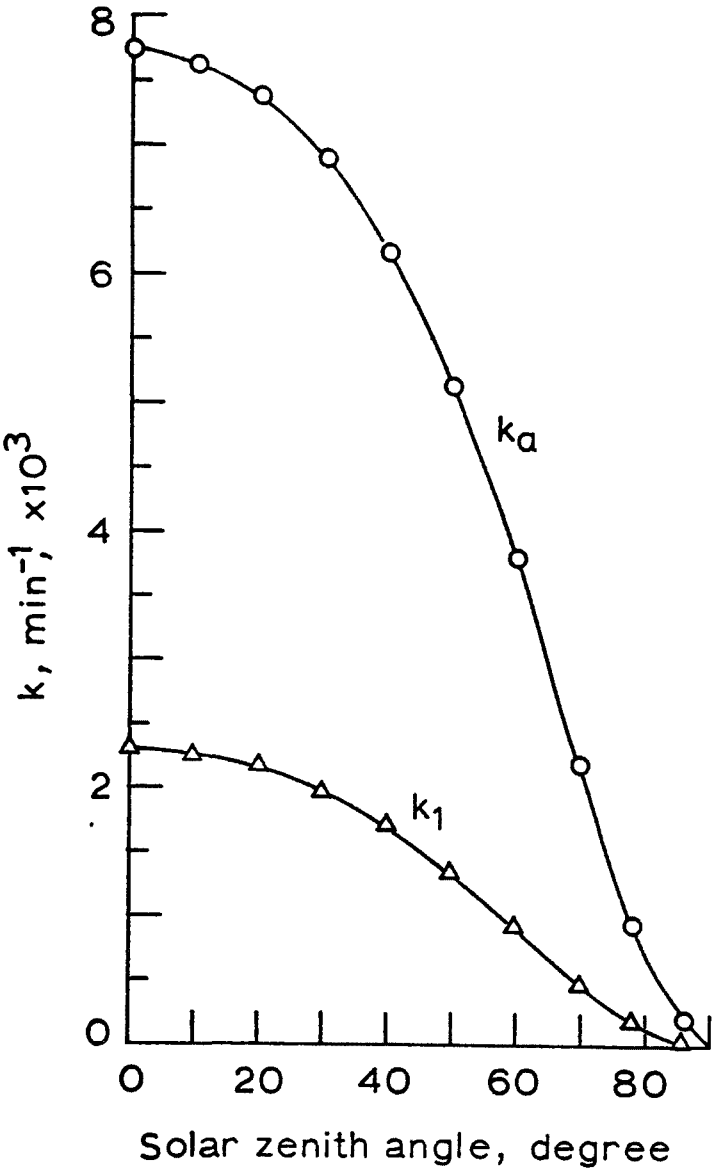

Figure 49. Variation with solar zenith angle of the apparent first order rate constants for sunlight absorption by CH_2O (k_a) and the decomposition of CH_2O by primary process (1): $CH_2O + h\nu \rightarrow H + HCO$ (1); values shown are estimated for the lower atmosphere employing Peterson's actinic irradiance estimates,[24] assuming no reflection from the earth's surface.

in the lower atmosphere is unclear at present. The recent observations of Osif and Heicklen[26] suggest that $R_4/R_5 \cong 5$ in air at 1 atm pressure, while Niki, et al., suggest that $R_4/R_5 > 9$ for these conditions. However our recent studies of the CH_2O-O_2 system have disclosed some hitherto unforseen complications in the mechanism of the formic acid and CO formation in the irradiated CH_2O-O_2 system, and it appears that this rate ratio may be much lower than the other recent studies suggest. Further work is now underway in our laboratory to derive this important rate constant ratio for atmospheric conditions.

REFERENCES

1. J. Heicklen, K. Westberg, and N. Cohen, Pennsylvania State Center Air Environment Studies, Publication No. 115-69 (1969).

2. K. Westberg, N. Cohen, and K.W. Wilson, Science, 171, 1013 (1971).

3. J.G. Calvert, J.A. Kerr, K.L. Demerjian, and R.D. McQuigg, Science, 175, 751 (1972).

4. K.L. Demerjian, J.A. Kerr, and J.G. Calvert, Advan. Environ. Sci. Technol., 4, 1 (1974).

5. J.J. Bufalini and K.L. Brubaker in "Chemical Reactions in the Urban Atmospheres", C.S. Tuesday, Ed., Elsevier, Amsterdam, 1971, p. 225.

6. J.T. Peterson, K.L. Demerjian, and K.L. Schere, "Actinic Solar Flux and Photolytic Rate Constants in the Troposphere", in Proceedings, Vol. 2, International Conference on Photochemical Oxidant Pollution and Its Control, EPA Report 600/3-77-001b, January, 1977, p 763.

7. R.D. McQuigg and J.G. Calvert, J. Amer. Chem. Soc., 91, 1590 (1969).

8. E. Gorin, J. Chem Phys., 7, 256 (1939).

9. R. Klein and L.J. Schoen, J. Chem. Phys., 24, 1094 (1956).

10. B.A. DeGraff and J.G. Calvert, J. Amer. Chem. Soc., 89, 2247 (1967).

11. H.P. Sperling and S. Toby, Can. J. Chem., 51, 471 (1973).

12. R.S. Lewis, K.Y. Tang, and E.K.C. Lee, J. Chem. Phys., 65, 2910 (1976).

13. K. Tadasa, N. Imai, and T. Inaba, Bull. Chem. Soc. Japan, 49, 1758 (1976).

14. J.H. Clark, Ph.D. Thesis, "Laser Photochemistry and Isotope Separation in Formaldehyde", University of California, Berkeley, 1976.

15. J. Marling, J. Chem. Phys., 66, 4200 (1977).

16. R. Walsh and S.W. Benson, J. Amer. Chem. Soc., 88, 4570 (1966).

17. P. Warneck, Z. Naturforsch., 26A, 2047 (1971).

18. M. Venugopalan and K.O. Kutschke, Can. J. Chem., 42, 2451 (1964).

19. A. Horowitz and J.G. Calvert, Int. J. Chem. Kinet., submitted for publication.

20. R.S. Lewis and E.K.C. Lee, referenced by Lewis, et al. [20].

21. A. Horowitz, J.G. Calvert, and F. Su, Int. J. Chem. Kinet., to be submitted.

22. a) E.S. Young and C.B. Moore, J. Chem. Phys., 58, 3988 (1973); b) Ibid., 60, 2139 (1974).

23. F. Su, J.W. Bottenheim, H.W. Sidebottom, J.G. Calvert, and E.K. Damon, Int. J. Chem. Kinet., in press.

24. J.T. Peterson, "Calculated Actinic Fluxes (290-700 nm) for Air Pollution Photochemistry Applications", EPA-600/4-76-025, 1976.

25. P.A. Leighton, "Photochemistry of Air Pollution", Academic Press, New York, 1961.

26. T.L. Osif and J. Heicklen, J. Phys. Chem., 80, 1526 (1976).

27. H. Niki, P. Maker, C. Savage, and L. Breitenbach, Abstracts, 173rd American Chemical Society Meeting, New Orleans, La., March 20-25, 1977.

AN UNUSUAL H_2-FORMING REACTION IN THE 3130Å PHOTOLYSIS OF CH_2O-O_2 MIXTURES AT 25°C.

Introduction

The chemistry and photochemistry of the formaldehyde-oxygen system have been studied extensively for a number of years.[1-16] The importance of CH_2O oxidation in hydrocarbon combustion and the potentially important role of CH_2O photooxidation in the chemistry of the atmosphere have helped to renew the interest in this system in recent years. However several important aspects of the photochemistry of the CH_2O-O_2 system remain unexplained: the detailed mechanism of formic acid formation;[14,16] hydrogen formation in quantum yields that apparently exceed unity;[9] and the detrimental effect of oxygen addition to HDCO on the isotope enrichment of the products of the laser photolysis of HDCO.[18,19]

It is well established that pure CH_2O vapor photoexcited within its first electronic absorption band (2400-3800 Å) decomposes by way of the primary processes (1) and (2), and CO and H_2 products are formed ultimately in about equal amounts through the reactions (3), (4), and (5) in experiments near 25°C:

$$CH_2O + h\nu \rightarrow H + HCO \qquad (1)$$

$$CH_2O + h\nu \rightarrow H_2 + CO \qquad (2)$$

$$H + CH_2O \rightarrow H_2 + HCO \qquad (3)$$

$$2HCO \rightarrow H_2 + 2CO \qquad (4)$$

$$2HCO \rightarrow CO + CH_2O \qquad (5)$$

O_2 addition to CH_2O leads to several additional products since O_2 will scavenge H-atoms and HCO radicals[20-22] rather effectively. Indeed, in addition to H_2 and CO products of CH_2O-O_2 photolyses, the formation of formic acid, CO_2, and H_2O have been observed, and the possible products, peroxyformic acid[14,15] and H_2O_2 [Ref. 2] have been inferred from indirect methods of analysis. Recent results of Niki, et al.[16] suggest strongly that peroxyformic acid is not formed in the photooxidation of CH_2O. In view of the fact that CO_2 is an unimportant product of the reactions in this system, the mechanism of formic acid formation through the HCO_2 radical reactions is unclear; one might expect the highly exothermic reaction, $HCO_2 + O_2 \rightarrow HO_2 + CO_2$, to compete successfully with formic acid formation: $HCO_2 + CH_2O \rightarrow HCO_2H + HCO$.

The early work of Horner, et al.[9] showed that the quantum yields of formation of H_2 and CO as well as formic acid were above unity in CH_2O-O_2 mixture photolyses at temperatures > 100°C. This observation seems to have attracted little attention in the years since its publication. In view of the relative stability of the HCO radical and the efficient scavenging of the HCO radical by oxygen, a chain sequence for H_2 formation in this system is unexpected; certainly confirmation of this unusual observation is required.

Another interesting effect of O_2 addition on CH_2O photolysis has been observed. Oxygen may change the efficiency of the primary steps (1) and (2) as Houston and Moore have suggested.[23] They found that the quantum yield of vibrationally excited CO(v = 1) significantly increased in the laser photolysis of CH_2O at 3055 Å in the presence of small amounts of O_2. This result was attributed to the O_2-enhancement of the molecular reaction mode (2) of CH_2O photodecomposition. It is of both theoretical interest and of great practical value to establish the mechanism and importance of this process in order to evaluate adequately the rate of H-atom and HCO radical generation in the earth's O_2-rich atmosphere.

Our interest in the CH_2O-O_2 system was stimulated by the several unanswered problems which we have reviewed, and it was heightened further by a most unexpected result which we obtained in another recent study of formaldehyde photolysis.[24] We redetermined the primary quantum yields of free radical (1) and molecular (2) processes in photolyses at 3130 Å. Various free radical scavengers were employed as potential reactants for H and HCO radicals in an attempt to determine Φ_2 from Φ_{H_2} values in experiments at high scavenger concentrations. Isobutene, nitric oxide, and trimethylsilane were found to be effective reactants, and CH_2O photolyses in mixtures with each of these compounds gave useful data related to Φ_1 and Φ_2. However we were very surprised to find that the addition of small amounts of O_2 to CH_2O did not suppress the hydrogen quantum yields in experiments at 25°C. On the contrary Φ_{H_2} significantly increased to values as high as $\Phi_{H_2} = 6$, yet CO_2 was only a minor product in these experiments. Thus the unusual observations of Horner et al.[9] made in experiments at temperatures of 100°C and above, are confirmed for CH_2O-O_2 photolyses even at 25°C. It was apparent that new kinetic information was necessary to rationalize these unusual findings. The present work was initiated to attempt to answer these many puzzling questions related to this interesting system. The results presented here provide some of the answers.

Experimental

Materials--

Formaldehyde was prepared from paraformaldehyde (Eastman) according to the procedure of Spence and Wild[25] and stored in a trap cooled to dry-ice temperature. Isobutene (Phillips) and CO_2 (Matheson) were purified by trap-to-trap distillation. As a further precaution against moisture introduction to the cell, each time that CO_2 and O_2 were introduced, their storage bulbs were cooled first to dry-ice temperature and then the gases were expanded into the cell.

Procedures and Product Analysis--

The experimental apparatus was the same as that described in our previous study.[24] In the present work actinometry was based upon the photolysis of pure CH_2O at 25°C, accepting Φ_{H_2}=1.10 as determined for these conditions in our earlier work. Any polymer and acid which deposited on the walls of the cell as the CH_2O-O_2 photolysis progressed in each experiment, was removed between runs by warming the cell to about 110°C while evacuating it with the high vacuum

system. The technique of gas transfer from the cell and chromatographic procedures were somewhat modified from those of our previous work. The products H_2, CO, and CO_2 and the amount of O_2 which reacted were directly determined in this study. The Molecular Sieve 5A column held at 30°C and with N_2 as carrier gas was employed here to determine H_2 in the presence of relatively large amounts of oxygen. The same column held at 100°C and with helium as carrier gas was used in O_2 and CO determinations. In these analyses at least four determinations of the sample were made to increase the accuracy of the O_2 disappearance measurement. In a few experiments CO_2 was estimated by Toepler-pumping the product gases through a glass bead - containing trap immersed in pentane-dry-ice slush. The untrapped gases were then analyzed for CO_2 using a Poropak Q column held at 100°C and He carrier gas. The CO_2 quantum yields were found to be very small; in experiments with 8 Torr of CH_2O, Φ_{CO_2} = 0.21, 0.11, and 0.16 (± 40% uncertainty) with P_{O_2} = 1, 2, and 4 Torr, respectively. Thus this analysis procedure was not continued in the later experiments. In most runs only the gases which did not condense at liquid nitrogen temperature (H_2, CO, and O_2) were determined. Duplicate runs were carried out for each set of experimental conditions. The gases from one of the runs were analyzed for H_2 while CO and O_2 were determined in the other run. The total pressure of these gases was also measured in each run as an independent check on the overall reproducibility of the system.

The key factor which limited the accuracy of the quantum yield measurements in this work was the estimation of the final and the average formaldehyde concentrations during the run and the number of quanta of light absorbed during the reaction. In theory the final P_{CH_2O} could be estimated from the measured absorbance at the end of the run; for our conditions this would amount to a 15-20% change from the initial value. However the addition of O_2 in the CH_2O photolyses leads to a much lowered stability of the monomer CH_2O; apparently acid and H_2O products of the CH_2O-O_2 mixture photolysis catalyzes the polymerization of the monomer, even during very short light exposures. As a result the transmitted light intensity was not a true measure of the gaseous formaldehyde absorption as the run progressed. Thus the formaldehyde remaining after a run was estimated by two other less direct methods: (1) the material balance of the products; and (2) the thermal jump in the pressure which was observed at the start and the finish of the irradiation. In the former method we have assumed that HCO_2H is the only acid product as Niki, et al.[16] have shown recently. We also assumed that H_2O (and not H_2O_2) is a final product and have estimated the chemical loss of formaldehyde during the run (other than polymerization) from the mass balance relation: $\Phi_{-CH_2O} = \Phi_{H_2} + 2\Phi_{-O_2}$. The amount of CH_2O that polymerized was obtained from the recorded pressure-time profiles of the reaction. Typical pressure records are shown in Figure50 for the CH_2O-O_2 system (curve A) and the CH_2O-O_2-CO_2 system (curve B). The sudden jump in pressure (point a) as the photochemical reaction began resulted largely from the very exothermic nature of the overall oxidation reactions which occurred as well as the ultimate conversion of the absorbed light energy to heat. The former source is dominant here. After a short induction period following the initial exposure, the pressure dropped at a

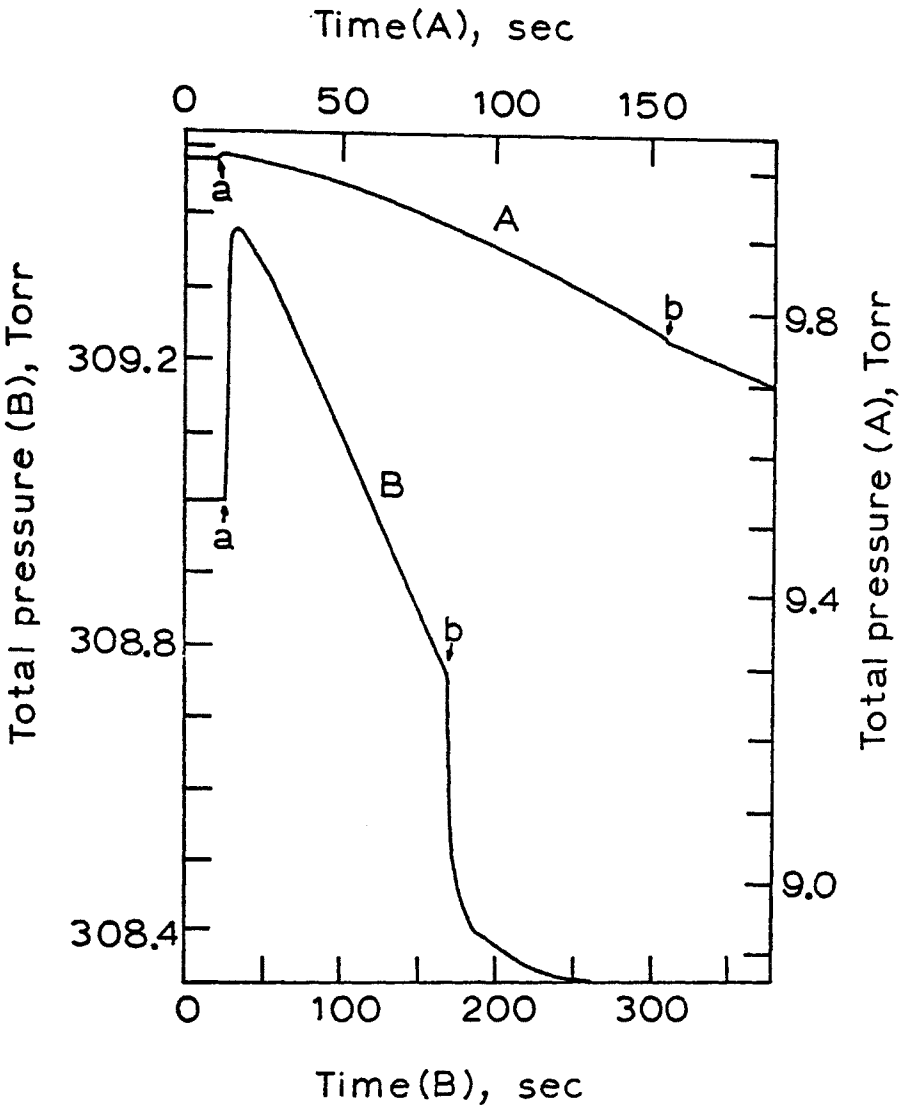

Figure 50. Pressure-time profiles in the photo-oxidation of CH_2O; 3130 Å excitation; temperature, 25°C; initial conditions: curve A, 8 Torr CH_2O, 2 Torr O_2; curve B, 8 Torr CH_2O, 1 Torr O_2, 300 Torr CO_2; points a and b designate the start and finish of the irradiation, respectively.

rate which was essentially constant during the entire irradiation period. As the light was extinguished a sudden pressure drop was observed (point b in Figure 50). This was followed by a further decrease in pressure which proceeded with a rate equal to or lower than the rate observed when the cell was irradiated. The amount of products formed was found to be independent of the time elapsed between the end of the irradiation and the time that the gases were transferred to the analytical system. Evidently the acid- and water- catalyzed polymerization of CH_2O was the sole origin of the pressure drop after the irradiation. Since the pressure in the cell decreased nearly linearly throughout the photochemical run, the rate of polymerization had to be essentially constant and equal to the rate observed immediately after the thermal jump at the end of the run. This rate was taken from the pressure-time profile and multiplied by the irradiation time to determine the amount of CH_2O which polymerized during the run; this together with the estimated amount of CH_2O which reacted chemically, gave the final CH_2O pressure using the mass balance method.

The thermal jump in pressure provided an independent method of estimating the final CH_2O pressure at the end of the run in our experiments with added CO_2. The large excess of CO_2 insured that the heat capacity of the reactant mixture was essentially unchanged during the run. In a typical experiment at initial pressures: $P_{O_2} = 1$, $P_{CH_2O} = 8$, and $P_{CO_2} = 155$ Torr, the heat released per mole of quanta absorbed was about 1461 kcal.[26,27] Only about 91 kcal $mole^{-1}$ of quanta would be released from the conversion of the light energy to heat and about 151 kcal $mole^{-1}$ from polymerization;[28] the latter energy probably would be released at the wall of the cell. The equilibrium between heat generating and heat dissipating processes at the wall is reached rapidly at a temperature which is slightly higher than the initial temperature. Our studies of the thermal jump observed in irradiated SO_2-isobutane systems[29] have shown that when the heat capacity of the system is relatively unchanged during the run, the pressure jump is directly proportional to the heat generated in the cell as a result of the light absorption and subsequent chemistry. This condition is met in our system at high CO_2 pressures. The results of Tables 28-30 show that within a narrow pressure range the rate of the chemical reaction was directly proportional to the absorbed light intensity and independent of the P_{O_2}. Thus in the CH_2O-O_2-CO_2 system, the initial and final pressure jumps should be proportional to the rate that light was absorbed by CH_2O at these points in the reaction. Since the limiting form of Beer s law applies to the CH_2O absorption for our conditions, the ratio of the initial and final pressure jumps could be used to estimate the final P_{CH_2O}. The average value of P_{CH_2O} calculated by both the product balance method (column 1, Table and the pressure jump method (in parentheses, column 1, Table reasonably well, and some confidence is added to the results of these two indirect methods.

Discussion

The Nature of the H_2, CO_2 HCO_2H-forming Chain Reactions in the Photolysis of CH_2O-O_2 Mixtures--

The present kinetic study of the 3130Å photolysis of formaldehyde-oxygen mixtures provides some interesting and unexpected results. One of

TABLE 28. EXPERIMENTAL DATA FROM THE PHOTOLYSIS OF CH_2O-O_2 MIXTURES AT 3130Å AND 25°C[a]

Pressure of reactant, Torr			Irrad. time, sec	Quanta abs./ cell-sec, x 10^{-15}	Φ_{H_2}	Φ_{CO}	Φ_{-O_2}	Φ_{CO_2}	$\frac{R_3}{R_3 + R_6}$	$\frac{\Phi_{H_2} - \Phi_2}{\frac{R_3}{R_3 + R_6}}$
CH_2O (aver)	O_2 (init)	O_2 (aver)								
7.98	0.020	-----	20	7.07	2.96(----)[b]	----(----)[b]	----(----)[b]	----(----)[b]	----	---
7.92	0.050	0.035	20	7.02	4.50(4.79)	7.01(6.54)	3.60(4.19)	----(0.25)	0.99	4.2
7.67	0.120	----	150	6.80	3.89(----)	----(----)	----(----)	----(----)	----	---
7.92	0.150	0.131	30	7.02	----(4.66)	7.07(6.41)	2.98(4.19)	----(0.25)	0.96	---
7.84	0.150	0.119	60	6.95	4.42(4.63)	6.77(6.38)	2.53(4.15)	----(0.24)	0.96	4.3
7.88	0.300	0.277	30	7.01	4.37(4.45)	6.66(6.21)	3.75(4.17)	----(0.24)	0.92	4.4
7.71	0.300	-----	75	6.83	4.42(----)	----(----)	----(----)	----(----)	----	---
7.76	0.500	0.453	75	6.88	4.26(4.20)	6.15(5.95)	3.08(4.11)	----(0.22)	0.87	4.5
7.75	0.500	0.447	75	6.87	----(4.20)	6.35(5.95)	3.50(4.11)	----(0.22)	0.88	---
7.49	1.00	0.887	150	6.64	3.75(3.67)	6.00(5.40)	3.83(3.98)	0.21(0.20)	0.78	4.4
7.49	1.00	0.885	150	6.64	----(3.68)	5.61(5.41)	3.90(3.98)	----(0.20)	0.78	---
7.49	1.00	0.882	150	6.64	----(3.68)	5.51(5.41)	4.00(3.98)	----(0.20)	0.80	---
7.21	1.00	0.774	300	6.50	----(3.66)	5.44(5.35)	3.92(3.84)	----(0.20)	0.80	---
7.94[c]	1.00	0.979	150	7.04	0.33(0.32)	1.15(1.00)	0.69(0.68)	----(----)	----	---
7.51	2.00	-----	150	6.66	3.15(----)	----(----)	----(----)	----(----)	----	---
7.02	2.00	1.77	300	6.22	----(2.91)	5.03(4.60)	4.18(3.75)	0.11(0.16)	0.63	4.5
7.05	2.00	1.78	300	6.26	----(2.91)	4.82(4.61)	3.89(3.77)	----(0.16)	0.63	---
7.51	4.00	----	75	6.67	2.25(----)	----(----)	----(----)	----(----)	----	---
7.02	4.00	3.68	300	6.22	2.11(2.14)	4.02(3.87)	5.75(3.75)	0.16(0.12)	0.45	4.0
7.23	4.00	3.79	300	6.41	----(2.16)	3.80(3.92)	3.71(3.86)	----(0.12)	0.44	---
7.76	8.00	7.9	100	6.88	1.44(1.48)	3.19(3.37)	----(4.11)	----(0.09)	----	---
7.00	8.00	7.71	400	6.21	1.41(1.40)	2.85(3.16)	3.90(3.74)	----(0.09)	0.26	4.2

[a]Initial P_{CH_2O} = 8.00 Torr. [b]The values in the parentheses were calculated by computer solution of the rate equations based upon the reaction mechanism and rate constants given in Table IV. [c]Isobutene at 2.0 Torr was added in this experiment.

TABLE 29. THE EFFECT OF ABSORBED LIGHT INTENSITY ON THE PRODUCT QUANTUM YIELDS IN THE PHOTOLYSIS OF CH_2O-O_2 MIXTURES[a]

Pressure (average) Torr P_{CH_2O}	Pressure (average) Torr P_{O_2}	Irrad. time, sec	Quanta abs./cell-sec, x 10^{-14}	Φ_{H_2}	Φ_{CO}	Φ_{-O_2}
A) $P^o_{CH_2O}$ = 8.00; $P^o_{O_2}$ = 1.00 Torr						
7.96	0.980	1000	2.70	2.10	3.55	2.50
7.67	0.971	1000	4.51	2.22	4.10	2.15
7.63	0.940	770	11.3	2.58	4.05	2.35
7.63	0.938	770	11.3	----	3.89	2.43
7.64	0.938	770	11.3	----	3.89	2.41
7.40	0.863	450	26.6	2.84	4.75	3.90
7.14	0.827	400	38.3	3.19	5.45	3.84
B) $P^o_{CH_2O}$ = 8.00; $P^o_{O_2}$ = 1.00; $P^o_{CO_2}$ = 117 Torr						
7.40	0.818	1500	4.39	4.49	7.22	6.81
7.47	0.877	600	11.1	5.02	8.11	6.27
6.60	0.594	770	24.2	5.79	8.69	7.41
7.26	0.754	300	38.8	5.19	8.26	7.18

[a]Excitation was at 3130 Å; temperature, 25°C.

TABLE 30. EXPERIMENTAL DATA FROM THE PHOTOLYSIS OF CH_2O-O_2-CO_2 MIXTURES AT 3130Å AND 25°C[a]

Pressure reactants, Torr (average) CH_2O[b]	O_2	CO_2	Quanta abs./cell-sec, x 10^{-15}	Φ_{H_2}	Φ_{CO}	Φ_{-O_2}	Φ_{CO_2}
7.24(7.24)	0.775	55	6.68	6.05 (5.61)[c]	8.62 (8.46)[c]	7.62 (7.79)[c]	(0.39)[c]
7.21(7.35)	0.769	117	6.67	5.53 (5.21)	8.79 (8.32)	7.86 (8.72)	(0.46)
7.24(7.36)	0.781	117	6.68	---- (5.20)	8.74 (8.32)	7.44 (8.76)	(0.46)
7.22(7.41)	0.744	155	6.67	5.42 (5.10)	8.60 (8.58)	8.68 (9.28)	(0.52)
7.28(7.35)	0.754	300	6.62	4.02 (4.01)	6.69 (7.38)	8.34 (9.79)	(0.56)

[a]Initial pressures of reactants: P_{CH_2O} = 8.00; P_{O_2} = 1.00 Torr; irradiation time, 150 sec in all experiments. [b]The two values shown here were estimated by the mass balance method and the pressure jump method (in parentheses) as described in the text. [c]Calculated by computer from the reaction mechanism and rate constant data given in Table IV; k_7 was assumed to be 2.0×10^{10} $\ell.^2 mole^{-2} sec^{-1}$ for M = CO_2.

the most puzzling results is the formation of H_2 in a chain mechanism; note in Tables 28-30 that the quantum yields of hydrogen are as high as 6 in some of these experiments at 25°C. One anticipates that formic acid, or possibly peroxyformic acid, carbon monoxide, and carbon dioxide may be formed in chain reactions following primary process (1) in this system through the reactions (6)-(12):

$$CH_2O + h\nu \rightarrow H + HCO \quad (1)$$

$$H + CH_2O \rightarrow H_2 + HCO \quad (3)$$

$$H + O_2 + M \rightarrow HO_2 + M \quad (6)$$

$$HCO + O_2 + M \rightarrow HCOO_2 + M \quad (7)$$

$$HCO + O_2 \rightarrow HO_2 + CO \quad (8)$$

$$HCOO_2 + CH_2O \quad HCOO_2H + HCO \quad (9)$$

$$2HCOO_2 \rightarrow 2HCO_2 + O_2 \quad (10)$$

$$HCO_2 + CH_2O \rightarrow HCO_2H + HCO \quad (11)$$

$$HCO_2 + O_2 \rightarrow HO_2 + CO_2 \quad (12)$$

Apparently peroxyformic acid is not formed in significant amounts in this system,[16] so we have neglected reaction (9) in our further considerations. However conventional reaction schemes cannot rationalize H_2 formation in a chain for experiments at 25°C. The formyl radicals formed in the CH_2O-O_2 system will react almost exclusively with O_2, even in experiments at P_{O_2} = 0.05 Torr, and H_2 formation through the reaction (4) which may occur in O_2-free CH_2O photolyses at 25°C, is unimportant here.[21,22,30,31] However H_2 formation through reaction (3) is expected to compete with the H-atom reaction (6) with O_2 for the relatively low $[O_2]/[CH_2O]$ ratios which we employed. Only a small fraction of the H-atoms formed in this system will be captured by O_2 in experiments at low added O_2 pressures; most of them will react with CH_2O in reaction (3).* Note in Table 1 the rate ratio $R_3/(R_3 + R_6)$; in experiments with $P^o_{CH_2O}$ = 8 Torr, the ratio decreases from 0.99 with $P^o_{O_2}$ = 0.050 Torr to 0.26 with $P^o_{O_2}$ = 8 Torr. However without some

---

*In making these rate estimates we have used the following rate constants: k_3 = 2.8 x 10^7 ℓ. $mole^{-1}sec^{-1}$ [Ref. 20], k_6 = 1.64 x 10^{11} (M = CH_2O; assumed equal to that for M = CH_4 [Ref. 20e]), and 2.1 x 10^{10} $\ell.^2mole^{-2}sec^{-1}$ (M = O_2 [Ref. 20a,20e]).

chain reaction which regenerates H-atoms or H_2, the Φ_{H_2} resulting from the sequence (1)-(12) must equal $\Phi_2 + \Phi_1 R_3/(R_3 + R_6)$, 1.00 at $P^o_{O_2}$ = 0.05 Torr and 0.50 at $P^o_{O_2}$ = 8 Torr. Obviously some undefined reaction steps must regenerate H-atoms to explain the much higher Φ_{H_2} values actually observed for these conditions: 4.5 at $P^o_{O_2}$ = 0.05 and 1.4 at $P^o_{O_2}$ = 8 Torr. Observe in Table 28 that the ratio of the quantum yield of H_2 exclusive of H_2 produced in the primary molecular process (2), $\Phi_{H_2} - \Phi_2$, to the fraction of H-atoms formed which lead to H_2, $R_3/(R_3 + R_6)$, is essentially a constant for all of the conditions employed in Table 28. This suggests that the unknown H-atom generating species provides a large and fairly constant source of H-atoms which has about the same rate in runs at both low and high pressures of added O_2; in experiments at the higher O_2 pressures, H_2 formation in (3) is ultimately attenuated through the increasing importance of reaction (6).

The reactive species which generates H-atoms cannot be the HCO or the HCO_2 radicals. The conventional reactions (1), (3), and (13) cannot constitute a significant chain, since reaction (13) is very slow compared to (7) and (8) even at very low pressures of O_2:

$$HCO + M \rightarrow H + CO + M \qquad (13)$$

$$HCO + O_2 + M \rightarrow HCOO_2 + M \qquad (7)$$

$$HCO + O_2 \rightarrow HO_2 + CO \qquad (8)$$

Taking $k_7[M] + k_8 = 3.4 \times 10^9$ ℓ. mole^{-1}sec^{-1} [Ref. 21] for an experiment with P_{O_2} = 0.05 and P_{CH_2O} = 8 Torr, $R_{13}/(R_7 + R_8)$ $\quad 5 \times 10^{-10}$ [Ref. 24]. It is equally unlikely that the H-atom generating species is the HCO_2 radical, since its reaction with O_2 in (12) or its decomposition in (14) would generate CO_2 in amounts equal to those of H-atoms; experimentally it is observed that $\Phi_{CO_2} \ll \Phi_{H_2}$.

$$HCO_2 + O_2 \rightarrow HO_2 + CO_2 \qquad (12)$$

$$HCO_2 \ (+M) \rightarrow H + CO_2 \ (+M) \qquad (14)$$

It is clear that the obvious conventional reaction steps which one might invoke are inadequate to account for the present results.

One reaction sequence which seems consistent with our findings, involving an HO_2-HO radical chain (15)-(19) and radical addition to the C-atom of the CH_2O:

$$HO_2 + CH_2O \rightarrow (HO_2CH_2O) \rightarrow HO + HCO_2H \qquad (15)$$

$$HO + CH_2O \rightarrow H_2O + HCO^{\ddagger} \qquad (16)$$

$$HO + CH_2O \rightarrow H_2O + HCO \quad (17)$$

$$HO + CH_2O \rightarrow (HOCH_2O) \rightarrow HCO_2H + H \quad (18)$$

$$HCO^{\ddagger} \rightarrow H + CO \quad (19)$$

The reaction (15), exothermic by 60 kcal/mole overall, is somewhat analogous to the overall reaction proposed by McKeller and Norrish[10] in the flash photolysis of CH_2O-O_2 mixtures at temperatures 140°C: $HO_2^* + CH_2O \rightarrow H_2O + CO + HO$; here HO_2^* is a vibrationally-rich HO_2 radical. Reaction (15) appears to require a much less complicated rearrangement of the reactants, and hence it appears to us to be a more realistic choice. In reaction (15), presumably the simultaneous shift of an H-atom on the carbon atom to an O-atom must accompany the rupture of the HO-bond as this reaction occurs. Reaction (18) is exothermic by 22 kcal/mole and requires rupture of single C-H bond following HO addition to CH_2O to form a formic acid molecule and an H-atom. One might speculate that H-atoms may result as well from a vibrationally excited HCO product of the reaction (16). The reaction (17) is exothermic by 33 kcal/mole, and it is conceivable that a fair fraction of the reaction will proceed by (16) in which the initial HCO product will contain more than the ~18 kcal/mole necessary for the decomposition of the radical:

$$HO + CH_2O \rightarrow HCO^{\ddagger} + H_2O \quad (16)$$

$$HCO^{\ddagger} \rightarrow H + CO \quad (19)$$

$$HCO^{\ddagger} + M \rightarrow HCO + M \quad (20)$$

Indeed without reactions (16) and (19), all of the CO molecules formed in CH_2O-O_2 mixture photolysis at 25°C must be generated in reactions (2) and (8), and for these conditions one expects $\Phi_{CO} - \Phi_{H_2} \leq \Phi_1 = 0.68$; this is contrary to the experimental results. By analogy with the proposed HO_2 radical addition to CH_2O, reaction (21), the addition of the peroxyformyl radical to CH_2O, and the subsequent rearrangement by H-atom transfer should be considered as well:

$$HCOO_2 + CH_2O \rightarrow (HCOO_2CH_2O) \rightarrow HCO_2 + HCO_2H \quad (21)$$

The relative insensitivity of Φ_{H_2} to variations in the absorbed light intensity (Table 29) points to the first order termination of the radical chains at the wall of the reaction cell for our conditions. A reaction such as (22) is suggested:

$$HO_2 + Wall \rightarrow Products\ (H_2O, O_2) + Wall \quad (22)$$

Presumably the Φ_{H_2} values increase with added CO_2 (Compare Φ_{H_2} values in sections A and B in Table 29.) as a result of the slowing of the diffusion of HO_2 (and/or other chain carried radicals) to the wall and the increased length of the chains which would result for these conditions.

Although the nature of the chain source of H-atoms must remain unclear at this time, it appears to us that the reactions (18), (16) and (19) are attractive candidates. Whatever the nature of the chain carrier, it is clear that it and/or its precursor radicals react rapidly with added butene. Thus in the experiment involving an initial mixture of 8 Torr of CH_2O, 1 Torr of O_2, and 2 Torr of isobutene shown in Table I (footnoted with a "c"), the residual Φ_{H_2} found (0.33) is equal within the experimental error to that estimated earlier in binary mixtures of CH_2O and isobutene at 3130 Å; this limiting value of Φ_{H_2} was attributed to the quantum yield of H_2 from the molecular process (2). The transients H, HO, and HO_2 which are involved in our sequence would react with isobutene as these experiments require.[33]

The proposed reaction sequence including reactions (15)-(19) and (21) also provides a realistic alternative to the HCO_2H formation in the CH_2O-O_2 photolysis system. It avoids the apparent contradiction between the required rapidity of the HCO_2 reaction (11) with CH_2O and the required slowness of the highly exothermic reaction (12) of the HCO_2 radical with O_2(ΔH_{12} = -53 kcal mole^{-1}) which seems necessary to avoid significant CO_2 formation in the system.

Using the steady state assumption for the transient radicals HO, HO_2, etc., in our system and the reaction mechanism (1)-(3), (6)-(8), (11), (12), (15)-(19), (21) and (22), the relation (A) can be derived:

$$\frac{\Phi_{H_2} - \Phi_2}{R_3/(R_3 + R_6)} = \Phi_1 \left[1 + \frac{2(k_{16} + k_{18})k_{15}[CH_2O]}{(k_{16} + k_{17} + k_{18})k_{22}} \right] \qquad (A)$$

For our experimental conditions $[CH_2O]$ is approximately constant (average P_{CH_2O} = 7.5 ± 0.5 Torr), and hence in terms of the mechanism outlined, the function $(\Phi_{H_2} - \Phi_2)/[R_3/(R_3 + R_6)]$, should be approximately constant as is observed experimentally; see Table 28.

A more quantitative test of the compatibility of the proposed mechanism with the present data will be made after a consideration of the mechanism of the HCO reactions with O_2 in the next section.

The mechanism of the formyl radical reactions with O_2. There has been considerable interest in recent years concerning the relative importance of the two competing reactions (7) and (8) of the HCO radical with O_2:

$$HCO + O_2 + M \rightarrow HCOO_2 + M \qquad (7)$$

$$HCO + O_2 \rightarrow HO_2 + CO \qquad (8)$$

Direct measurements at low pressures suggest that the HCO reaction with O_2 is in the second order region and that reaction (8) is dominant.[21,22,30] However in the recent study of the Cl-atom sensitized decomposition CH_2O-O_2

mixtures, Osif and Heicklen[14,15] estimated the ratio of $R_7/R_8 = 5 \pm 1$, independent of the pressure in the range 60-700 Torr. Niki, et al.,[16] came to the conclusion that $R_7/R_8 > 9$ in similar Cl_2-CH_2O-O_2 studies at atmospheric pressures. However the conclusions of Osif and Heicklen and those of Niki, et al., must be reexamined in view of the present findings. Both research groups have made the reasonable assumption on the basis of the data then available that the rates of HCO_2H and CO formation can be taken as measures of the rates of reactions (7) and (8), respectively. They have assumed that all $HCOO_2$ radicals formed in (7) will ultimately form HCO_2H, presumably through the reactions (10) and (11). However in view of the present findings, other sources of HCO_2H in addition to $HCOO_2$ radicals formed in (7) are likely.

The absence of peroxyformic acid among the products of the photooxidation of CH_2O[16] and the very exothermic nature of the HCO_2 reaction with O_2, suggest to us that CO_2 formation may represent a large fraction of the ultimate products formed following the HCO radical addition to O_2, reaction (7). The possible direct reaction of HCO with O_2 to give CO_2, $HCO + O_2 \rightarrow HO + CO_2$, is considered here to be an unimportant source of CO_2. Assuming the mechanism outlined and the inequalities $R_{12} \gg R_{17}$, we may estimate a lower limit to the ratio, $R_7/(R_7 + R_8)$ through the approximate relation (B):

$$\frac{R_7}{R_7 + R_8} \geq \frac{\Phi_{CO_2}}{\Phi_{H_2} + \Phi_1 - \Phi_2} \qquad (B)$$

From our data obtained in experiments at 8 Torr of CH_2O and 1, 2, and 4 Torr of O_2, we estimate $R_7/(R_7 + R_8) \geq 0.051$, 0.031, and 0.065, respectively. The CH_2O molecule should be a much more effective M in reaction (7) than O_2, so that for our conditions $R_7/(R_7 + R_8) \cong k_7[CH_2O]/(k_7[CH_2O] + k_8) = 0.049 \pm 0.017$ for $[CH_2O] = 4.0 \times 10^{-4}$ M. Taking $k_8 = 3.4 \times 10^9$ l. $mole^{-1}sec^{-1}$ [Ref. 21], we find the lower limit for the rate constant $k_7 \geq (4.4 \pm 1.6) \times 10^{11}$ $\ell.^2mole^{-2}sec^{-1}$. This estimate for k_7 is in reasonable accord with those for other third order reactions of similar complexity of reactants and similar exothermicities ($\Delta H_7 = -39$ kcal $mole^{-1}$): $HO + SO_2 + N_2 \rightarrow HOSO_2 + N_2$, $\Delta H = -37$, $k = (2.6 \pm 1.0) \times 10^{11}$ [Ref. 34]; $NO + HO + N_2 \rightarrow HONO + N_2$, $\Delta H = -36$ kcal $mole^{-1}$, $k = (2.1 \pm 0.4) \times 10^{11}$ $\ell.^2mole^{-2}sec^{-1}$. Obviously the quantum yield of CO_2 which would give a clearer picture of the pressure dependence of R_7/R_8, could not be determined from the present experiments with added CO_2. The only measurements of Φ_{CO_2} in CH_2O photooxidation at high pressures are those of Osif and Heicklen[15] who found Φ_{CO_2} values ranged from 0.08 to 0.31 in the presence of 81-458 Torr of N_2, 21-122 Torr of O_2 and 1-10 Torr of CH_2O. This is the magnitude of the Φ_{CO_2} values which we predict for the higher pressures from the present mechanism (Table30). Since k_7 for M=

N_2 would be smaller than that for CO_2, the Φ_{CO_2} values found by Osif and Heicklen should be smaller than those presented here.

The relative dominance of reaction (8) compared to (7) for the $P^o_{CH_2O}$ = 8 Torr experiments at low added O_2 pressures is also consistent with the results of our experiment in which 2 Torr of isobutene was added to 8 Torr of CH_2O and 2 Torr of O_2 (the run footnoted with a "c" in Table I). In this run about 91% of the H-atoms formed should add to isobutene,[24] so that Φ_{H_2} should be very close to $\Phi_2 = 0.32$ [Ref. 24]. Indeed we found $\Phi_{H_2} = 0.33$. We also found in this experiment that $\Phi_{CO} = 1.15$ and $\Phi_{-O_2} = 0.69$; for these conditions and $R_8 \gg R_7$, we expect $\Phi_{CO} \cong 1.0 = \Phi_1 + \Phi_2$ and $\Phi_{-O_2} = \Phi_1 = 0.68$. If R_7 were equal in magnitude or greater than R_8, then we would expect $\Phi_{CO} < \Phi_1 + \Phi_2$. Obviously the present data appear to require that $R_8 \gg R_7$, at least in the 8-12 Torr pressure range employed in these experiments.

Although the present data do not establish an accurate estimate of k_7, they do lead to a theoretically reasonable value and point to some unrecognized complications in other recent studies of this system. If we accept the true k_7 value as the lower limit of this constant which we have estimated here ($k_7 = 4.4 \times 10^{11}$ $\ell.^2 mole^{-2} sec^{-1}$), and we assume that the relative efficiency of N_2 and O_2 as M in (7) is about one-quarter of that for CH_2O and that the third order dependence of reaction (7) extends to a pressure of 1 atm of air, then we predict that about equal fractions of HCO radicals formed in the atmosphere will react by (7) and (8). Obvisouly further more definitive experiments are required to redetermine accurately the pressure dependence of the important rate ratio, $R_7/(R_7 + R_8)$. These are now underway in our laboratory.

Tests of the compatibility of the present mechanism with the experimental data obtained in this work were made using reasonable choices for the rate constants and a computer solution of the differential equations. The rate constant choices are summarized in Table 31 together with the references and reasoning used in arriving at the rate constants used. The quantum yields of the various products which are calculated using these constants are shown (in parentheses) with the experimental Φ data in Tables 1 and 3. Note that there is reasonable accord between the experimental and calculated quantum yields. Obviously the mechanism suggested is compatible with the present data, and it appears to be deserving of further detailed testing.

The Effect of O_2 Addition on the Laser Isotope Enrichment in CHDO--

Clark[18] and Marling[19] have studied the laser photolysis of CHDO at 3050Å and 3140Å, respectively, in the absence and presence of small amounts of added O_2. Both workers have found that the addition of O_2 to CHDO sharply increased the H_2/HD and HD/D_2 ratios in the products. Thus Marling found the addition of O_2 (2 Torr) to CHDO (4 Torr) increased the H_2/D_2 ratio to

TABLE 31. SUMMARY OF THE REACTION MECHANISM AND RATE CONSTANTS EMPLOYED IN THE SIMULATION OF THE CH_2O, O_2, AND CO_2 MIXTURE PHOTOLYSES

Reaction	Rate constant[a]	Reference
(1) $CH_2O + h\nu \rightarrow H + HCO$	3.68×10^{-5}	[36][b]
(2) $CH_2O + h\nu \rightarrow H_2 + CO$	1.73×10^{-5}	[36][b]
(3) $H + CH_2O \rightarrow H_2 + HCO$	2.80×10^{7}	[20]
(4) $2HCO \rightarrow H_2 + 2CO$	0.32×10^{10}	[24]
(5) $2HCO \rightarrow CO + CH_2O$	1.88×10^{10}	[24]
(6a) $H + O_2 + CH_2O \rightarrow HO_2 + CH_2O$	1.64×10^{11}	[20a]
(6b) $H + O_2 + O_2 \rightarrow HO_2 + O_2$	2.10×10^{10}	[20e][c]
(6c) $H + O_2 + CO_2 \rightarrow HO_2 + CO_2$	2.50×10^{10}	d
(7) $HCO + O_2 + M \rightarrow HCOO_2 + M$	4.2×10^{11} (M = CH_2O)	This work
(8) $HCO + O_2 \rightarrow HO_2 + CO$	3.40×10^{9}	[21]
(21) $HCO_3 + CH_2O \rightarrow HCO_2H + HCO_2$	5.35×10^{4}	e
(10) $2HCO_3 \rightarrow 2HCO_2 + O_2$	1.50×10^{6}	e
(11) $HCO_2 + CH_2O \rightarrow HCO_2H + HCO$	8.60×10^{5}	e
(12) $HCO_2 + O_2 \rightarrow HO_2 + CO_2$	3.00×10^{10}	e
(15) $HO_2 + CH_2O \rightarrow HO + HCO_2H$	7.30×10^{4}	[17b][e]
(16) $HO + CH_2O \rightarrow H_2O + HCO$	2.92×10^{9}	[37][f]
(17) $HO + CH_2O \rightarrow H_2O + HCO$	3.44×10^{7}	[37][f]
(18) $HO + CH_2O \rightarrow HCO_2H + H$	5.64×10^{9}	[37][f]
(19) $HCO^{\dagger} \rightarrow H + CO$	7.00×10^{8}	g
(22) $HO_2 + wall \rightarrow Products(H_2O,O_2) + wall$	11 - 4.1	h

[a]Reactions (1), (2), (19), and (22) are first order (sec^{-1}); reactions (6a), (6b), (6c), and (7) are third order ($\ell.^2 mole^{-2} sec^{-1}$), and all others are second order ($\ell.\ mole^{-1} sec^{-1}$). [b]Values for k_1 and k_2 were calculated from the measured light intensity and ϕ_1 and ϕ_2 values of ref. [36]. [c]See footnote 1 of the text. [d]Value was chosen to optimize the fit of the data in Table III. [e]The value of k_{21} was picked to be consistent with that taken for the analogous reaction (15); k_{15} was assumed to be equal to the total HO_2-CH_2O reaction rate constant (presumably for H-abstraction) estimated in reference [17b]; k_{10} was assigned by analogy with the observed rate constant for sec-alkyl peroxy radical reaction, $2R_2CHO_2 \rightarrow 2R_2CHO + O_2$, in ref. [38]; the relative rate constants, k_{11}/k_{12}, were picked to match best the Φ_{CO_2} data; the Φ_{H_2} and Φ_{CO} values calculated were relatively insensitive to the choices of k_9, k_{10}, k_{11}, and k_{12}. [f]The value of $k_{16} + k_{17} + k_{18}$ was taken as the total measured HO-CH_2O rate constant of ref. [37]; the relative values were assigned to give the best computer fit to the data. [g]The rate constant k_{19} was estimated to give a fast unimolecular dissociation rate which would be relatively unperturbed by the deactivation step (20) for the pressures of added gases we have employed here. [h]k_{22} was assigned so that a match of the experimental chain length was achieved; values of k_{22} = 11, 5.2, 4.6, 4.3, and 4.1 sec^{-1} were used for runs at 0, 55, 117, 155, and 300 Torr, respectively, of added CO_2.

70 from its value of 5.4 in the absence of O_2. This observation is in accord with the isotopic discrimination which one might expect with the H-atom chain reactions observed in this work. A small degree of isotopic discrimination is expected in the primary decomposition of CHDO in (1a) and (1b) such that $\Phi_{1a} > \Phi_{1b}$:

$$CHDO + h\nu \rightarrow H + DCO \qquad (1a)$$

$$CHDO + h\nu \rightarrow D + HCO \qquad (1b)$$

Also the subsequent reactions of the H and D atoms will favor H_2 formation in CHDO mixtures with added O_2, since $E_{3a} < E_{3b} = E_{3c} < E_{3d}$:

$$H + CHDO \rightarrow H_2 + DCO \qquad (3a)$$

$$H + CHDO \rightarrow HD + HCO \qquad (3b)$$

$$D + CHDO \rightarrow HD + DCO \qquad (3c)$$

$$D + CHDO \rightarrow D_2 + HCO \qquad (3d)$$

$$H + O_2 + M \rightarrow HO_2 + M \qquad (6a)$$

$$D + O_2 + M \rightarrow DO_2 + M \qquad (6b)$$

If the reactions (1) and (3) were the exclusive sources of H_2 and D_2 in the O_2-CHDO mixture photolysis, and sufficient O_2 is present to capture all HCO and DCO radicals ($P_{O_2} > 0.05$ Torr), then the ratio of H_2/D_2 in the products should be given by relation (C):

$$\frac{H_2}{D_2} = \left(\frac{k_{3a}}{k_{3d}}\right)\left(\frac{\Phi_{1a}}{\Phi_{1b}}\right)\left(\frac{k_{3c} + k_{3d} + k_{6d}\,[O_2]\,M}{k_{3a} + k_{3b} + k_{6a}\,[O_2]\,M}\right) \qquad (C)$$

When the reactions (6a) and (6b) remove a major fraction of the H and D atoms ($[O_2]/[CHDO] > 0.5$), then one expects the residual H_2/D_2 formed to be given approximately by: $(H_2/D_2) = (k_{3a}/k_{3d})(\Phi_{1a}/\Phi_{1b})(k_{6b}/k_{6a})$. We may make the reasonable estimates that $k_{6b} = k_{6a}$, $\Phi_{1a}/\Phi_{1b} \leq 2$, and $k_{3a}/k_{3d} \leq 5$; thus in the unscavenged H_2 and D_2 product from CHDO photolysis with several Torr of added O_2, we expect $H_2/D_2 \leq 10$. The much higher discrimination favoring H_2 formation in the studies of Marling and Clark can be rationalized in terms of the additional hydrogen forming chain reactions considered here. In this case the intermediate which forms H or D atoms in the chain sequence, reactions (16a)-(16d), (19a), (19b), and (18a)-(18d), will also reflect isotopic preferences for H-atom formation.

$$HO + CHDO \rightarrow HDO + HCO^{\ddagger} \qquad (16a)$$

$$HO + CHDO \rightarrow H_2O + DCO^{\ddagger} \qquad (16b)$$

$$DO + CHDO \rightarrow D_2O + HCO^{\ddagger} \quad (16c)$$

$$DO + CHDO \rightarrow HDO + DCO^{\ddagger} \quad (16d)$$

$$HCO^{\ddagger} \rightarrow H + CO \quad (19a)$$

$$DCO^{\ddagger} \rightarrow D + CO \quad (19b)$$

$$HO + CHDO \rightarrow (HOCHDO) \rightarrow DCO_2H + H \quad (18a)$$

$$HO + CHDO \rightarrow (HOCHDO) \rightarrow HCO_2H + D \quad (18b)$$

$$DO + CHDO \rightarrow (DOCHDO) \rightarrow DCO_2D + H \quad (18c)$$

$$DO + CHDO \rightarrow (DOCHDO) \rightarrow HCO_2D + D \quad (18d)$$

The reactions (16a)-(16d) all have very large rate constants and are expected to show only a small isotopic discrimination favoring DCO over HCO formation. However we expect the inequalities: $k_{19a} > k_{19b}$, $k_{18a} > k_{18b}$, and $k_{18c} > k_{18d}$. Thus it appears that the combined isotopic preferences shown in the chain sequence for H_2, HD, and D_2 formation can rationalize the experimentally observed detrimental effect of O_2 on the laser isotope separation in $CHDO-O_2$ mixtures. Without such a chain, the effect is difficult to explain.

Marling[19] also observed that the addition of 1 Torr of O_2 to 4 Torr of CH_2O with natural isotopic abundance of $^{13}CH_2O$ (1.1%), decreased the isotope enrichment in the CO product induced by $^{22}Ne_{II}$ laser photolysis at 3323.7 Å. In this case however the decrease was by a factor of 2-3, while in the CHDO experiments the H_2/D_2 ratio changed by a factor of 13. The present mechanism is not inconsistent with these results since CO formation occurs in primary process (2) rather efficiently at this wavelength ($\Phi_2 \cong 0.8$ [Ref. 36]), and in reactions (8a)-(8d) only a small difference in the rates of the reactions of the ^{13}C and ^{12}C species is expected:

$$H^{13}CO + O_2 \rightarrow HO_2 + {}^{13}CO \quad (8a)$$

$$H^{12}CO + O_2 \rightarrow HO_2 + {}^{12}CO \quad (8b)$$

$$D^{13}CO + O_2 \rightarrow DO_2 + {}^{13}CO \quad (8c)$$

$$D^{12}CO + O_2 \rightarrow DO_2 + {}^{12}CO \quad (8d)$$

The Effect of O_2 Addition on the Primary Photodissociation Steps in Formaldehyde--

In their study of CH_2O photolysis at 3050Å, Houston and Moore[23] found that the addition of NO or O_2 to formaldehyde increased markedly the yield of vibrationally excited CO(v = 1) and the vibrationally relaxed CO(v = 0). The relative yield of CO(v = 1) was higher for NO addition than for O_2 addition, while the reverse trend was observed for CO(v = 0). The effect was

attributed to interactions between NO or O_2 and the vibronically excited ground state [$S_0(v)$] formaldehyde molecules. The decomposition of CH_2O by primary processes (1) and (2) was assumed to occur from $S_0(v)$, and collisions with NO and O_2 presumably "catalyzed" the latter molecular mode of decomposition at the expense of the free radical decomposition. The authors did not, however, exclude the possibility that the increased rates of CO formation were caused by chemical reaction between the HCO radicals and added NO and O_2. The present results allow a seemingly unambiquous choice between these alternatives.

In our previous study of CH_2O photolysis at 3130 Å,[24] the addition of a sufficient amount of isobutene and NO lowered the hydrogen quantum yield to the same limiting value, presumably equal to Φ_2. The agreement between the two values seems to indicate that the molecular mode of decomposition is not enhanced by NO. The present results with added isobutene which we have discussed previously show that this is also true for oxygen. In the experiment in which 2 Torr of isobutene was added to 8 Torr of CH_2O and 2 Torr of O_2 (see Table 28.), we find $\Phi_{H_2} = 0.33 \cong \Phi_2$. Houston and Moore[23] observed a two-fold increase in the relative CO(v = 1) quantum yield when 0.5 Torr of O_2 was added to 2 Torr of CH_2O; for the same CH_2O/O_2 ratio we find no effect of O_2 on Φ_2. Thus we feel that reactions (8) and (23) are responsible for the enhanced formation of the vibronically excited CO.

$$HCO + O_2 \rightarrow HO_2 + CO(v = 1) \qquad (8e)$$

$$HCO + NO \rightarrow HNO + CO(v = 1) \qquad (23)$$

The reactions (8) and (23) are sufficiently exothermic (30 and 34 kcal $mole^{-1}$, respectively[27]) that they can in theory provide readily the necessary 6.2 kcal $mole^{-1}$ to create vibrationally excited CO(v = 1) molecules. The stronger effect of NO on the relative yield of CO(v = 1) could possibly be related to the somewhat higher exothermicity of reaction (23). Finally the observed smaller effect of NO on CO(v = 1) formation at the longer wavelengths can also be explained by the occurrence of reaction (23), since the amount of HCO formed in reaction (1) is significantly decreased at the longer wavelengths.

REFERENCES

1. R. Fort and C.N. Hinshelwood, Proc. Roy. Soc., A, 129, 284 (1930).

2. W.A. Bone and J.B. Gardner, Proc. Roy. Soc., A, 154, 297 (1936).

3. J. Spence, J. Chem. Soc., 1936, 649.

4. J.E. Carruthers and R.G.W. Norrish, J. Chem Soc., 1936, 1036.

5. F.F. Snowdon and D.W.E. Style, Trans. Faraday Soc., 35, 426 (1939).

6. D.W.E. Axford and R.G.W. Norrish, Proc. Roy. Soc., A, 192, 518 (1948).

7. D.W.G. Style and D. Summers, Trans. Faraday Soc., 42, 388 (1946).

8. E.C.A. Horner and D.W.G. Style, Trans. Faraday Soc., 50, 1197 (1954).

9. E.C.A. Horner, D.W.G. Style and D. Summers, Trans. Faraday Soc., 50, 1201 (1954).

10. J.F. McKellar and R.G.W. Norrish, Proc. Roy. Soc., A, 254, 147 (1960).

11. J.J. Bufalini and K.L. Brubaker in "Chemical Reactions in Urban Atmospheres", C.S. Tuesday Ed., Elsevier, Amsterdam, 1971, p. 225.

12. D.E. Hoare and G.S. Milne, Trans. Faraday Soc., 63, 101 (1967).

13. a) R.R. Baldwin, A.R. Fuller, D. Longthorn, and R.W. Walker, J. Chem. Soc., Faraday I, 68, 1362 (1972); b) Ibid., 70, 1257 (1974).

14. T.L. Osif, Ph.D. Thesis, "The Reactions of $O(^1D)$ and OH with CH_3OH, the Oxidation of HCO Radicals, and the Photochemical Oxidation of Formaldehyde Formaldehyde", Pennsylvania State University, 1976.

15. T.L. Osif and J. Heicklen, J. Phys. Chem., 80, 1526 (1976).

16. H. Niki, P. Maker, C. Savage, and L. Breitenbach, Abstracts 173rd American Chemical Society Meeting, New Orleans, La., March 20-25, 1977.

17. a) J.G. Calvert, J.A. Kerr, K.L. Demerjian, and R.D. McQuigg, Sci., 175, 751 (1972); b) K.L. Demerjian, J.A. Kerr, and J.G. Calvert, Adv. Environ. Sci. Technol., 4, 1 (1974).

18. J.H. Clark, Ph.D. Thesis, "Laser Photochemistry and Isotope Separation in Formaldehyde", University of California, Berkeley, 1976.

19. J. Marling, J. Chem. Phys., 66, 4200 (1977).

20. a) D.L. Baulch, D.D. Drysdale, D.G. Horne, and A.C. Lloyd, Evaluated Kinetic Data for High Temperature Reactions, Vol. 1, Butterworth, London, 1972; b) W.P. Bishop and L.M. Dorfman, J. Chem. Phys., 52, 3210 (1970); c) T. Hikida, J.A. Eyre, and L.M. Dorfman, J. Chem. Phys., 54, 3422 (1971); d) M.J. Kurylo, J. Phys. Chem., 76, 3518 (1972); e) W. Wong and D.D. Davis, Int. J. Chem. Kinet., 6, 401 (1974).

21. N. Washida, R.I. Martinez, and K.D. Bayes, Z. Naturforsch., 29a, 251 (1974).

22. a) I. Tanaka, private communication of the results of Dr. Shibuya, Ph.D. Thesis, Tokyo Institute of Technology, Tokyo, Japan, 1976; b) I. Tanaka, private communication of the results of Dr. Ebata, Ph.D. Thesis, Tokyo Institute of Technology, Tokyo, Japan, 1976.

23. P.L. Houston and C.B. Moore, J. Chem. Phys., 65, 757 (1976).

24. A. Horowitz and J.G. Calvert, Int. J. Chem. Kinet., in press.

25. R. Spence and W. Wild, J. Chem. Soc., 1935, 338.

26. R.A. Fletcher and G. Pilcher, Trans. Faraday Soc., 66, 794 (1970)

27. S.W. Benson, Thermochemical Kinetics, Sec. Ed., John Wiley, New York, 1976.

28. G.S. Parks and H.P. Mosher, J. Polymer Sci., A, 1, 1979 (1963).

29. F. Su and J.G. Calvert, Int. J. Chem Kinet., submitted for publication.

30. J.H. Clark, C.B. Moore, and J.P. Reilly, paper submitted for publication; the authors are grateful to Dr. Clark for a preprint of this work.

31. a) M.J. YeeQuee and J.C.Y. Thynne, Trans Faraday Soc., 63, 1656 (1967); b) Ibid., Ber. Bunsenges. Phys. Chem., 72, 211 (1968).

32. F. Su, J.W. Bottenheim, H.W. Sidebottom, J.G. Calvert, and E.K. Damon, Int. J. Chem. Kinet., in press.

33. A.C. Lloyd, Evaluated and Estimated Kinetic Data for the Gas Phase Reactions of the Hydroperoxy Radical, N.B.S. Report 10447, 1970.

34. G.W. Harris and R.P. Wayne, J. Chem. Soc., Faraday I, 71, 610 (1975).

35. J.G. Anderson, J.J. Margitan, and F. Kaufman, J. Chem. Phys., 60, 3310 (1974).

36. A. Horowitz and J.G. Calvert, Int. J. Chem. Kinet., in press.

37. E.D. Morris and H. Niki, J. Chem. Phys., 55, 199 (1971).

38. J.E. Bennett, D.M. Brown, and B. Mile, Trans. Faraday Soc., 66, 376 (1970).

SECTION 4

STUDIES RELATED TO THE REMOVAL MECHANISMS OF NITROGENOUS COMPOUNDS IN THE ATMOSPHERE

THE NEAR UV ABSORPTION SPECTRUM OF GASEOUS HONO AND H_2O_3

Introduction

In recent years there has been a renewed interest in the study of the gas phase reactions of HONO. This has been stimulated largely by two factors: (1) The need for a quantitative evaluation of the reaction pathways which form and destroy HONO in the atmosphere; and (2) the increasing use of HONO as a convenient photochemical source of HO radicals in the laboratory.

The atmospheric chemistry of nitrous acid remains poorly defined today. Nash[1] seemingly identified HONO in the atmosphere of southern England (0.4-11 ppb), but the analytical method employed could, at best, provide only a very indirect identification of this compound.[2] In theory nitrous acid is expected to be present in the NO_x-RH-polluted, sunlight-irradiated atmosphere at levels in the range estimated by Nash. It may be formed in the atmosphere through several reaction pathways; for example, the reactions (1)-(3) have been considered in the computer simulation of the chemistry of the polluted atmosphere:[3,4]

$$HO + NO\ (+M) \rightarrow HONO\ (+M) \qquad (1)$$

$$HO_2 + NO_2 \rightarrow HONO + O_2 \qquad (2)$$

$$NO + NO_2 + H_2O \rightarrow 2HONO \qquad (3)$$

The ultimate concentration to which HONO will build is limited by the rates of its various removal reactions such as (4)-(6):

$$2HONO \rightarrow NO + NO_2 + H_2O \qquad (4)$$

$$HONO + HO \rightarrow H_2O + NO_2 \qquad (5)$$

$$HONO + h\nu(\lambda < 400nm) \rightarrow HO + NO \qquad (6)$$

Existing rate data suggest that reaction (6) is probably the dominant loss reaction for HONO in the atmosphere,[4,5] but the large difference between recent estimates of the absorption cross sections of HONO,[6-8] make its rate uncertain by as much as a factor of six. The methods used in the previous studies appear to be uncomplicated. In the HONO spectral studies of Johnston and Graham,[7] nitrous acid was prepared by reactions (3) and (4), presumably at its equilibrium concentration, from starting gaseous mixtures of NO, NO_2, and H_2O in He. Corrections were made for absorptions due to NO_2, N_2O_4, and

N_2O_3 in the spectrum. In the studies of HONO by Cox and Derwent,[8] relatively pure, dilute mixtures of HONO were prepared in a nitrogen carrier gas which was allowed to flow over an acidified nitrite salt solution. With this method corrections for NO_2 absorption were relatively small, and those due to N_2O_4 and N_2O_3 were negligible. In principle both of these recent quantitative studies of HONO absorption should provide reliable absorption cross section data, and it is not clear from the published information as to what problems led to the very different results. Obviously a further study of this system is necessary to establish the correct HONO absorption cross sections and to provide a more quantitative evaluation of the potential reactions of HONO in the atmosphere.

Cox has shown recently that nitrous acid vapors are an excellent photochemical source of HO radicals through reaction (6).[9-11] Following his lead, we have studied some of the thermal and photochemical reactions of HONO vapors employing an FTS IR, long-path spectroscopy system to follow HONO and various reactants and products.[5,12,13] In the course of these studies, we observed that the rates of HONO photolysis were very much faster in dilute gaseous mixtures than we had anticipated from the measured intensities in our experiments at simulated solar intensities (290-410nm region) and the HONO absorption cross section data then available.[7] The present spectral study of HONO was initiated at that time in an attempt to reevaluate the near uv absorption cross sections of HONO and to allow an unambiguous and independent check on our measured rates of reaction 6 in the reaction chamber. We utilized the equilibrium method employed by Johnston and Graham.[7] As our work neared completion, the recent study of Cox and Derwent[8] appeared. The new results which we report here are in qualitative accord with those reported by Cox and Derwent, although some significant differences appear.

Experimental

Spectral measurements of the gaseous mixtures of HONO, NO_2, N_2O_3, N_2O_4, NO and H_2O were made using a Cary 17 uv-visible spectrophotometer in a 10 cm path gas cell equipped with a Teflon vacuum stopcock and Supracil windows. The optical resolution varied with wavelength but was kept less than 1 nm in the 325-450 nm range and less than 5 nm in the 300-325 nm range. Since King and Moule[6] found no trace of fine structure in the HONO spectrum when they employed a 20 ft grating spectrograph with a resolving power of 150,000, our equipment was sufficient to resolve the structure of the HONO. The reactant gases NO and NO_2 (Matheson), and H_2O were purified by fractional distillation and degassing in two conventional high vacuum systems which were equipped with Teflon high vacuum stopcocks, calibrated volumes, pressure gauges, and a quartz spiral manometer.

In the study of the N_2O_3 spectra, small quantities (1-14 Torr) of an NO_2-N_2O_4 gaseous mixture were added to the cell. Then a large measured quantity of NO (112-753 Torr) was introduced into the cell. The cell contents were allowed to equilibrate for about 30 min, and then the absorption spectrum of the mixture (300-450 nm) was determined. The NO_2 pressure in the cell was estimated from the visible absorption at 430, 440, and 448 nm using the absorption cross section data for these wavelengths reported by Hall and Blacet;[14] the three independent estimates of the P_{NO_2} checked well

with one another, usually within a few percent. From the measured P_{NO_2} in the equilibrium mixture and the P^{o}_{NO}, $P_{N_2O_4}$ and $P_{N_2O_3}$ were calculated using the known equilibrium constants K_7 and K_8 for the given temperature of the particular experiment.

$$2NO_2 \rightleftharpoons N_2O_4 \qquad (7)$$

$$NO + NO_2 \rightleftharpoons N_2O_3 \qquad (8)$$

The values of K_7 and K_8 which we employed were derived from the JANAF enthalpy, entropy, and heat capacity data[15] and should be reliable for temperatures used in this work (24-30°C):

$$K_7 = \exp[6989T^{-1} + 0.791 \ln(T/298) - 21.52] \qquad (9)$$

$$K_8 = \exp[4834T^{-1} - 0.144 \ln(T/298) - 16.854] \qquad (10)$$

These expressions yield estimates which are in reasonable accord with the measured values of K_7 and K_8 at 298°K [Ref. 16,18] and 300°K [Ref. 17]. The absorption data of Bass, et al.[19] were used to determine absorbances due to NO_2 and N_2O_4 in the 300-400 nm range, and these were subtracted from the measured absorbance to determine that due to N_2O_3. Absorbances determined in this fashion at several wavelengths followed well the linear Beer's law dependence on $[N_2O_3]$ over the entire pressure range which could be studied here (0.54-6.32 Torr); data for the 300, 310, and 320 nm measurements are shown in Figure 51. Summarized in Table 32 are the absorption cross sections, $\sigma_\lambda = \ln (I_{o\lambda}/I_\lambda)/[N_2O_3]\ell$ $cm^2 molec^{-1}$ for N_2O_3 at each nm in the 300-400 nm range.

In the HONO studies, HONO was formed from NO_2, NO, and H_2O vapors through the equilibrium 11:

$$NO + NO_2 + H_2O \rightleftharpoons 2HONO \qquad (11)$$

Mixtures were prepared by adding small amounts of NO_2, N_2O_4 as before. Then H_2O vapor at its equilibrium pressure at 0°C was introduced to a calibrated volume in the manifold, and a measured fraction of this was distilled into the cell. This procedure provided the same 1.57 Torr (298°K) initial pressure of H_2O in each run which was made. A measured quantity of nitric oxide gas was then added to the cell as before. The mixture was allowed to warm to room temperature and to equilibrate. Spectra of the mixtures were determined every day for three successive days; they did not change detectably after the first 24 hour period, so it seems clear that equilibrium was established in the mixtures used for the HONO absorption cross section measurements in this work. The equilibrium P_{NO_2} was measured as before. Using the initial pressures of H_2O and NO, and the measured amount of NO_2 in the equilibrium mixture, the pressures of the other components in the equilibrium mixture were calculated using relations (9), (10), and (12):

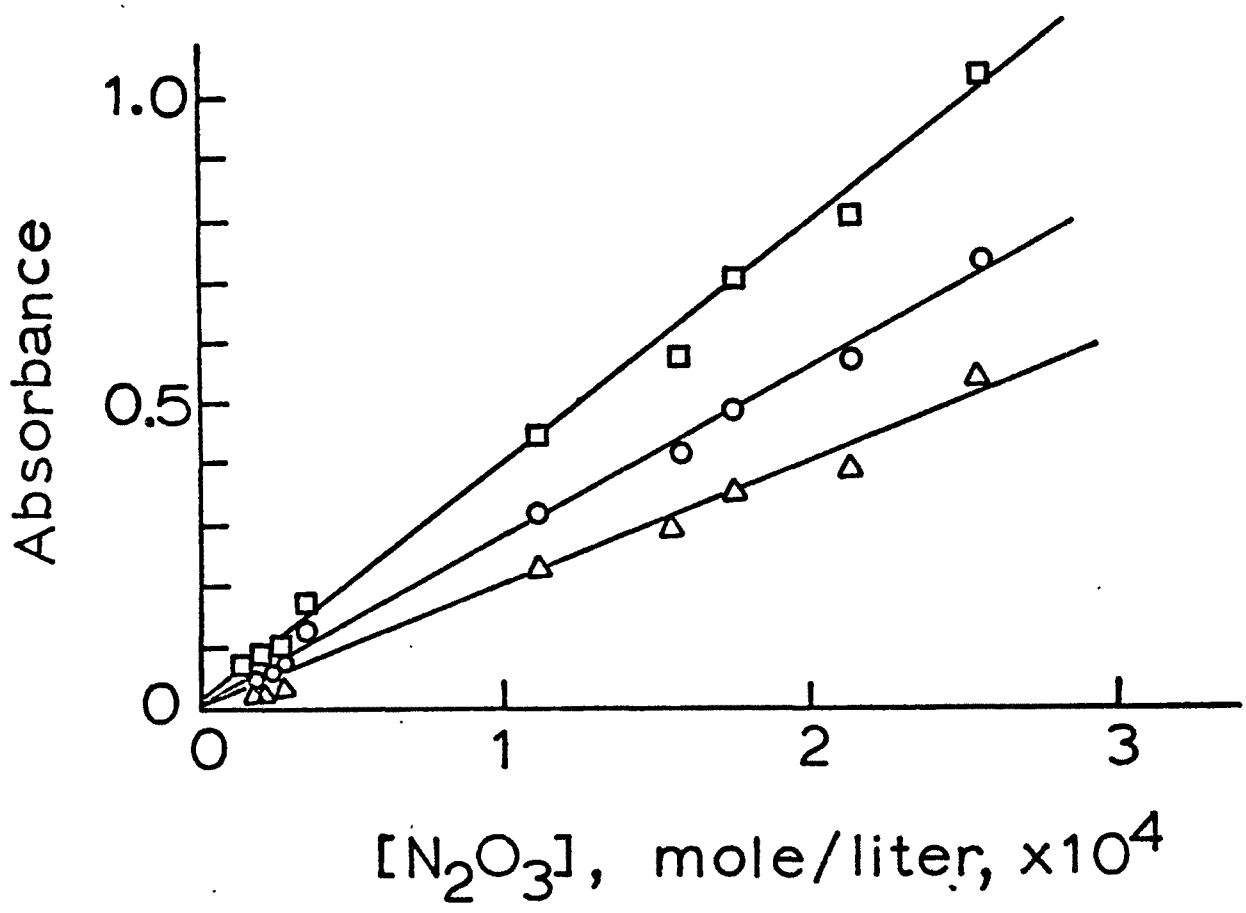

Figure 51. Beer's law plots for $N_2O_3(g)$ at some representative wavelengths; data for wavelengths 300, 310, 320 nm are shown as squares, circles, and triangles, respectively.

TABLE 32. DINITROGEN TRIOXIDE ABSORPTION CROSS SECTIONS*

Wavelength, nm	σ, cm^2 $molec^{-1}$ x 10^{20}	Wavelength, nm	σ, cm^2 $molec^{-1}$ x 10^{20}	Wavelength, nm	σ, cm^2 $molec^{-1}$ x 10^{20}
300	150	334	68.4	368	29
301	146	335	66.8	369	27
302	141	336	65.7	370	26
303	136	337	63.8	371	26
304	132	338	62.3	372	26
305	128	339	60.3	373	26
306	123	340	58.1	374	26
307	118	341	57.3	375	26
308	113	342	56.1	376	26
309	109	343	55.4	377	27
310	106	344	54.2	378	27
311	101	345	53.5	379	27
312	97.4	346	53.1	380	27
313	94.0	347	52.7	381	25
314	90.9	348	52.3	382	24
315	88.6	349	51.9	383	23
316	85.6	350	51.6	384	21
317	83.3	351	50.4	385	20
318	81.7	352	49.7	386	18
319	79.8	353	48.9	387	17
320	78.3	354	48.1	388	15
321	77.5	355	47.7	389	13
322	76.8	356	47.0	390	12
323	76.4	357	45.8	391	10
324	76.0	358	44.7	392	8.8
325	75.6	359	43.9	393	7.3
326	75.2	360	43.2	394	5.7
327	74.9	361	41.2	395	4.6
328	74.5	362	39.7	396	3.8
329	74.1	363	38.2	397	3
330	73.7	364	36	398	2
331	71.8	365	35	399	1
332	70.7	366	33	400	0
333	69.9	367	31		

* $\sigma = \ln (I_o/I)/[N_2O_3]\ell$, cm^2 $molec^{-1}$.

$$K_{11} = \exp[-15.56 + 4.73 \times 10^3 T^{-1}] \quad (12)$$

Relation (12) was derived by Chan, et al.[5] from the combined experimental data of Wayne and Jost,[20] Waldorf and Babb,[21] and Ashmore and Tyler.[22] The JANAF data for the HONO species must be in error since constants derived from these data do not reproduce the experimental equilibrium data.[5] Using these composition data, the known absorption cross sections for NO_2 and N_2O_4 [Ref. 19] together with our absorption data for N_2O_3 (Table 32), absorbances due to NO_2, N_2O_4, and N_2O_3 were calculated at 1 nm wavelength intervals from 300 to 400 nm. These were subtracted from the total measured absorbance of the equilibrium mixture to obtain the absorbance due to HONO. The fraction of the measured absorbance at 332 and 368 nm which was attributable to HONO was in the range 15 to 67% of the total absorbance measured. The absorbances for HONO followed reasonably well the linear dependence on concentration expected from Beer's law for the very limited range of concentrations which could be determined for this system (1.47-3.73 Torr, 25°C). The absorption cross sections which we have estimated from this study are summarized in Table 33. The accumulated error in these estimates which could result from the absorbance measurements and equilibrium data employed should be less than 10% at the maxima in the HONO absorption spectrum.

The near uv absorption spectrum of N_2O_3 vapor

The absorption cross sections estimated for $N_2O_3(g)$ in the near ultraviolet region are presented in Table 32 and plotted in Figure 52. The continuous nature of the absorption reported previously is confirmed.[23] However there is a weak, but readily discernible structure which can be seen. We attribute this tentatively to the $N_2O_3(g)$. It is not likely that such an effect would result from impurity bands of HONO which may have formed inadvertently from the reaction of the oxides of nitrogen with H_2O impurity released from the cell wall. The amount of such water vapor must be below a few hundred ppm at most, and the equilibrium level of HONO in such a mixture could not create the relatively intense absorption of the broad structure observed here. Furthermore the positions of the strongest HONO bands at 368 and 340 nm are near minima in the broad structure exhibited in Figure 52. Conceivably the structure could arise due to the faulty correction for NO_2 present in the N_2O_3 mixture, but experiments in which NO_2 absorption was matched in the reference beam of the spectrometer also showed this broad structure. We are not aware of any tabular data with which we can compare these cross section estimates. Johnston and Graham[7] did not publish their measured data for N_2O_3. That of Shaw and Vosper[23] were presented in graphical form only, and the scale of the plot chosen makes impossible an accurate reading at the wavelength of most intense absorption in our work (300 nm); however it appears to be qualitatively consistent with our estimates.

The near uv spectrum of HONO vapor

The absorption cross section data for HONO determined in this study are summarized in Table 33 and plotted in Figure 53 (the solid curve). These data

TABLE 33. NITROUS ACID ABSORPTION CROSS SECTIONS*

Wavelength, nm	σ, cm^2 $molec^{-1}$ x 10^{20}	Wavelength, nm	σ, cm^2 $molec^{-1}$ x 10^{20}	Wavelength, nm	σ, $cm^2 molec^{-1}$ x 10^{20}
310	0.0	339	16.3	368	45.0
311	0.0	340	10.5	369	29.3
312	0.2	341	8.70	370	11.9
313	0.42	342	33.5	371	9.46
314	0.46	343	20.1	372	8.85
315	0.42	344	10.2	373	7.44
316	0.3	345	8.54	374	4.77
317	0.46	346	8.32	375	2.7
318	3.6	347	8.20	376	1.9
319	6.10	348	7.49	377	1.5
320	2.1	349	7.13	378	1.9
321	4.27	350	6.83	379	5.8
322	4.01	351	17.4	380	7.78
323	3.93	352	11.4	381	11.4
324	4.01	353	37.1	382	14.0
325	4.04	354	49.6	383	17.2
326	3.13	355	24.6	384	19.9
327	4.12	356	11.9	385	19.0
328	7.55	357	9.35	386	11.9
329	6.64	358	7.78	387	5.65
330	7.29	359	7.29	388	3.2
331	8.70	360	6.83	389	1.9
332	13.8	361	6.90	390	1.2
333	5.91	362	7.32	391	0.5
334	5.91	363	9.00	392	0.0
335	6.45	364	12.1	393	0.0
336	5.91	365	13.3	394	0.0
337	4.58	366	21.3	395	0.0
338	19.1	367	35.2	396	0.0

* $\sigma = \ln(I_o/I)/[HONO]\ell$, cm^2 $molec^{-1}$.

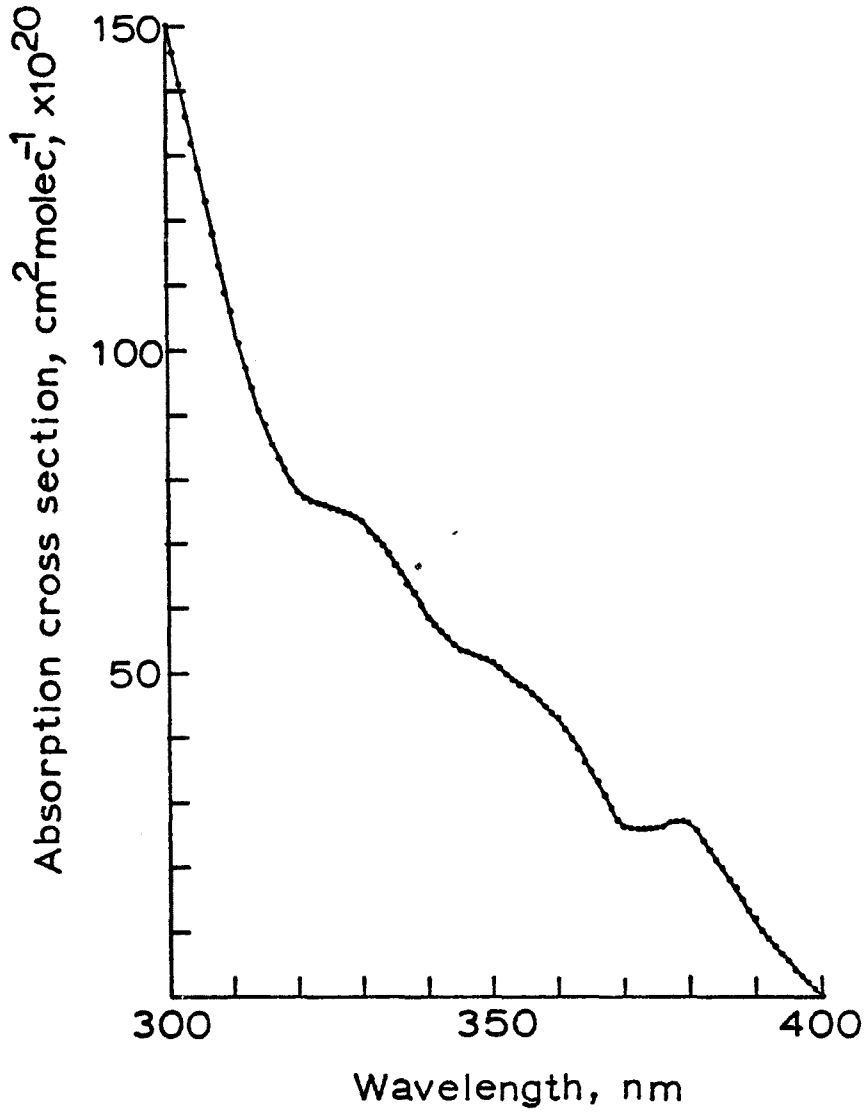

Figure 52. The absorption cross section for $N_2O_3(g)$ as a function of wavelength.

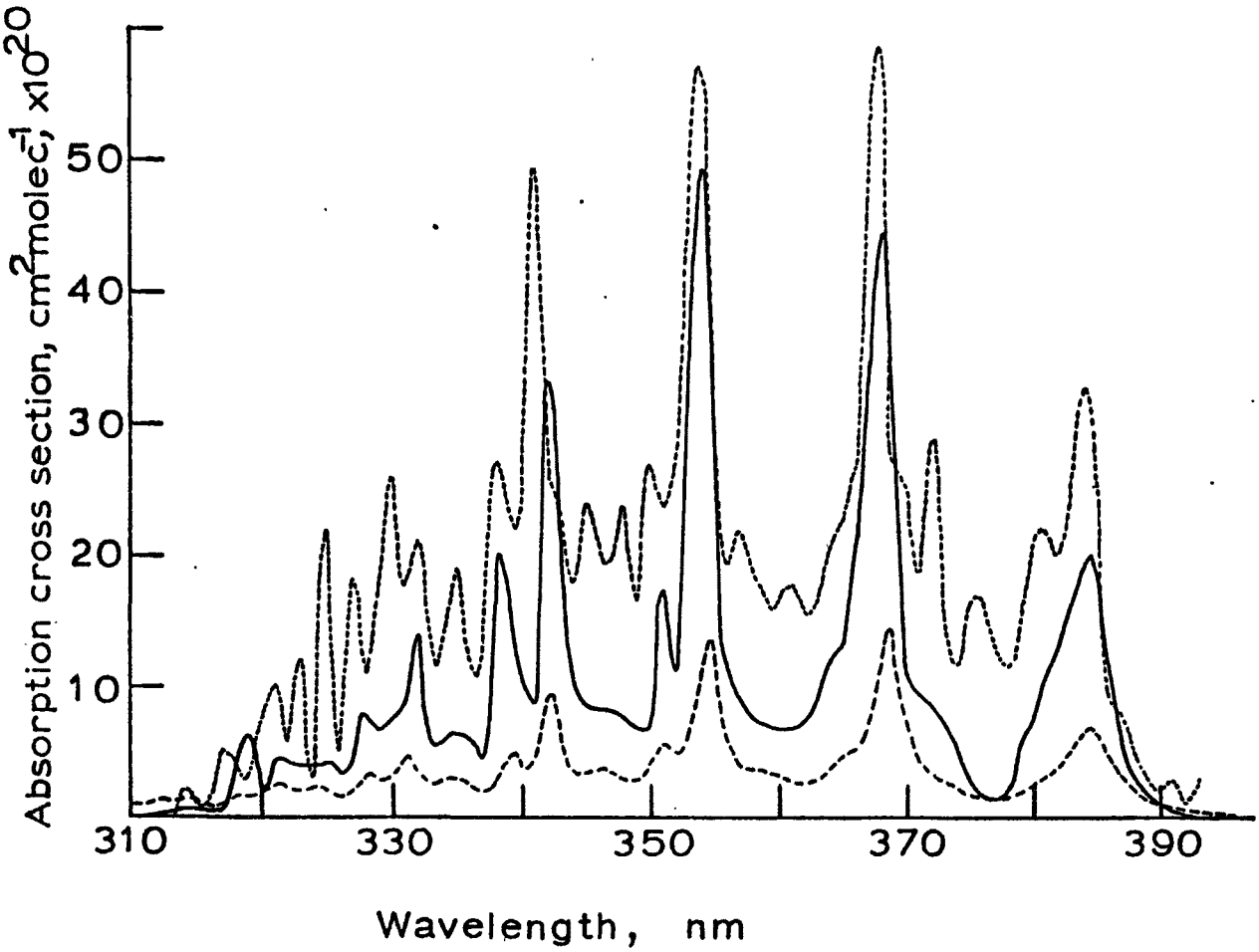

Figure 53. The absorption cross section for HONO(g) as a function of wavelength; data from present work are shown as solid curve; those of Cox and Derwent[8] and Johnston and Graham[7] are given by the lower and upper dashed curves, respectively.

can be compared with those estimated in the studies of Johnston and Graham[7] (the lower dashed curve) and Cox and Derwent[8] (the upper dashed curve). It is apparent that the magnitude of the cross sections for the peaks in absorption estimated in our work are more nearly equal to those of Cox and Derwent, although the vibrational structure which we observe correlates better with the data of Johnston and Graham.[7] The peaks seen in the Cox and Derwent spectrum near 325, 330, 345, 348, 357, 361, 373, 376, 380, and 391 nm do not appear in our HONO absorption spectrum or in those reported by Johnston and Graham[7] and King and Moule.[6] We noted that maxima occur very near these wavelengths in the spectrum of NO_2 gas.[19] The magnitude of these peaks is within the uncertainty in the HONO cross sections reported by Cox and Derwent. However if these peaks are real, then it is likely that the Cox and Derwent spectral data for HONO include some uncorrected absorptions from NO_2 impurity in their mixtures. In making the corrections for NO_2 absorption, they employed the Johnston and Graham absorption data for NO_2 which lists only values at wavelength intervals of 5 nm [Ref. 7]. It seems inevitable that some peak structure of NO_2 must be retained in the corrected spectrum of HONO using this procedure. If one assumes that this is the origin of the difference between our absorption data and that of Cox and Derwent and that they have correctly estimated the concentration of HONO in their mixtures, then we expect the uncorrected NO_2 to be given by: $[NO_2]_{uncor} \cong [HONO]\{(\sigma_{HONO} - \sigma_{HONO})/\sigma_{NO_2}\}$; σ'_{HONO} is the apparent absorption cross section observed by Cox and Derwent, and σ_{HONO} and σ_{NO_2} are the correct values for HONO and NO_2, respectively. Using the Cox and Derwent data from 345, 348, 357, 361, 372, 376, and 380 nm and assuming our σ_{HONO} values to be correct, we estimate $[NO_2]_{uncor}/[HONO] \cong 0.24 \pm 0.07$ in the Cox and Derwent experiments. Of course the net effect of having uncorrected absorption due to NO_2 present is to raise the σ_{HONO} estimate. It seems likely to us that this may have occurred in the experiments of Cox and Derwent.

The seemingly low values of absorption cross sections for HONO derived by Johnston and Graham, may reflect non-equilibrium levels of HONO in their reaction mixtures as Cox and Derwent have suggested, since reactions 3 and 4 are relatively slow in the NO_2, NO_2 H_2O, He gas mixtures employed. These workers do not describe the time dependence of the growth of HONO observed nor the period of delay before final measurements were made, so such a suggestion must remain as conjecture. The ratio of peak to valley cross sections in the three data sets now available for HONO are inconsistent. Thus $\sigma_{354}/\sigma_{360} = 3.74$, 3.29, and 7.26 from the data Johnston and Graham,[7] Cox and Derwent,[8] and our data, respectively. Conceivably this difference may have resulted from an overcorrection for NO_2 in our study. However if this were the case one should observe minima in the HONO calculated spectrum which would correspond to the NO_2 peaks. This is not observed. It seems more likely to us that the data of the other workers were undercorrected for the presence of NO_2.

A test of the reliability of the HONO absorption cross section data can be made using rate data derived in our large photochemical reactor system. The ultraviolet light which bathes the cell contents rather uniformly, mimics quite well the ground level solar flux both in intensity and wavelength distribution in the 2900 to 4100 Å region. FTS IR spectrometric analysis of reactants and products can give a fairly continuous record of the chemistry which occurs in the reactor. The apparent first order rate constant for reaction (7) was determined in a series of experiments employing low concentrations of HONO in 700 Torr of air and in mixtures with small quantities of added CO, NO, and NO_2 in 700 Torr of air.[24] Rate data on reaction 13 were obtained in another series of experiments at low concentrations of NO_2 carried out both in the absence and the presence of 700 Torr of air.

$$HONO + h\nu \rightarrow HO + NO \qquad (7)$$

$$NO_2 + h\nu \rightarrow O + NO \qquad (13)$$

The kinetic treatment of these data gave $k_7 \cong 0.11$ and $k_{13} \cong 0.60$ min^{-1} [Ref. 13]. The relative light intensity versus wavelength distribution function $F(\lambda)$ for the uv light within the cell was determined using an absolute spectrofluorimeter as detector. These data were coupled with our present $\sigma_{HONO}(\lambda)$ estimates, $\sigma_{NO_2}(\lambda)$ data of Bass, et al.,[19] primary quantum yield data for (Ref. 13), $\Phi_{13}(\lambda)$, of Jones and Bayes,[24] and the assumption that $\Phi_7 = 1$ at all HONO absorbing wavelengths in the 290-410 nm range,[8] to derive the theoretically expected relative rates of reactions (7) and (13) in our photochemical reactor:

$$\frac{R_7}{R_{13}} = \frac{\int \sigma_{HONO}(\lambda)\, F(\lambda)\, \Phi_7(\lambda)\, d\lambda}{\int \sigma_{NO_2}(\lambda)\, F(\lambda)\, \Phi_{13}(\lambda)\, d\lambda} \qquad (14)$$

Using relation (14) and integrating over the 290 to 410 nm range of non-zero values, we obtained $R_7/R_{13} \cong 0.18 \pm 0.02$. This checks well with the ratio of the independently estimated experimental rates: $R_7/R_{13} \cong 0.11/0.06 \cong 0.18 \pm 0.04$. Thus some support is provided for the accuracy of the present HONO cross section data and the conclusion of Cox and Derwent that $\Phi_7 \cong 1.0$ within the first absorption band of HONO. If the σ_{HONO} values of Johnston and Graham are used in relation (14), we obtained $R_7/R_{13} \cong 0.065$; use of the Cox and Derwent estimates of σ_{HONO} yields $R_7/R_{13} \cong 0.32$.

We feel that our present estimates of the absorption cross sections of HONO are the most reliable of those available today, and we recommend their use in the modeling of the tropospheric chemistry. We may combine our σ_{HONO} values with Peterson's recent estimates of the flux of solar radiation at ground level[25] to derive new theoretical estimates of k_7

applicable for the lower troposphere at various solar zenith angles. These estimates are shown in Figure 54 for the choice of zero surface albedo. They may be increased by the appropriate reflection factor which describes best the properties of the earth's surface at the point of interest.

The unambiguous detection of HONO in ambient air has not yet been accomplished to our knowledge. Simulations using these estimates suggest that for a typical NO_x-RH-polluted, sunlight-irradiated atmosphere, the levels of HONO, controlled largely by reactions (1)-(6), which are expected to be present near ground level should be in the ppb range. Obviously a sensitive detector system will be necessary to successfully identify HONO in the ambient air.

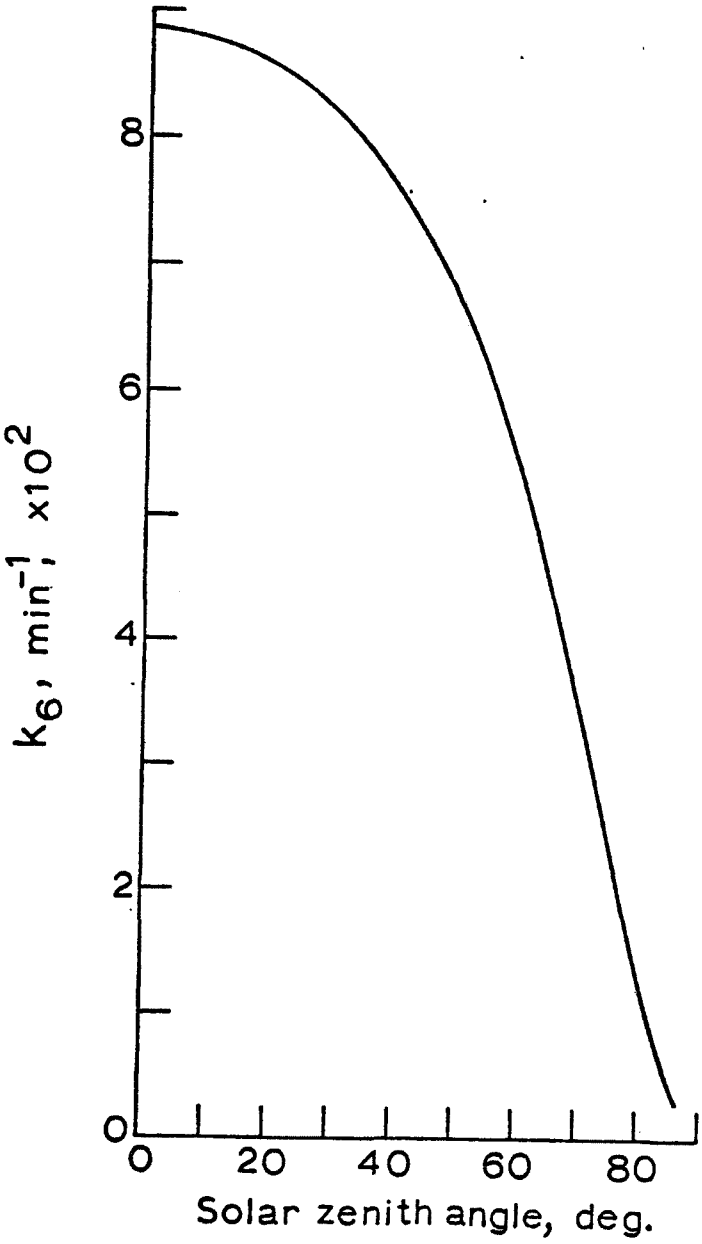

Figure 54. Estimated first order rate constants for HONO(g) photolysis in sunlight, HONO + sunlight → HO + NO; data are calculated for sea level and surface albedo equal zero for various solar zenith angels; actinic flux data from Peterson.[25]

REFERENCES

1. T. Nash, Tellus, 26 (1974) 175-179.

2. T. Nash, Am. Occup. Hyg., 11 (1968) 235-239.

3. K.L. Demerjian, J.A. Kerr, and J.G. Calvert, Adv. Environ. Sci. Technol., 4 (1974) 1-262.

4. J.G. Calvert and R.D. McQuigg, Int. J. Chem. Kinet., Symp. 1 (1975) 113-154.

5. W.H. Chan, R.J. Nordstrom, J.G. Calvert, and J.H. Shaw, Environ. Sci. Technol., 10 (1976) 674-682.

6. G.W. King and D. Moule, Can. J. Chem., 40 (1962) 2057-2065.

7. H.S. Johnston and R. Graham, Can. J. Chem., 52 (1974) 1415-1423.

8. R.A. Cox and R.G. Derwent, J. Photochem., 6 (1976/77) 23-34.

9. R.A. Cox, J. Photochem, 3 (1974) 175-188.

10. R.A. Cox, J. Photochem., 3 (1974) 291-304.

11. R.A. Cox, Int. J. Chem. Kinet. Symp. 1 (1975) 379-398.

12. W.H. Chan, W.M. Uselman, J.G. Calvert, and J.H. Shaw, Chem. Phys. Letters, 45 (1977) 240-244.

13. S.Z. Levine, W.M. Uselman, W.H. Chan, J.G. Calvert, and J.H. Shaw, Chem. Phys. Letters, 48 (1977) 528-535.

14. T.C. Hall, Jr., and F.E. Blacet, J. Chem. Phys., 20 (1952) 1745-1749.

15. JANAF Thermodynamic Tables, 2nd Edition, Nat. Stand. Ref. Data Ser., Nat. Bur. Stand. 37 (1971).

16. F.H. Verhoek and F. Daniels, J. Amer. Chem. Soc., 53 (1931) 1250-1263.

17. E.W. Kaiser and C.H. Wu, J. Phys. Chem., 81 (1977) 187-190.

18. E.R. Beatte and S.W. Bell, J. Chem. Soc. (1957), 1681-1686.

19. A.M. Bass, A.E. Ledford, and A.H. Laufer, J. Res. Nat. Bur. Stand. Sect. A, 80A (1976), 143-166.

20. L.G. Wayne and D.M. Yost, J. Chem. Phys., 19 (1951) 41-47.

21. D.M. Waldorf and A.L. Babb, J. Chem. Phys., 39 (1963), 432-435; ibid., 40 (1964) 1165.

22. P.G. Ashmore and B.J. Tyler, J. Chem. Soc. (1961) 1017-1021.

23. A.W. Shaw and A.J. Vosper, J. Chem. Soc., Dalton (1972) 961-964.

24. I.T.N. Jones and K.D. Bayes, Chem. Phys. Letters, 11 (1971) 163-166.

25. J.T. Peterson, "Calculated actinic fluxes (290-700nm) for air pollution photochemical applications", Report EPA-600/4-76-025, June, 1976, Environmental Protection Agency, Research Triangle Park, N.C.

THE KINETICS OF DIMETHYLAMINO RADICAL REACTION IN SIMULATED ATMOSPHERES: THE FORMATION OF DIMETHYLNITROSAMINE AND DIMETHYLNITRAMINE

Introduction

There has been increasing concern over the possible generation of nitrosamines within the atmosphere because of their unusually high carcinogenic activity.

In 1956, dimethylnitrosamine (DMN) was shown to cause cancer in rats,[1] and concern has continued to grow about this and other N-nitrosamines and their relation to human health. Although there have been no studies directly linking DMN with cancer in humans, DMN has been shown to cause tumors in mice, hamsters, mink, rats, guinea pigs, rabbits and rainbow trout.[2] To date, no animal species studied has shown any resistance to the carcinogenic action of DMN. It would seem rather presumptuous to assume that man is the uniquely immune species.

DMN has been shown to be an effective carcinogen regardless of the manner of application. Ingestion, inhalation, injection and topical application of DMN have all been shown to cause tumors, generally far from the site of administration. For example, long-term, low-dosage ingestion of DMN was found to lead to liver cancer, while higher concentrations in the foodstuff produced kidney cancer in a shorter amount of time -- in several cases after just one dose.[3] A single dose of 5 ppm caused tumors in 70% of the animals in another study.[4] Inhalation of DMN was shown to be an effective means of exposure at levels of 200 $\mu g/m^3$ (67 ppb); furthermore, the study showed that a small daily dose led to a smaller cumulative dose before the appearance of cancer.[5]

It is from the overall picture rather than from any individual study that concern arises. It is these considerations that prompt researchers to classify DMN as one of the most potent carcinogens.[3,6,7]

The first reported finding of nitrosamines in the atmosphere, the detection of DMN and diethylnitrosamine (DEN) near a factory producing secondary amines in Germany,[8] generated considerable interest in the atmospheric occurence and behavior of these species. Since that time, nitrosamine concentrations in several U.S. cities have been measured.[2,9,10] The highest concentrations of DMN were found near an FMC plant synthesizing unsymmetrical dimethylhydrazine and utilizing DMN as an intermediate. These concentrations peaked at 36 $\mu g/m^3$ (12 ppb), and levels in the nearby community of Baltimore ranged from 0.03 to 8 $\mu g/m^3$ (0.01 - 2.6 ppb). In Belle, W. Va., where both DuPont and Union Carbide manufacture or use dimethylamine (DMA), levels of from 0.2 to 1.0 $\mu g/m^3$ were found.[10] This is comparable to levels observed in New York City.[11] These levels are much higher than those found for other airborne carcinogens, e.g., benzo(a)pyrene at 2 ng/m^3 [Ref. 12], and thus these levels are cause for concern.

The origins of DMN in ambient air are not clear. Presumably, the nitrosamine will either be emitted as a primary pollutant, or conceivably it could be formed from precursors in the atmosphere.

The only known major emitter of DMN, the FMC plant near Baltimore, was shut down in April, 1976.[13] Small amounts of DMN have also been found to be by-products of the combustion of rocket fuel[14] and tabacco;[15] DMN is also produced in the preparation of fish products,[16,17] which are rich in amines.

The main precursors of nitrosamines in the atmosphere are felt to be secondary and tertiary amines, and oxides of nitrogen. Both are widely distributed. Amines are emitted as a result of a wide variety of industrial activity, including amine manufacture, food processing, coking, the refining of petroleum, and incineration. They are also given off in appreciable concentrations from sewage treatment plants, animal feed lots, and swamps.[11] Nitrogen oxide sources include fossil fuel combustors, refuse incineration, home heating, automobile exhausts, and industrial processes related to the manufacture and use of nitric acid.[12]

Bretschneider and Matz[8] have shown that mixtures of dimethylamine and nitrogen dioxide at 50 to 100 ppm combine within seconds to form DMN. Neurath et al.[18] have shown that the stoichiometry of this reaction is 1:1, but the mechanism of the reaction remains unclear. Recent work by Hanst[19] at much lower concentrations (2 ppm NO, 2 ppm NO_2, 1 ppm DMA) indicate that this reaction is too slow to be an important source of nitrosamine under atmospheric conditions.

Hanst[19] has also studied the reaction of HONO with DMA. The reaction of 0.5 ppm HONO (in equilibrium with 2 ppm NO, 2 ppm NO_2, and 13,000 ppm H_2O) with 1 ppm DMA gave DMN from DMA in about 10 to 30% yield. Glasson[20] repeated this work, finding the same rate of loss of the amine, but obtaining only about 1% yield of the nitrosamine. He suggests that this is evidence that the reaction does not take place homogeneously, but is controlled by a reaction occurring at the cell wall.

Further work by Hanst[19] includes a study of the photolysis of DMN in sunlight. The sample was prepared by mixing 20 Torr DMA with 20 Torr NO, adding room air, and pumping out the volatile components. A value for $t_{1/2}$ of 30 minutes for photolysis in bright sunlight at noon was obtained, corresponding to an apparent first order photolysis rate constant, $k_1 = 0.02\ min^{-1}$.

$$(CH_3)_2N\text{-}NO + h\nu \rightarrow (CH_3)_2N + NO \qquad (1)$$

Products found include nitric oxide, carbon monoxide, formaldehyde, and an unidentified compound with absorbances at 1560 cm^{-1}(s), 1480 cm^{-1}(m-s), 1310 cm^{-1}(s), 1000 cm^{-1}(m) and 775 cm^{-1}(w).

In light of the work of Hanst, Pitts et al.[21] have initiated a study of amine-NO_x photolyses. One of the amines employed was DMA. DMA was combined with NO and NO_2 at a relative humidity of about 40% and allowed to react for two hours in the dark before being exposed to sunlight. The qualitative results agree with Hanst; that is, DMN is formed in the dark, and disappears during photolysis with $t_{1/2} \cong 1 - 2$ hr. The unknown product of Hanst is identified as dimethylnitramine, $(CH_3)_2N\text{-}NO_2$.[22] This is the

same product obtained by Althorpe et al.[23] by the sunlight photolysis of dilute solutions of DMN in hexane.

The detailed mechanism of nitrosamine formation is still obscure, although some speculation about it has been made. Attack of the amine by a hydroxyl group has been suggested as an initiating step for reaction of the amine.[21,24]

$$(CH_3)_2NH + OH \rightarrow (CH_3)_2N + HOH \quad (2a)$$

$$\rightarrow CH_2NHCH_3 + HOH \quad (2b)$$

Atkinson et al.[25] have measured the rate constants for the reaction of OH with dimethylamine and trimethylamine to be 9.67×10^4 $ppm^{-1}min^{-1}$ and 9.00×10^4 $ppm^{-1}min^{-1}$. If we make the naive assumption that the rate constant can be separated into a value for each bond (analogous to Greiner's work with alkanes),[26] then the results of Atkinson et al. lead to $k_{C-H} = 1.00 \times 10^4$ $ppm^{-1}min^{-1}$, and $k_{N-H} = 3.67 \times 10^4$ $ppm^{-1}min^{-1}$. From this we can estimate the rate constants of $k_{2a} = 3.67 \times 10^4$ $ppm^{-1}min^{-1}$ and $k_{2b} = 6.00 \times 10^4$ $ppm^{-1}min^{-1}$, or a relative rate of $k_{2b}/k_{2a} = 1.63$.

Once the radical $(CH_3)_2N$ has been formed, it is expected to react in the atmosphere according to the following scheme:

$$(CH_3)_2N + O_2 \rightarrow (CH_3)_2N\text{-}O_2 \text{ and other products} \quad (3)$$

$$(CH_3)_2N + NO \quad (CH_3)_2N\text{-}NO \quad (4)$$

$$(CH_3)_2N + NO_2 \rightarrow (CH_3)_2N\text{-}NO_2 \text{ and other products} \quad (5)$$

$$(CH_3)_2N\text{-}NO + h\nu \rightarrow (CH_3)_2N + NO \quad (1)$$

At first glance, it might seem that the only reaction of any importance in the O_2-rich atmosphere would be reaction 3; oxygen is present at concentrations approximately 10^6 times greater than NO or NO_2 in urban air, and most organic radicals react very quickly with oxygen. However, Lesclaux[27,28] has shown that the radical NH_2 is very much less reactive towards O_2 than it is toward NO.

$$NH_2 + O_2 \rightarrow \text{products} \quad (6)$$

$$NH_2 + NO \rightarrow \text{products} \quad (7)$$

His flash photolysis studies show that $k_6 < 5 \times 10^{-3}$ $ppm^{-1}min^{-1}$ [Ref. 27], while $k_7 = 3 \times 10^4$ $ppm^{-1}min^{-1}$ [Ref. 28]. If the dimethylamine radical is analogous to the NH_2 species, it is conceivable that its reactions with pollutant molecules could dominate the system, and may contribute heavily to the nitrosamine concentrations observed in urban atmospheres.

This hypothesis was tested in this work through the quantitative study of the reactions 1, 3, 4, and 5 using FT IR spectroscopy. Relative rates for the reaction of the amine radical with NO, NO_2, and O_2 were determined. The data presented here may be used to derive the first quantitative estimates of the importance of the nitrosamines and nitramines formed through these homogeneous reactions in the atmosphere.

Experimental Study of the Dimethylamino Radical

In this study, reactions of amines of probable importance in the atmosphere were investigated. To understand these reactions, it is advisable to study gaseous systems which contain reactants at concentrations approximating those found in ambient air and which can be irradiated at light levels similar to sunlight.

Although many techniques have been proposed for monitoring low levels of gaseous pollutants, infrared absorption remains among the most specific, sensitive and accurate methods for the detection of many molecules. The ability to detect a given molecular species increases with path length and with spectral resolution.

The time required to collect an infrared spectrum typically increases as the spectral resolution or the spectral interval surveyed is increased. The slow response typical of grating and prism infrared systems has been largely overcome by Fourier transform spectroscopy (IRFTS), which can collect spectral information over wide spectral regions in relatively short times.

The instrumentation available for the present study includes a glass-walled multiple pass cell with a maximum path length of more than 500 m. The cell is surrounded by fluorescent bulbs which result in an irradiance inside the cell similar in spectral distribution and magnitude to ground level solar radiation between 300 and 400 nm.

The infrared spectra were taken using a Michelson interferometer (Digilab Model FTS 20). The time required to collect a single scan interferogram from 0 to 3950 cm^{-1} at 1 cm^{-1} resolution and to store the information on magnetic tape is 28 seconds. This rapid collection speed allows chemical reactions to be monitored rapidly so that rate constants can be determined.

The FTS Photolysis System

Photolysis Cell --

The main body of the cell consists of four 1.5 m lengths of Corning low-expansion borosilicate glass separated by stainless steel spacers with Teflon gaskets. Stainless steel endplates are also used. One endplate contains KBr windows to allow infrared radiation to enter and leave the cell; the other has an outlet to a vacuum pump and mechanical feed throughs to adjust the mirrors. Each endplate and spacer has been provided with a gas

inlet port to help ensure a uniform distribution of gases throughout the cell.

The entire length of the cell can be irradiated by four banks of fluorescent lights surrounding the cell. The lamps installed in the system are GE FT2T12/BL/HO and F40BL black lights. The emission spectrum of one of these lamps after passing through the cell wall was measured with a Turner spectrophotometer operated in the luminescence and energy mode. The spectrum obtained is shown in Figure 55, together with the estimated relative spectral distribution of solar radiation for a solar angle of 45° [Ref. 29].

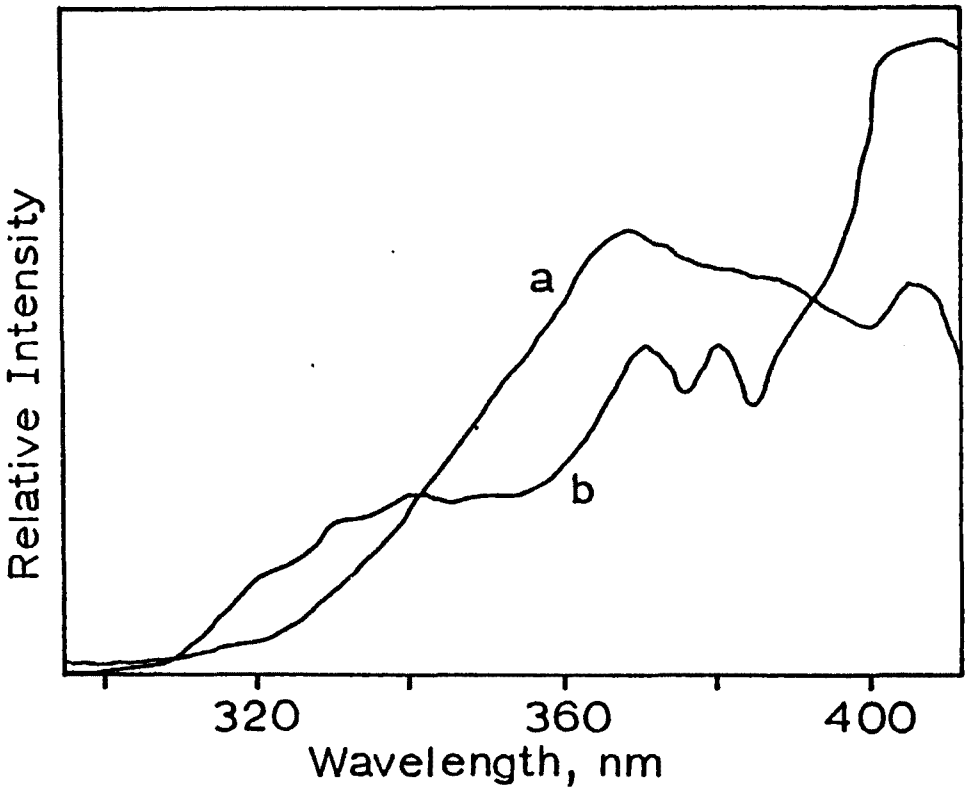

Figure 55. Comparison of irradiance inside photolysis cell with solar irradiance.
(a) spectral distribution of fluorescent lamp output after passing through glass walls of cell (unpublished data of Eugene Beer);
(b) relative spectral distribution of solar energy at ground level.

The fluorescent lamp assembly is surrounded by an aluminum foil reflector to increase the intensity and improve the uniformity of the light within the cell.

Gas Introduction System --

Figure 56 shows the gas handling system used to inject known amounts of gases into the photolysis cell. This grease-free, mercury-free system was constructed entirely of glass with Teflon stopcocks. Connections are made with stainless steel Cajon unions using Viton O-rings. Pressures are read on one of two Wallace and Tiernan absolute pressure guages (0-20 and 0-800 Torr) which are separated from the system by a quartz spiral manometer used as a null meter.

This gas handling system was designed to minimize dead volumes and to permit positive injections of samples with a carrier gas; positive injection capability is essential for forming multicomponent mixtures in the photolysis cell.

The seven volumes built into the vacuum system (2.7 to 92.4 cm^3) allow convenient injection of samples from less than 0.01 to over 200 ppm. Larger concentrations can be injected by attaching larger bulbs to the system at the direct inlet port. Weighed amounts of solids or liquids with reasonable vapor pressure can also be injected through this port.

A manifold of stainless steel tubing (0.25 in. o.d.) connects the gas handling system to the photolysis cell. Five inlet ports (one in each spacer and endplate) help to ensure a uniform distribution of gases throughout the cell.

Optical Arrangement Within the Photolysis Cell --

A standard White cell is shown in Figure 57, and consists of three spherical mirrors of equal focal length. The light from the source is focused into a real image at the entrance aperture of the cell, and above the horizontal centerline of the field mirror M_f (see Figure 58). It then diverges and is collected on mirror D_1. Since D_1 is located two focal lengths from the image, the inverted image from D_1 is focused on M_f. D_1 is adjusted so the image (marked 2) falls below the horizontal centerline of M_f. The reflected diverging beam falls entirely on D_2, and D_2 is adjusted so the real image formed (marked 4) is beside the aperture image. If this image is placed in the exit aperture, the total number of traversals is the minimum of four. If it is placed symmetrically opposite the first image (marked 2), there will be at least four more passes through the system.

The optical system used in this study was a modified White cell, and has been described by Hanst.[30] As shown in Figure 59, the single field mirror M_f in Figure 3 has been replaced by four rectangular spherical mirrors M_a, M_b, M_c, and M_d, and the pair of mirrors D_1 and D_2 have been replaced by

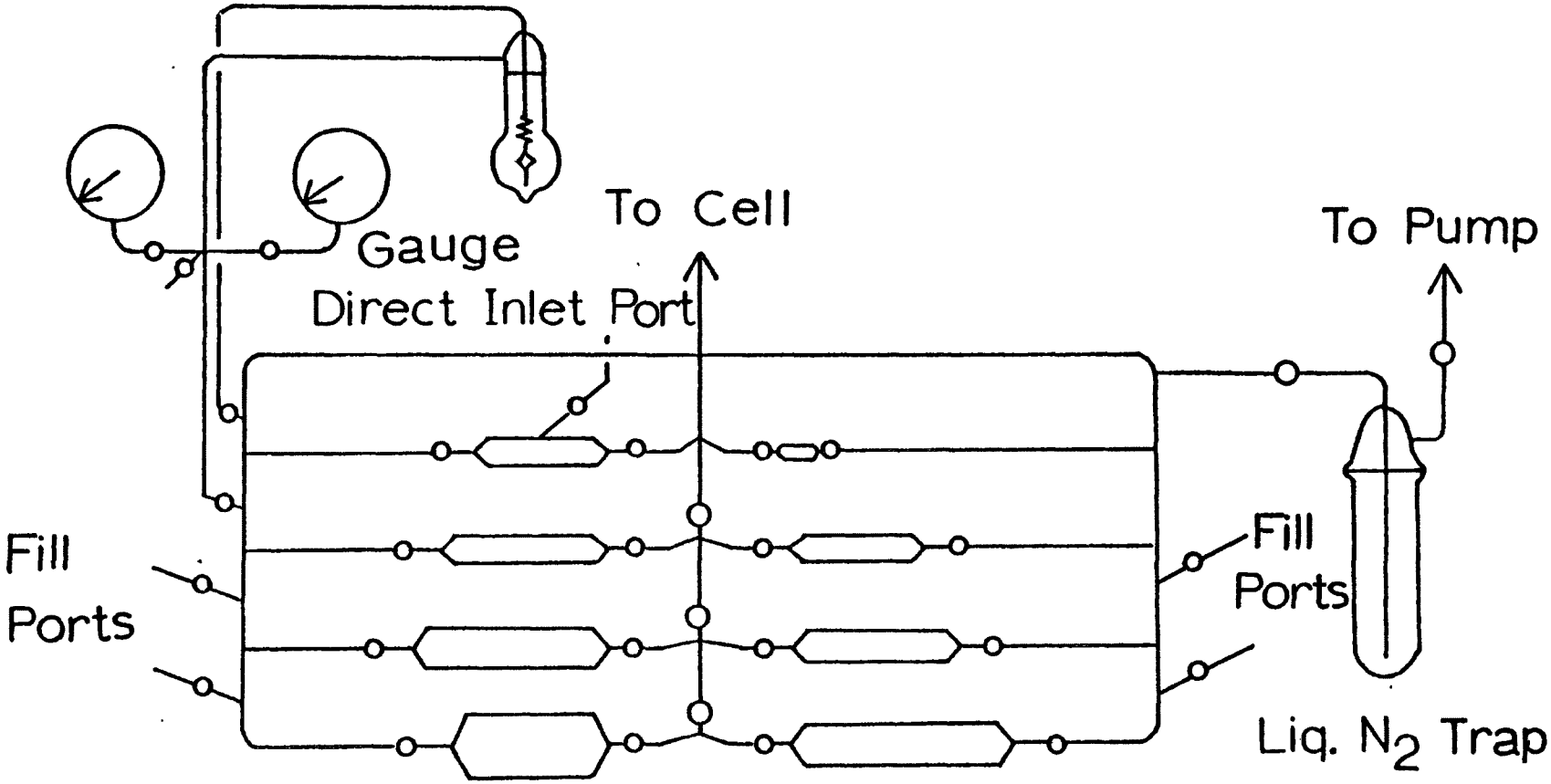

Figure 56. Gas handling system for introducing known amounts of chemicals into the photolysis cell.

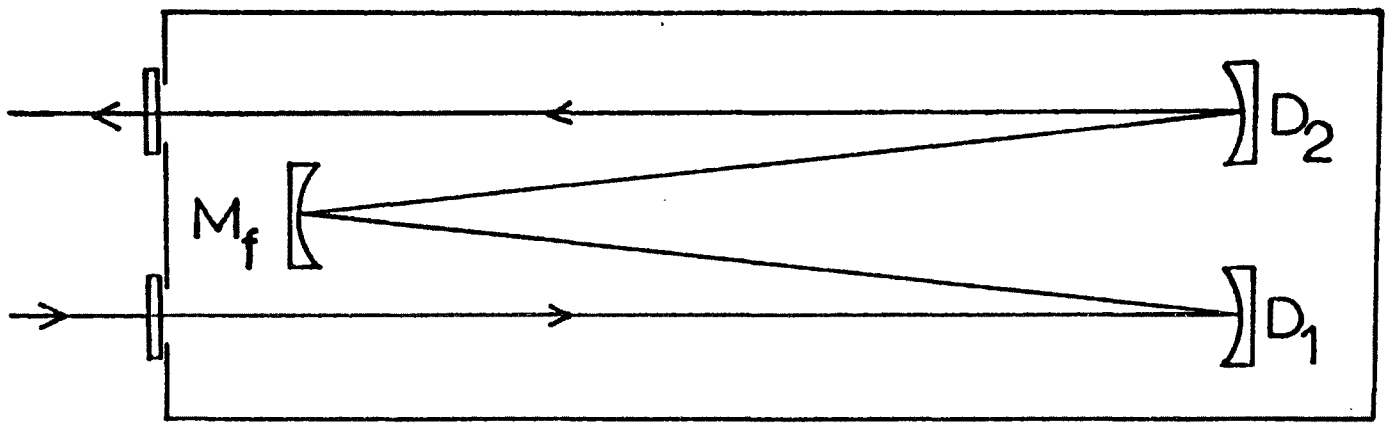

Figure 57. Optical paths in a standard White cell (4n pass).

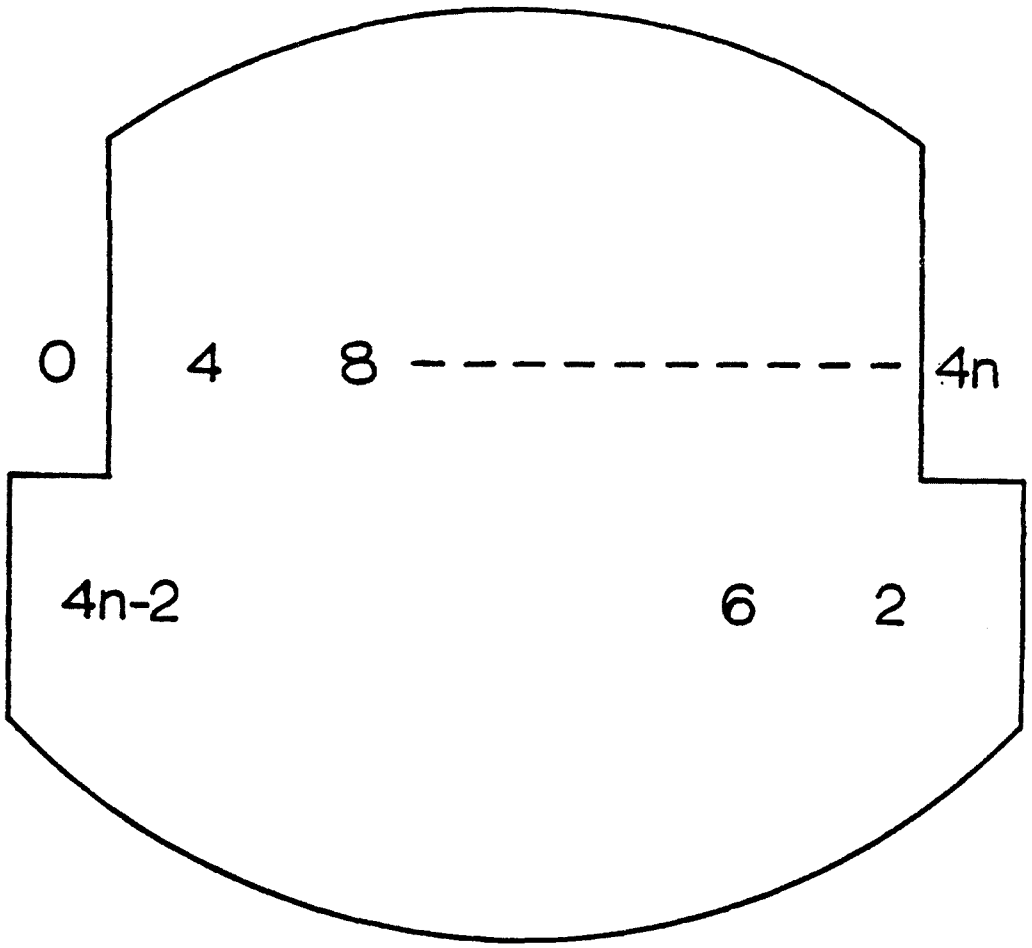

Figure 58. Placement of images on M_f in a standard White cell. The numbers refer to consecutive reflections by the mirrors.

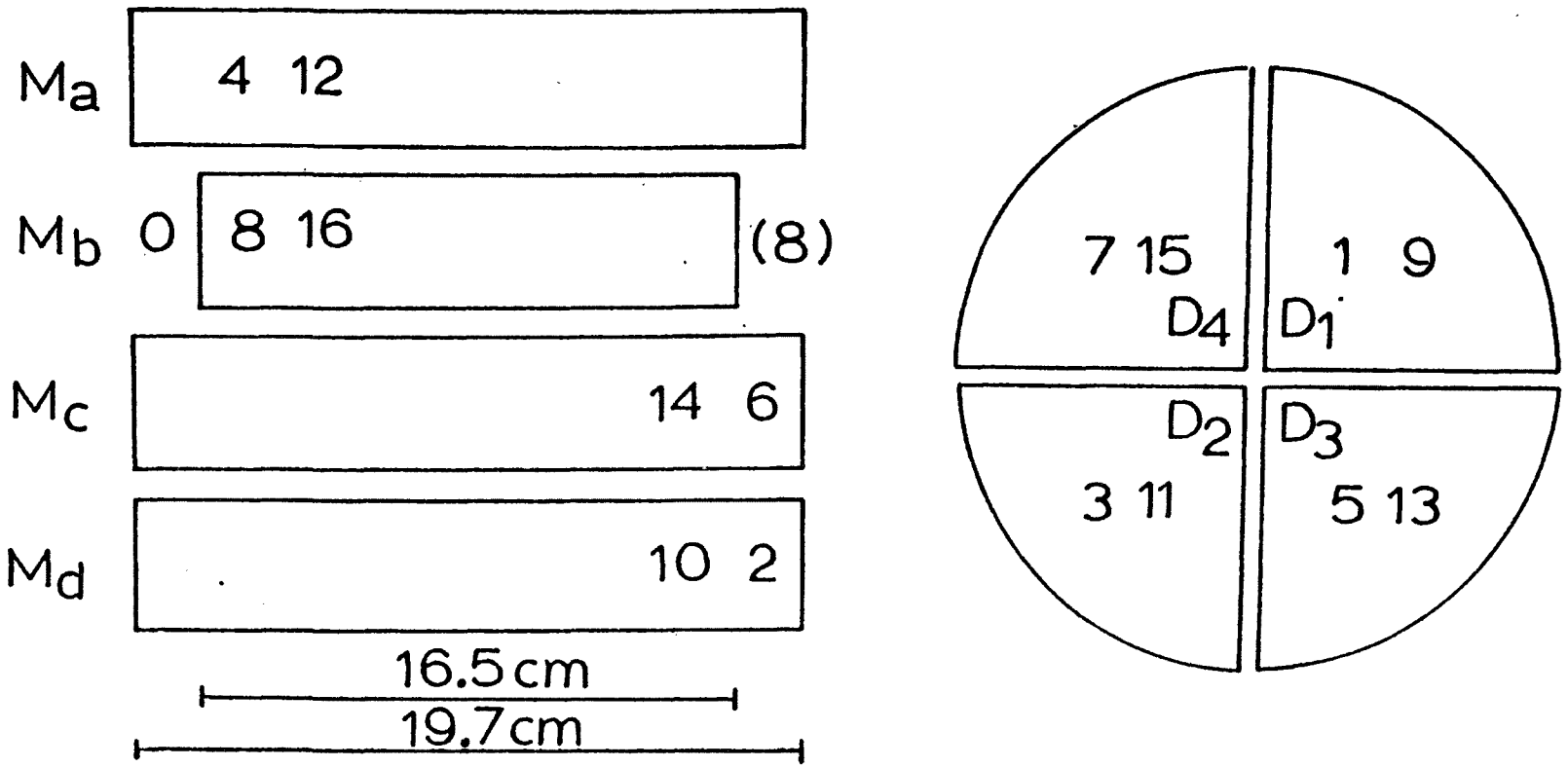

Figure 59. Mirror system for the modified White cell. The numbers refer to consecutive reflections by the mirrors. The number of traversals is altered by turning D_4.

four quadrant shaped spherical mirrors D_1, D_2, D_3, and D_4. In an aligned system, an image of the source is formed in the plane of the mirrors near M_b (marked O). Rows of images are formed on M_a, M_b, M_c, and M_d after reflections by the mirrors D_1, D_2, D_3, and D_4. The beam leaves on the opposite side of M_b.

The number of traversals used throughout this work was 32. The distance between the mirrors is 5.31 m, giving a total path length of 170 m.

Transfer Optics --

A schematic of the optical arrangements used in this work is given in Figure 60. The entire optical system outside the cell is mounted on an aluminum slab and enclosed in a transparent plastic box sealed to be essentially airtight. The box is purged with dry nitrogen gas during operation, and residual water and carbon dioxide in the gas are removed by placing traps of sodium hydroxide and activated alumina on the floor of the box.

Radiation from a Nernst glower (N) is reflected by the spherical mirror M_1 (f_1 = 15 cm) to an off-axis paraboloid mirror M_2 (f_2 = 27 cm) which results in parallel radiation to the interferometer. Within the interferometer, the collimated beam is amplitude-divided at a beam splitter (BS) consisting of germanium on a KBr substrate. Half of the radiation is reflected to the movable mirror M_4 and half is transmitted to a stationary mirror M_5 (Figure 61). These two beams recombine at the beam splitter and exit the interferometer. The resultant beam is reflected by two plane mirrors (M_6 and M_8 in Figure 60) and two spherical mirrors (M_7, f_7 = 60 cm; M_9, f_9 = 45 cm) before entering the absorption cell. Optics are adjusted so an image of the Nernst is formed at N_3 in the plane of the field mirrors and an image of the beam splitter is formed on the top left quadrant at the far end of the cell. Intermediate images of the Nernst are also found at positions N_1 and N_2.

Results and Discussion

Dimethylnitrosamine (DMN) has been found to be one of the most carcinogenic chemicals in experimental animals.[3,6,7] In view of this, the detection of DMN in industrial atmospheres[2,8,11] has generated considerable interest in the atmospheric sources and sinks of this and other similar compounds.

Formation of Dimethylnitrosamine by the Photooxidation of Dimethylamine in Simulated Atmospheres --

Through the formation of nitrosamines from amines in the condensed phase has been studied extensively,[31] few investigations of their formation from amines in the atmosphere have been made. Our original intention in

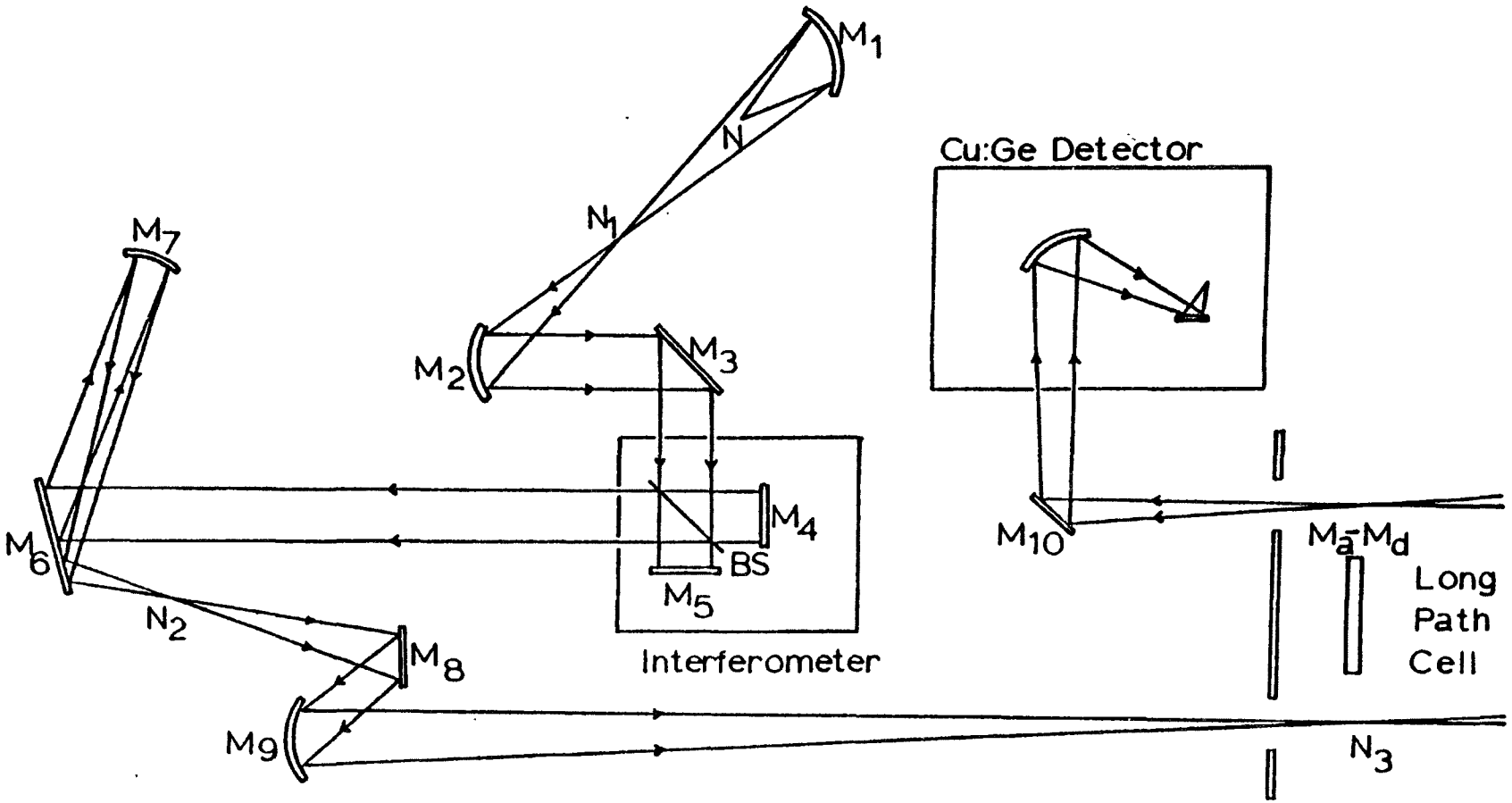

Figure 60. Optical transfer system from interferometer to photochemical cell.

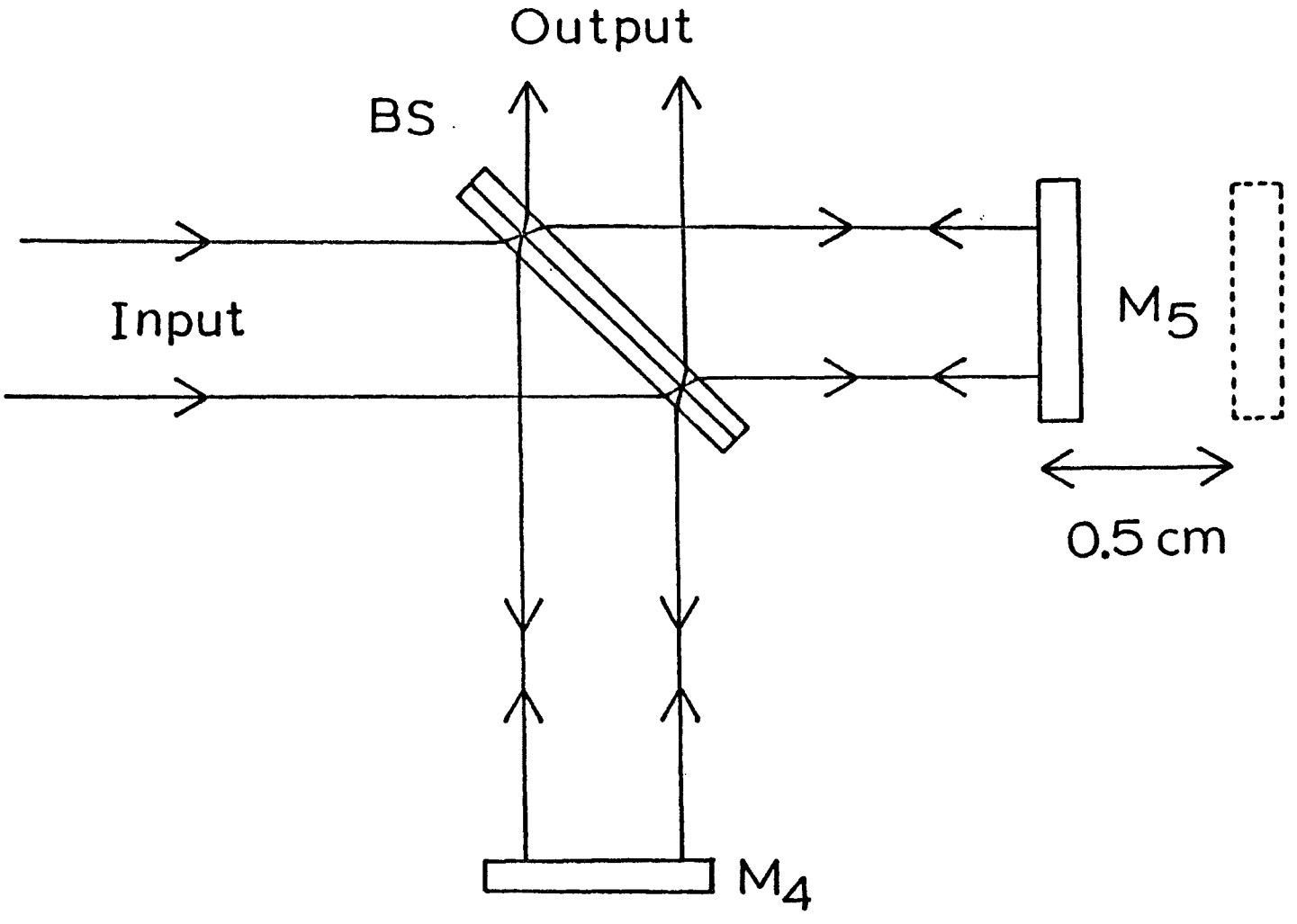

Figure 61. Optical diagram of interferometer

this work was to characterize the products and kinetics of the photo-oxidation of dimethylamine (DMA) in simulated atmospheres, with particular attention being paid to the question of nitrosamine formation.

Results from experiments designed to investigate the reaction of DMA with nitrous acid, concentration-time profiles were derived from the data; a typical one is shown in Figure 62.

Formation of Dimethylnitrosamine in the Dark --

Dimethylnitrosamine was produced by the reaction of DMA with HONO in the dark. A yield of DMN from DMA of about 5% was found in each case before photolysis was initiated, though a considerably lower yield (< 2%) was found in the dark period directly following the photolysis. These values are greater than those reported by some workers[20,21] and less than that obtained by others,[19] supporting the idea that the reaction is heterogeneous.[20]

Initially, DMN was produced quite rapidly, with a concurrent rapid loss of HONO and DMA. The rate of DMN formation decreased to a fairly steady value within five minutes. This is similar to behavior noted by Pitts et al.[21] However, in our system considerable nitrous acid and amine were left, indicating that the reaction was limited by wall reactions rather than by the availability of nitrous acid.

Nitrosamine Formation During Photolysis --

The rate of nitrosamine formation in both experiments increases dramatically when photolysis is initiated, and slows as photolysis is continued. In the first experiment, an initial rate of DMN formation of 0.26 ppm/min decreases to 0.04 ppm/min after 10 minutes. In the experiment with 10 ppm NO added, the initial rate of 0.18 ppm/min decreases to about 0.08 ppm/min after 10 minutes.

The sequence of reactions leading to the formation of DMN presumably begins with the photolysis of nitrous acid to produce OH radicals, which then attack the amine.

$$HONO + h\nu \rightarrow OH + NO \qquad (22)$$

$$OH + (CH_3)_2NH \rightarrow (CH_3)_2N + H_2O \qquad (2a)$$

$$\rightarrow CH_3NHCH_2 + H_2O \qquad (2b)$$

The radical $(CH_3)_2N$ formed in reaction 2a can, among other possibilities, react with NO to form DMN.

$$(CH_3)_2N + NO \rightarrow (CH_3)_2N\text{-}NO \qquad (4)$$

In the experiment where 10 ppm NO was added, the reaction of the dimethylamino radical with NO will be enhanced. In this experiment, a maximum yield of DMN from DMA of 31% was found during the first few minutes of photolysis. This indicates that at least 31% of the amine reacts with OH

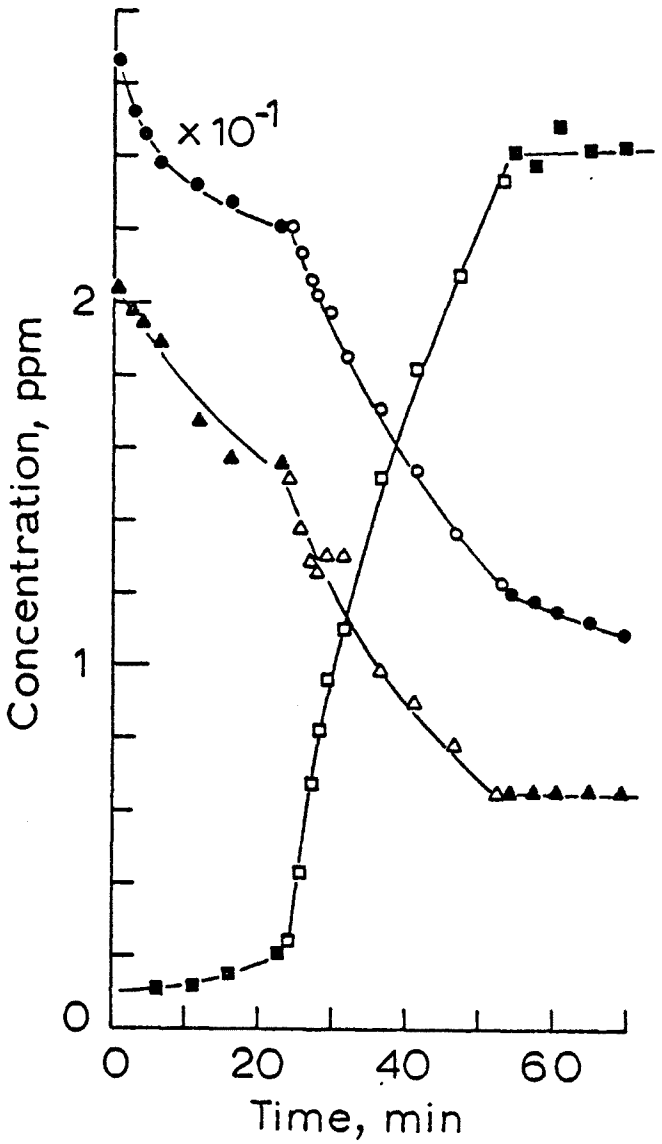

Figure 62. Concentration/time profile for the reaction of dimethylamine with nitrous acid. Open symbols indicate data collected during the photolysis. Circles, dimethylamine; triangles, nitrous acid; squares, dimethylnitrosamine.

to form the dimethylamino radical, or $k_{2a}/k_{2b} \cong 0.45$. This is in good agreement with our estimation of 0.61 from the data of Atkinson et al.,[25] and supports the contention of Pitts et al.[21] that H-abstraction from the N-H bond is competitive with H-abstraction from the C-H bonds in secondary alkyl amines.

The reduction in the rate of formation of nitrosamine can be explained by a combination of factors. These include lower concentrations of the reactants HONO and DMA, and removal of DMN from the system, either by photolysis or reaction with other species in the system. The observed reduction in the yield of DMN from DMA can best be explained by the removal of DMN.

At this point in the study we became aware that the group directed by Dr. J.N. Pitts in Riverside, California, had initiated an IRFTS study of the irradiation of amine-NO_x systems essentially identical to the one we had begun.[22] Rather than duplicate their efforts, the emphasis of our study was changed from a general consideration of amine reactions in NO_x -polluted atmospheres to concentration on the reactions of the dimethylamino radical in these atmospheres.

Determination of the Photolysis Rate of Dimethylnitrosamine--

The ultraviolet absorption spectrum of dimethylnitrosamine and the measured spectral irradiance inside of the photolysis cell (Figure 55) overlap in the region from 300 to 420 nm. The dissociation energy of the N-N bond in DMN has been given by various authors as 32 kcal/mole,[32] 43 kcal/mole,[33] and 55.2 kcal/mol.[34] Taking the largest (and most recent) of these values, we can expect possible dissociation of the nitrosamine at wavelengths below 518 nm. Thus our photolysis cell is suited to this study.

Photolysis of Dimethylnitrosamine in Nitrogen--

Dimethylnitrosamine is expected to photolyze according to reaction 1:

$$(CH_3)_2N\text{-}NO + h\nu \rightarrow (CH_3)_2N + NO \qquad (1)$$

Data from the photolysis of DMN in nitrogen were determined in a series of runs and shown as circles in Figure 63. As can be seen from a plot of the logarithm of the nitrosamine concentration as a function of time, (circles in Figure 64, a first-order loss of nitrosamine is not observed. Presumably this is because of the recombination of the amine radical with nitric oxide.

$$(CH_3)_2N + NO \rightarrow (CH_3)_2N\text{-}NO \qquad (4)$$

Photolysis of Dimethylnitrosamine with Nitric Oxide in Nitrogen--

To test this contention, a sample of nitrosamine was photolyzed in the presence of 5 ppm nitric oxide. This should enhance reaction 4, suppressing the radical concentration and lowering the rate of nitrosamine decay. The expected behavior is observed, and the rates of nitrosamine photolysis with and without nitric oxide are compared in Figure 63.

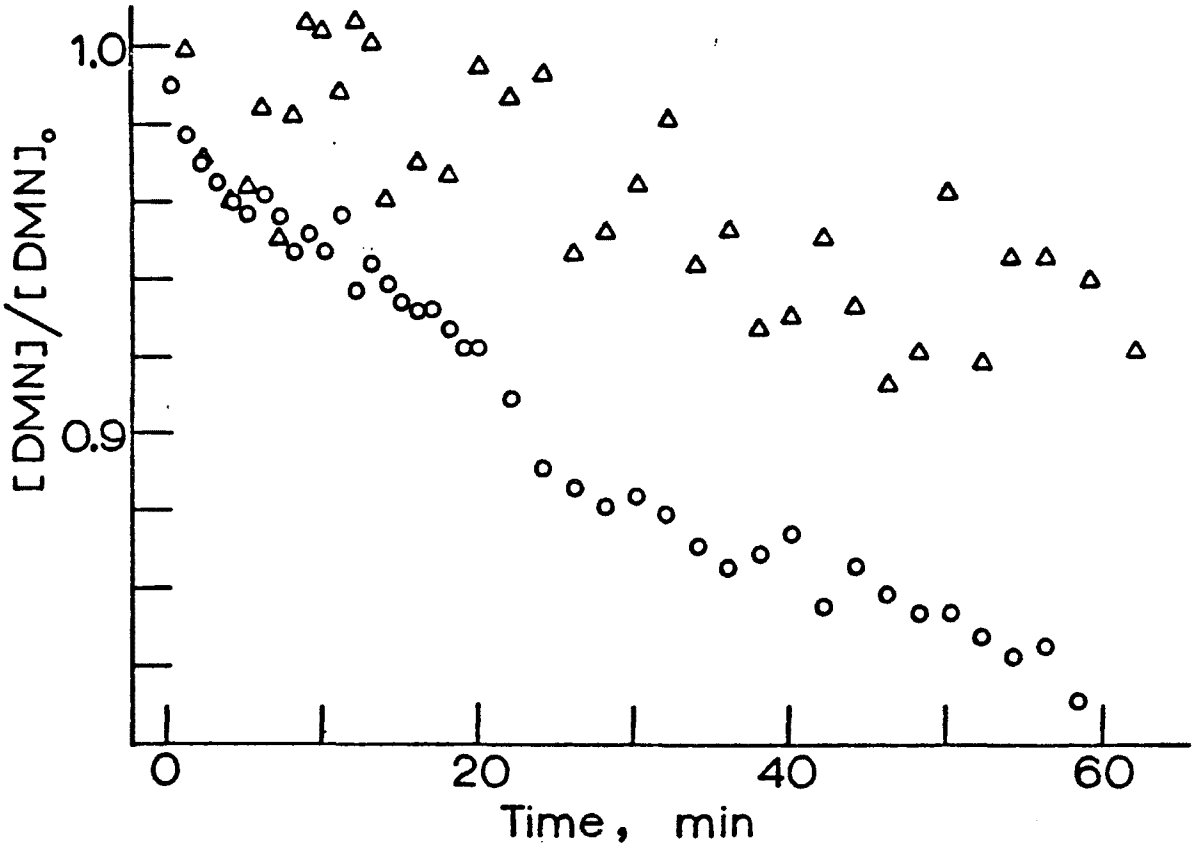

Figure 63. Plot of the disappearance of dimethylnitrosamine as a function of photolysis time. Circles, [DMN] = 3.96 ppm, [NO] = 0; triangles, [DMN] = 3.16 ppm, [NO] = 5.0 ppm.

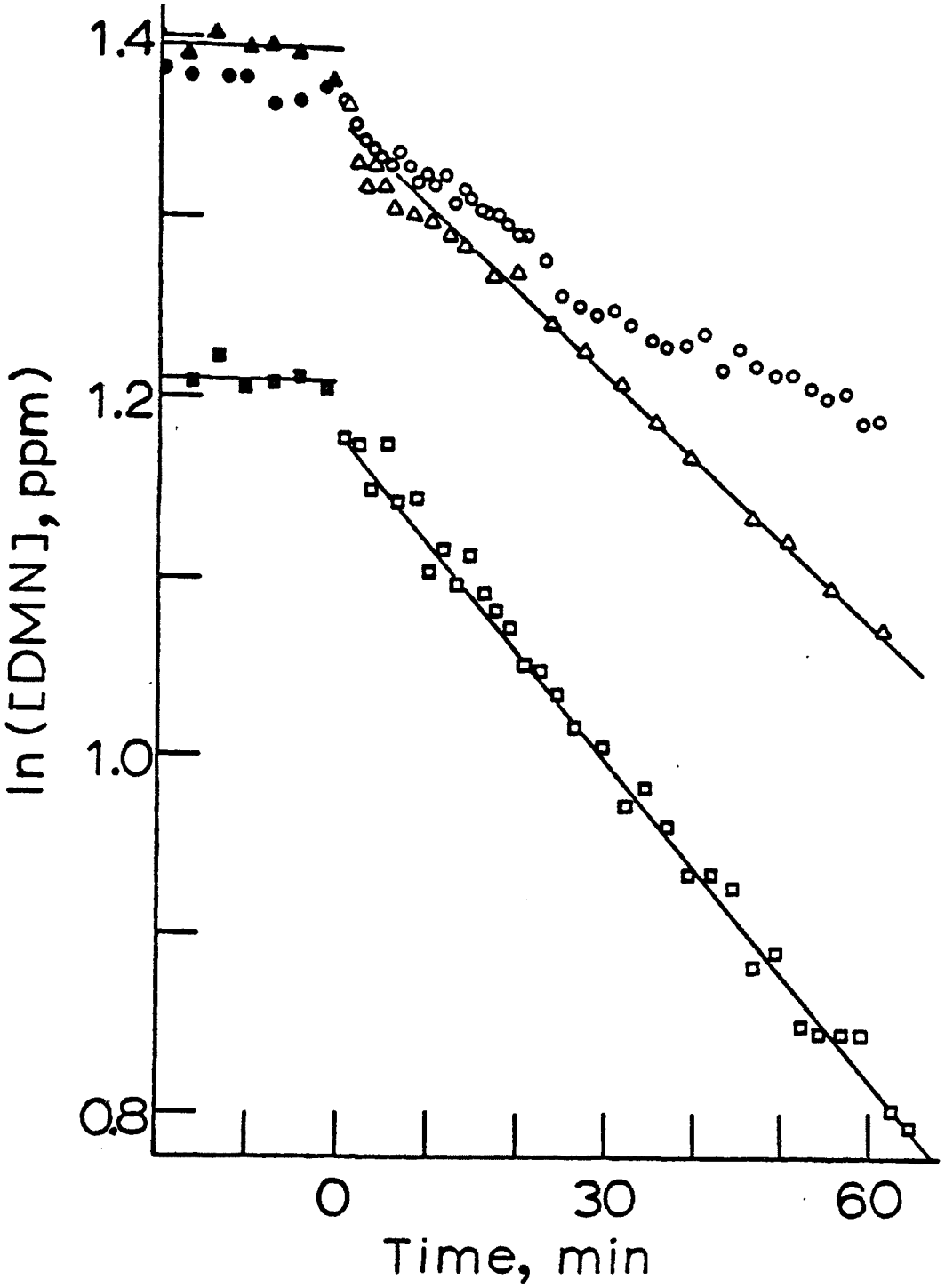

Figure 64. Plot of the logarithm of dimethylnitrosamine concentration as a function of time. Closed symbols indicate data taken before photolysis was begun. Circles, nitrosamine in nitrogen; triangles, nitrosamine with 50 ppm isobutane, slope = -0.0046 min^{-1}; squares, nitrosamine with 6.4 ppm trimethylsilane, slope = -0.0061 min^{-1}.

In addition, a plot of 1/[DMN] as a function of time gives a straight line (Figure 65). This is consistent with a rapid equilibrium followed by bimolecular decay of the radical.

$$(CH_3)_2N\text{-}NO \underset{}{\overset{h\nu}{\rightleftharpoons}} (CH_3)_2N + NO \qquad \text{(fast)}$$

$$2(CH_3)_2N \longrightarrow \text{products} \qquad \text{(slow)} \qquad (23)$$

In this event the radical concentration at any time is given by the equilibrium expression.

$$[(CH_3)_2N] = \frac{k_1[DMN]}{k_4[NO]} \qquad (24)$$

In the case where 5 ppm of nitric oxide is present initially, its concentration will remain fairly constant during the photolysis. The radical concentration will then be proportional only to the concentration of the nitrosamine, and the behavior of the radical will be reflected by the behavior of the nitrosamine.

Photolysis of Dimethylnitrosamine with Trimethylsilane and Isobutane in Nitrogen --

One way to measure the photolysis rate of DMN is to add another species that will react with the dimethylamino radical much faster than it reacts with NO. Two candidates for this added species are trimethylsilane (TMS) and isobutane (IBU), either of which may react to donate a hydrogen atom.

$$(CH_3)_2N + (CH_3)_3CH \rightarrow (CH_3)_2NH + (CH_3)_3C \qquad (25)$$

$$(CH_3)_2N + (CH_3)_3SiH \rightarrow (CH_3)_2NH + (CH_3)_3Si \qquad (26)$$

Data from these two experiments were used to estimate the concentration-time profiles, and the logarithm of nitrosamine concentration as a function of time is plotted in Figure 64. The slopes of the linear portions of the two graphs give rate constants of 0.0061 min^{-1} and 0.0046 min^{-1} for the experiments with TMS and IBU, respectively. These low values, together with the fact that the concentrations of nitrosamine at the onset of photolysis predicted by these lines are considerably lower than the actual concentration measured before photolysis, indicate that an appreciable fraction of the radicals are still reacting with NO to reform the nitrosamine. The use of larger concentrations of either TMS or IBU was not practical because of their strong infrared absorbances.

Estimation of Photolysis Rate Constant from Initial Slope Data --

An estimate of the photolysis rate constant k_1 can be obtained by considering only the initial data and extrapolating back to the onset of photolysis when the concentration(s) of radical and/or nitric oxide are zero. This technique is illustrated in Figure 66 for the photolysis of DMN in nitrogen, giving a value of $k_1 = 0.042\ min^{-1}$ in this case.

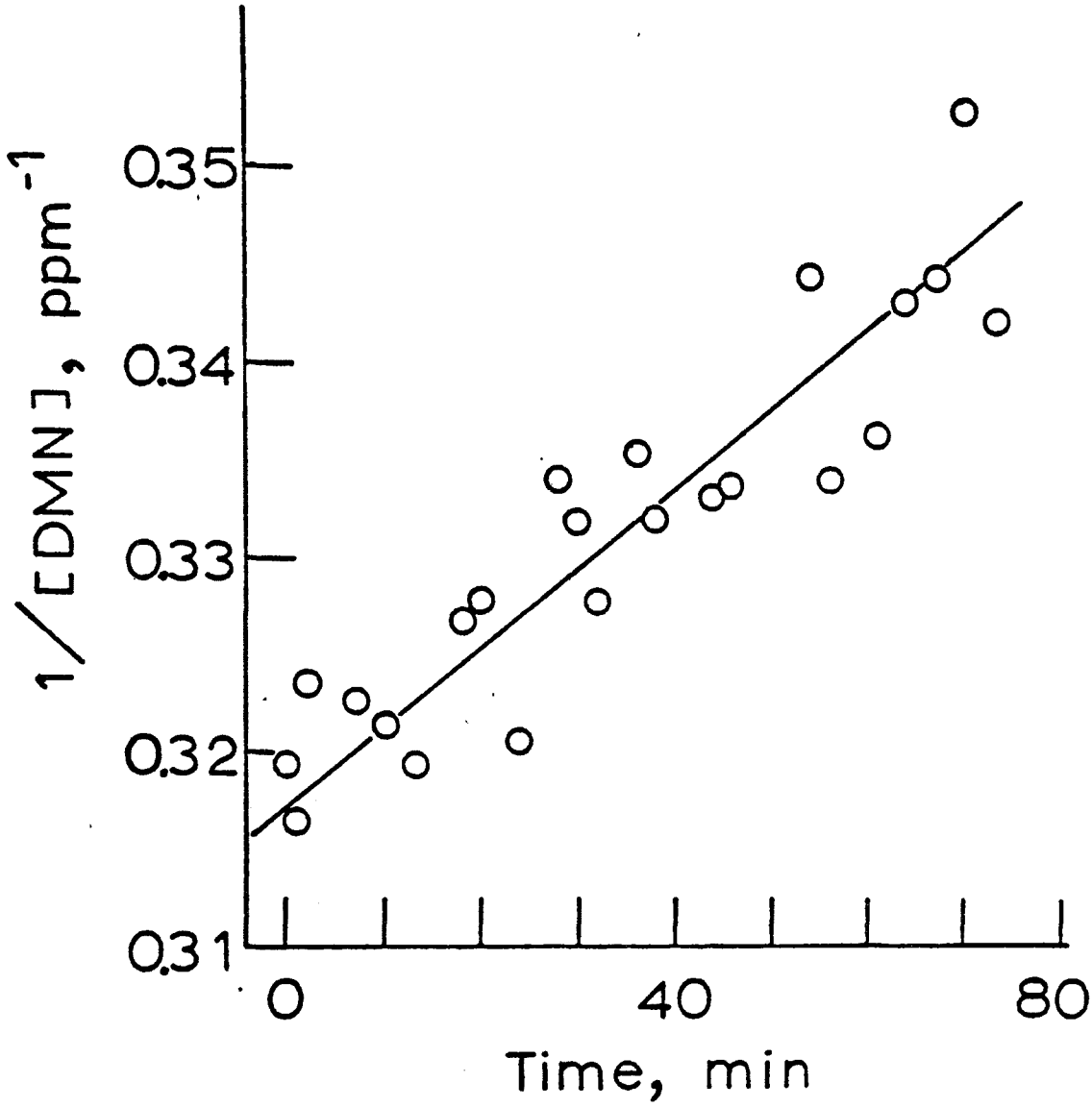

Figure 65. Plot of the reciprocal concentration of dimethylnitrosamine as a function of time for the photolysis of DMN with 5.0 ppm nitric oxide in nitrogen.

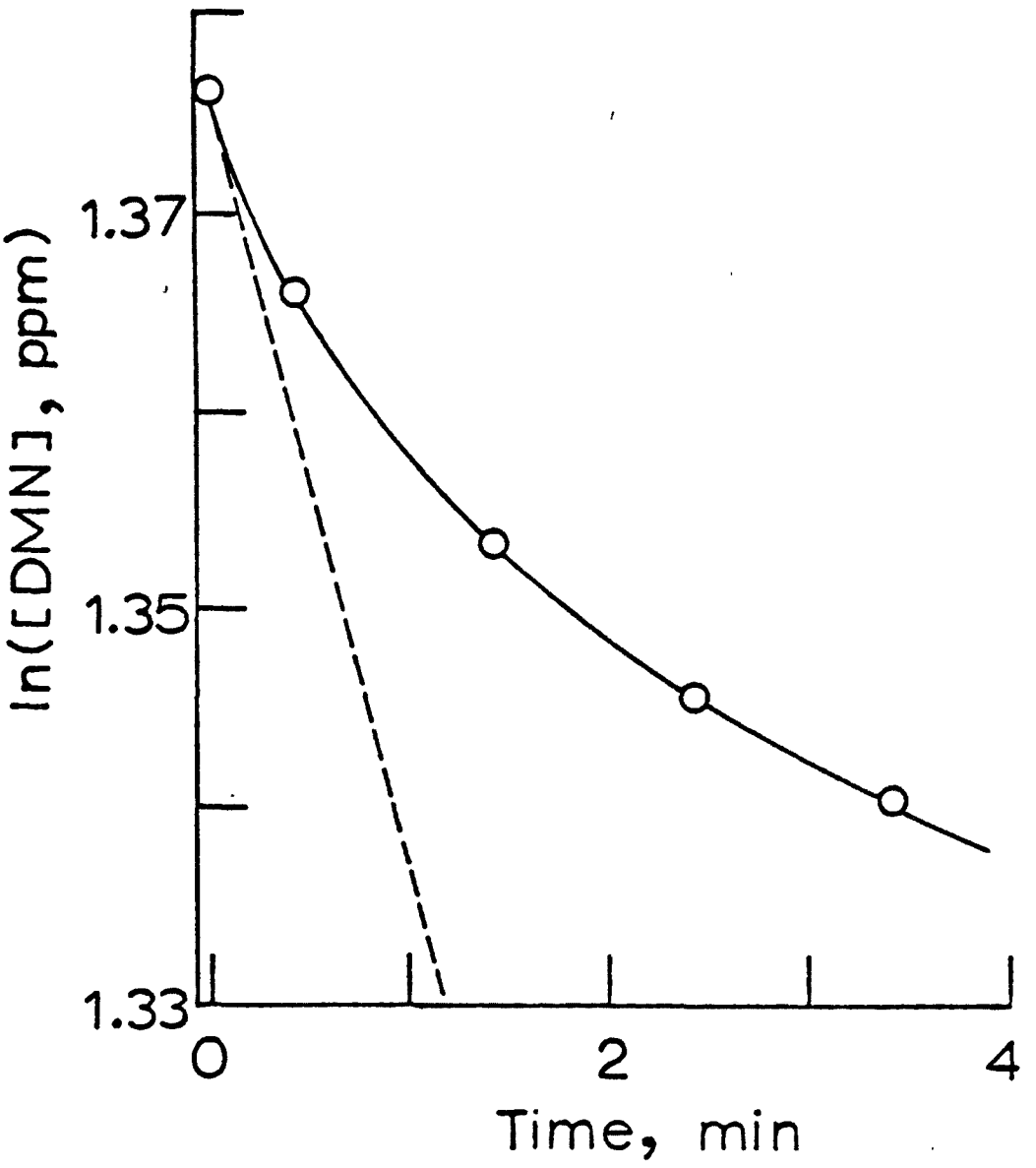

Figure 66. Initial data from the photolysis of DMN in nitrogen illustrating determination of initial slope (shown as dashed line).

Values obtained using this technique for the experiments indicated are listed in Table 34. The deviation from first-order behavior is considerable even at the shortest times measured here, and so the values given are subject to the prejudices of the person making the measurements. However, as the concentration of oxygen increases, the absolute value of the initial slope increases, indicating that the oxygen acts to remove the radical. Thus the larger values (i.e., 0.11 - 0.12 min^{-1}) should be closest to the true photolysis rate constant.

Theoretical Estimation of the Photolysis Rate from Ultraviolet Absorption and Quantum Yield Data --

The photochemical rate constant for a species X in the cell is proportional to the integral

$$F_x = \int_{\lambda_1}^{\lambda_2} \epsilon(\lambda)\ \Phi(\lambda)\ I^o(\lambda) \qquad (27)$$

where $\epsilon(\lambda)$ is the extinction coefficient at wavelength λ, $\Phi(\lambda)$ is the quantum yield for the decomposition, and $I^o(\lambda)$ is the relative light intensity. The ratio of two rate constants is therefore equal to the ratio of their integrals, or

$$k_x = (F_x/F_y)k_y \qquad (28)$$

Thus the rate constant for photolysis of DMN can be estimated from its ultraviolet absorption spectrum and the relative light intensity by comparison to a system whose photochemical decomposition is more easily measured.

One such system is the photolysis of NO_2 at low pressure. Absorption coefficients[35] and quantum yield data[36] are available in the literature, and the primary photolysis rate constant, k_{29}, is readily measured since, at low pressures of nitrogen, only reactions 29 and 30 are important.[31]

$$NO_2 + h\nu \rightarrow NO + O \qquad (29)$$

$$NO_2 + O \rightarrow NO + O_2 \qquad (30)$$

In this case, two molecules of NO_2 are destroyed for each molecule destroyed photochemically, and the primary photolysis rate constant k_{29} is given by the relationship $k_{29} = (1/2t)\ln(A_o/A)$, where A_o and A are the values of the absorbance due to NO_2 at time zero and time t, respectively.

Data from the photolyses of NO_2 at low pressures were determined and the Figure 67 consists of a plot of the logarithm of NO_2 absorbance as a function of time for each run. The slopes of these plots give values of k_{29} of 0.280 ± 0.004(2σ) min^{-1}, 0.253 ± 0.005(2σ) min^{-1}, and 0.260 ± 0.005 (2σ) min^{-1}, for an average value of k_{29} = 0.264 min^{-1}.

TABLE 34. VALUES OF THE RATE CONSTANT FOR THE PHOTOLYSIS OF DIMETHYLNITROSAMINE OBTAINED FROM THE INITIAL SLOPE OF THE LOGARITHM OF THE DIMETHYLNITROSAMINE CONCENTRATION AS A FUNCTION OF TIME

k, min^{-1}	Reactants	Expt #
0.042	4.0 ppm DMN	770917-1
0.081	4.0 ppm DMN, 50 ppm isobutane	770929
0.084	2.9 ppm DMN, 50 Torr O_2	770919
0.112	1.8 ppm DMN, 140 Torr O_2	770917-2
0.122	11.4 ppm DMN, 730 Torr O_2	770930-2
0.008	8.2 ppm DMN, 5.5 ppm NO, 69 Torr O_2	770930-1
0.014	5.9 ppm DMN, 5.2 ppm NO, 138 Torr O_2	771003-1
0.057	5.9 ppm DMN, 3.7 ppm NO, 1.2 ppm NO_2, 700 Torr O_2	771003-2
0.056	2.9 ppm DMN, 20 ppm NO, 4.8 ppm NO_2, 145 Torr O_2	770920-1

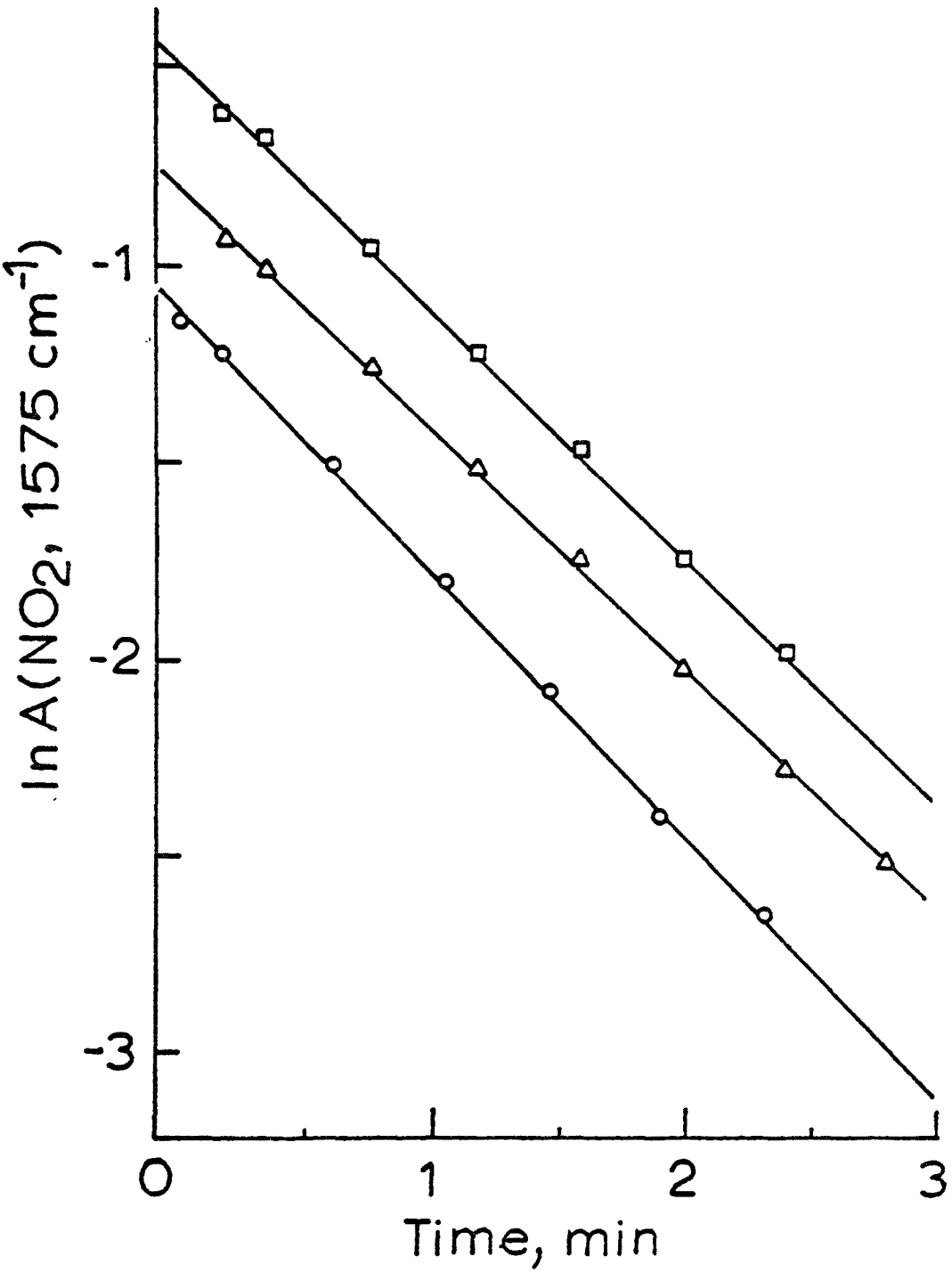

Figure 67. Plot of ln (absorbance) for three low-pressure photolyses of nitrogen dioxide. Circles, slope = -0.559 ± 0.008(2σ) min^{-1}; triangles, slope = -0.505 ± 0.010(2σ) min^{-1}; squares, slope = -0.519 ± 0.010(2σ) min^{-1}.

Table 35. shows the light intensity, extinction coefficient and quantum yield data used in the estimation of the photolysis rate of DMN in our photolysis cell. A quantum yield of unity is assumed for the nitrosamine, and the integral of Equation 29 is approximated by the sum at 1 nm increments. The following values were obtained:

F_{NO_2} = 51693 (arbitrary units)

F_{DMN} = 15183 (arbitrary units)

From equation 28, $k_1 = (15183/51693)(0.264\ min^{-1})$

$= 0.078\ min^{-1}$

This value is lower than that predicted by the method of initial rates. The most probable explanation is that the light intensity within the cell has decreased during the course of this work. The measurement of k_{29} = 0.264 min^{-1} was made about six months after the bulk of the nitrosamine photolyses were performed. Measurements of the same rate constant made in the same way some two years earlier gave values of k_{29} = 0.515 min^{-1}. An intermediate value of k_{29} = 0.40 min^{-1} gives k_1 = 0.12 min^{-1}, in line with the values predicted from the initial rate data.

Photolysis of Dimethylnitrosamine in the Presence of Oxygen--

The relative rates of the reactions of dialkylamino radicals with oxygen and oxides of nitrogen at the concentrations typical of polluted atmospheres are not now known, although some workers have assumed that the reaction with oxygen is small enough that it can be ignored.[21] If this is the case, then the photolysis of DMN in nitrogen/oxygen mixtures should be largely independent of the amount of oxygen present. By comparison of the work in the previous section (DMN photolyzed in nitrogen) with the results of Hanst et al.[19] in air, it can be seen that this is not the case. Thus if we are to understand the chemistry of dimethylnitrosamine in the atmosphere, it is imperative that a direct experimental estimate of the relative importance of the reactions of the radical $(CH_3)_2N$ with oxygen and the oxides of nitrogen be made.

Formation of Products: The Mechanism of Photooxidation--

The two main products formed during the initial stage of the photolysis of DMN in the presence of oxygen are dimethylnitramine[21,22] (DMNA) and a species having a sharp absorbance at 1025 cm^{-1}. This absorbance has been tentatively assigned to tetramethylhydrazine ($(CH_3)_2N\text{-}N(CH_3)_2$) by Tuazon et al.,[22] but our work shows it to be due to monomethylmethyleneamine (MMA). This assignment was verified by comparison with the spectrum of an authentic sample.

TABLE 35. EXTINCTION COEFFICIENTS, QUANTUM YIELDS AND VALUES OF THE LIGHT INTENSITY WITHIN THE CELL USED IN THE DETERMINATION OF THE PHOTOLYSIS RATE OF DIMETHYL-NITROSAMINE

		Nitrogen dioxide			Dimethylnitrosamine	
λ, nm	$I^{o}(\lambda)$,[a]	$\varepsilon(\lambda)$,[b] ℓ/mol-cm	$\phi(\lambda)$,[c]	$F(\lambda)$,[d]	$\varepsilon(\lambda)$,[e] ℓ/mol-cm	$F(\lambda)$,[d]
300	0.00	33.5	0.990	0.00	2.40	0.00
301	0.00	35.1	0.990	0.00	2.28	0.00
302	0.00	39.2	0.990	0.00	2.28	0.00
303	0.00	45.5	0.990	0.00	2.03	0.00
304	0.00	45.6	0.990	0.00	2.28	0.00
305	0.00	47.3	0.990	0.00	1.90	0.00
306	0.00	45.2	0.990	0.00	2.28	0.00
307	0.01	46.6	0.990	0.46	2.40	0.03
308	0.02	46.2	0.990	0.91	2.28	0.04
309	0.04	52.5	0.990	2.08	2.53	0.10
310	0.05	50.2	0.990	2.48	2.66	0.13
311	0.08	53.7	0.990	4.25	3.29	0.27
312	0.10	56.0	0.990	5.54	3.42	0.34
313	0.11	58.1	0.990	6.33	3.29	0.36
314	0.13	55.5	0.990	7.14	3.42	0.44
315	0.15	64.3	0.990	9.55	3.93	0.59
316	0.19	60.9	0.990	11.46	4.94	0.94
317	0.23	66.5	0.990	15.14	5.45	1.25
318	0.27	70.9	0.990	18.95	6.08	1.64
319	0.30	66.1	0.990	19.63	6.46	1.94
320	0.30	72.4	0.990	21.50	7.09	2.13
321	0.32	75.7	0.990	23.98	8.49	2.72
322	0.38	75.6	0.990	28.44	8.87	3.37
323	0.42	79.0	0.990	32.85	10.26	4.31
324	0.50	76.4	0.990	37.82	11.27	5.64
325	0.55	79.5	0.990	43.29	11.91	6.55
326	0.60	82.2	0.990	48.83	13.30	7.98
327	0.72	83.1	0.990	59.23	13.93	10.03
328	0.85	87.8	0.990	73.88	15.20	12.92
329	0.96	85.6	0.990	81.35	16.85	16.17
330	1.10	85.3	0.990	92.89	17.73	19.51
331	1.20	87.1	0.990	103.47	18.62	22.34
332	1.30	85.8	0.990	110.42	19.63	25.52
333	1.42	106.4	0.990	149.58	20.65	29.32
334	1.52	85.1	0.990	128.06	21.91	33.31
335	1.65	98.6	0.990	161.06	23.31	38.45
336	1.75	100.2	0.990	173.60	24.95	43.67
337	1.87	98.9	0.990	183.09	26.60	49.74
338	2.02	99.3	0.990	198.58	28.50	57.57
339	2.19	113.9	0.990	246.95	30.53	66.85
340	2.30	110.8	0.985	251.02	32.30	74.29
341	2.55	118.9	0.985	295.65	33.44	85.27

(Continued)

TABLE 35. (Continued)

λ, nm	$I^{o}(\lambda)$,[a]	Nitrogen dioxide $\varepsilon(\lambda)$,[b] ℓ/mol-cm	$\phi(\lambda)$,[c]	$F(\lambda)$,[d]	Dimethylnitrosamine $\varepsilon(\lambda)$,[e] ℓ/mol-cm	$F(\lambda)$,[d]
342	2.68	109.4	0.985	288.74	34.83	93.35
343	2.83	101.2	0.985	282.10	35.97	101.80
344	2.92	115.9	0.985	333.35	36.73	107.26
345	3.13	116.2	0.984	357.89	38.13	119.34
346	3.25	122.6	0.984	392.07	39.39	128.02
347	3.45	122.1	0.984	414.51	41.80	144.21
348	3.60	137.6	0.984	487.43	44.97	161.87
349	3.70	131.7	0.984	485.97	48.13	180.49
350	3.88	117.0	0.983	446.24	51.42	199.53
351	4.15	129.0	0.983	526.25	54.21	224.98
352	4.30	126.7	0.983	535.55	55.48	238.56
353	4.49	113.9	0.983	502.72	55.73	250.23
354	4.62	143.9	0.983	653.52	54.72	252.80
355	4.73	146.5	0.982	680.47	54.21	256.42
356	4.88	131.5	0.982	630.17	54.08	263.93
357	5.05	159.3	0.982	789.98	53.70	271.21
358	5.18	143.8	0.981	730.73	55.10	285.41
359	5.35	130.0	0.981	682.29	57.12	305.62
360	5.55	128.8	0.980	700.54	60.54	336.02
361	5.75	153.8	0.979	865.78	64.98	373.62
362	6.20	143.9	0.978	872.55	70.04	434.27
363	6.25	146.2	0.977	892.73	72.70	454.40
364	6.40	139.1	0.976	868.87	73.34	469.36
365	6.49	165.0	0.975	1044.08	71.31	462.81
366	6.60	154.1	0.974	990.62	68.40	451.42
367	6.65	148.0	0.973	957.63	64.22	427.05
368	6.69	152.5	0.972	991.66	60.42	404.20
369	6.70	147.9	0.971	962.19	57.50	385.28
370	6.72	154.7	0.970	1008.40	54.84	368.56
371	6.65	148.8	0.969	958.84	53.20	353.77
372	6.52	170.8	0.968	1077.98	53.07	346.03
373	6.46	157.1	0.967	981.38	54.08	349.39
374	6.42	153.0	0.966	948.86	57.25	367.56
375	6.36	152.8	0.965	937.79	60.42	384.26
376	6.30	178.0	0.964	1081.03	62.44	393.40
377	6.27	161.9	0.963	977.55	61.96	388.35
378	6.22	147.7	0.962	883.78	59.28	368.71
379	6.17	156.1	0.961	925.57	55.22	340.73
380	6.13	170.9	0.960	1005.71	51.55	316.01
381	6.12	161.6	0.958	947.45	46.61	285.26
382	6.09	160.9	0.956	936.77	43.57	265.35
383	6.08	153.4	0.954	889.77	39.39	239.51
384	6.06	170.3	0.952	982.48	35.72	216.45

(Continued)

TABLE 35. (Continued)

λ, nm	$I^{o}(\lambda)$,[a]	Nitrogen dioxide $\varepsilon(\lambda)$,[b] ℓ/mol-cm	$\phi(\lambda)$,[c]	$F(\lambda)$,[d]	Dimethylnitrosamine $\varepsilon(\lambda)$, ℓ/mol-cm	$F(\lambda)$,[d]
385	6.02	169.6	0.950	969.94	32.43	195.20
386	6.00	157.2	0.948	894.15	29.51	177.07
387	5.99	159.9	0.946	906.08	26.35	157.81
388	5.95	170.7	0.944	958.79	23.69	140.93
389	5.90	171.9	0.942	955.37	21.53	127.04
390	5.85	171.3	0.940	941.98	19.63	114.85
391	5.78	166.4	0.935	899.28	17.73	102.50
392	5.70	172.7	0.933	918.44	16.21	90.25
393	5.62	155.7	0.930	813.78	14.19	79.73
394	5.55	158.2	0.925	812.16	13.17	73.11
395	5.48	168.1	0.920	847.49	11.40	62.47
396	5.42	175.4	0.905	860.25	10.89	59.04
397	5.35	161.7	0.885	765.61	9.37	50.15
398	5.27	182.9	0.860	828.94	8.61	45.39
399	5.22	160.9	0.800	671.92	7.60	39.67
400	5.21	193.0	0.680	683.76	6.46	33.65
401	5.22	186.3	0.600	593.49	6.08	31.74
402	5.45	163.0	0.500	444.18	5.32	28.99
403	5.68	145.7	0.440	364.13	4.43	25.18
404	5.75	173.2	0.360	358.52	4.31	24.76
405	5.86	180.4	0.330	348.86	3.67	21.53
406	5.87	153.9	0.280	252.95	3.17	18.59
407	5.73	135.0	0.230	177.92	2.91	16.69
408	5.63	170.2	0.180	172.48	2.53	14.26
409	5.40	168.4	0.160	145.50	2.03	10.94
410	5.05	164.8	0.150	124.84	1.77	8.96
411	5.05	164.0	0.120	99.38	1.90	9.59
412	4.75	164.0	0.080	62.32	1.52	7.22
413	4.60	164.0	0.060	45.26	1.27	5.83
414	4.48	164.0	0.050	36.24	1.14	5.10
415	4.45	164.0	0.030	21.89	0.89	3.95
416	4.40	163.0	0.020	14.34	0.89	3.90
417	4.35	163.0	0.000	0.00	0.89	3.86

[a] Unpublished work of Eugene Beer; arbitrary units.

[b] A. M. Bass, A. E. Ledford, Jr., A. H. Laufer, J. Res. Nat. Bur. Stand., 80A, 143(1973).

[c] Values from J. G. Calvert's curve from the data of I. T. N. Jones and K. D. Bayes, J. Chem. Phys., 59, 4836(1973).

[d] Arbitrary units.

Concentration/time profiles of several experiments are shown in Figures 68 through 75. Figures 68 through 70 depict photolyses of pure DMN samples in synthetic nitrogen/oxygen mixtures of varied composition. Figures 70 through 74 illustrate a similar series of experiments where 5 ppm NO was added initially. General observations from these data include the following.

1. The loss of DMN is enhanced by both O_2 and NO_2, but inhibited by NO.
2. The formation of DMNA is enhanced by NO_2, but inhibited by NO (cf. Figures 69, 73 and 75).
3. The formation of MMA is enhanced by O_2, but inhibited by NO.
4. The formation of HONO is enhanced by both oxygen and NO_x.

The simplest mechanism which can account for the products found initially and the general trends noted above includes the following reactions of DMN and the dimethylamino radical.

$$(CH_3)_2N\text{-}NO + h\nu \rightarrow (CH_3)_2N + NO \tag{1}$$

$$(CH_3)_2N + O_2 \rightarrow CH_2{=}N\text{-}CH_3 + HO_2 \tag{3}$$

$$(CH_3)_2N + NO \rightarrow (CH_3)_2N\text{-}NO \tag{4}$$

$$(CH_3)_2N + NO_2 \rightarrow (CH_3)_2N\text{-}NO_2 \tag{5a}$$

If these are the only important reactions of DMN and the radical $(CH_3)_2N$, then the rates of change for species involved can be expressed as follows.

$$\frac{d[DMN]}{dt} = k_1[DMN]\left(\frac{k_4[NO]}{F_1}\right) - k_1[DMN]$$

$$= -k_1[DMN]\left(\frac{k_3[O_2] + k_{5a}[NO_2]}{F_1}\right) \tag{31a}$$

$$\frac{d[DMN]}{dt} + k_1[DMN] = k_1[DMN]\left(\frac{k_4[NO]}{F_1}\right) \tag{31b}$$

$$\frac{d[DMNA]}{dt} = k_1[DMN]\left(\frac{k_{5a}[NO_2]}{F_1}\right) \tag{32}$$

$$\frac{d[MMA]}{dt} = k_1[DMN]\left(\frac{k_3[O_2]}{F_1}\right) \tag{33}$$

where $F_1 = k_3[O_2] + k_4[NO] + k_{5a}[NO_2]$ (34)

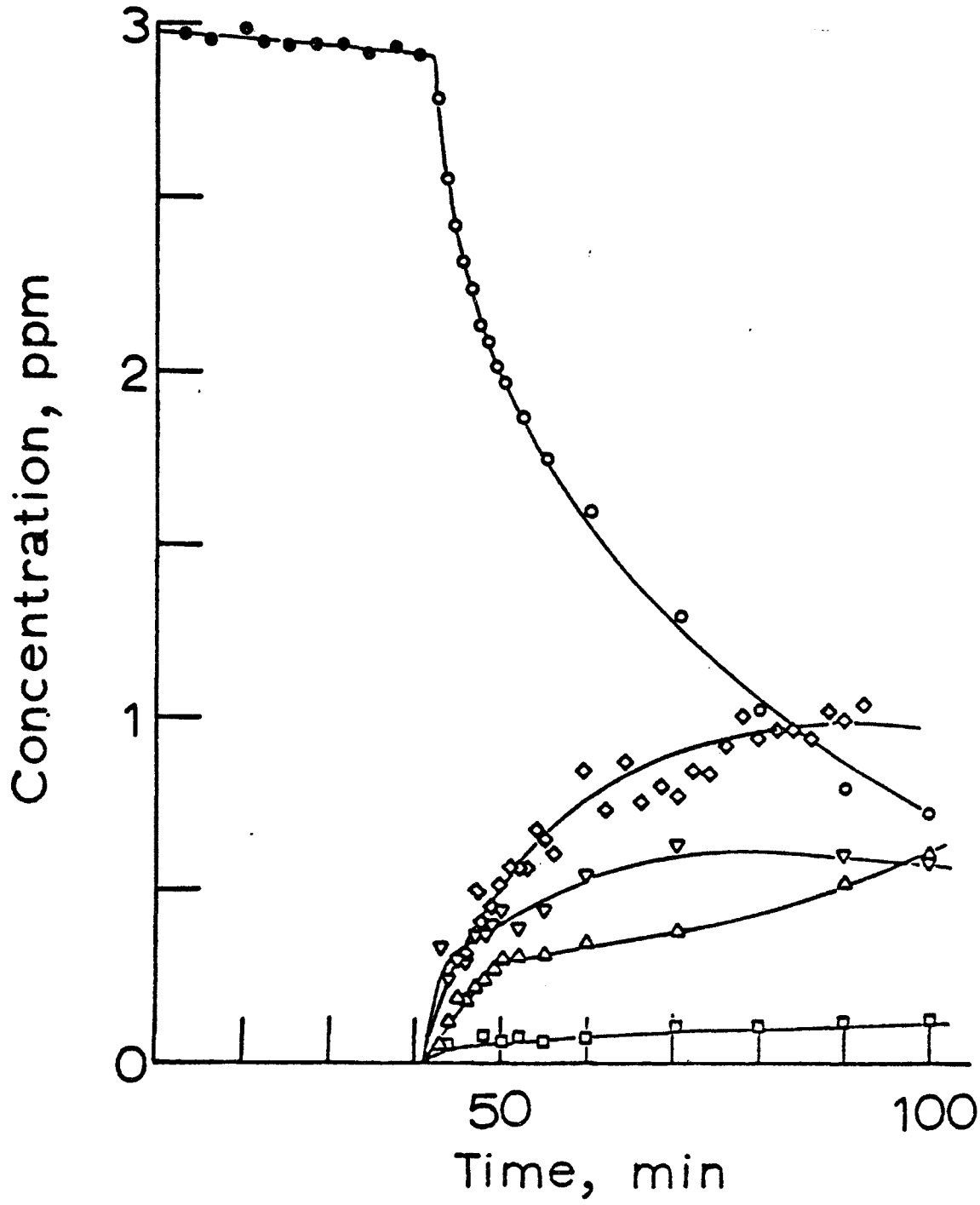

Figure 68. Concentration-time profile from the photolysis of dimethylnitrosamine in a mixture of 49 Torr oxygen and 651 Torr of nitrogen. Open symbols indicate data taken during photolysis; circles, dimethylnitrosamine; upright triangles, dimethylnitramine; inverted triangles, monomethylmethyleneamine; squares, nitrous acid; diamonds, nitric oxide; hexagons, nitrogen dioxide.

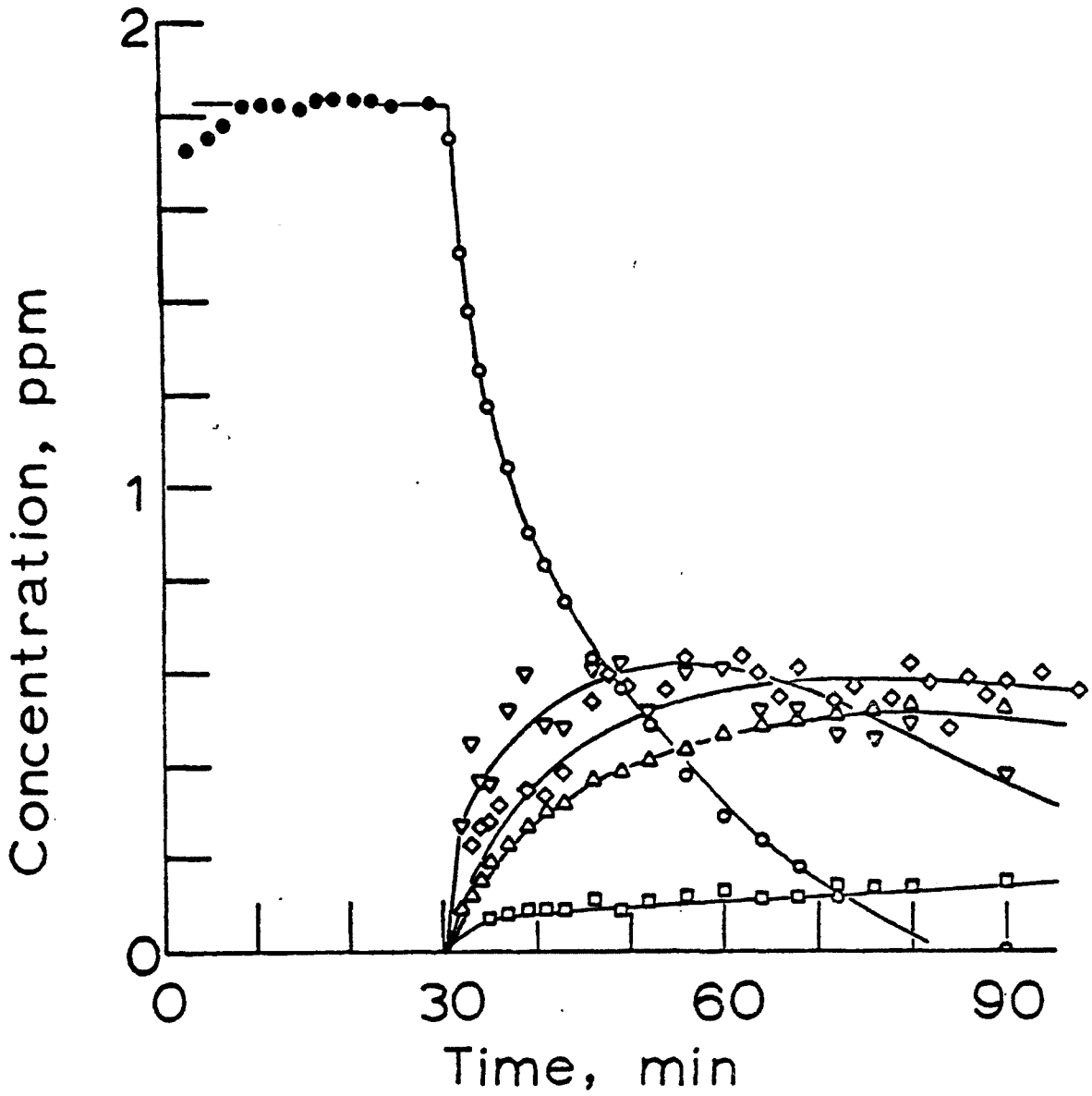

Figure 69. Concentration-time profile from the photolysis of dimethylnitrosamine in a mixture of 140 Torr of O_2 and 560 Torr nitrogen. Symbols same as Figure 68.

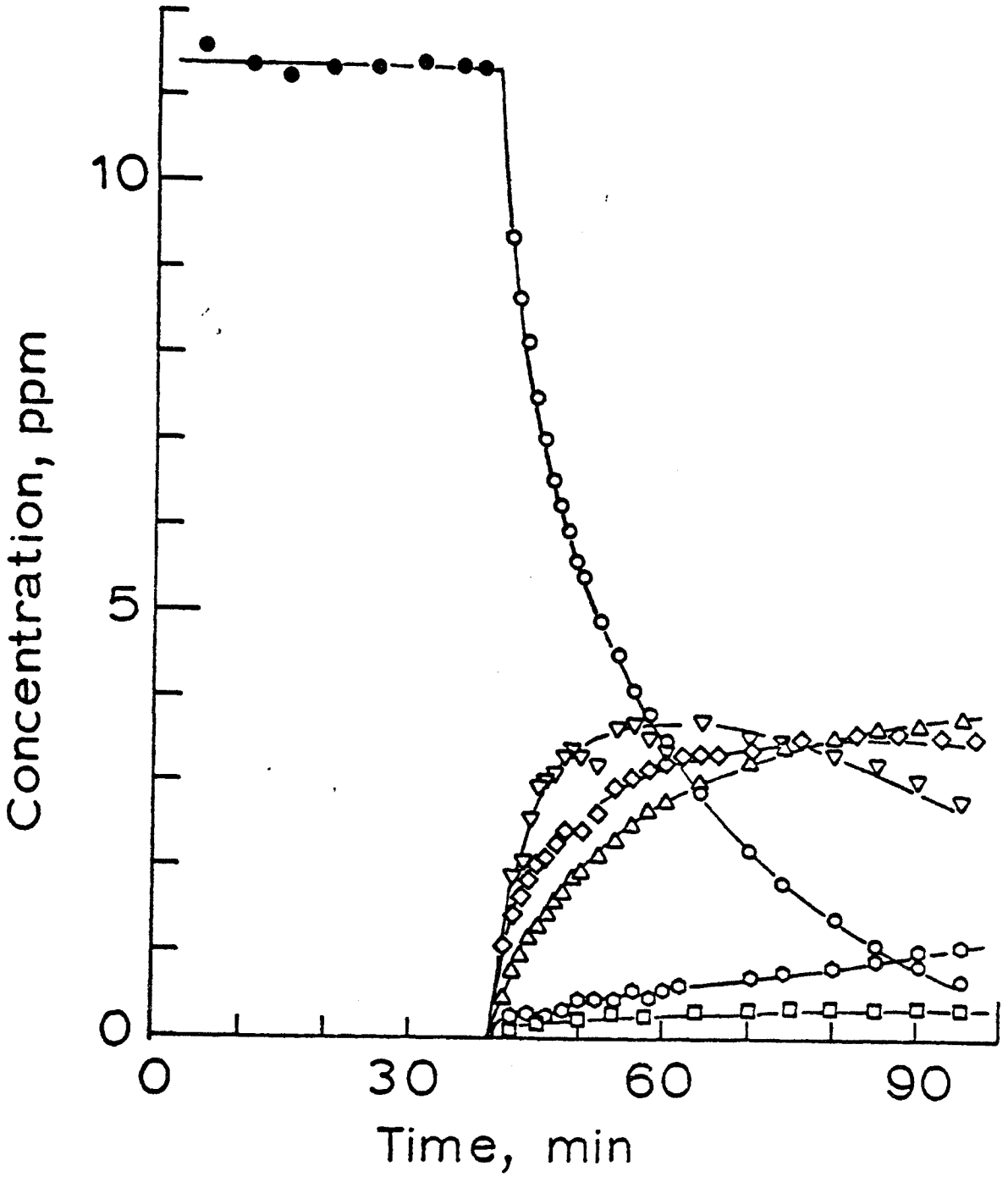

Figure 70. Concentration-time profile from the photolysis of dimethylnitrosamine in 730 Torr oxygen; symbols same as Figure 68.

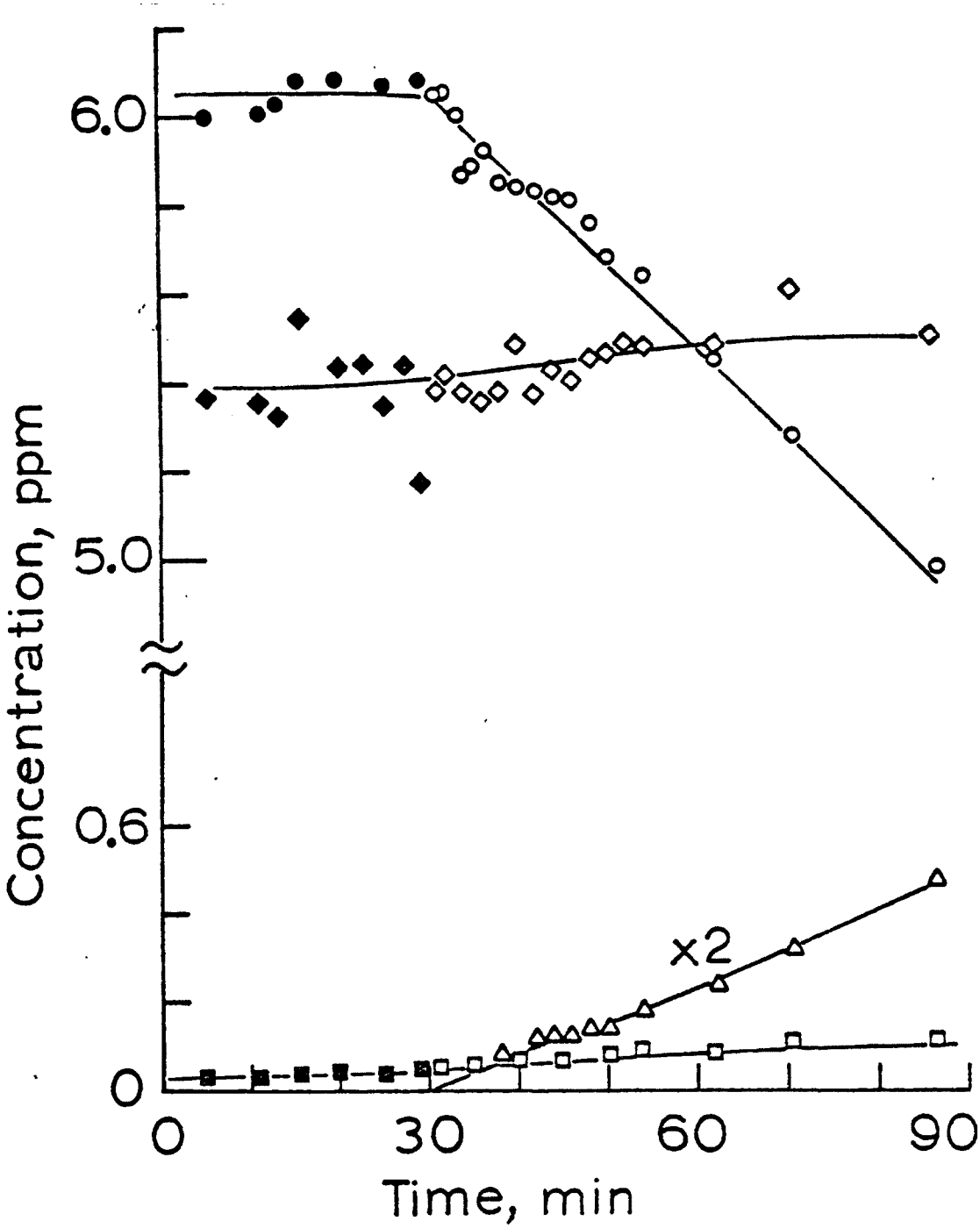

Figure 71. Concentration-time profile from the photolysis of dimethylnitrosamine with 5.4 ppm nitric oxide in a mixture of 23 Torr oxygen and 677 Torr nitrogen; symbols are same as Figure 68.

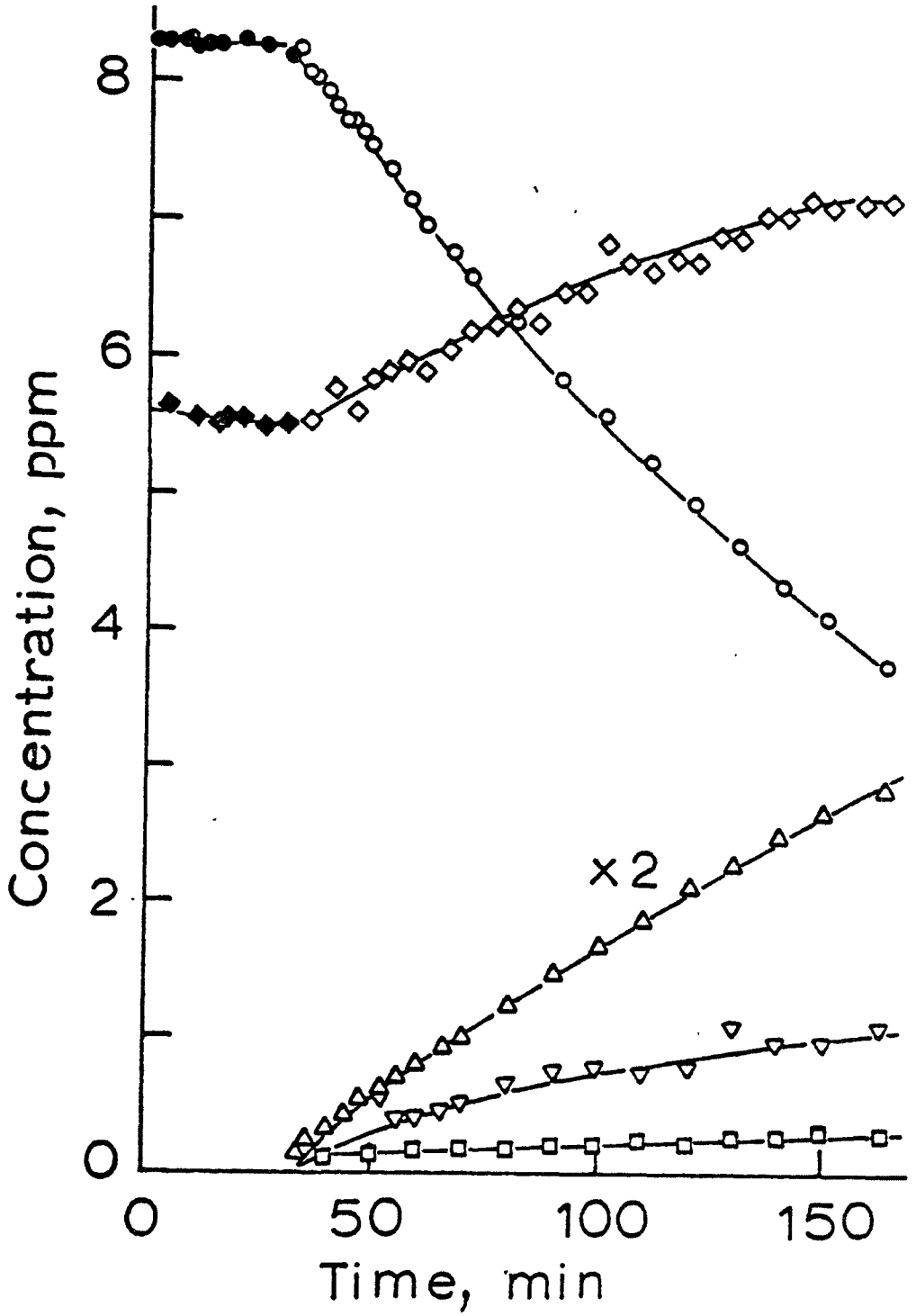

Figure 72. Concentration-time profile from the photolysis of dimethylnitrosamine with 5.5 ppm nitric oxide in a mixture of 69 Torr oxygen and 621 Torr nitrogen; symbols same as Figure 68.

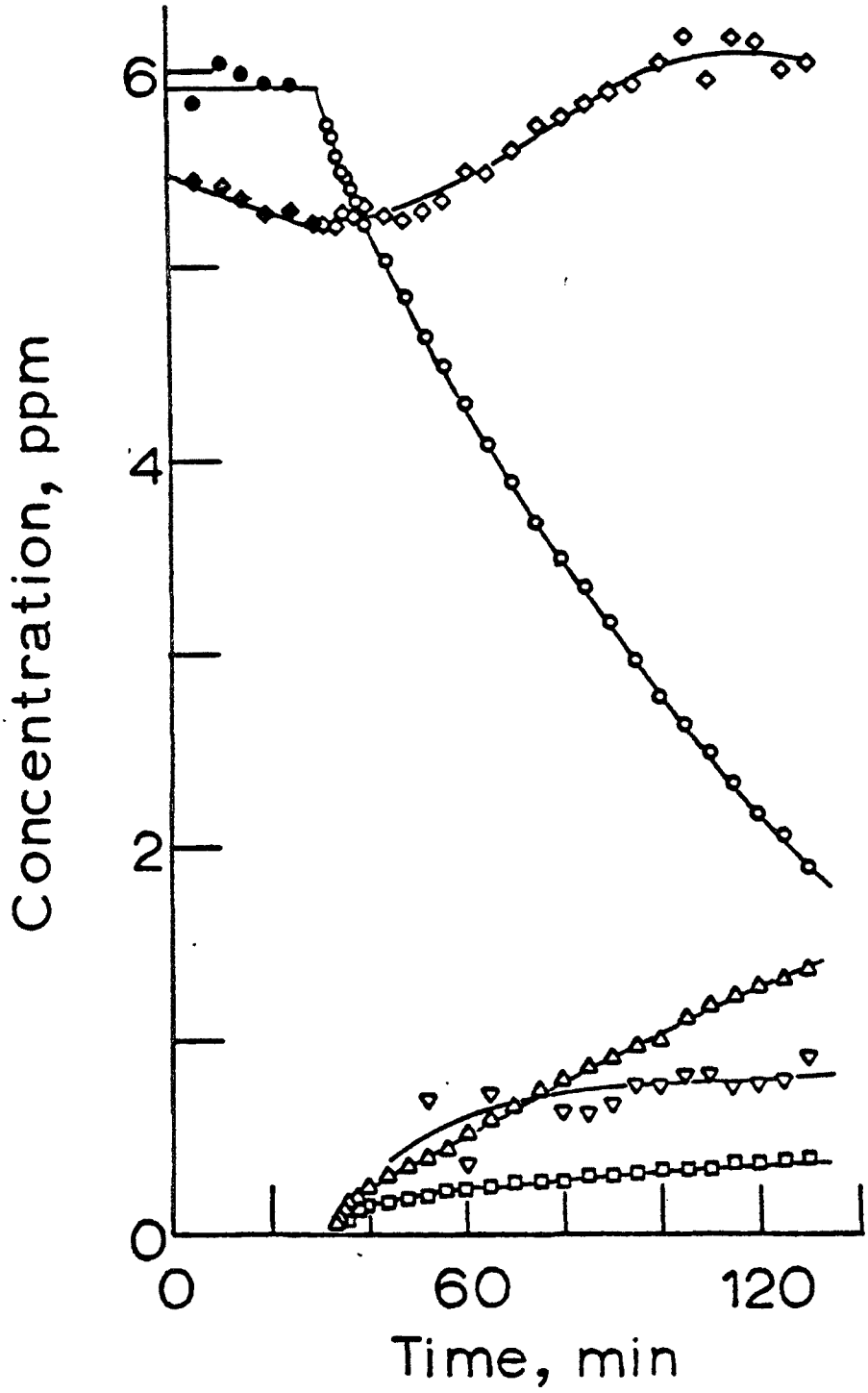

Figure 73. Concentration-time profile from the photolysis of dimethylnitrosamine with 5.5 ppm nitric oxide in a mixture of 138 Torr oxygen and 562 Torr nitrogen; symbols as in Figure 68 .

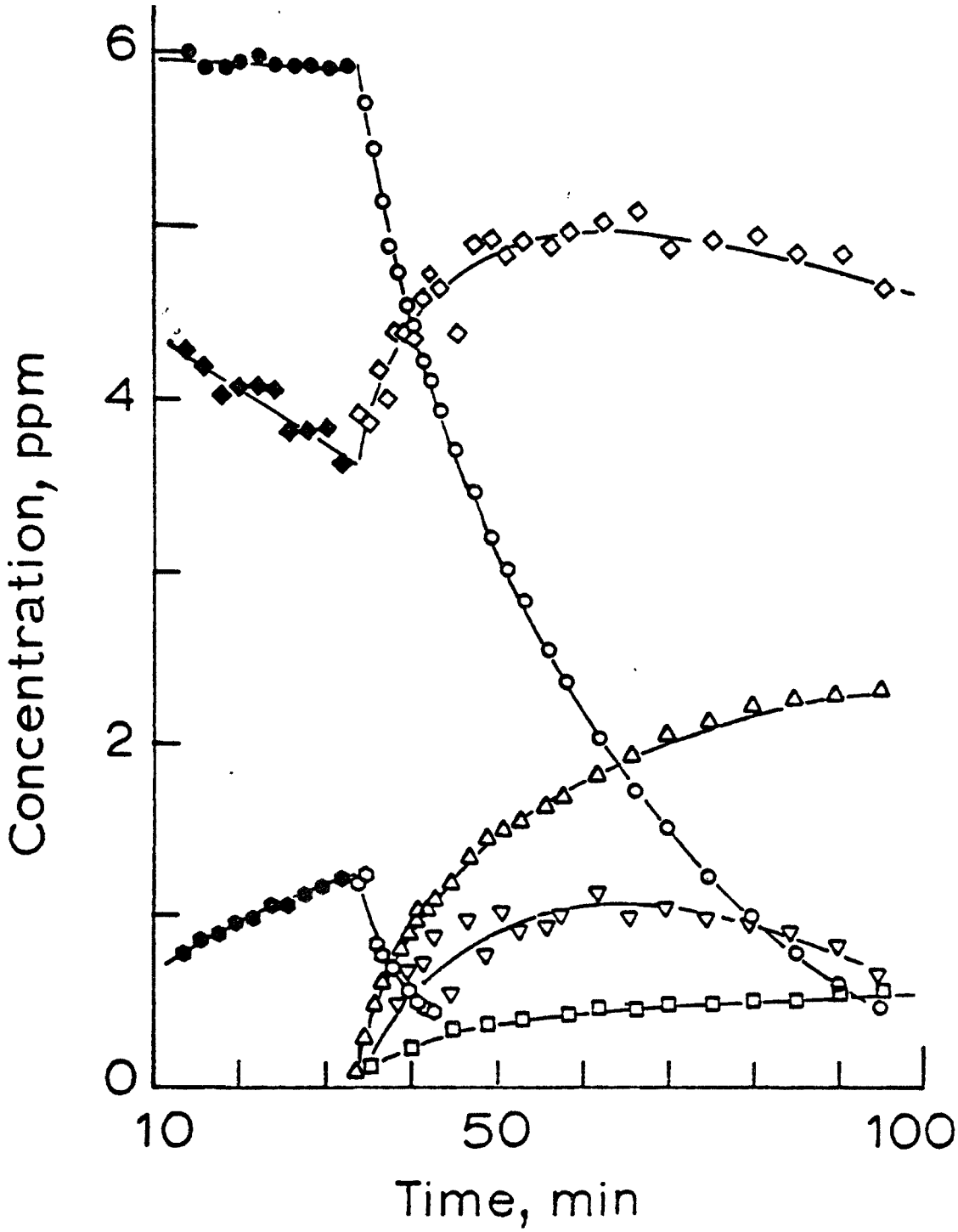

Figure 74. Concentration-time profile from the photolysis of dimethylnitrosamine with 5.0 ppm nitric oxide in 700 Torr oxygen; symbols as in Figure 68.

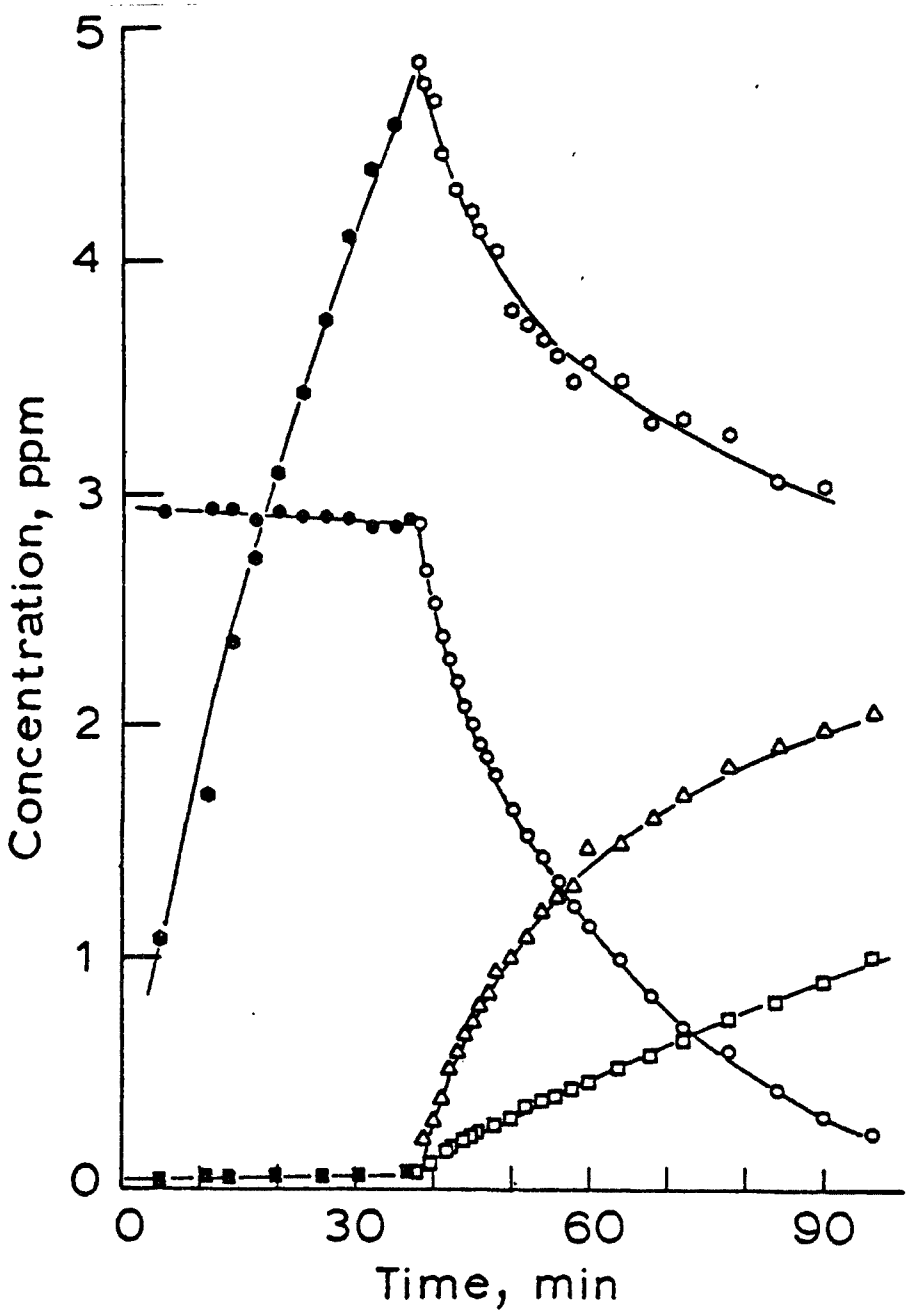

Figure 75. Concentration-time profile from the photolysis of dimethylnitrosamine with 25 ppm nitric oxide in a mixture of 145 Torr oxygen and 555 Torr nitrogen; symbols same as in Figure 68.

Determination of k_4/k_3 --

From the rate equations, the following expressions can be derived.

From equations 31a, 31b, and 32,

$$\frac{k_3[O_2]}{k_4[NO]} = \frac{-d[DMNA]/dt - d[DMN]/dt}{k_1[DMN] + d[DMN]/dt} \equiv B \qquad (35)$$

and from equations 31b and 33,

$$\frac{k_3[O_2]}{k_4[NO]} = \frac{d[MMA]/dt}{k_1[DMN] + d[DMN]/dt} \equiv B' \qquad (36)$$

The quantities B and B′ can be calculated from values of the concentrations obtained experimentally and a knowledge of the photolysis rate constant k_1.

Only data from the first few minutes of the photolysis were used in the calculation of B and B′ . At later times, secondary reactions of the products DMNA and MMA become important, as one might expect. This is especially evident in the case of MMA, which is seen to decrease at later times in most of the photolyses.

The results of these calculations for several experiments using k_1 = 0.12 min^{-1} are listed in Table 36. A plot of B and B′ as a function of $[O_2]/[NO]$ should have a slope of k_3/k_4 and an intercept of zero. This is illustrated in Figure 76. The reciprocal of the slope of the line shown gives $k_4/k_3 = (6.76 \pm 0.33(2\sigma)) \times 10^5$.

Determination of k_{5a}/k_3 --

A similar data treatment can be made to determine k_{5a}/k_3. The following relationships are derived from equations 31-33.

$$\frac{k_3[O_2]}{k_{5a}[NO_2]} = \frac{-d[DMN] - d[DMNA]}{d[DMNA]} \equiv C \qquad (37)$$

$$\frac{k_3[O_2]}{k_{5a}[NO_2]} = \frac{d[MMA]}{d[DMNA]} \equiv C' \qquad (38)$$

Values calculated for C and C′ are listed in Table 37. A concentration of NO_2 large enough to allow measurement was present in the few experiments shown in this table. It could be detected in most of the experiments where oxygen was present, although overlap of the spectral features with water and other products prevent quantitative analysis in most cases.

TABLE 36. CALCULATED VALUES OF B AND B′ USED IN THE ESTIMATION OF k_4/k_3. CONCENTRATIONS LISTED ARE TAKEN FROM GRAPHS OF THE DATA FROM THE EXPERIMENTS INDICATED

time, min	[DMN], ppm	[DMNA], ppm	[MMA], ppm	[NO], ppm	$\frac{[O_2]}{[NO]} \times 10^{-5}$	B[a]	B'[b]
			Experiment number 770919. 49 Torr O_2.				
43.00	2.570	0.074	0.142	0.18	2.93	0.51	0.41
44.00	2.438	0.121	0.211	0.26	2.19	0.38	0.30
45.00	2.330	0.161	0.265	0.33	1.82	0.33	0.25
46.00	2.236	0.195	0.310	0.38	1.61	0.30	0.22
47.00	2.154	0.222	0.349	0.42	1.47	0.23	0.18
48.00	2.087	0.246	0.382	0.46	1.36	0.21	0.16
49.00	2.026	0.268	0.412	0.49	1.27	0.20	
50.00	1.972	0.284		0.53	1.19	0.19	
51.00	1.925	0.296		0.56	1.13	0.18	
52.00	1.882	0.306		0.59	1.07	0.17	
53.00	1.843	0.314		0.62	1.02	0.16	
54.00	1.807	0.320		0.64	0.98	0.17	
55.00	1.772	0.325					
			Experiment number 770917-2. 140 Torr O_2.				
33.00	1.342	0.118	0.299	0.18	9.01	1.57	1.40
34.00	1.234	0.153	0.364	0.23	7.31	0.87	
35.00	1.152	0.182		0.28	6.40	0.85	
36.00	1.077	0.207		0.30	5.84	0.71	
37.00	1.012	0.229		0.33	5.38	0.73	
38.00	0.952	0.247		0.36			
			Experiment number 770930-2. 730 Torr O_2.				
42.00	8.73	0.740	1.910	1.40	6.26	0.96	1.00
43.00	8.13	0.947	2.320	1.67	5.43	0.78	0.77
44.00	7.61	1.136	2.645	1.87	4.93	0.66	0.58
45.00	7.16	1.300	2.900	2.03	4.60	0.60	
46.00	6.75	1.456	3.100	2.15	4.35	0.645	
47.00	6.36	1.590		2.27	4.13	0.54	
48.00	6.02	1.712		2.38			
			Experiment number 770930-1. 69 Torr O_2.				
32.00	8.244	0.007		5.50	0.165	0.023	
33.00	8.187	0.043		5.52	0.164	0.033	
34.00	8.128	0.072		5.54	0.164	0.037	
35.00	8.071	0.095		5.56	0.163	0.033	
36.00	8.020	0.116		5.58	0.163	0.030	
37.00	7.976	0.132		5.59	0.162	0.030	
38.00	7.933	0.148		5.61	0.161	0.035	
40.00	7.842	0.176		5.65	0.160	0.037	
42.00	7.752	0.200		5.69			

(Continued)

TABLE 36. (Continued)

time, min	[DMN], ppm	[DMNA], ppm	[MMA], ppm	[NO], ppm	$\frac{[O_2]}{[NO]} \times 10^{-5}$	B^a	B'^b
			Experiment number 771003-1. 138 Torr O_2.				
34.00	5.561	0.097		5.22			
35.00	5.494	0.129		5.22	0.353	0.059	
36.00	5.436	0.157		5.22	0.353	0.050	
37.00	5.378	0.182		5.22	0.353	0.056	
38.00	5.322	0.204		5.23	0.352	0.061	
39.00	5.271	0.225		5.23	0.352	0.051	
40.00	5.219	0.244			0.352	0.057	

[a] B is defined in equation 35.

[b] B' is defined in equation 36.

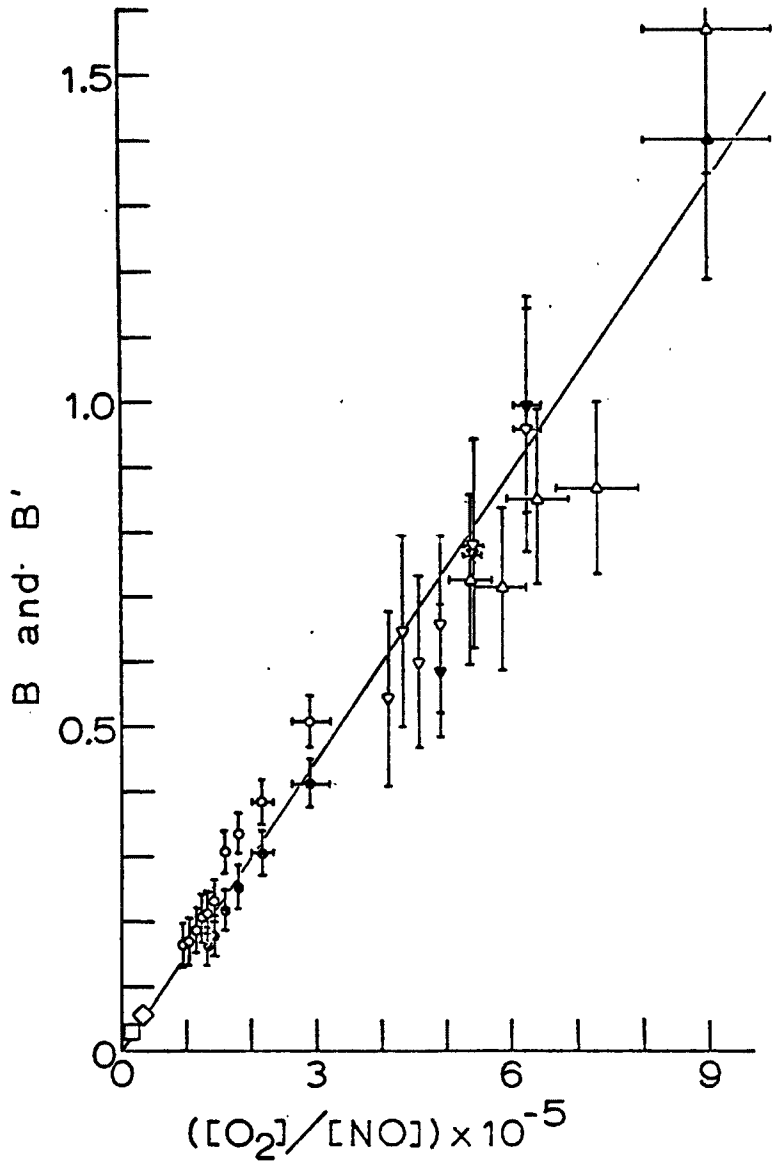

Figure 76. Plot of B and B′ as a function of $[O_2]/[NO]$ used to estimate k_4/k_3; open symbols, B; closed symbols, B′.

TABLE 37. CALCULATED VALUES OF C AND C′ USED IN THE ESTIMATION OF k_{5a}/k_3 AND k_{5b}/k_3. CONCENTRATIONS LISTED ARE TAKEN FROM GRAPHS OF THE DATA FROM THE EXPERIMENTS INDICATED

time, min	[DMN], ppm	[DMNA], ppm	[MMA], ppm	$[NO_2]$, ppm	$\frac{[O_2]}{[NO_2]} \times 10^{-6}$	C[a]	C′[b]
			Experiment number 770930-2. 730 Torr O_2.				
42.00	8.73	0.740	1.910	0.182	4.67	1.90	1.98
43.00	8.13	0.947	2.320	0.229	3.90	1.75	1.72
44.00	7.61	1.136	2.645	0.264	3.44	1.74	1.55
45.00	7.16	1.300	2.900	0.295	3.13	1.63	1.28
46.00	6.75	1.456	3.100	0.318			
			Experiment number 771003-2. 700 Torr O_2.				
34.00	5.755	0.086	0.040	1.11	0.89	0.59	0.48
35.00	5.430	0.291	0.139	0.97	1.01	0.61	0.53
36.00	5.155	0.462	0.230	0.86	1.13	0.70	0.62
37.00	4.920	0.600	0.316	0.765	1.27	0.65	0.69
38.00	4.730	0.715	0.395	0.685	1.41	1.07	0.87
39.00	4.550	0.802	0.471	0.620	1.56	0.80	0.83
40.00	4.395	0.888	0.542	0.560	1.72	0.95	0.83
41.00	4.245	0.965	0.606	0.510			
			Experiment number 770920-1. 145 Torr O_2.				
38.00	2.812	0.052		4.880	0.040	0.33	
39.00	2.644	0.178		4.742	0.041	0.19	
40.00	2.501	0.298		4.618	0.042	0.10	
41.00	2.380	0.408		4.507	0.043	0.09	
42.00	2.271	0.508		4.409	0.044	0.15	
43.00	2.169	0.597		4.318	0.045	0.33	
44.00	2.081	0.663		4.228	0.046	0.32	
45.00	1.995	0.728		4.148			

[a] C is defined in equation 37.

[b] C′ is defined in equation 38.

The quantities C and C′ are plotted as a function of $[O_2]/[NO_2]$ in Figure 23. The linear relation between the variables is in qualitative agreement with expectations. A weighted least squares gives the line shown, and the inverse of the slope of this line gives $k_{5a}/k_3 = (2.40 \pm 0.17\ (2\sigma)) \times 10^6$. A non-weighted least squares give $k_{5a}/k_3 = (2.56 \pm 0.18) \times 10^6$.

Refinement of the Mechanism --

Hydrogen Atom Abstraction by Nitrogen Dioxide: The Determination of k_{5b}/k_3--

There are two deficiencies in the simple mechanism considered in the previous section. First, it does not explain the non-zero intercept found in the plot of C and C′ as a function of $[O_2]/[NO_2]$. Secondly, this mechanism does not predict the quantities of nitrous acid that were observed experimentally.

Both of these shortcomings may be overcome by the addition of a reaction in which NO_2 abstracts a hydrogen atom from the dimethylamino radical.

$$(CH_3)_2N + NO_2 \rightarrow CH_2{=}N{-}CH_3 + HONO \qquad (5b)$$

If this reaction is added to the scheme, the following more complete expression for the relation of C and C′ to the concentrations of reactants may be derived.

$$C,\ C = \frac{k_3[O_2]}{k_{5a}[NO_2]} + \frac{k_{5b}}{k_{5a}} \qquad (39)$$

From the intercept of the graph in Figure 77, $k_{5b}/k_{5a} = 0.154 \pm 0.063$. Dividing by the slope, $k_{5b}/k_3 = (3.7 \pm 1.1(2\sigma)) \times 10^5$.

The effect of this change in mechanism on B and B′ is also of interest. Using the new mechanism,

$$B,\ B = \frac{k_3[O_2]}{k_4[NO]} + \frac{k_{5b}[NO_2]}{k_4[NO]} \qquad (40)$$

Since the experiments used to evaluate k_3/k_4 were chosen to be those in which little NO_2 was present, this should have little effect on the value of k_4/k_3 obtained.

Evidence for the Direct Oxidation of Dimethylnitrosamine--

Some indication is given that DMN may react directly (without dissociation) with oxidizing species to produce DMNA. Specifically, in the

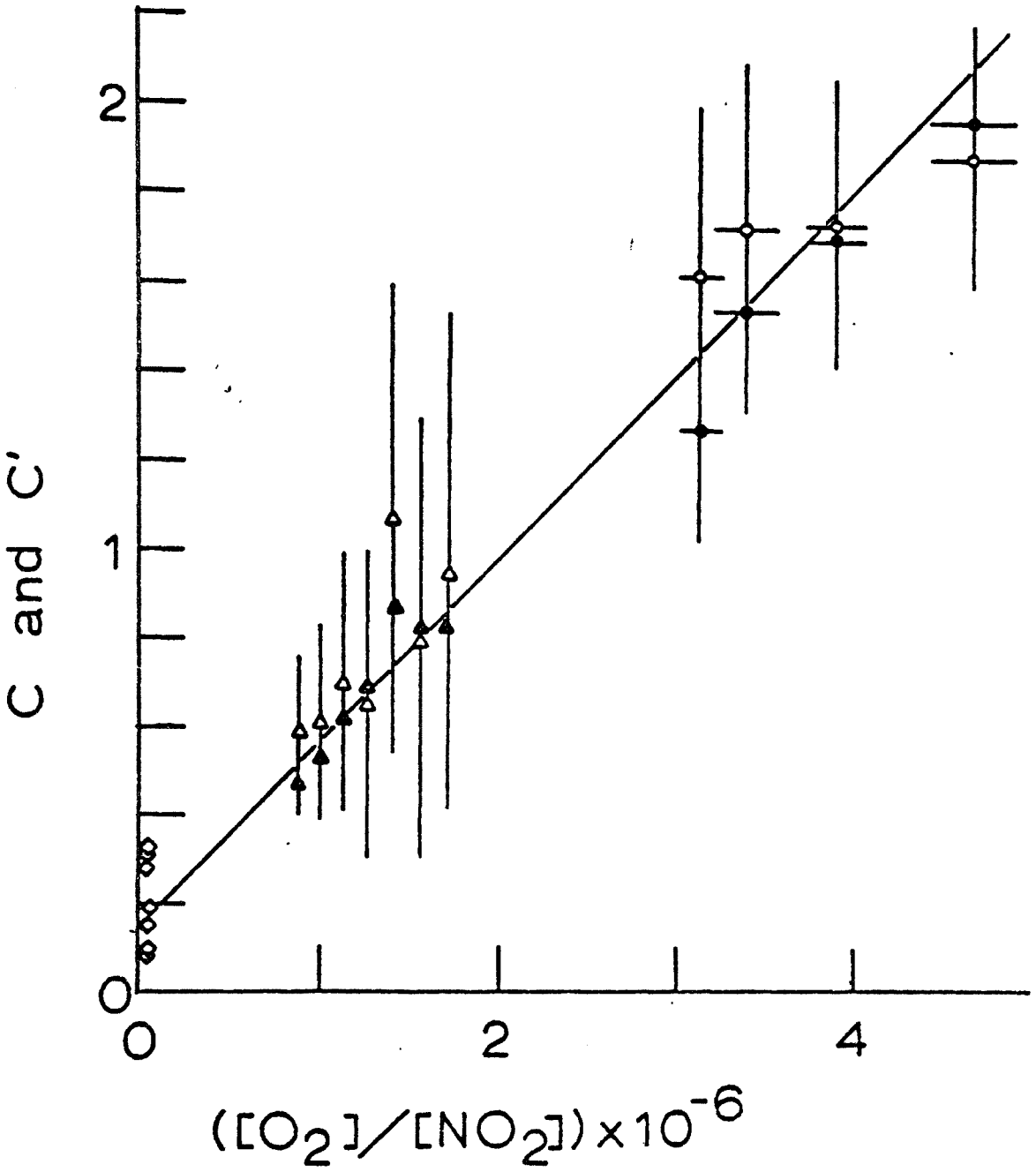

Figure 77. Plot of C and C′ as a function of $[O_2]/[NO_2]$ for the estimation of the rate constant ratio k_{5a}/k_3 and k_{5b}/k_3; open symbols, C; closed symbols, C′.

experiment where 11.4 ppm DMN was photolyzed in 730 Torr O_2, an initial enhancement of DMNA formation seemed to be present. This can be thought of as occurring from the subsequent reactions of the HO_2 radical formed in reaction 3.

$$(CH_3)_2N\text{-}NO + h\nu \rightarrow (CH_3)_2N + NO \quad (1)$$

$$(CH_3)_2N + O_2 \rightarrow CH_2{=}N\text{-}CH_3 + HO_2 \quad (3)$$

When NO is present, either as an added gas or as a photolysis product at later times, HO_2 will react with it rapidly to convert it to NO_2.

$$HO_2 + NO \rightarrow OH + NO_2 \quad (41)$$

However, in the beginning of an experiment such as the one under consideration, no oxides of nitrogen are present, and the HO_2 may react to oxidize DMN directly.

$$HO_2 + (CH_3)_2N\text{-}NO \rightarrow OH + (CH_3)_2N\text{-}NO_2 \quad (42)$$

From the present data, no crucial test of this hypothesis is possible, although they are consistent with it. A series of photochemical experiments using $Cl_2/H_2/O_2$/DMN mixtures might be used to test this point further.

Summary and Conclusions

A Fourier transform infrared spectrometer system was employed to study the kinetics of the reactions of the $(CH_3)_2N$ radical in simulated atmospheres. The radical was prepared by the photolysis of both dimethylnitrosamine and tetramethyl-2-tetrazene, and by the reaction of OH with dimethylamine. The following reactions appear to be important in the determination of nitrosamine levels in the atmosphere.

$$(CH_3)_2N\text{-}NO + h\nu \rightarrow (CH_3)_2N + NO \quad (1)$$

$$(CH_3)_2NH + OH \rightarrow (CH_3)_2N + H_2O \quad (2a)$$

$$\rightarrow CH_3NHCH_2 + H_2O \quad (2b)$$

$$(CH_3)_2N + O_2 \rightarrow CH_2{=}N\text{-}CH_3 + HO_2 \quad (3)$$

$$(CH_3)_2N + NO \rightarrow (CH_3)_2N\text{-}NO \quad (4)$$

$$(CH_3)_2N + NO_2 \rightarrow (CH_3)_2N\text{-}NO_2 \quad (5a)$$

$$\rightarrow CH_2{=}N\text{-}CH_3 + HONO \quad (5b)$$

A kinetic analysis of the data gave the following rate constant ratio estimates:

$$k_4/k_3 = (6.76 \pm 0.33) \times 10^5$$

$$k_{5a}/k_3 = (2.40 \pm 0.17) \times 10^6$$

$$k_{5b}/k_3 = (3.7 \pm 1.1) \times 10^5$$

These data may be used to make a preliminary estimate of the concentration of dimethylnitrosamine in a polluted atmosphere.

If the above scheme is valid,

$$\frac{d[DMN]}{dt} = \left(k_1[DMN] + k_{2a}[OH]\,[DMA]\right)\left[\frac{k_4[NO]}{k_3[O_2] + k_4[NO] + k_5[NO_2]}\right] - k_1[DMN]$$

Assuming that a steady state concentration of dimethylnitrosamine is reached,

$$k_1[DMN]\left[1+\frac{k_4[NO]}{k_3[O_2] + k_4[NO] + k_5[NO_2]}\right] = k_{2a}[OH][DMA]\left[\frac{k_4[NO]}{k_3[O_2] + k_4[NO] + k_5[NO_2]}\right]$$

$$[DMN]_{ss} = \left[\frac{k_{2a}[OH][NO]}{k_1((k_3/k_4)[O_2] + (k_5/k_4)[NO_2])}\right][DMA]$$

In sunlight irradiated polluted atmospheres, [OH] is generally estimated to be about 10^{-7} ppm. Using this value, the value $k_{2a} = 3.67 \times 10^4$ $ppm^{-1}min^{-1}$ derived from the data of Atkinson et al.,[25] and values of the rate constant ratios and k_1 derived in this work,

$$[DMN]_{ss} = \left[\frac{0.037[NO]}{0.30 + 4.10[NO_2]}\right][DMA]$$

Assuming NO and NO_2 concentrations in the range 0.1 to 0.5 ppm normally encountered in highly polluted air, then nitrosamine levels of about 1% of the dimethylamine in the air will result at the steady state.

Dimethylnitrosamine is not an end product in the photooxidation of dimethylamine in the atmosphere, since it photolyzes in sunlight to reform the dimethylamino radical. The two other products formed in our system from the reactions of the dimethylamino radical were monomethylmethyleneamine and dimethylnitramine. Of these two, monomethylmethyleneamine went on to further oxidation, while dimethylnitramine was reasonably stable.

If this stability of dimethylnitramine carries over to the atmosphere, as seems likely, the potential for a considerable accumulation of this compound exists. Using the rate constant ratios derived in this work, together with the estimation of k_{2a} derived from the work of Atkinson

et al.,[25] the rate of formation of dimethylnitramine from dimethylamine in a polluted atmosphere can be estimated.

$$\frac{d[DMNA]}{dt} = k_{2a}[OH][DMA]\left[\frac{k_{5a}[NO_2]}{(k_{5a} + k_{5b})[NO_2] + k_3[O_2]}\right]$$

$$= (3.67 \times 10^4 ppm^{-1}min^{-1})(10^{-7} ppm)[DMA]\left[\frac{[NO_2]}{1.15[NO_2] + 0.083}\right]$$

Even at the moderate NO_2 concentration of 0.1 ppm, this gives a rate of conversion of dimethylamine to the nitramine of about 0.2%/minute. Thus our data predicts that appreciable levels of dimethylnitramine may be built up where amine levels are high. Since dimethylnitramine has demonstrated carcinogenic activity in laboratory animals,[38,39] these high levels are of concern. These results suggest that analysis for dimethylnitramine in the real atmosphere be initiated.

REFERENCES

1. P.N. Magee and J.M. Barnes, Brit. J. Cancer, 10, 114 (1956).

2. D.H. Fine, D.P. Rounbehler, N.M. Belcher, and S.S. Epstein, Science, 192, 1328 (1976).

3. P.N. Magee and J.M. Barnes, Adv. Cancer Res., 10, 163 (1967).

4. B. Terracini, P.N. Magee, and J.M. Barnes, Brit. J. Cancer, 21, 559 (1967).

5. G.E. Moiseyev and V.V. Benemanskiy, Vopr. Onkol., 21, 106 (1975).

6. H. Druckrey, R. Preussman, S. Ivankovic, and D. Schmahl, Z. Krebsforsch., 69, 103 (1967).

7. P. Walker, J. Gordon, L. Thomas, and R. Ouellette, MITRE Technical Report #MTR-7152, February 1976.

8. K. Bretschneider and J. Matz, Arch. Geschwulstforsch., 42, 36 (1974).

9. D.H. Fine, D.P. Rounbehler, A. Rounbehler, A. Silvergleid, E. Sawicki, K. Krost, and G.A. DeMarrais, Environ. Sci. Technol., 11, 581 (1977).

10. D.H. Fine, D.P. Rounbehler, E.D. Pellizzari, J.E. Bunch, R.W. Berkeley, J. McCrae, J.T. Bursey, E. Sawicki, and G.A. DeMarrais, Bull. Environ. Contam. Toxicol., 15, 739 (1976).

11. Atmospheric Nitrosamine Assessment Report. Environmental Protection Agency Draft, March 12, 1976.

12. R.B. Faoro, J. Air Pollut. Control Assoc., 25, 638 (1975).

13. D. Shapley, Science, 191, 268 (1976).

14. B.R. Simoneit and A.L. Burlingame, Nature (London), 234, 210 (1971).

15. J.W. Rhoades and D.E. Johnson, J. Nat. Cancer Inst., 48, 1841 (1972).

16. T. Fazio, J.N. Damico, J.W. Howard, R.H. White, and J.O. Watts, J. Agr. Food Chem., 19, 250 (1971).

17. D.F. Gadbois, E.M. Ravesi, R.C. Lundstrom, and R.S. Maney, J. Agr. Food Chem., 23, 665 (1975).

18. G. Neurath, B. Pirmann, H. Luttich, and H. Wichern, Beitr. Tabakforsch., 3, 251 (1965).

19. P.L. Hanst, J.W. Spence, and M. Miller, Environ. Sci. Technol., 11, 403 (1977).

20. W.A. Glasson, General Motors Research Laboratory, Warren, Michigan, private communication with J.G. Calvert.

21. J.N. Pitts, Jr., D. Grosjean, K.A. Van Cauwenberghe, J.P. Schmid, and D.R. Fitz, Environ. Sci. Technol., 12, 946 (1978).

22. E.C. Tuazon, A.M. Winer, R.A. Graham, J.P. Schmid, and J.N. Pitts, Jr., Environ. Sci. Technol., 12, 954 (1978).

23. J. Althorpe, D.A. Goddard, D.J. Sissons, and G.M. Telling, J. Chromatogr., 53, 371 (1970).

24. J.G. Calvert, Report of Ad Hoc Committee on Assessment of Nitrosamines in the Atmosphere, August 1976, preliminary draft.

25. R. Atkinson, R.A. Perry, and J.N. Pitts, Jr., J. Chem. Phys., 68, 1850 (1978).

26. N.R. Greiner, J. Chem. Phys., 53, 1070 (1970).

27. R. Lesclaux and M. Demissey, to appear in Nouv. J. Chem.

28. R. Lesclaux, P. Vankhe, J.C. Soulignac, and J. Joussot-Dubien, Abstracts, VII International Conference on Photochemistry, Edmonton, Canada, August 1975.

29. K. Ya. Kondratzev, "Radiation in the Atmosphere", Academic Press, New York, N.Y., 1969, p. 225.

30. P.L. Hanst in "Advances in Environmental Science and Technology," Vol. II, J.N. Pitts, Jr. and R.L. Metcalf, eds., Wiley Interscience, New York, N.Y., 1971, pp. 154-164.

31. C.H. Wu and H. Niki, Environ. Sci. Technol., 9, 46 (1975).

32. C.H. Bamford, J. Chem. Soc., 12 (1939).

33. B.G. Gowenlock, F. Jones, and J. Mayer, Trans. Faraday Soc., 57, 23 (1961).

34. B.L. Korsunskii, V.N. Pepkin, Yu. A. Lebevdev, and A. Ya. Apin, Izv. Akad. Nauk SSSR, Ser. Khim., 525 (1967).

35. A.M. Bass, A.E. Ledford, Jr., and A.H. Laufer, J. Res. Nat. Bur. Stand., 80A, 143 (1976).

36. I.T.N. Jones and K.D. Bayes, J. Chem. Phys., 59, 4836 (1973).

37. B.G. Gowenlock and K.E. Thomas, J. Chem. Soc., B, 409 (1966).

38. H. Druckrey, R. Preussmann, D. Schmahl, and M. Muller, Naturwissenschaften, 48, 134 (1961).

39. C.M. Goodall and T.H. Kennedy, Cancer Lett., 1, 295 (1976).

TECHNICAL REPORT DATA
(Please read Instructions on the reverse before completing)

1. REPORT NO.	2.	3. RECIPIENT'S ACCESSION NO.
EPA-600/2-80-024		

4. TITLE AND SUBTITLE	5. REPORT DATE
KINETIC STUDIES OF SIMULATED POLLUTED ATMOSPHERES	January 1980
	6. PERFORMING ORGANIZATION CODE

7. AUTHOR(S)	8. PERFORMING ORGANIZATION REPORT NO.
Jack G. Calvert	

9. PERFORMING ORGANIZATION NAME AND ADDRESS	10. PROGRAM ELEMENT NO.
Department of Chemistry The Ohio State University Columbus, Ohio 43212	1AA603A AC-24 (FY-78)
	11. CONTRACT/GRANT NO.
	R804348-01

12. SPONSORING AGENCY NAME AND ADDRESS	13. TYPE OF REPORT AND PERIOD COVERED
Environmental Sciences Research Laboratory-RTP, NC Office of Research and Development U.S. Environmental Protection Agency Research Triangle Park, North Carolina 27711	Final 1/76 - 4/79
	14. SPONSORING AGENCY CODE
	EPA/600/09

15. SUPPLEMENTARY NOTES

16. ABSTRACT

The kinetics and reaction mechanisms of several important atmosheric contaminants - SO_2, formaldehyde, nitrous acid, and the nitrosamines - were assessed to help quantify some key aspects of the chemistry of polluted atmospheres. The reactions and lifetimes of excited sulfur dioxide with various atmospheric components including hydroxyl, hydroperoxy, and methylperoxy radicals were studied. These data and other published rate data were reviewed and evaluated. The photolysis of formaldehyde was investigated as a major source of hydroperoxyl radicals, and a quantitative evaluation made of its apparent first order rate constants at various solar zenith angles. The absolute extinction coefficients for nitrous acid were determined, and estimates made of the rates of hydroxyl radical generation in the troposphere by photolysis of nitrous acid. Long path Fourier transform infrared spectroscopy was used to help evaluate the potential for nitrosamine formation in the polluted atmosphere.

17. KEY WORDS AND DOCUMENT ANALYSIS

a. DESCRIPTORS	b. IDENTIFIERS/OPEN ENDED TERMS	c. COSATI Field/Group
*Air pollution		13B
*Ozone		07B
*Nitrogen oxides		07C
*Sulfur inorganic compounds		07E
*Photochemical reactions		

18. DISTRIBUTION STATEMENT	19. SECURITY CLASS *(This Report)*	21. NO. OF PAGES
RELEASE TO PUBLIC	UNCLASSIFIED	280
	20. SECURITY CLASS *(This page)*	22. PRICE
	UNCLASSIFIED	

EPA Form 2220-1 (9-73)